Chemical-proteomic strategies to study cysteine posttranslational modifications

Author: Shalise Monique Couvertier

CHEMICAL-PROTEOMIC STRATEGIES TO STUDY CYSTEINE POSTTRANSLATIONAL MODIFICATIONS

Shalise Monique Couvertier

A dissertation

submitted to the Faculty of

the department of Chemistry

in partial fulfillment

of the requirements for the degree of

Doctor of Philosophy

Boston College
Morrissey College of Arts and Sciences
Graduate School

April 2016

Chemical-proteomic strategies to study cysteine posttranslational modifications

by

Shalise Monique Couvertier

Thesis Advisor: Eranthie Weerapana, Ph.D.

Abstract

Cysteine residues on proteins play important catalytic and regulatory roles in complex proteomes. These functional residues can be modified under physiological conditions by posttranslational modifications (PTMs) to regulate protein activities and modulate cysteine reactivity. Many PTMs are highly labile and dynamic, rendering it difficult to detect modified proteins within complex systems. To contribute to the chemical-proteomic methods currently available, chemical probe-Mass Spectrometry (MS) platforms were developed to study oxidative cysteine modifications. A MS platform for the assessment of *S*-nitrosation *in vitro* identified Cys329 of Cathepsin D (CTSD) as highly sensitive to *S*-nitrosothiol formation. To achieve a more physiological relevant representation of *S*-nitrosation, this platform was later adapted for study in live cells using a caged electrophile, Caged BK. Additionally, oscillation of cysteine oxidation as a function of circadian rhythm in *Drosophila melanogaster* and human samples was explored. As a compliment to these MS platforms, a 4-aminopiperidine-based cysteine-reactive probe library was developed. These probes have been used to target specific reactive cysteines as an alternate way to regulate protein function and can be used as tools to provide insight into the roles of these residues in protein activities.

Table of Contents

List of Tables

Appendix.

List of Figures

Chapter 1.

Chapter 2.

Chapter 4.

Chapter 5.

in the a' domain. SMC-18 shows selectivity for C53 in the a-domain. (C) Structures of probes used site of labeling experiments.

List of Schemes

Chapter 5.

List of Abbreviations

Standard 3-letter and 1-letter codes are used for the 20 natural amino acids.

AGE	advanced glycation endproducts
AKT1	RAC-alpha serine/threonine-protein kinase/ Protein Kinase B
Akt2	RAC-beta serine/threonine-protein kinase
AMP	Adenosine monophosphate
ARP	aldehyde-reactive probe
Asp-AMC	L-aspartic acid 7-amido-4-methylcoumarin
ATP	Adenosine triphosphate
biotin-HPDP	N-[6-(biotinamido)hexyl]-3'-(2'-pyridyldithio)propionamide
BCN	9-hydroxymethylbicyclo[6.1.0]nonyne
BH	biotin hydrazide
BioGEE	biotinoylated glutathione ethyl ester
BioGSH	biotinylated GSH
BioGSSG	biotinylated GSSG
BK	bromomethyl ketone
BMAL	Brain and Muscle ARNT-Like
BST	Biotin-switch technique
CA	chloroacetamide
cAMP	cyclic AMP
CASP3	caspase-1
CBK	caged bromomethyl ketone

cCMP	cyclic cytidine monophosphate
CID	collision-induced dissociate
Clk	CLOCK
CLOCK	Circadian Locomotor Output Cycles Kaput
CO	carbon monoxide
COX	cyclooxygenase
C_p	peroxidatic cysteine
C_r	resolving cysteine
CSA	congenital sideroblastic anemia
CTSD	cathepsin D
CuAAC	copper(I)-catalyzed azide-alkyne cycloaddition
CysNO	S-nitrosocysteine
DCXR	L-xylulose reductase
DJ-1	Protein deglyase
DNA	deoxyribonucleic acid
Dnp	2,4-dinitrophenol
DNPEP	Aspartyl aminopeptidase
DNPH	dinitrophenylhydrazine
15d-PGJ2	15-deoxy12,13-prostaglandin J2
DUBs	deubiquitinating enzymes
EGF	epidermal growth factor
EGFR	epidermal growth factor receptor
eNOS	endothelial NOS

ER	endoplasmic reticulum
FAD	flavin adenine dinucleotide
FRET	Förster Resonance Energy Transfer
FTase	farnesyl transferase
GAPDH	glyceraldehyde-3-phosphate dehydrogenase
GFP	Green fluorescent protein
GGTase-I/II	geranylgeranyltransferase
Glrx1	Glutaredoxin 1
Glrx2	Glutaredoxin 2
Glrx3	Glutaredoxin 3
Glrx5	glutaredoxin 5
Glrxs	Glutaredoxins
GSH	reduced glutathione
GS	glutathione synthetase
GSNO	S-nitrosoglutathione
GSSG	oxidized glutathione
GST	Glutathione S-transferase
GSTO1	glutathione S-transferase Omega 1
2-HD	2-trans-hexadecenal
HEK293T	human embryonic kidney 293T
HNE	4-hydroxy-2-nonenal
iNOS	inducible NOS
IA	iodoacetamide

ICAT	isotope-coded affinity tags
isoTOP-ABPP	isotopic Tandem Orthogonal Proteolysis – Activity-Based Protein Profiling
IAA	iodoacetamide alkyne
Isc	Iron sulfur cluster
JNK	c-Jun N-terminal kinase
L:H	light to heavy ratio
LC	liquid chromatography
LCBH	long-chain biotin hydrazide
LDE	lipid derived electrophile
L-NAME	N_{ω}-Nitro-L-arginine methyl ester
LOX	lipooxygenases
Luc	Luciferase
Mca	4-methoxylcoumarin
MCF-7	Michigan Cancer Foundation-7
MMTS	methyl methanethiosulfonate
MRM	multiple reaction MS
MS	mass spectrometry
NAD^+	Nicotinamide adenine dinucleotide
NADP	Nicotinamide adenine dinucleotide phosphate
NEt_3	triethyl amine
nNOS	neuronal NOS
NO	nitric oxide
NOS	nitric oxide synthase

OxICAT	oxidation ICAT
PACMA	propynoic acid carbamoyl methyl amide
PBS	Phosphate buffered saline
PDI	Protein Disulfide Isomerase
PDIA1	protein disulfide isomerase A 1
PDIA3	protein disulfide isomerase A 3
PDIA4	protein disulfide isomerase A 4
PER/per	PERIOD/ period circadian protein homolog
Per2	Period circadian protein homolog 2
PKB	Protein Kinase B
Prx	peroxiredoxin
Prxs	peroxiredoxins
Prx5	Peroxiredoxin 5
Prdx6	Peroxiredoxin 6
PTM	posttranslational modification
PTPs	protein-tyrosone phosphatases
RAS	Renin-angiotensin system
RBCs	red blood cells
Rh-N_3	rhodamine azide
RNA	Ribonucleic acid
RNase	Ribonuclease
R-NO	nitroso group
RNS	reactive nitrogen species

ROS	reactive oxygen species
SILAC	stable isotope labeling by amino acids in cell culture
SPH	solid-phase hydride
SNO	*S*-nitrosothiol
SNO-RAC	SNO resin-assisted capture
SNOSID	SNO site identification
sRNase	scrambled RNase
sulfo-NHS-biotin	sulfosuccinimidyl-6-(biotinamido)-hexanoate
STS	staurosporine
TEV	Tobacco Etch Virus
THF	tetrahydrofuran
TIM	TIMELESS
TK1	thymidine kinase 1
TMT	tandem mass tags
TrxNO	S-nitrosothioredoxin
Trxr-1	drosophila thioredoxin reductase 1
TrxR2	mammalian thioredoxin reductase 2
TrxRs	Thioredoxin reductases
TsCl	tosyl chloride
TXPTS	tris(4,6dimethyl-3-sulfonatophenyl)phosphine trisodium salt hydrate
UV	ultra violet
UPR	Unfolded Protein Response

U2OS_P	human osteosarcoma cell line with Per-Luc promoter
vNKH	variant nonketotic hyperglycemia
WT	wild-type
ZAK kinase	Sterile alpha motif and leucine zipper containing kinase

Acknowledgements

Firstly, I would like to thank my advisor, Professor Eranthie Weerapana. I cannot thank you enough for giving me the opportunity to work in your lab. Your patience and graceful approach to mentoring helped to create an excellent place to learn and work. I could not have asked for a better advisor. Because of you, I have developed into a far better scientist than I thought I would become and I hope that, as I continue in my scientific career, I am able to emulate all that I have learned under your tutelage. It was truly a pleasure working in your lab and I will look back at my time here fondly. I would also like to extend a sincere thank you to my thesis committee, Jianmin Gao and Abhishek Chatterjee, for all of your help, our stimulating discussions about research and your advice over the course of my time at Boston College.

Thank you to all of my collaborators. A special thanks goes to Dr. Kimberly Kerr, Jennifer Sherk, and Dr. Michael Rosbash from Brandeis University. Thank you for always going above and beyond whenever I needed help with data analysis or more (yes, more) fly heads. I am thankful for all that you have done for me and I owe a lot of the success with the circadian oscillation project to you. Collaborating with you has provided me with greater appreciation for research outside of chemistry and for that I am grateful.

I would like to thank all of the members of the Weerapana lab past and present: Lisa, Tyler, Dan, Alex S., Julie, Yani, Nick, Masahiro, Haley, Ranjan, Katie, Kyle and Aaron. You have all been a pleasure to work with and learn from. I would also like to thank the undergraduate students, Paige, Inchul and Alex W., who worked with me throughout my Ph.D. I would like to give a special thank you to my fellow "year-mate"

Lisa. I cannot thank you enough for the friendship and support, scientifically speaking and otherwise, which you have given me throughout our time together in graduate school. I can honestly say that surviving graduate school would have been impossible without you and that I treasure the friendship that we share. I would also like to thank my beloved bench-mate, Dan. From putting up with my antics to our shared love of Cher Lloyd, your friendship and mentorship over the past few years has really had an impact on my time at BC. Graduate school would not have been the same without you. Last but not least, I would like to thank my "little brother" of the lab, Tyler. You are one of the most unique, funny and happy people I know. Because of you, lab was always entertaining and I would like to thank you for always making even the most mundane lab work fun.

I would also like to thank my family and friends outside of Boston College. More specifically, I would like to thank my brothers for their love and support. You three are my best friends and laughter is infectious when the four of us are together. Thank you for keeping me grounded and reminding me to enjoy the present by not sweating the small stuff. I also need to thank my parents. Both of you have had such a great influence on all that I have done. Thank you for all of your support and always encouraging me to never do less than my best. Finally, I would like to end by thanking Thomas Blaisdell. You are always there for me when I need someone to talk science and for some reason you are still putting up with my crazy moments. For this I am grateful. I would not have been able to make it through graduate school without your never-ending love and support. I look forward to what the future has in store for us.

Chapter 1

Chemical-proteomic strategies for the assessment of cysteine posttranslational modifications

A significant portion of the work described in this chapter has been published in:

Couvertier, S. M.; Zhou, Y.; Weerapana, E. Chemical-proteomic strategies to investigate cysteine posttranslational modifications. *Biochim. Biophys. Acta* **2014**, *1844*, 2315–2330.

Introduction

Cysteine residues on proteins play critical functional roles within a complex proteome. Cysteines can act as sites of nucleophilic and redox catalysis, metal binding, structural stabilization and allosteric regulation. [1] The various functions of cysteine arise from of the intrinsic nucleophilicity and redox properties of the cysteine free thiol. As a result of the low dissociation energy of the S−H bond, 82 kcal/mol, and the large atomic radius of sulfur, 1.27 Å, the cysteine thiol has a pKa value of ~8.0. [2] Within a local protein environment, the thiol side-chain pKa is easily perturbed. Cysteine thiol pKa values as low as 3.5 have been reported for members of the glutaredoxin family. [3,4] Reduced thiol pKa enhances the reactivity of protein thiols, which can promote a variety of electrophilic and oxidative posttranslational modifications (PTMs) (Figure 1-1).

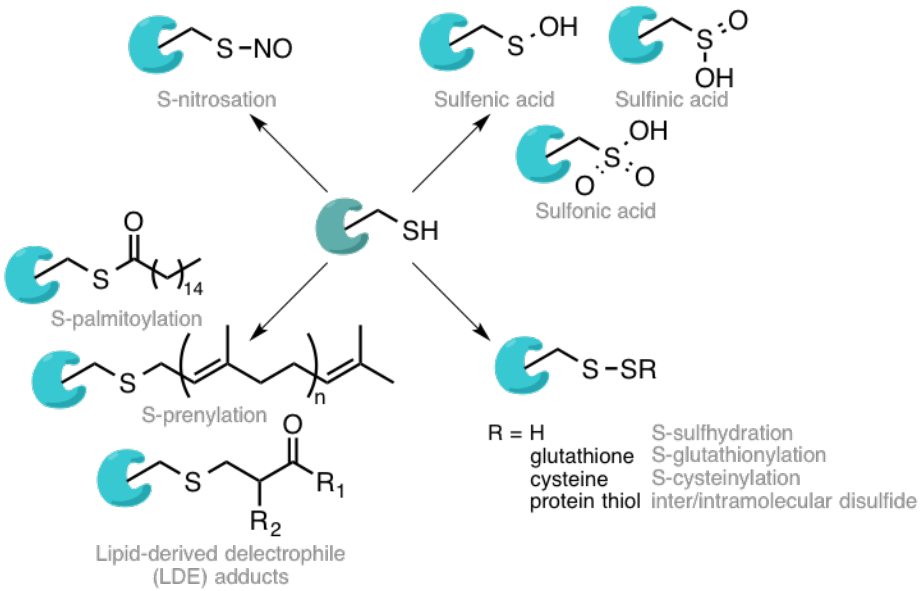

Figure 1-1 Common posttranslational modifications of cysteine residues.

Cysteine PTMs can be categorized as either spontaneous or enzyme-catalyzed modifications. Spontaneous modifications are generally seen as the perturbation of the cysteine thiol with endogenous oxidants and highly reactive electrophiles, such as reactive nitrogen/oxygen species (RNS/ROS) and lipid-derived electrophiles (LDEs). Oxidative modifications result in the formation of sulfenic/sulfinic/sulfonic acids[5], *S*-nitrosothiols[6], intra- and inter-protein disulfides[7], persulfides[8] and mixed disulfides with glutathione and free cysteine[9]. LDEs, such as 4-hydroxy-2-nonenal (HNE), commonly form Michael Addition adducts with nucleophilic cysteines[10]. Enzyme-catalyzed cysteine PTMs include palmitoylation[11] and prenylation[12]. For these PTMs, enzyme-mediated transfer of lipids or isoprenoids from activated donors to cysteine thiols occur. It is of note that some modifications, such as disulfide-bond formation, can be both spontaneous and enzyme catalyzed. In addition to the common eukaryotic cysteine PTMs listed above, many other rare modifications are also observed, such as methylation, ubiquitination and phosphorylation, in eukaryotes and prokaryotes. [13] All PTMs of cysteine have been shown to modulate protein activity and localization. Dysregulation of these PTMs causes a variety of proliferative and degenerative diseases.[14–16]

Methods that enrich, identify and quantify specific cysteine PTMs are of vital importance for the enhancement of our understanding of the scope and physiological roles of these modifications. Chemical-proteomic strategies to investigate these modifications in complex proteomes have been developed over several decades and have enabled detailed evaluation of cysteine PTMs. [17] These methods range from early radioisotope-labeling experiements to more recent advances in chemical-probe design and the use of mass spectrometry (MS). Additionally, the development of bioorthogonal

reactions has allowed for the selective tagging of specific functional groups, permitting the assessment of these PTMs under physiologically relevant conditions. Though a variety of methods to study PTMs are available, further development of new methods is necessary to gain a more complete picture of these modifications' role in regulating proteins activities under healthy conditions and diseased states.

Cysteine Nitrosation

The free thiol group on cysteine can react with RNS to generate *S*-nitrosothiols (SNO). [18,19] This transformation is known as cysteine nitrosation. The term *S*-nitrosylation is also commonly used to refer to this PTM, however this term is chemically erroneous. Nitrosylation refers to the coordination of a nitrosyl group, formally a NO radical, with a transition metal. Conversely, a nitrosation reaction is the transfer of a nitroso group (R-NO), generated by NO synthase (NOS), to a cysteine thiol resulting in *S*-nitrosothiol formation. Thus, *S*-nitrosation is the proper term for the formation of R-NO from NO. [20] *S*-nitrosothiols in cells can be formed through three distinct pathways (Figure 1-2A): (1) reaction of cysteine thiols with nitrogen trioxide (N_2O_3), an autoxidation product of cellular nitric oxide (NO); (2) recombination of NO and thiyl radicals; and (3) transition metal-catalyzed addition of NO to a cysteine thiol. *S*-NO formation is regulated by cellular NO levels, which are in turn regulated by three isoforms of NOS; neuronal NOS (nNOS), endothelial NOS (eNOS), and inducible NOS (iNOS). NO synthases modulate NO levels by catalyzing the oxidation of L-arginine to afford NO and L-citrulline[21]. Protein *S*-nitrosation can also occur by a process called transnitrosation, or the transfer of a NO group from a low-molecular NO donor (e.g. *S*-

nitrosocysteine (CysNO)/*S*-nitrosoglutathione (GSNO)) or other nitrosated proteins (e.g. *S*-nitrosothioredoxin (TrxNO)) to free thiols on other proteins[22].

Over 3000 *S*-nitrosation sites on proteins have been reported,[23] yet pathways that lead to selective *S*-nitrosation still remain unknown. Additionally, no sequence motif or pKa trend has been observed for the identification of sites of *S*-nitrosation.[24,25] Sites of nitrosation that have been identified include active-site cysteines in proteins like caspase-3 (CASP3) and glyceraldehyde-3-phosphate dehydrogenase (GAPDH). Nitrosation of the active site cysteine of CASP3 has been shown to inhibit CASP3 protease activity and regulation of cellular NO levels helps govern the initiation of apoptosis though perturbation of this activity.[26,27] When active site Cys150 of GAPDH is nitrosated an increased binding to ubiquitin ligase Siah1 is observed. This binding facilitates GAPDH translocation into the nucleus.[28,29] The characterization of these proteins and other nitrosation targets was made possible by chemical-proteomic strategies that enrich and identify *S*-nitroso modified proteins from complex proteomes.

The low abundance and reactive nature of endogenous SNO adducts has rendered the direct enrichment and identification of protein *S*-nitrosothiols difficult. Early work toward the study of *S*-nitrosation used UV-visible and chemiluminescence detections, as well as photolysis to homolytically cleave S-NO bonds, followed by the detection of freed NO.[30,31] These methods allow for the quantification of total nitrosothiols in a sample, but do no allow for the direct identification of individual *S*-nitrosated proteins. More recently, several commonly utilized proteomic strategies have been developed that allow for the enrichment, identification and differentiation of *S*-nitrosated protein species in complex systems.

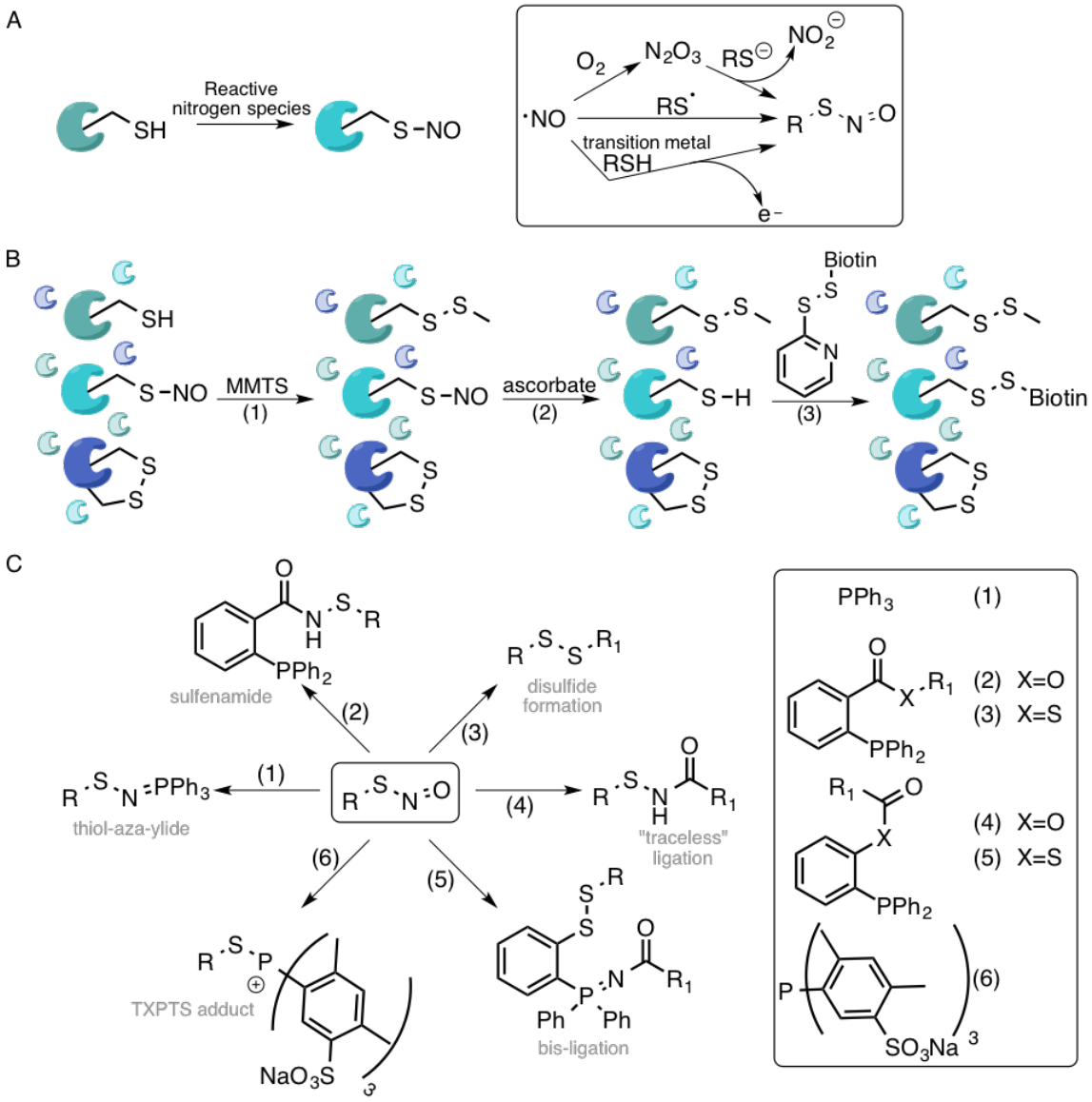

Figure 1-2 Cysteine nitrosation. (A) Nitrosation is the transfer of a nitroso-group onto cysteine residues. Thisi process can occur through three pathways to form *S*-nitrosothiols. (B) The biotin switch technique (BST) uses capping of reduced thiols with MMTS, followed by selective reduction of S-nitrosothiols with ascorbate and subsequent disulfide bond formation to append biotin to formally s-nitrosated cysteines for enrichment and identification. (C) Chemical probes for the detection of S-nitrosothiols.

Biotin-switch technique

One of the most widely utilized methods for protein-SNO detection is the biotin-switch technique (BST). The original BST includes three steps: (1) cap free cysteine thiols with the cysteine alkylating agent methyl methanethiosulfonate (MMTS); (2) selective reduction of S-NOs to free thiols using ascorbate; and, (3) label newly reduced thiols with the biotinylating cysteine-reactive agent N-[6-(biotinamido)hexyl]-3'-(2'-pyridyldithio)propionamide (biotin-HPDP) (Figure 1-2B).[32,33] The resulting biotinylated proteins can be detected by immunoblotting or subjection to avidin enrichment for more detailed MS analysis. The original BST has since been modified for the study of biotinylated peptides instead of proteins (SNOSID)[34] and has been enhanced with the use of resin-assisted capture (SNO-RAC).[35] Recent methods have combined BST with existing quantitative proteomic methods, such as isotope-coded affinity tags (ICAT), stable isotope labeling by amino acids in cell culture (SILAC), and tandem mass tags (TMT). The above mentioned methods incorporate an isotopic label through the metabolic incorporation of heavy amino acids prior to BST or through the labeling of reactive amino-acid residues with isotopically labeled tags after BST. Overall, these modified BST approaches allow for the identification and quantification of endogenous sites of protein nitrosation.

Despite the wide variety of applications of BST, several limitations are of note. BST requires complete capping of free thiols in the first alkylation step of the protocol; incomplete alkylation will result in false positives. Additionally, the lengthy sample preparation protocol increases the potential for SNO decomposition and scrambling of *S*-nitrosation with disulfide formation. *S*-nitrosothiols are known to be highly labile in the

presence of UV-irradiation, a characteristic exploited in early SNO detection methods, leading to the generation of further false positives. The selectivity of ascorbate reduction of nitrosated cysteines relies on a mechanism proposed as an indirect reduction. Ascorbate does not directly donate electrons to the nitrosothiol, but instead undergoes a transnitrosation reaction with the nitrosated cysteine. Under similar conditions, ascorbate was thought to reduce disulfide bonds thus further questioning the false positives generated by BST. However, Stamler *et al.* have shown that ascorbate-mediated reduction is highly specific and that unintentional exposure of samples to sunlight is the cause of false positives. [36] They suggest that samples in which all SNO species are photolyzed prior to the BST protocol can act as an additional control to reduce false positives in BST experiments.

BST has enabled multiple biological studies to shed light on the role cysteine nitrosation plays in cellular function. Recently, a study used BST to study red blood cells (RBCs) and showed that *S*-nitrosation of cytoskeletal proteins is critical in maintenance of RBC structure. [37] Similarly, BST has also been used in the identification of proteins that mediate NO-induced resistance of melanoma cells to anticancer agents such as cisplatin. [38] In this study, several nitrosated proteins were identified, including caspase-3 and prolyl-hydroxylase-2. Both are directly involved in the development of resistance to cisplatin.

Chemical probes for the detection of nitrosothiols

The limitations and potential false positives associated with BST have led to significant efforts made toward the development of chemical probes to selectively detect

nitrosothiols over other cysteine oxoforms. Similar to the Staudinger ligation, [39] that exploits the selective reactivity of phosphines with azides to afford aza-ylides, nitrosothiols can react with triarylphosphines to generate thiol-aza-ylides[40] (Figure 1-2C). This method has been advanced further by the substitution of arylphosphines for phosphine esters, resulting in the rearrangement of aza-ylide intermediates that form sulfonamides (Figure 1-2C). With these SNO ligation methods, the product formed is rather bulky and not suitable for downstream analytical platforms. In an effort to improve these methods, 'traceless' SNO ligation has been pursued. [41] When using phosphine ester or thioester derivatives, *S*-nitrosothiols are modified to form a stable and less sterically encumbered bis-ligation disulfide product. [42,43] Despite these improvements on SNO ligation, this method still suffers from poor water solubility of the phosphine reagents. In recent work, the use of water-soluble tris(4,6dimethyl-3-sulfonatophenyl)phosphine trisodium salt hydrate (TXPTS) was used to modify *S*-nitrosothiols and form the corresponding aza-ylide with high efficiency and stability (Figure 2C). [44] To further improve SNO ligation compatibility with aqueous samples and MS ionization, Tannenbaun and coworkers generated a panel of triphenylphosphine derivatives with sulfonate ester and tertiary amines (Figure 1-2C). [45] These modified probes were used to measure cellular GSNO levels using multiple reaction (MRM)-MS in macrophages and malignant cancer cells. These studies were the first to show successful application of phosphine probes for the detection of nitrosothiols within a complex biological sample, however, only low molecular-weight *S*-nitrosothiols were analyzed. To date, there are no reports of the use of phosphine probes for the detection of protein nitrosothiols in a complex proteome. Nevertheless, the continued effort toward the improvement of water

solubility and chemo-selectivity of novel chemical probes has resulted in successful study of *S*-nitrosation events in complex biological samples.[46] Majmudar et al. have recently developed biotin-conjugate probes that utilize the cross reactivity of *S*-sulfination and *S*-nitrosation to form stable thiosulfonates. These biotinylated thiosulfonates have been used to analyze *S*-nitrosothiols and sulfinic acid formation in cell and mouse tissue homogenates.

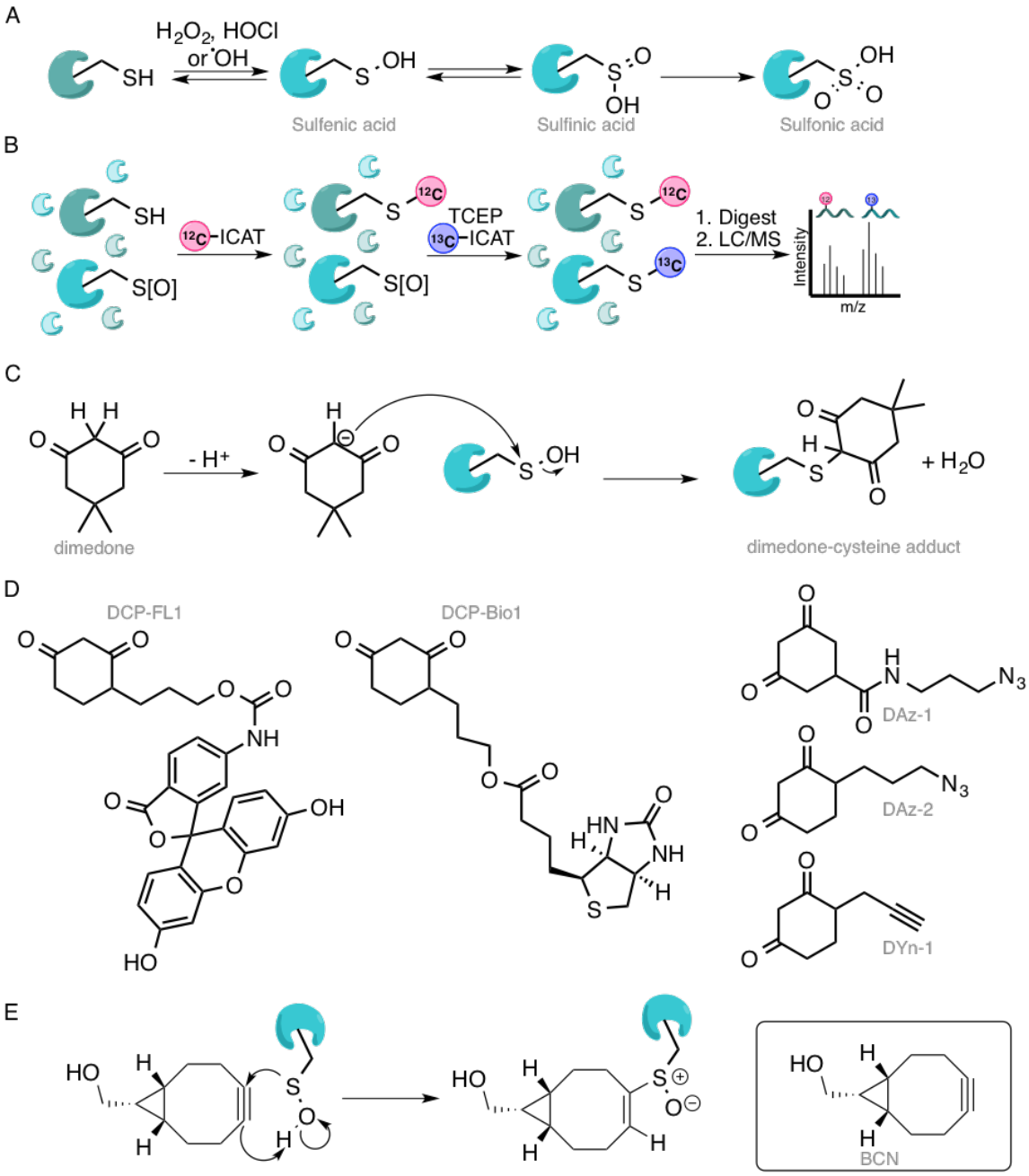

Figure 1-3 Cysteine oxidation. (A) Cysteine can be oxidized to sulfenic, sulfinic and sulfonic acids by reaction with hydrogen peroxide, perchloric acid and hydroxyl radicals. (B) OxICAT is a modified version of ICAT used to study cysteine oxidation. (C) The nucleophilic addition of dimedone to sulfenic acids generates a covalent adduct with cysteine residues. (D) Dimedone-based probes for chemical proteomics. (E) A strained alkyne probe, BCN, reacts with sulfenic acis to generate a sulfenic acid covalent adduct.

Cysteine Oxidation

Cysteine residues are highly sensitive to oxidation, resulting in a variety of cysteine oxoforms[47]. The most common oxoforms are intra- and inter-molecular disulfide-bond formation, known for facilitating protein folding and maintaining structural stability. Cysteine can also take part in disulfide bonds with non-protein thiol sources. Glutathione (L-γ-glutamyl-L-cysteinylglycine) is a non-protein peptide primarily found in the cytosol in both a reduced (GSH) and oxidized form (GSSG). The process by which cysteine residues on proteins form mixed disulfides with glutathione is known as *S*-glutathionylation.[48,49] The extent to which proteins are *S*-glutathionylated is dependent on the relative GSH/GSSG ratio in the cytosol and the process involves an exchange between a protein thiol/disulfide and GSSG/GSH. *S*-glutathionylation can also result from a reaction of reduced glutathione with activated *S*-nitrosated cysteines or sulfenic acids.[50] Glutathionylation is highly reversible and reduction of glutathionylated cysteines can result from thiol/disulfide exchange with free GSH or can be enzymatically catalyzed by glutaredoxins.

Similar to *S*-glutathionylation, *S*-cysteinylation is also the formation of mixed disulfides with protein thiols, and a non-protein peptide cytosolic free cysteine to form the disulfide pair. This PTM is less characterized in eukaryotes but has been shown to play important regulatory roles in prokaryotic systems.[51] Lastly, cysteine sulfhydration is a modification that results from the reaction of protein cysteine thiols with free hydrogen sulfide (H_2S) and this PTM is critical in cell signaling.[8] The resulting persulfide (-S-SH) has similar reactivity to thiol groups, thus making further study and method development to detect this PTM difficult.

In addition to disulfide bonds, other oxoforms include sulfenic, sulfinic and sulfonic acids[5] (Figure 1-3A). Sulfenic acids are a product of the reaction of cysteine thiols with biological oxidants such as hydrogen peroxide, hypochlorous acid and hydroxyl radicals. Additionally, sulfenic acids can form as a product of the hydrolysis of *S*-nitrosothiols.[47] Sulfenic acids can be further oxidized to generate sulfinic and sulfonic acids. Sulfinic acids are stable to most cellular reductants, unlike sulfenic acids, and are reduced only in the presence of a newly discovered ATP-dependent sulfiredoxin enzyme.[52] Sulfonic acids are the most highly oxidized cysteine thiol species and oxidation is considered to be irreversible. The reversible nature of cysteine sulfenic and sulfinic acids has resulted in the evolution of these PTMs as key regulators of protein activity and biological processes.[53] Examples include, the protein-tyrosine phosphatases (PTPs), whereby sulfenylation of the active-site cysteine nucleophile results in inactivation of these enzymes.[54] Additionally, cysteine proteases such as deubiquitinating enzymes (DUBs) that cleave ubiquitin from target proteins are known to possess active sites cysteine sensitive toward cysteine sulfenylation.[55,56]

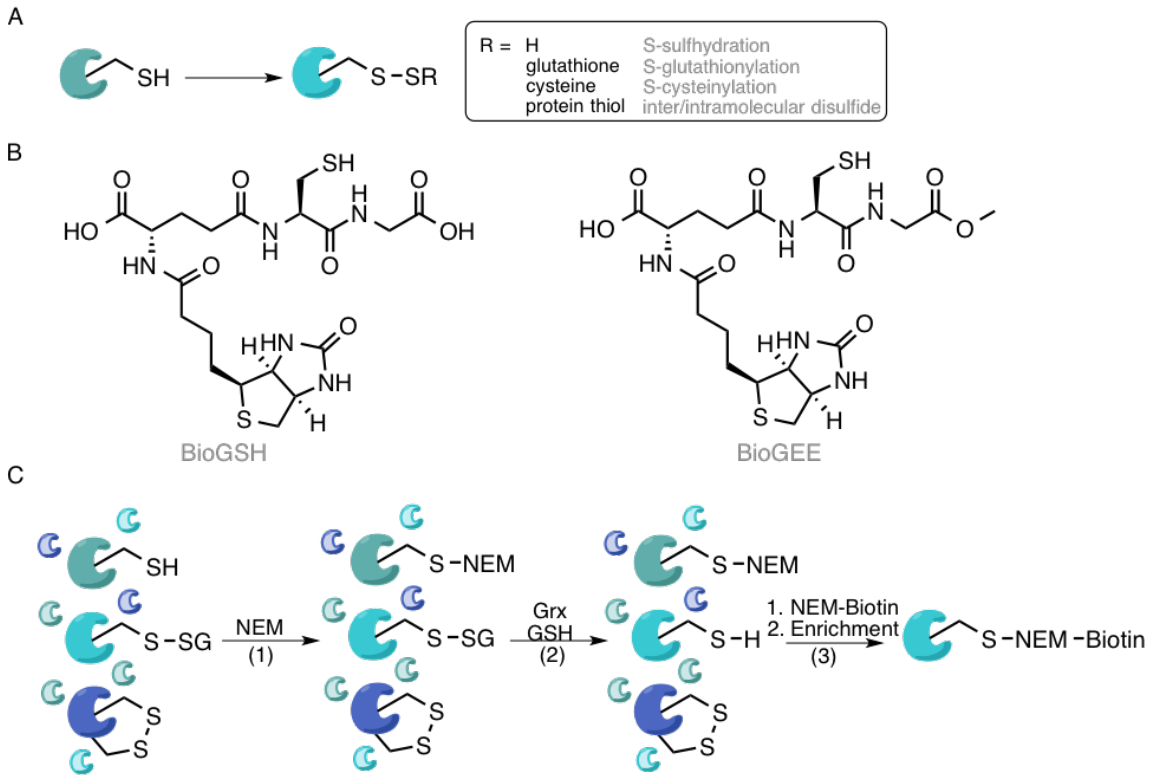

Figure 1-4 Cysteine glutathionylation and disulfide formation. (A) can form mixed disulfides with a variety of sulfur/thiol containing proteins, peptides and small molecules in cells. (B) Biotinylated proteins can be identified by capping reduced cysteines with NEM followed by glutaredoxin (Grx)-mediated reduction of glutathionylated cysteines. The newly formed thiols are subsequently capped with NEM-biotin for later enrichment of glutathionylated proteins.

Study of glutathionylation using modified glutathione derivatives

Early methods to study glutathionylation relied on the use of radiolabeled GSH both *in vitro*, by the treatment of cell lysates with ^{3}H or ^{35}S-labeled GSH, and *in situ*, by metabolic labeling of ^{35}S-cysteine. [57,58] Incorporation of radiolabeling *in situ* was facilitated by endogenous glutathione-synthesis machinery, γ-glutamylcysteine synthetase and glutathione synthetase. Additionally, cellular studies require the use of cycloheximide to inhibit cellular protein synthesis, to ensure that the radiolabeled cysteine will only be incorporated into proteins through *S*-glutathionylation. The *S*-

glutathionylated proteins can be separated by SDS-PAGE and imaged by autoradiography. ^{35}S-GSH radiolabeling gave rise to many early discoveries including the identification of glyceraldehyde-3-phosphate dehydrogenase (GAPDH) as a target of S-glutathionylation.[59] Though a highly useful early method of detection, the radiolabeling method has many limitations, including specialized training for working with radiolabelled samples and the potential of false positives resulting from other forms of *S*-thiolation such as cysteinylation.

To overcome many of the limitations found with the use of radiolabeled glutathione, biotinylated glutathione derivatives were developed. Biotinylated glutathione is easily generated *in vitro* using water-soluble biotinylation reagent, sulfosuccinimidyl-6-(biotinamido)-hexanoate (sulfo-NHS-biotin). This reagent couples biotin to the free primary amine group of GSH/GSSG in amine free buffer to generate BioGSH/BioGSSG (Figure 1-4B) [60]. A cell-permeable GSH source can be synthesized under similar conditions by substituting glutathione ethyl ester for GSH, resulting in biotin-labeled glutathione ethyl ester or BioGEE[61]. Once glutathionylated, the now biotinylated proteins can be enriched by exposing samples to streptavidin beads. The bound proteins can be eluted by treatment with reducing agents to cleave the mix disulfide between the protein target and the biotinylated-GSH. This method has been used *in vitro* and in whole cells to identify S-glutathionylated proteins. One example used BioGEE to identify proteins that undergo S-glutathionylation following treatment of cells with carbon monoxide (CO).[62] CO generated low levels of ROS through inhibition of cytochrome c oxidase, indirectly perturbing the GSH/GSSG ratio in cells and increasing protein glutathionylation. This study identified p65 as a target of glutathionylation and found that this PTM blocks NF-

κB-p65 nuclear translocation. Though the use of biotinylated glutathione is an improvement to previous radiolabelled glutathione techniques, a significant drawback to this method is the presence of the bulky biotin group that may artificially perturb the subset of protein targets with this PTM. This method is also limited by the necessary addition of exogenous glutathione, which does not allow for the identification of native glutathionylation targets.

To overcome the limitations present in radiolabelled and biotinylated glutathione methods, a recent technique optimized the synthesis of glutathione containing an azide bioorthogonal handle in living cells.[63] A mutant of glutathione synthetase (GS) was generated to accommodate azido-Ala and promote its coupling to γ-Glu-Cys to generate azido-GSH. Cells transfected with mutant GS are capable of *in situ* azido-GSH generation, which is used by the cells to label glutathionylated proteins. Azido-GSH-modified proteins are later identified using click chemistry. This elegant method was utilized in cells to monitor the increase in S-glutathionylation in the presence of hydrogen peroxide.[63]

Isotope-coded affinity tags (ICAT) for the study of cysteine oxoforms

The use of isotope-coded affinity tags (ICAT) has allowed for the expansion of a shotgun proteomic strategy that can isotopically label and compare proteins across two different samples.[64] Cysteines labeled with ICAT reagents are enriched on streptavidin beads and analyzed by quantitative MS. The tagged cysteine containing peptides can be identified and the relative abundance between light- and heavy-tagged samples can be quantified. The first use of ICAT for the study of redox proteomics involved the use of

light and heavy ICAT reagents to compare reduced thiol content across two samples. [65,66] In the case of cysteine oxidation, this method takes advantage of differential labeling of oxidized over reduced cysteines. Cysteines that are not oxidized will remain reactive toward biotinylated-iodoacetamide (IA) derivatives, which possess either isotopically light or heavy linkers, for later differentiation between two different samples. In this case, ICAT reagents are used to compare a control proteome to one that is treated with hydrogen peroxide, enabling the identification of cysteines sensitive to oxidation. Later iterations utilized ICAT to differentially label oxidized versus reduced cysteine residues within a single sample. [67] This method, termed OxICAT (Fig. 1-3B), allows for the quantification of the oxidized: reduced cysteine ratio, which can then be compared across numerous biological samples. Furthermore, to control for changes in protein levels, ICAT methods have been coupled with stable isotope dimethyl labeling to quantify protein abundance prior to cysteine enrichment. [68,69] These MS methods allow for increased accuracy in quantification, and global identification of all oxidized cysteines in a single experiment. One major drawback, however, is that the method relies on the cysteine of interest existing on tryptic peptides that can be identified by MS. Cysteines that are located within very short or long tryptic peptides will not be detected by this method. Additionally, this method requires complete tagging of reduced cysteines in the samples to eliminate false positives.

Chemical probes for sulfenic acids

The OxICAT method cannot differentiate between sulfenic acids, sulfinic acids and cysteine disulfides. For this reason, alternative methods have been pursued to discern and

annotate cysteines based on their susceptibility toward specific oxidation states. Sulfenic acids are highly reversible in nature and have been found to act as a mode of regulation of protein activity. To better identify sulfenic acids in complex systems, chemical probes have been developed to specifically react with and tag sulfenic acid moieties. These probes include 5,5-dimethyl-1,3-cyclohexanedione, commonly known as dimedone (Figure. 1-3C). Dimedone selectively reacts with electrophilic sulfenic acids through a nucleophilic addition of the enolate intermediate generated from the 1,3-dicyclohexadione moiety. Dimedone has been further modified to possess fluorophores and biotin (e.g. DCP-Fl1 and DCP-Bio1 (Figure 1-3D)) to allow for visualization and avidin-enrichment for gel-based and MS analysis, respectively.[70–73]

Though more amenable to protein detection than dimedone, biotin and fluorophore-tagged analogs possess bulky reporter tags that are unable to target buried sulfenic acids within proteins and these dimedone derivatives also demonstrate poor cell-permeability for *in vivo* applications. The high lability of sulfenic acids requires the use of methods that trap these modifications *in vivo* with minimal disruptions to endogenous redox environments. To overcome issues of cell-permeability, less sterically encumbered bioorthogonal handles were used. Azide-tagged probes (DAz-1 and DAz-2) [74,75] as well as an alkyne-tagged probe (DYn-1) [76] have been developed for more efficient in-cell sulfenic acid labeling. After initial modification of sulfenic acid moieties, these probes undergo conjugation with reporter tags using modified Staudinger reaction or copper-catalyzed azide-alkyne cycloaddition (CuAAC) chemistry for later analysis.

An additional limitation of the dimedone chemotype for sulfenic acid modification is the low reaction rate, which requires the use of high millimolar

concentrations of probe for efficient protein labeling. In recent efforts to overcome high probe loading, strained cycloalkynes, such as 9-hydroxymethylbicyclo[6.1.0]nonyne (BCN) (Figure 1-3E), have been developed.[77] Strained cycloalkynes selectively modify sulfenic acids with reaction rates over two orders of magnitude greater than those of dimedone. These probes can be used to study cell lysates and in live-cell labeling experiments at micromolar concentrations.

Despite the limitations that arise when using dimedone-based probes for the study of sulfenic acids, these molecules have been used to identify many protein sulfenic acids in a variety of biological systems. For example, biotin-functionalized dimedone has been used to characterize the site of oxidation of the protein kinase, Akt2.[78] Oxidation of Cys124 has been shown to inhibit Akt2 activity, thus presenting a mechanism by which Akt2 is modified concurrently by phosphorylation and cysteine oxidation. Biotin-functionalized dimedone has also been applied to investigate cysteine sulfenylation present in T-cell activation.[48] These studies show that sulfenic acid formation is an essential step in immune-cell signaling and function. Lastly, Dyn-2 (Figure 1-3D), the alkyne-functionalized dimedone, enabled the global assessment of protein sulfenylation upon epidermal growth factor receptor (EGFR)-mediated signaling.[76] Sulfenylation of EGFR itself, at Cys797, was shown to increase kinase activity. These examples showcase the diverse functions of sulfenic acids in essential cellular signaling pathways.

Cysteine adducts with lipid-derived electrophiles

Lipid-derived electrophiles (LDEs) are products of cellular metabolism, cellular lipid nitrosation and peroxidation.[79] Formation of LDEs can occur spontaneously or

under enzymatic control. Reactive oxygen species (ROS) and reactive nitrogen species (RNS) can trigger the non-enzymatic peroxidation of unsaturated fatty acids to afford α-β unsaturated aldehydes and nitroalkenes. [80,81] Examples include: 4-hydroxy-2-nonenal (HNE) [82] and 2-trans-hexadecenal (2-HD) (Figure 1-5). Enzymatic LDE formation is typically the result of oxidation of prostaglandins, such as 15-deoxyΔ12,13-prostaglandin J2 (15d-PGJ2). The oxidation occurs in response to stimuli such as inflammation caused by cyclooxygenases (COX), lipooxygenases (LOX), cytochrome P450s and $NAD^+/NADP^+$ -dependent dehydrogenases. [83,84] All LDEs share common characteristics of being electron poor and able to react with nucleophilic cysteines via a Michael addition reaction. The LDE adducts generated are reversible and can regenerate the unmodified cysteine depending on cellular conditions.

LDE-modifications of proteins are known to regulate critical cellular functions. For example, Kelch-like ECH-Associate Protein 1 (Keap1) is a cysteine rich protein containing five functional domains. Keap1 acts as a cytoplasmic inhibitor of Nuclear Factor (Erythroid-derived-2)-like-2 (Nrf2) to prevent its translocation into the nucleus, where it binds to the antioxidant response elements (ARE) to activate ARE-dependent genes. Exposure of Keap1 to 15d-PGJ2 results in dissociation and nuclear translocation of Nrf2, thus regulating ARE-dependent genes for cytoprotection. [85] Heat shock proteins (HSPs) are another well-characterized target of LDE adduct formation. HSPs are molecular chaperones that are involved in protein trafficking and degradation. In rats subject to high fact/high-ethanol diet, both Hsp72 and Hsp90 have been shown to form HNE adducts with Cys267 and Cys572, respectively. [86,87] In both cases, HNE

modification inhibits the chaperone activity of the HSP and results in impaired cellular stress response.

To improve our understanding of the endogenous targets of LDE-modification, many proteomic methods have been developed to visualize, enrich and identify LDE-modified proteins. Characterization of endogenous sites of LDE modification is limited by the low abundance of LDE adducts, the reversible nature of the Michael addition and potential side reactions of the carbonyl group found in the LDE adduct. Initial studies utilized monoclonal and polyclonal antibodies generated for LDE-amino acid adducts. These antibodies aided in the visualization and enrichment of LDE-modified proteins.[88–90] More recently, methods to selectively modulate and enrich LDE-modified proteins have been developed.

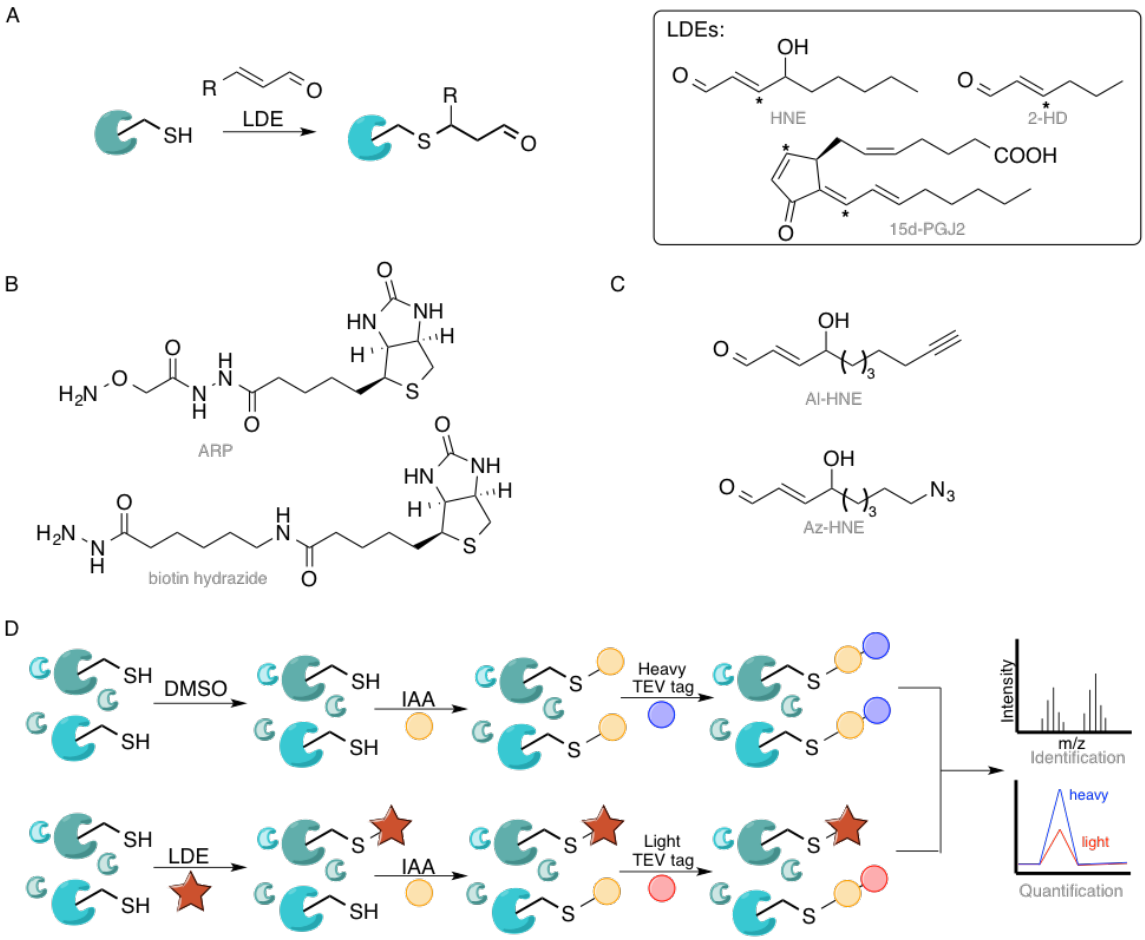

Figure 1-5 Cysteine adducts with lipid-derived electrophiles (LDEs). (A) LDEs contain an α-β unsaturated carbonyl that can react with cysteine residues via a Michael addition. Examples of common LDEs include: HNE, 2-HD and 15d-PGJ2; * denotes carbon of nucleophilic attack. (B) Chemical derivatization of the carbonyl group that results from LDE-protein modification. (C) Azide and alkyne-derivatized HNE allow for labeling of LDE-modified proteins in living cells. (D) A competitive labeling platform allows for quantification of the extent of LDE formation by labeling free reactive cysteines with an iodoacetamide-alkyne (IAA) probe. LDE labeling is identified as a loss in cysteine reactivity, which is quantified through incorporation of isotopic labels during MS analysis.

Chemical derivatization of LDEs

The carbonyl group formed upon LDE modification of cysteines can serve as a selective chemical-derivatization handle for the enrichment of LDE targets.[91] This carbonyl moiety can be subject to trapping with hydrazines and hydrazides to form

hydrazones that can be later reduced to a more stable adduct. Initial chemical-derivatization platforms for LDE-modified proteins used dinitrophenylhydrazine (DNPH) in a method known as "Oxyblot". For this method, lysates are treated with DNPH and then are later analyzed by Western blot using an anti-DNPH antibody. [92,93] A similar reagent, known as Girard's P reagent, has also been used to tag carbonylated proteins. [94] Additionally, the development of fluorescently labeled hydrazides has resulted in facile visualization of protein carbonylation. [95] The incorporation of an enrichment handle, such as an alkyne or azide, would greatly facilitate proteomic analysis. Therefore, biotinylated aldehyde-capture reagents, such as N'-aminooxymethylcarbonylhydrazino D-biotin (aldehyde-reactive probe, ARP) and biotin hydrazide have been developed (Figure 1-5B). [96,97] Biotinylation of LDE modified proteins in cell lysates is achieved by treatment with either hydrazide probes or hydroxylamine-based ARP. Treatment with the hydrazide probe requires sodium addition of exogenous HNE. [98] Lastly, a comparative analysis of four hydrazine-based aldehyde-reactive probes (DNPH, biotin hydrazide (BH), ARP and a long-chain biotin hydrazide (LCBH)) showed that ARP and DNPH perform better than BH and LCBH, on a limited set of model peptides. [90] This study confirmed that carbonyl modification of HNE-adducted peptides serves to prevent neutral loss of the HNE group during collision-induced dissociate (CID) fragmentation, thus facilitating identification of the exact site of HNE modification.

Additional derivations of the biotin-hydrazide tagging approach have been developed, such as the solid-phase hydride (SPH) reagent for enrichment and subsequent release of LDE-modified peptides using acid treatment. [99] This method enables identification of the exact site of modification by eliminating the biotin group prior to MS

analysis. This reagent has also been used to quantify SPH enriched peptides across multiple samples by use of ^{18}O incorporation, [100] stable isotope dimethyl labeling of peptide amine groups, [101] and d0/d4-succinic anhydride labeling. [102] These carbonyl derivatization methods have enhanced our knowledge of protein LDE modification during the last decade. However, limitations to these methods result from the promiscuity of the hydrazide reagents. These reagents are known to also react with aldehydes, ketones and sulfenic acids on biomolecules, [103] resulting in potential false-positive protein-LDE adduct identification.

Bioorthogonal reporters of LDE adducts

Biotinylated LDE analogs, such as 15d-PGJ2, have been used to identify potential LDE-adducts in biological systems. [104,105] However, like many bulky reporter analogs, there is the potential for disruption of LDE-binding due to the presence of the large biotin group. Less intrusive functionalities have been pursued to facilitate accurate detection of LDE adducts. Similar to the alkyne and azide-tagged isoprene and palmitoyl derivative discussed previously, methods for identification of LDE adducts have also exploited bioorthogonal-tagging methods. Both azido HNE (Az-HNE) and alkynyl HNE (Al-HNE) (Figure 1-5C) have been synthesized and used to label proteins in intact RKO cells. [106] Az-HNE and Al-HNE modified proteins were conjugated to biotin reporter group using either Staudinger ligation or CuAAC. Subsequent MS analysis of the HNE-derivative treated RKO cells identified HNE-adduction of numerous stress-related proteins, such as HSPs at Az-HNE and Al-HNE concentrations as low as 5μM. [106] The Al-HNE tag was also used to identify HNE-modified proteins in healthy human plasma. [107] After treatment

with Al-HNE, CuAAC was used to incorporate a photocleavable biotin linker for enrichment and ultimate release of HNE-adducted peptides for subsequent MS analysis. The photocleavable linker minimizes the elution of non-specifically bound peptides to the streptavidin beads. This strategy was used to identify 18 sites of HNE modification in human plasma, including human serum albumin and apolipoprotein A1. The HNE-analogs containing a bioorthogonal reporter group help overcome the non-specificity of the carbonyl-derivatization methods described above. However, these methods require addition of exogenous HNE derivatives to cells or lysates and they do not provide a means of identification and quantification of endogenous HNE-modified sites.

Competitive labeling strategies

In order to quantify the extent of HNE adduction in a complex proteome, a competitive chemical proteomic strategy has been developed (Figure 1-5D). [108] This method relies on the use of iodoacetamide alkyne (IAA) probe to label reactive cysteines, coupled with a quantitative MS platform termed isotopic Tandem Orthogonal Proteolysis–Activity-Based Protein Profiling (isoTOP-ABPP), for quantification of cysteine labeling. [109] Typically, cell lysate is treated with a LDE, followed by the IAA probe to cap all non-LDE modified reactive cysteines. The IAA-tagged proteins are conjugated to isotopically labeled cleavable linkers (TEV-light and TEV-heavy) for enrichment and selective release as well as MS-based identification/ quantification of IAA-modified peptides. Direct comparison of an LDE-treated (TEV-light) sample to an untreated (TEV-heavy) sample allows for quantification of the extent of LDE-modification of reactive cysteines within a proteome. Using this method, MDA-

MD-231 human breast cancer cells were treated with three LDEs (HNE, 15d-PGJ2, or 2-HD) and 750-1000 cysteines were quantified in terms of their sensitivity toward each LDE modification. Several LDE-sensitive cysteines were identified, including a conserved cysteine adjacent to the active site of ZAK kinase.[108] HNE modification of these cysteines inhibits enzyme function and suppresses activation of JNK signaling pathways during oxidative stress. This competitive isoTOP-ABPP platforms provides indirect measurement of LDE-modified cysteines and has the potential for false positives generated by other cysteine modifications that modulate cysteine reactivity, such as oxidation and nitrosation. Additionally, the observed changes in reactivity toward IAA could be a reflection of inconsistent protein concentrations across two biological samples. Despite these limitations, one important benefit to this platform is the ability to quantify the sensitivity of cysteine toward a particular LDE, which is not possible with the previous methods. This method can also be applied to the assessment of other cysteine PTMs described above and has served as the basis for identifying cysteine PTMs in a variety of biological systems as described in this thesis.

Summary

Cysteine PTMs have been shown to be highly dynamic and therefore are responsible for spatial and temporal regulation of a variety of proteins. The dynamic nature of many of these modifications provides a great challenge in the study of these proteins within endogenous cellular environments. During the past decade, significant advancements in the development of analytical platforms for the global assessment of these cysteine PTMs have provided insight into their functional roles in complex systems.

[110] These methods are diverse and exploit the unique chemical reactivity of these modified adducts as handles to selectively enrich PTM-modified cysteines. In parallel, the advances with MS instrumentation and quantification accuracy have further benefitted this field by facilitating the identification of sites of cysteine modification and quantification of the abundance of these PTMs. As these analytical platforms continue to improve and our understanding of the reactivity of cysteine PTMs expand, the methods described above are likely to improve in both selectivity and sensitivity. Until then, the many diverse techniques available for each cysteine PTM allow for the use of multiple orthogonal methods to demonstrate and confirm the presence of a particular modification on a protein of interest.

References

(1) Pace, N.; Weerapana, E. Diverse Functional Roles of Reactive Cysteines. *ACS chemical biology* **2013**, *8*, 283-296.
(2) Cannan, R. K.; Knight, B. C. Dissociation Constants of Cystine, Cysteine, Thioglycollic Acid and Alpha-Thiolactic Acid. *Biochem. J.* **1927**, *21*, 1384–90.
(3) Gan, Z. R.; Wells, W. W. Identification and Reactivity of the Catalytic Site of Pig Liver Thioltransferase. *J. Biol. Chem.* **1987**, *262*, 6704–7.
(4) Yang, Y. F.; Wells, W. W. Identification and Characterization of the Functional Amino Acids at the Active Center of Pig Liver Thioltransferase by Site-Directed Mutagenesis. *J. Biol. Chem.* **1991**, *266*, 12759–65.
(5) Lo Conte, M.; Carroll, K. S. The Redox Biochemistry of Protein Sulfenylation and Sulfinylation. *J. Biol. Chem.* **2013**, *288*, 26480–8.
(6) Gould, N.; Doulias, P.-T. T.; Tenopoulou, M.; Raju, K.; Ischiropoulos, H. Regulation of Protein Function and Signaling by Reversible Cysteine S-Nitrosylation. *J. Biol. Chem.* **2013**, *288*, 26473–9.
(7) Azimi, I.; Wong, J. W.; Hogg, P. J. Control of Mature Protein Function by Allosteric Disulfide Bonds. *Antioxid. Redox Signal.* **2011**, *14*, 113–26.
(8) Kabil, O.; Motl, N.; Banerjee, R. H2S and Its Role in Redox Signaling. *Biochim. Biophys. Acta* **2014**, *1844*, 1355–66.
(9) Grek, C. L.; Zhang, J.; Manevich, Y.; Townsend, D. M.; Tew, K. D. Causes and Consequences of Cysteine S-Glutathionylation. *J. Biol. Chem.* **2013**, *288*, 26497–504.
(10) Guéraud, F.; Atalay, M.; Bresgen, N.; Cipak, A.; Eckl, P. M.; Huc, L.; Jouanin, I.;

Siems, W.; Uchida, K. Chemistry and Biochemistry of Lipid Peroxidation Products. *Free Radic. Res.* **2010**, *44*, 1098–124.
(11) Tom, C.; Martin, B. R. Fat Chance! Getting a Grip on a Slippery Modification. *ACS chemical biology* **2012**, *8*, 46–57.
(12) Zhang, F. L.; Casey, P. J. Protein Prenylation: Molecular Mechanisms and Functional Consequences. *Annu. Rev. Biochem.* **1996**, *65*, 241–69.
(13) Shannon, D. A.; Weerapana, E. Orphan PTMs: Rare, yet Functionally Important Modifications of Cysteine. *Biopolymers* **2014**, *101*, 156–64.
(14) Garcia-Garcia, A.; Zavala-Flores, L.; Rodriguez-Rocha, H.; Franco, R. Thiol-Redox Signaling, Dopaminergic Cell Death, and Parkinson's Disease. *Antioxid. Redox Signal.* **2012**, *17*, 1764–84.
(15) Go, Y.-M. M.; Jones, D. P. Cysteine/cystine Redox Signaling in Cardiovascular Disease. *Free Radic. Biol. Med.* **2011**, *50*, 495–509.
(16) Resh, M. D. Targeting Protein Lipidation in Disease. *Trends Mol Med* **2012**, *18*, 206–14.
(17) Murray, C. I.; Van Eyk, J. E. Chasing Cysteine Oxidative Modifications: Proteomic Tools for Characterizing Cysteine Redox Status. *Circ Cardiovasc Genet* **2012**, *5*, 591.
(18) Smith, BC; Marletta, MA Mechanisms of S-Nitrosothiol Formation and Selectivity in Nitric Oxide Signaling. *Current opinion in chemical biology* **2012**, *16*, 498-506.
(19) Hess, D. T.; Matsumoto, A.; Kim, S.-O. O.; Marshall, H. E.; Stamler, J. S. Protein S-Nitrosylation: Purview and Parameters. *Nat. Rev. Mol. Cell Biol.* **2005**, *6*, 150–66.
(20) Smith, B. C.; Marletta, M. A. Mechanisms of S-Nitrosothiol Formation and Selectivity in Nitric Oxide Signaling. *Curr Opin Chem Biol* **2012**, *16*, 498–506.
(21) Marletta, M. A.; Hurshman, A. R.; Rusche, K. M. Catalysis by Nitric Oxide Synthase. *Curr Opin Chem Biol* **1998**, *2*, 656–63.
(22) Wu, C.; Liu, T.; Chen, W.; Oka, S.; Fu, C.; Jain, M. R.; Parrott, A. M.; Baykal, A. T.; Sadoshima, J.; Li, H. Redox Regulatory Mechanism of Transnitrosylation by Thioredoxin. *Mol. Cell Proteomics* **2010**, *9*, 2262–75.
(23) Lee, T.-Y. Y.; Chen, Y.-J. J.; Lu, C.-T. T.; Ching, W.-C. C.; Teng, Y.-C. C.; Huang, H.-D. D.; Chen, Y.-J. J. dbSNO: A Database of Cysteine S-Nitrosylation. *Bioinformatics* **2012**, *28*, 2293–5.
(24) Marino, S. M.; Gladyshev, V. N. Structural Analysis of Cysteine S-Nitrosylation: A Modified Acid-Based Motif and the Emerging Role of Trans-Nitrosylation. *J. Mol. Biol.* **2010**, *395*, 844–59.
(25) Doulias, P.-T. T.; Greene, J. L.; Greco, T. M.; Tenopoulou, M.; Seeholzer, S. H.; Dunbrack, R. L.; Ischiropoulos, H. Structural Profiling of Endogenous S-Nitrosocysteine Residues Reveals Unique Features That Accommodate Diverse Mechanisms for Protein S-Nitrosylation. *Proc. Natl. Acad. Sci. U.S.A.* **2010**, *107*, 16958–63.
(26) Benhar, M.; Forrester, M. T.; Hess, D. T.; Stamler, J. S. Regulated Protein Denitrosylation by Cytosolic and Mitochondrial Thioredoxins. *Science* **2008**, *320*, 1050–4.
(27) Mitchell, D. A.; Morton, S. U.; Fernhoff, N. B.; Marletta, M. A. Thioredoxin Is Required for S-Nitrosation of Procaspase-3 and the Inhibition of Apoptosis in Jurkat Cells. *Proc. Natl. Acad. Sci. U.S.A.* **2007**, *104*, 11609–14.

(28) Kornberg, M. D.; Sen, N.; Hara, M. R.; Juluri, K. R.; Nguyen, J. V.; Snowman, A. M.; Law, L.; Hester, L. D.; Snyder, S. H. GAPDH Mediates Nitrosylation of Nuclear Proteins. *Nat. Cell Biol.* **2010**, *12*, 1094–100.
(29) Hara, M. R.; Agrawal, N.; Kim, S. F.; Cascio, M. B.; Fujimuro, M.; Ozeki, Y.; Takahashi, M.; Cheah, J. H.; Tankou, S. K.; Hester, L. D.; et al. S-Nitrosylated GAPDH Initiates Apoptotic Cell Death by Nuclear Translocation Following Siah1 Binding. *Nat. Cell Biol.* **2005**, *7*, 665–74.
(30) Diers, A. R.; Keszler, A.; Hogg, N. Detection of S-Nitrosothiols. *Biochim. Biophys. Acta* **2014**, *1840*, 892–900.
(31) Samouilov, A.; Zweier, J. L. Development of Chemiluminescence-Based Methods for Specific Quantitation of Nitrosylated Thiols. *Anal. Biochem.* **1998**, *258*, 322–30.
(32) Jaffrey, S. R.; Erdjument-Bromage, H.; Ferris, C. D.; Tempst, P.; Snyder, S. H. Protein S-Nitrosylation: A Physiological Signal for Neuronal Nitric Oxide. *Nat. Cell Biol.* **2001**, *3*, 193–7.
(33) Jaffrey, S. R.; Snyder, S. H. The Biotin Switch Method for the Detection of S-Nitrosylated Proteins. *Sci. STKE* **2001**, *2001*, pl1.
(34) Hao, G.; Derakhshan, B.; Shi, L.; Campagne, F.; Gross, S. S. SNOSID, a Proteomic Method for Identification of Cysteine S-Nitrosylation Sites in Complex Protein Mixtures. *Proc. Natl. Acad. Sci. U.S.A.* **2006**, *103*, 1012–7.
(35) Forrester, M. T.; Thompson, J. W.; Foster, M. W.; Nogueira, L.; Moseley, M. A.; Stamler, J. S. Proteomic Analysis of S-Nitrosylation and Denitrosylation by Resin-Assisted Capture. *Nat. Biotechnol.* **2009**, *27*, 557–9.
(36) Forrester, M. T.; Foster, M. W.; Stamler, J. S. Assessment and Application of the Biotin Switch Technique for Examining Protein S-Nitrosylation under Conditions of Pharmacologically Induced Oxidative Stress. *J. Biol. Chem.* **2007**, *282*, 13977–83.
(37) Grau, M.; Pauly, S.; Ali, J.; Walpurgis, K.; Thevis, M.; Bloch, W.; Suhr, F. RBC-NOS-Dependent S-Nitrosylation of Cytoskeletal Proteins Improves RBC Deformability. *PLoS ONE* **2013**, *8*, e56759.
(38) Godoy, L. C.; Anderson, C. T.; Chowdhury, R.; Trudel, L. J.; Wogan, G. N. Endogenously Produced Nitric Oxide Mitigates Sensitivity of Melanoma Cells to Cisplatin. *Proc. Natl. Acad. Sci. U.S.A.* **2012**, *109*, 20373–8.
(39) Saxon, E.; Bertozzi, C. R. Cell Surface Engineering by a Modified Staudinger Reaction. *Science* **2000**, *287*, 2007–10.
(40) Wang, H.; Xian, M. Fast Reductive Ligation of S-Nitrosothiols. *Angew. Chem. Int. Ed. Engl.* **2008**, *47*, 6598–601.
(41) Zhang, J.; Wang, H.; Xian, M. Exploration of the "Traceless" Reductive Ligation of S-Nitrosothiols. *Org. Lett.* **2009**, *11*, 477–80.
(42) Zhang, J.; Wang, H.; Xian, M. An Unexpected Bis-Ligation of S-Nitrosothiols. *J. Am. Chem. Soc.* **2009**, *131*, 3854–5.
(43) Zhang, J.; Li, S.; Zhang, D.; Wang, H.; Whorton, A. R.; Xian, M. Reductive Ligation Mediated One-Step Disulfide Formation of S-Nitrosothiols. *Org. Lett.* **2010**, *12*, 4208–11.
(44) Bechtold, E.; Reisz, J. A.; Klomsiri, C.; Tsang, A. W.; Wright, M. W.; Poole, L. B.; Furdui, C. M.; King, S. B. Water-Soluble Triarylphosphines as Biomarkers for Protein S-Nitrosation. *ACS Chem. Biol.* **2010**, *5*, 405–14.

(45) Seneviratne, U.; Godoy, L. C.; Wishnok, J. S.; Wogan, G. N.; Tannenbaum, S. R. Mechanism-Based Triarylphosphine-Ester Probes for Capture of Endogenous RSNOs. *J. Am. Chem. Soc.* **2013**, *135*, 7693–704.
(46) Majmudar, J. D.; Konopko, A. M.; Labby, K. J.; Tom, C. T.; Crellin, J. E.; Prakash, A.; Martin, B. R. Harnessing Redox Cross-Reactivity To Profile Distinct Cysteine Modifications. *J. Am. Chem. Soc.* **2016**, *138*, 1852–9.
(47) Reddie, K. G.; Carroll, K. S. Expanding the Functional Diversity of Proteins through Cysteine Oxidation. *Curr Opin Chem Biol* **2008**, *12*, 746–54.
(48) Michalek, R. D.; Nelson, K. J.; Holbrook, B. C.; Yi, J. S.; Stridiron, D.; Daniel, L. W.; Fetrow, J. S.; King, S. B.; Poole, L. B.; Grayson, J. M. The Requirement of Reversible Cysteine Sulfenic Acid Formation for T Cell Activation and Function. *J. Immunol.* **2007**, *179*, 6456–67.
(49) Pastore, A.; Piemonte, F. S-Glutathionylation Signaling in Cell Biology: Progress and Prospects. *Eur J Pharm Sci* **2012**, *46*, 279–92.
(50) Giustarini, D.; Milzani, A.; Aldini, G.; Carini, M.; Rossi, R.; Dalle-Donne, I. S-Nitrosation versus S-Glutathionylation of Protein Sulfhydryl Groups by S-Nitrosoglutathione. *Antioxid. Redox Signal.* **2005**, *7*, 930–9.
(51) Hochgräfe, F.; Mostertz, J.; Albrecht, D.; Hecker, M. Fluorescence Thiol Modification Assay: Oxidatively Modified Proteins in Bacillus Subtilis. *Mol. Microbiol.* **2005**, *58*, 409–25.
(52) Biteau, B.; Labarre, J.; Toledano, M. B. ATP-Dependent Reduction of Cysteine-Sulphinic Acid by S. Cerevisiae Sulphiredoxin. *Nature* **2003**, *425*, 980–4.
(53) Poole, L. B.; Nelson, K. J. Discovering Mechanisms of Signaling-Mediated Cysteine Oxidation. *Curr Opin Chem Biol* **2008**, *12*, 18–24.
(54) Salmeen, A; Andersen, JN; Myers, MP; Meng, TC Redox Regulation of Protein Tyrosine Phosphatase 1B Involves a Sulphenyl-Amide Intermediate. *Nature* **2003**.
(55) Cotto-Rios, X. M.; Békés, M.; Chapman, J.; Ueberheide, B.; Huang, T. T. Deubiquitinases as a Signaling Target of Oxidative Stress. *Cell Rep* **2012**, *2*, 1475–84.
(56) Kulathu, Y.; Garcia, F. J.; Mevissen, T. E.; Busch, M.; Arnaudo, N.; Carroll, K. S.; Barford, D.; Komander, D. Regulation of A20 and Other OTU Deubiquitinases by Reversible Oxidation. *Nat Commun* **2013**, *4*, 1569.
(57) Gao, X.-H. H.; Bedhomme, M.; Veyel, D.; Zaffagnini, M.; Lemaire, S. D. D. Methods for Analysis of Protein Glutathionylation and Their Application to Photosynthetic Organisms. *Mol Plant* **2009**, *2*, 218–35.
(58) Rokutan, K.; Thomas, J. A.; Johnston, R. B. Phagocytosis and Stimulation of the Respiratory Burst by Phorbol Diester Initiate S-Thiolation of Specific Proteins in Macrophages. *J. Immunol.* **1991**, *147*, 260–4.
(59) Ravichandran, V; Seres, T; Moriguchi, T S-Thiolation of Glyceraldehyde-3-Phosphate Dehydrogenase Induced by the Phagocytosis-Associated Respiratory Burst in Blood Monocytes. *Journal of Biological ...* **1994**.
(60) Brennan, J. P.; Miller, J. I.; Fuller, W.; Wait, R.; Begum, S.; Dunn, M. J.; Eaton, P. The Utility of N,N-Biotinyl Glutathione Disulfide in the Study of Protein S-Glutathiolation. *Mol. Cell Proteomics* **2006**, *5*, 215–25.
(61) Sullivan, D. M.; Wehr, N. B.; Fergusson, M. M.; Levine, R. L.; Finkel, T. Identification of Oxidant-Sensitive Proteins: TNF-Alpha Induces Protein Glutathiolation.

Biochemistry **2000**, *39*, 11121–8.
(62) Yeh, P.-Y. Y.; Li, C.-Y. Y.; Hsieh, C.-W. W.; Yang, Y.-C. C.; Yang, P.-M. M.; Wung, B.-S. S. CO-Releasing Molecules and Increased Heme Oxygenase-1 Induce Protein S-Glutathionylation to Modulate NF-κB Activity in Endothelial Cells. *Free Radic. Biol. Med.* **2014**, *70*, 1–13.
(63) Samarasinghe, K. T.; Munkanatta Godage, D. N.; VanHecke, G. C.; Ahn, Y.-H. H. Metabolic Synthesis of Clickable Glutathione for Chemoselective Detection of Glutathionylation. *J. Am. Chem. Soc.* **2014**, *136*, 11566–9.
(64) Gygi, S. P.; Rist, B.; Gerber, S. A.; Turecek, F.; Gelb, M. H.; Aebersold, R. Quantitative Analysis of Complex Protein Mixtures Using Isotope-Coded Affinity Tags. *Nat. Biotechnol.* **1999**, *17*, 994–9.
(65) Sethuraman, M.; McComb, M. E.; Heibeck, T.; Costello, C. E.; Cohen, R. A. Isotope-Coded Affinity Tag Approach to Identify and Quantify Oxidant-Sensitive Protein Thiols. *Mol. Cell Proteomics* **2004**, *3*, 273–8.
(66) Sethuraman, M.; McComb, M. E.; Huang, H.; Huang, S.; Heibeck, T.; Costello, C. E.; Cohen, R. A. Isotope-Coded Affinity Tag (ICAT) Approach to Redox Proteomics: Identification and Quantitation of Oxidant-Sensitive Cysteine Thiols in Complex Protein Mixtures. *J. Proteome Res.* **2004**, *3*, 1228–33.
(67) Leichert, L. I.; Gehrke, F.; Gudiseva, H. V.; Blackwell, T.; Ilbert, M.; Walker, A. K.; Strahler, J. R.; Andrews, P. C.; Jakob, U. Quantifying Changes in the Thiol Redox Proteome upon Oxidative Stress in Vivo. *Proc. Natl. Acad. Sci. U.S.A.* **2008**, *105*, 8197–202.
(68) García-Santamarina, S.; Boronat, S.; Espadas, G.; Ayté, J.; Molina, H.; Hidalgo, E. The Oxidized Thiol Proteome in Fission Yeast--Optimization of an ICAT-Based Method to Identify H2O2-Oxidized Proteins. *J Proteomics* **2011**, *74*, 2476–86.
(69) García-Santamarina, S.; Boronat, S.; Domènech, A.; Ayté, J.; Molina, H.; Hidalgo, E. Monitoring in Vivo Reversible Cysteine Oxidation in Proteins Using ICAT and Mass Spectrometry. *Nat Protoc* **2014**, *9*, 1131–45.
(70) Poole, L. B.; Klomsiri, C.; Knaggs, S. A.; Furdui, C. M.; Nelson, K. J.; Thomas, M. J.; Fetrow, J. S.; Daniel, L. W.; King, S. B. Fluorescent and Affinity-Based Tools to Detect Cysteine Sulfenic Acid Formation in Proteins. *Bioconjug. Chem.* **2007**, *18*, 2004–17.
(71) Nelson, K. J.; Klomsiri, C.; Codreanu, S. G.; Soito, L.; Liebler, D. C.; Rogers, L. C.; Daniel, L. W.; Poole, L. B. Use of Dimedone-Based Chemical Probes for Sulfenic Acid Detection Methods to Visualize and Identify Labeled Proteins. *Meth. Enzymol.* **2010**, *473*, 95–115.
(72) Poole, L. B.; Zeng, B.-B. B.; Knaggs, S. A.; Yakubu, M.; King, S. B. Synthesis of Chemical Probes to Map Sulfenic Acid Modifications on Proteins. *Bioconjug. Chem.* **2005**, *16*, 1624–8.
(73) Gupta, V.; Carroll, K. S. Sulfenic Acid Chemistry, Detection and Cellular Lifetime. *Biochim. Biophys. Acta* **2014**, *1840*, 847–75.
(74) Reddie, K. G.; Seo, Y. H.; Muse Iii, W. B.; Leonard, S. E.; Carroll, K. S. A Chemical Approach for Detecting Sulfenic Acid-Modified Proteins in Living Cells. *Mol Biosyst* **2008**, *4*, 521–31.
(75) Leonard, S. E.; Reddie, K. G.; Carroll, K. S. Mining the Thiol Proteome for Sulfenic Acid Modifications Reveals New Targets for Oxidation in Cells. *ACS Chem.*

Biol. **2009**, *4*, 783–99.
(76) Paulsen, C. E.; Truong, T. H.; Garcia, F. J.; Homann, A.; Gupta, V.; Leonard, S. E.; Carroll, K. S. Peroxide-Dependent Sulfenylation of the EGFR Catalytic Site Enhances Kinase Activity. *Nat. Chem. Biol.* **2012**, *8*, 57–64.
(77) Poole, T. H.; Reisz, J. A.; Zhao, W.; Poole, L. B.; Furdui, C. M.; King, S. B. Strained Cycloalkynes as New Protein Sulfenic Acid Traps. *J. Am. Chem. Soc.* **2014**, *136*, 6167–70.
(78) Wani, R.; Qian, J.; Yin, L.; Bechtold, E.; King, S. B.; Poole, L. B.; Paek, E.; Tsang, A. W.; Furdui, C. M. Isoform-Specific Regulation of Akt by PDGF-Induced Reactive Oxygen Species. *Proc. Natl. Acad. Sci. U.S.A.* **2011**, *108*, 10550–5.
(79) Higdon, A.; Diers, A. R.; Oh, J. Y.; Landar, A.; Darley-Usmar, V. M. Cell Signalling by Reactive Lipid Species: New Concepts and Molecular Mechanisms. *Biochem. J.* **2012**, *442*, 453–64.
(80) Geisler, A. C.; Rudolph, T. K. Nitroalkylation--a Redox Sensitive Signaling Pathway. *Biochim. Biophys. Acta* **2012**, *1820*, 777–84.
(81) Schopfer, F. J.; Cipollina, C.; Freeman, B. A. Formation and Signaling Actions of Electrophilic Lipids. *Chem. Rev.* **2011**, *111*, 5997–6021.
(82) Spickett, CM The Lipid Peroxidation Product 4-Hydroxy-2-Nonenal: Advances in Chemistry and Analysis. *Redox biology* **2013**.
(83) Lee, H. S.; Rangiah, K; Williams, MV Cyclooxygenase-2-Mediated Metabolism of Arachidonic Acid to 15-Oxo-Eicosatetraenoic Acid by Rat Intestinal Epithelial Cells. *Chem. Res. Toxicol.* **2007**, *20*, 1665-75.
(84) Surh, YJ; Na, HK; Park, JM; Lee, HN; Kim, W 15-Deoxy-Δ 12, 14-Prostaglandin J 2, an Electrophilic Lipid Mediator of Anti-Inflammatory and pro-Resolving Signaling. *Biochem. Pharmacol.* **2011**, *82*, 1335-51.
(85) Levonen, AL; Landar, A; Ramachandran, A Cellular Mechanisms of Redox Cell Signalling: Role of Cysteine Modification in Controlling Antioxidant Defences in Response to Electrophilic Lipid Oxidation Products. *Biochem. J.* **2004**, *378*, 373-82.
(86) Carbone, DL; Doorn, JA; Kiebler, Z Inhibition of Hsp72-Mediated Protein Refolding by 4-Hydroxy-2-Nonenal. *Chem. Res. Toxicol.* **2004**, *17*, 1459-67.
(87) Carbone, DL; Doorn, JA; Kiebler, Z; Ickes, BR Modification of Heat Shock Protein 90 by 4-Hydroxynonenal in a Rat Model of Chronic Alcoholic Liver Disease. *J. Pharmacol. Exp. Ther.* **2005**, *315*, 8-15.
(88) Jacobs, AT; Marnett, LJ Systems Analysis of Protein Modification and Cellular Responses Induced by Electrophile Stress. *Accounts of chemical research* **2010**.
(89) Fenaille, F; Tabet, JC; Guy, PA Immunoaffinity Purification and Characterization of 4-Hydroxy-2-Nonenal-and Malondialdehyde-Modified Peptides by Electrospray Ionization Tandem Mass Spectrometry *Anal. Chem.* **2002**, *74*, 6298-6304.
(90) Guo, J.; Prokai, L. To Tag or Not to Tag: A Comparative Evaluation of Immunoaffinity-Labeling and Tandem Mass Spectrometry for the Identification and Localization of Posttranslational Protein Carbonylation by 4-Hydroxy-2-Nonenal, an End-Product of Lipid Peroxidation. *J Proteomics* **2011**, *74*, 2360–9.
(91) Fritz, K. S.; Petersen, D. R. Exploring the Biology of Lipid Peroxidation-Derived Protein Carbonylation. *Chem. Res. Toxicol.* **2011**, *24*, 1411–9.
(92) Nakamura, A.; Goto, S. Analysis of Protein Carbonyls with 2,4-Dinitrophenyl Hydrazine and Its Antibodies by Immunoblot in Two-Dimensional Gel Electrophoresis.

J. Biochem. **1996**, *119*, 768–74.
(93) Shacter, E.; Williams, J. A.; Lim, M.; Levine, R. L. Differential Susceptibility of Plasma Proteins to Oxidative Modification: Examination by Western Blot Immunoassay. *Free Radic. Biol. Med.* **1994**, *17*, 429–37.
(94) Mirzaei, H.; Regnier, F. Identification and Quantification of Protein Carbonylation Using Light and Heavy Isotope Labeled Girard's P Reagent. *J Chromatogr A* **2006**, *1134*, 122–33.
(95) Tamarit, J.; de Hoogh, A.; Obis, E.; Alsina, D.; Cabiscol, E.; Ros, J. Analysis of Oxidative Stress-Induced Protein Carbonylation Using Fluorescent Hydrazides. *J Proteomics* **2012**, *75*, 3778–88.
(96) Chavez, J.; Wu, J.; Han, B.; Chung, W.-G. G.; Maier, C. S. New Role for an Old Probe: Affinity Labeling of Oxylipid Protein Conjugates by N'-Aminooxymethylcarbonylhydrazino D-Biotin. *Anal. Chem.* **2006**, *78*, 6847–54.
(97) Codreanu, S. G.; Zhang, B.; Sobecki, S. M.; Billheimer, D. D.; Liebler, D. C. Global Analysis of Protein Damage by the Lipid Electrophile 4-Hydroxy-2-Nonenal. *Mol. Cell Proteomics* **2009**, *8*, 670–80.
(98) Han, B.; Stevens, J. F.; Maier, C. S. Design, Synthesis, and Application of a Hydrazide-Functionalized Isotope-Coded Affinity Tag for the Quantification of Oxylipid-Protein Conjugates. *Anal. Chem.* **2007**, *79*, 3342–54.
(99) Roe, M. R.; Xie, H.; Bandhakavi, S.; Griffin, T. J. Proteomic Mapping of 4-Hydroxynonenal Protein Modification Sites by Solid-Phase Hydrazide Chemistry and Mass Spectrometry. *Anal. Chem.* **2007**, *79*, 3747–56.
(100) Roe, M. R.; McGowan, T. F.; Thompson, L. V.; Griffin, T. J. Targeted 18O-Labeling for Improved Proteomic Analysis of Carbonylated Peptides by Mass Spectrometry. *J. Am. Soc. Mass Spectrom.* **2010**, *21*, 1190–203.
(101) Rauniyar, N.; Prokai, L. Isotope-Coded Dimethyl Tagging for Differential Quantification of Posttranslational Protein Carbonylation by 4-Hydroxy-2-Nonenal, an End-Product of Lipid Peroxidation. *J Mass Spectrom* **2011**, *46*, 976–85.
(102) Han, B.; Hare, M.; Wickramasekara, S.; Fang, Y.; Maier, C. S. A Comparative "Bottom up" Proteomics Strategy for the Site-Specific Identification and Quantification of Protein Modifications by Electrophilic Lipids. *J Proteomics* **2012**, *75*, 5724–33.
(103) Dalle-Donne, I.; Carini, M.; Orioli, M.; Vistoli, G.; Regazzoni, L.; Colombo, G.; Rossi, R.; Milzani, A.; Aldini, G. Protein Carbonylation: 2,4-Dinitrophenylhydrazine Reacts with Both Aldehydes/ketones and Sulfenic Acids. *Free Radic. Biol. Med.* **2009**, *46*, 1411–9.
(104) Stamatakis, K.; Sánchez-Gómez, F. J.; Pérez-Sala, D. Identification of Novel Protein Targets for Modification by 15-Deoxy-Delta12,14-Prostaglandin J2 in Mesangial Cells Reveals Multiple Interactions with the Cytoskeleton. *J. Am. Soc. Nephrol.* **2006**, *17*, 89–98.
(105) Charles, R. L.; Burgoyne, J. R.; Mayr, M.; Weldon, S. M.; Hubner, N.; Dong, H.; Morisseau, C.; Hammock, B. D.; Landar, A.; Eaton, P. Redox Regulation of Soluble Epoxide Hydrolase by 15-Deoxy-Delta-Prostaglandin J2 Controls Coronary Hypoxic Vasodilation. *Circ. Res.* **2011**, *108*, 324–34.
(106) Vila, A.; Tallman, K. A.; Jacobs, A. T.; Liebler, D. C.; Porter, N. A.; Marnett, L. J. Identification of Protein Targets of 4-Hydroxynonenal Using Click Chemistry for Ex Vivo Biotinylation of Azido and Alkynyl Derivatives. *Chem. Res. Toxicol.* **2008**, *21*,

432–44.
(107) Kim, H.-Y. H. Y.; Tallman, K. A.; Liebler, D. C.; Porter, N. A. An Azido-Biotin Reagent for Use in the Isolation of Protein Adducts of Lipid-Derived Electrophiles by Streptavidin Catch and Photorelease. *Mol. Cell Proteomics* **2009**, *8*, 2080–9.
(108) Wang, C.; Weerapana, E.; Blewett, M. M.; Cravatt, B. F. A Chemoproteomic Platform to Quantitatively Map Targets of Lipid-Derived Electrophiles. *Nat. Methods* **2014**, *11*, 79–85.
(109) Weerapana, E.; Wang, C.; Simon, G. M.; Richter, F.; Khare, S.; Dillon, M. B.; Bachovchin, D. A.; Mowen, K.; Baker, D.; Cravatt, B. F. Quantitative Reactivity Profiling Predicts Functional Cysteines in Proteomes. *Nature* **2010**, *468*, 790–5.
(110) Couvertier, S. M.; Zhou, Y.; Weerapana, E. Chemical-Proteomic Strategies to Investigate Cysteine Posttranslational Modifications. *Biochim. Biophys. Acta* **2014**, *1844*, 2315–2330.

Chapter 2

Characterizing the role of *S*-nitrosation in regulating the activity of cathepsin D (CTSD)

A significant portion of the work described in this chapter has been published in:

Zhou, Y.*, Wynia-Smith, S. L.*, Couvertier, S. M.*, Kalous, K. S., Marletta, M. A., Smith, B. C., Weerapana. E. Chemoproteomic strategy to quantitatively monitor transnitrosation uncovers functionally relevant *S*-nitrosation sites on Cathepsin D and HADH2. *Cell Chemical Biology*, **2016**, *23*, 727-737.

Yani Zhou performed MS analysis on GSNO treated lysates and analyzed resulting data.

Introduction.

To date, one of the most commonly used methods for the study of cysteine *S*-nitrosation is the Biotin Switch Technique (BST). [1,2] This method takes advantage of the specific reduction of *S*-nitrosothiols by ascorbate to generate the free thiol. This thiol is later exposed to a cysteine reactive molecule, N-(6-(Biotinamido)hexyl)-3'-(2'-pyridyldithio)propionamide (biotin-HPDP), which allows for enrichment and identification of proteins and peptides that are formally nitrosated. This method has been utilized by many to enrich proteins for later immunoblot analysis and protein identification by MS, providing a database of known nitrosated cysteines. [3–5] Additional advances in S-NO detection led to the development of a variety of chemical probes for the detection of nitrosated cysteines. These probes also take advantage of the unique reactivity of *S*-nitrosothiols over other cysteine PTMs. [6–11] These probes have been employed in MS experiments to identify low molecular weight *S*-nitrosothiols, which provides promise for future use of probes in the identification of S-NO containing proteins.

Despite the ability to provide insight into cysteine nitrosation, these methods are not without limitations. BST is sensitive to false positives, which can arise from incomplete capping of free cysteines prior to S-NO reduction or non-specific S-NO reduction caused by exposure of the sample to light. [12] Additionally, the long sample preparation time increases the potential for S-NO decomposition or rearrangement of *S*-nitrosothiols in complex proteomes. Many of the phosphine-based chemical probes suffer from solubility issues as well as steric encumbrance, making efficient detection of *S*-nitrosated proteins in complex biological samples difficult. In an effort to expand the

methods available to detect nitrosated cysteines in complex proteomes and provide a means to monitor the extent to which a cysteine is nitrosated, our laboratory has developed an *in vitro* MS platform to quantify cysteine sensitivity to *S*-nitrosation.

Mass-spectrometry platform for the study of cysteine susceptibility toward *S*-nitrosation.

We focused on the development of a platform that would allow for the comparison of cysteine reactivity between two samples, a control sample and one with increased levels of NO-modified cysteines (Figure 2-1). To induce cysteine nitrosation, a low molecular weight transnitrosation donor, *S*-nitrosoglutathione (GSNO), was used. Transnitrosation is a reversible reaction between a nitrosothiol and a cysteine thiol. [13] The reaction proceeds through nucleophilic attack of the nitrosothiol nitrogen by a cysteine thiolate ion resulting in a nitroxyl disulfide intermediate. [13,14] The overall mechanism resembles an S_N2 reaction, where the rate of reaction is governed by the nucleophilicity of the cysteine thiol. *S*-nitrosation of a protein thiol will quench the nucleophilicity of that cysteine residue, and therefore monitoring loss of cysteine reactivity in the presence of a transnitrosation agent will allow for determination of sites of *S*-nitrosation. The degree of loss in cysteine reactivity is indicative of the extent of *S*-nitrosation, thereby providing the stoichiometry of *S*-nitrosation for a cysteine of interest. Cysteine reactivity was measured using an iodoacetamide alkyne (IAA) probe that is known to modify hundreds of cysteines within a human proteome.[15]

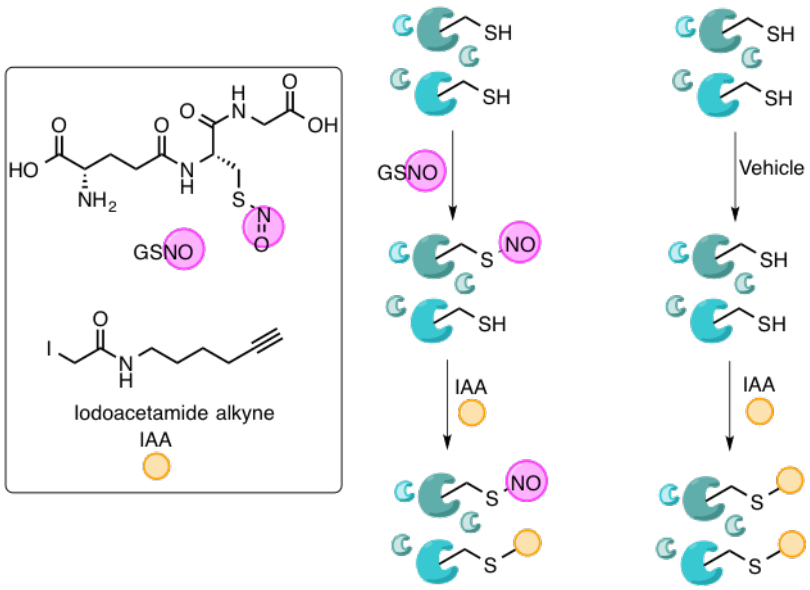

Figure 2-1 General Platform for the quantification and identification of cysteine sensitivity toward *S*-nitrosation.

To identify cysteine residues modified by the IAA probe, we utilized a mass-spectrometry (MS) platform previously developed in the Weerapana Lab. This platform applies a cleavable linker (azo-tag) that allows for enrichment and selective release of IAA-modified peptides for MS analysis. [16] The azo-tag used possesses three basic functionalities: (1) an azide, a bioorthogonal group for click chemistry derivatization of IAA-modified proteins; (2) a biotin group, for enrichment of modified IAA-modified proteins using the strong streptavidin-biotin interaction; (3) an azobenzene cleavable unit, for release of IAA-modified peptides from streptavidin beads after enrichment and on-bead trypsin digestion (Figure 2-2). IAA-treatment of proteomes is followed by Copper(I)-catalyzed Azide-Alkyne Cycloaddition (CuAAC) to conjugate the azo-tag to IAA-modified proteins. IAA-tagged proteins are then subjected to enrichment on streptavidin beads followed by an on-bead trypsin digestion. After the trypsin digestion,

the IA-modified peptides remain immobilized on the beads and can be selectively eluted using sodium dithionite, which chemically cleaves the azobenzene cleavable unit.

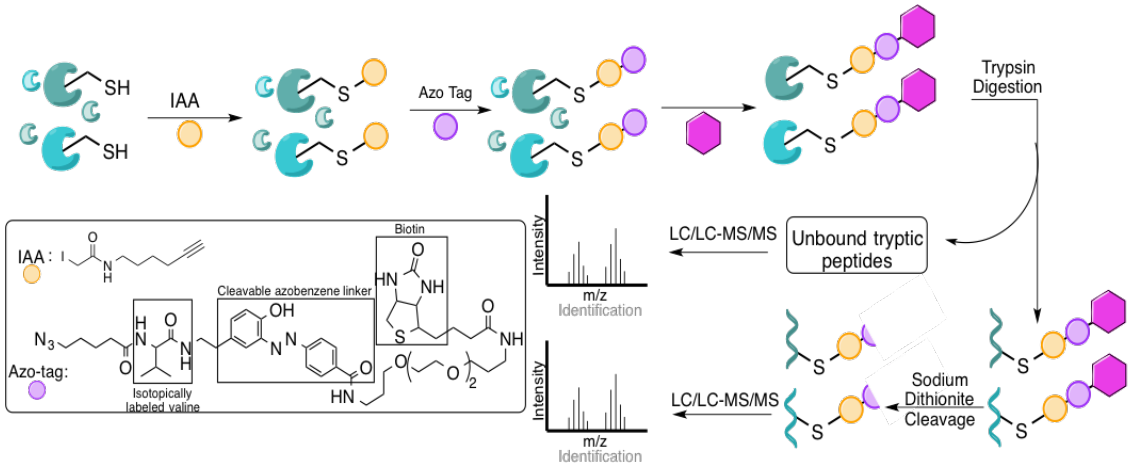

Figure 2-2 MS platform that takes advantage of the azo-tag for identification of specific cysteines modified by an iodoacetamide alkyne (IAA)

In order to globally assess cysteine reactivity across two different samples, the azo-tag was modified to include either an isotopically light (^{12}C and ^{14}N) or heavy (^{13}C and ^{15}N) valine moiety, generating azo-light and azo-heavy tags, respectively. Typically, a control sample is labeled with the azo-heavy tag and a modified sample with azo-light tag (Figure 2-3). After combining the two samples, differences in cysteine reactivity can be monitored by the generation of light to heavy (L:H) ratios. If the reactivity of a particular cysteine is decreased in the modified sample, a L:H ratio less than one will be observed. A cysteine assigned a L:H ratio that is equal to one, indicates that the reactivity of the cysteine has not changed. Lastly, cysteines may be assigned L:H ratios greater than one, which represent increased reactivity in the modified sample with respect to the heavy-labeled control.

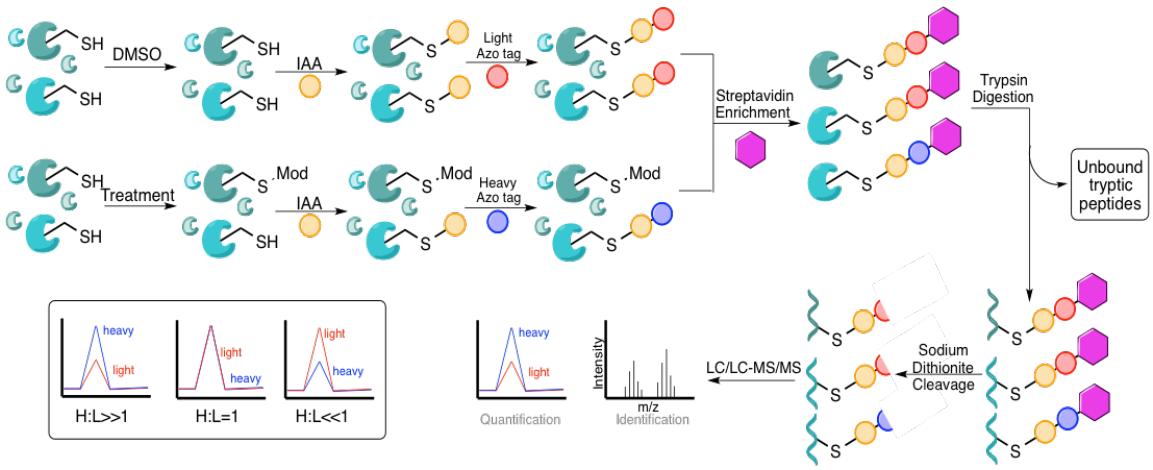

Figure 2-3 MS platform used for the identification and quantification of cysteine reactivity across two samples.

The MS platform described above can be applied to the study of cysteine nitrosation. Lysates treated with either buffer or GSNO were treated with IAA and conjugated with either azo-heavy or azo-light, respectively. The samples were combined and enriched on streptavidin beads. The bound proteins undergo a trypsin digestion and the tryptic peptides are isolated from the beads. The peptides that remain bound to the beads are eluted using sodium dithionite and the samples are later subjected to LC/LC-MS/MS analysis.

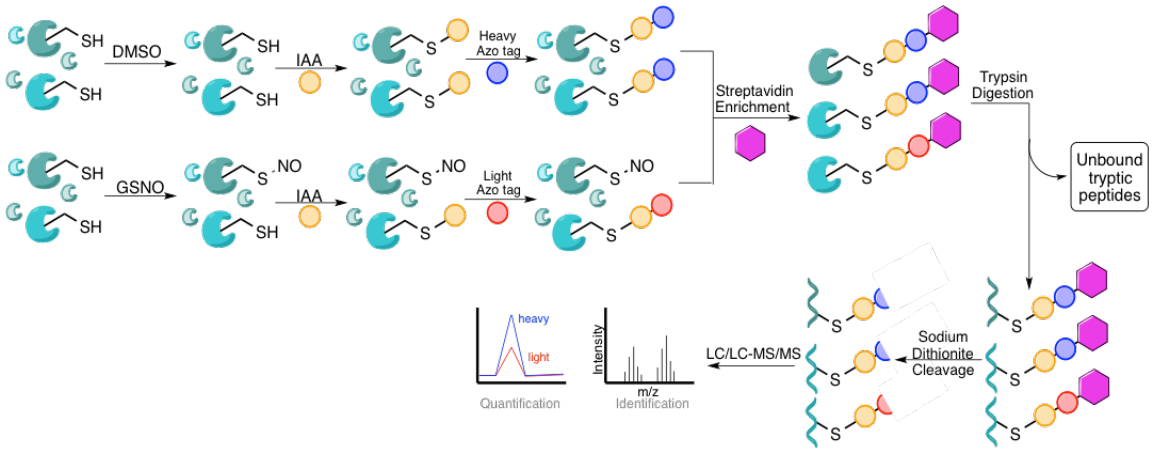

Figure 2-4 MS platform used for the identification and quantification of cysteine sensitivity to *S*-nitrosation in complex samples.

Initially, we prepared two MS samples. The first sample compared two vehicle treated lysates (0 µM versus 0 µM) and the second compared vehicle and 500 µM GSNO treated lysates (0 µM vs. 500 µM). The ratios observed for the "0 µM vs. 0 µM" sample were approximately 1, indicative of no change in cysteine reactivity between the buffer treated lysates. A majority of ratios identified for the "0 vs. 500 µM" sample were greater than one. Therefore, GSNO treatment causes a global decrease in cysteine reactivity toward IAA with respect to the buffer treated control (Figure 2-5).

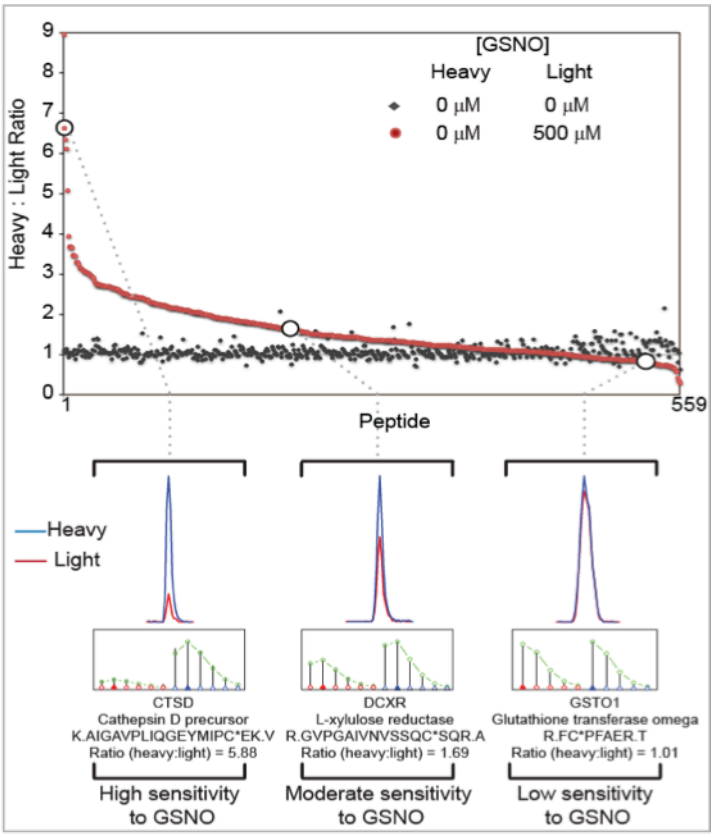

Figure 2-5 Plot of MS ratio obtained for comparison of DMSO treated sample and 500µM GSNO sample to a DMSO treated control. Ratios of representative ratios are highlighted with individual plots for CTSD, DCXR and GSTO1.

This MS platform allows for quantification of cysteine reactivity with IAA after nitrosation and ranking of cysteine sensitivity toward nitrosation in the human proteome. As validation for our method, we identified Cys152 of GAPDH to have the greatest H:L ratio indicating that this cysteine is the most sensitive to *S*-nitrosation. Cys152 has been previously annotated as a cysteine that readily undergoes nitrosation. [17,18] The resulting *S*-nitrosocysteine reversibly inhibits GAPDH activity and modification contributes to heme trafficking and apoptotic signaling. The remaining cysteines within the dataset were rank ordered by their relative ratios and S-NO susceptibility. One example, Cys32 of glutathione S-transferase Omega 1 (GSTO1) had a calculated H:L ratio of 1.01, suggesting that the active site cysteine of GSTO1 is not sensitive to nitrosation (Figure 2-5). Cysteines with moderate sensitivity were also identified, such as Cys138 of L-xylulose reductase (DCXR) with a relative H:L ratio of 1.69. Within the group of cysteine residues assigned H:L ratios greater than two, we identified Cys329 of cathepsin D (CTSD) with a ratio of 5.88, indicative of high sensitivity toward nitrosation. *S*-nitrosation of human CTSD has not been previously reported. Thus, we chose to further characterize *S*-nitrosothiol formation on Cys329 and the potential role this PTM plays on protease regulation.

Cysteine 329: a cysteine sensitive to *S*-nitrosation on Cathepsin D

Cys329 of CTSD is one of the most sensitive cysteines to nitrosation in the human proteome identified using our MS platform. Cathepsin D is an aspartyl protease active at pH 4 and is localized in human lysosomes. [19] Prior to lysosomal compartmentalization, CTSD is translated in the endoplasmic reticulum (ER) as a pre-/pre-pro-enzyme (Figure 2-6A). [20] Next, pre-CTSD is cleaved and shuttled to the Golgi where the protein becomes

glycosylated.[21] From the Golgi, CTSD is transported to the lysosome where the enzyme is proteolytically cleaved by other cysteine cathepsins to afford mature CTSD. The active form of CTSD consists of heavy (28 kDa) and light (17 kDa) chains, which interact non-covalently (Figure 2-6B). This enzyme also possesses 8 cysteines, all of which are assigned to annotated structural disulfide bonds.

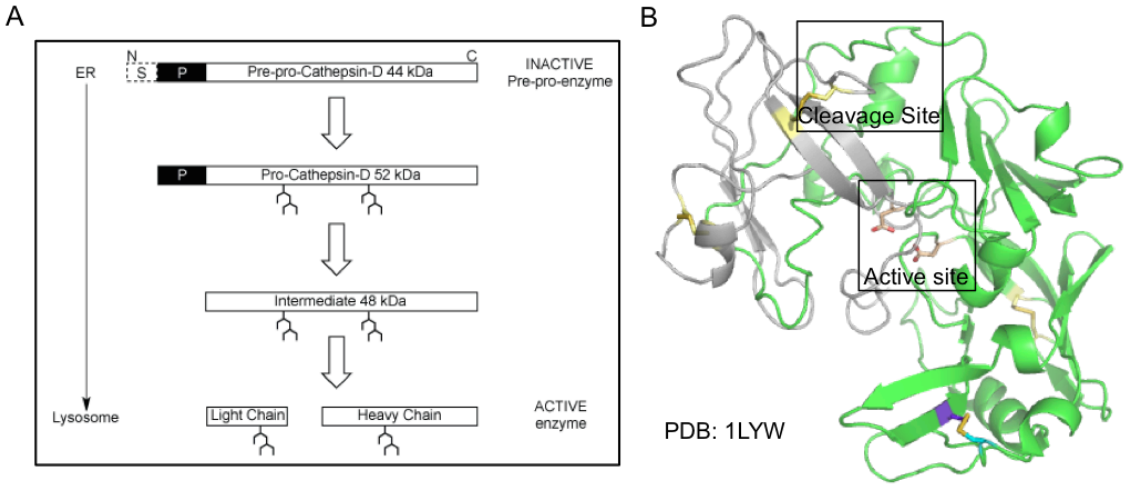

Figure 2-6 Cathepsin D (CTSD) is an aspartyl protease which undergoes a series of processing steps before becoming active in the lysosome. (A) General processing of CTSD. (B) Crystal structure of CTSD with disulfide bonds highlighted in yellow or marked.

The cysteine residue corresponding to Cys329 in the mouse CTSD homolog has been previously identified to undergo *S*-nitrosation in a proteomic analysis study of mouse heart tissue after myocardial ischemic preconditioning.[22,23] In crystal structures of mature CTSD, Cys329 forms a disulfide with Cys366 located distal to both the active site of the enzyme as well as the site of light and heavy chain-forming proteolytic cleavage (Figure 2-6B). This structural disulfide of CTSD is thought to help stabilize the mature protein and functional consequences of CTSD *S*-nitrosation at this residue have not been previously characterized. Initially, the annotation of Cys329 as a disulfide partner was surprising since the MS data as well as data from a previous study[15] found Cys329 highly reactive towards IAA. Typically structural disulfides are inert and cannot react with IAA

without prior reduction. However, covalent modification of Cys329 with IAA suggests that this disulfide is either dynamic and possesses redox properties or is an artifact of protein crystallization.

Cathepsin D has also been found to have implications in disease. CTSD is upregulated in breast cancer tumors and is used a biomarker for aggressive cases of the disease.[24] The role of CTSD in breast cancer is still unknown, however many potential roles for this enzyme in disease have been postulated. Some hypothesize that this protease may act as an autocrine mitogen, since the inactive pre/pre-pro form of the enzyme is secreted from diseased cells into the extracellular environment.[25,26] It is unknown whether CTSD is activated after secretion by extracellular proteases, however the secreted pre-pro CTSD may encourage neighboring tissue to become cancerous in nature.

Characterization of the role of *S*-nitrosation of Cys329 on CTSD activity.

Due to the numerous glycosylation and processing steps CTSD undergoes, recombinant expression and purification of a properly folded and active protease was not feasible. Instead transient transfection of HEK293T cells with CTSD WT, C329A, or C366A with a C-terminal Myc/His tag containing plasmids for overexpression of CTSD was used. After transfection of the WT and C329A mutant plasmids in HEK293T cells, soluble protein was isolated and used to perform CTSD protease activity assays to compare the effect mutagenesis has on CTSD activity. The substrate peptide, GlyLysProIleLysPhePheArgLeuLysAspArg, used in the Förster Resonance Energy Transfer (FRET)-based protease assay contains a N-terminal 7-methoxylcoumarin (Mca)

fluorophore and C-terminal 2,4-dinitrophenol (Dnp) quencher. Prior to cleavage by the protease, no fluorescent signal is detected from the substrate peptide. Once CTSD cleaves the peptide, the emitted fluorescent signal can be read as a measure of activity with respect to mock HEK293T lysates. In comparison to wild-type overexpressing lysates, the lysates with overexpressed C329A mutant exhibited protease activity comparable to that of the mock control (Figure 2-7B). The lack of fluorescence detected indicates that Cys329 is essential for CTSD protease activity.

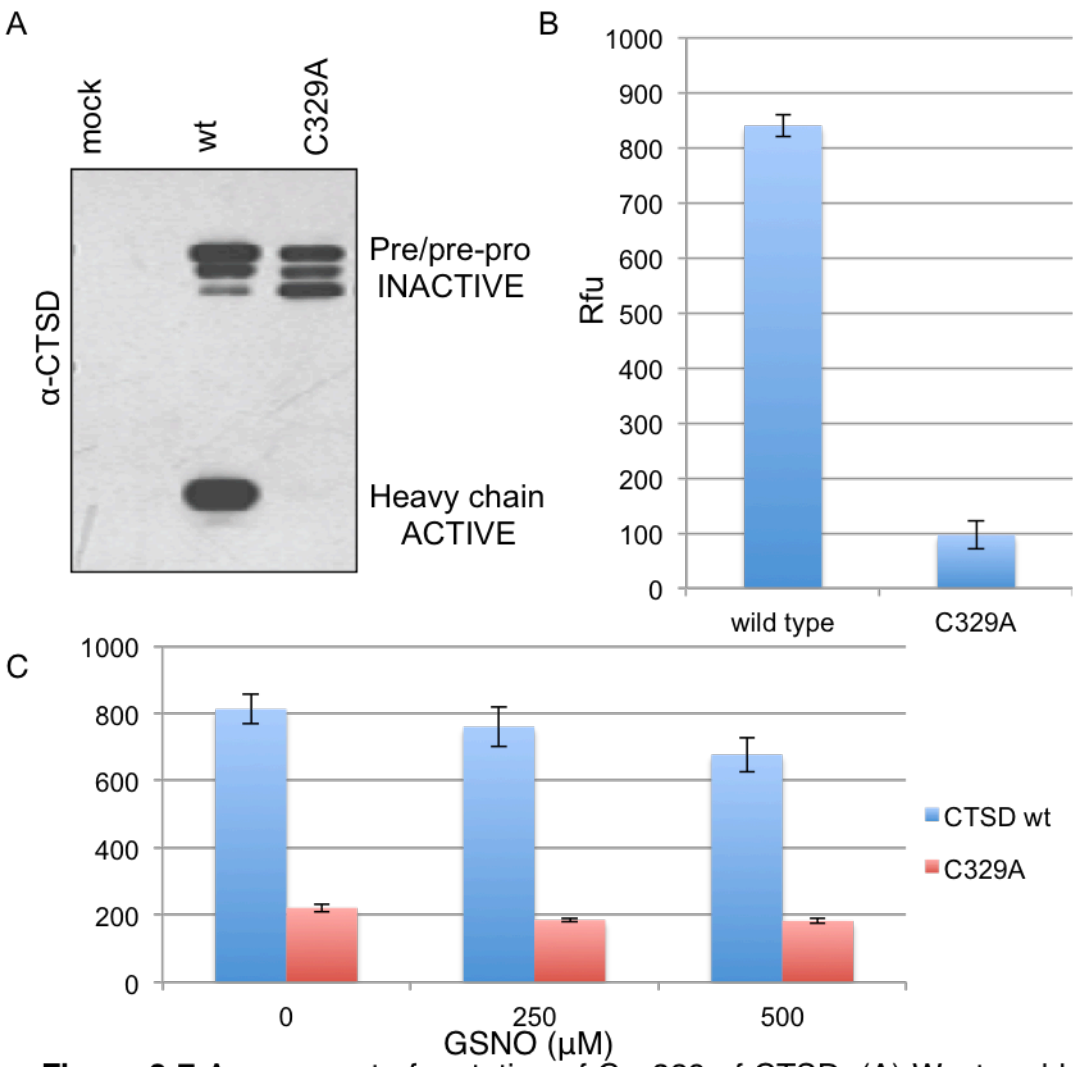

Figure 2-7 Assessment of mutation of Cys329 of CTSD. (A) Western blot of wt and C329A mutant Myc-tagged CTSD. (B) Quantification of wt and C329A mutant CTSD activity by fluorescence-based protease activity. Activity of C329A is comparable to mock lysates. (C) Quantification of CTSD activity in the presence of GSNO.

An immunoblot on CTSD containing lysates was performed to confirm that efficient overexpression of C329A mutant protein was achieved (Figure 2-7A). Both precursors of CTSD, pre-/pre-pro-CTSD, were overexpressed in cells transfected with WT and mutant CTSD. However, unlike the lysates from the WT transfection, the C329A mutant lysates did not contain CTSD heavy chain, indicating that the mutant protein is not processed to the mature active form. The lack of mature CTSD present in the C329A

mutant overexpressing lysates supports the data obtained from the protease activity assay. Additional mutagenesis of Cys366 and Cys91 was used to monitor the effect alternative cysteine residues have on CTSD processing (Figure 2-8). Mutation of Cys366 to an alanine results in similar inhibition of processing monitored by immunoblot as the Cys329 mutant. Alternatively, complete processing to the active form of CTSD is observed for the Cys91 mutant. Therefore, the lack of processing for the Cys329/Cys366 mutants shows that this disulfide is essential for proper processing of CTSD.

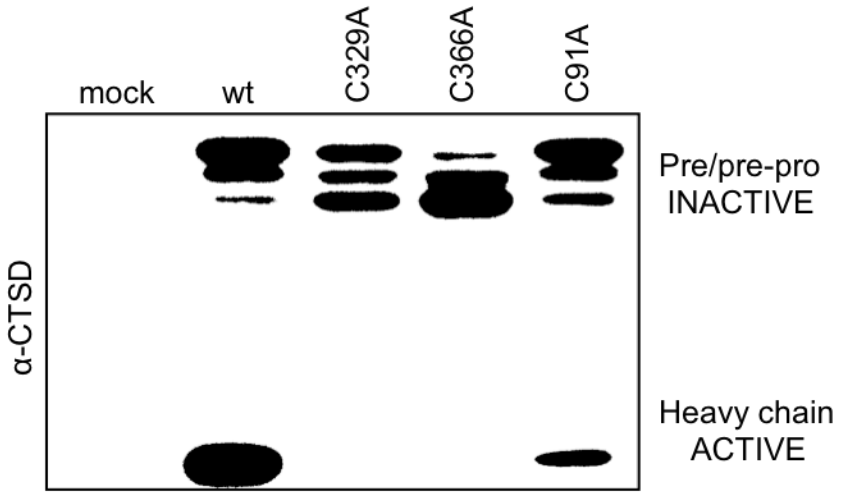

Figure 2-8 Assessment of disulfide cysteines in CTSD processing. Western blot was used to monitor processing of wt, C329A, C366A and C91A Myc-tagged mutants CTSD.

Though mutagenesis allows for the removal of reactive cysteine residues from proteins, it is not a direct substitute for perturbation of cysteine reactivity by *S*-nitrosothiol formation. To confirm that inhibition of processing is also caused by *S*-nitrosation, CTSD WT was transiently transfected into HEK293T cells and the cells were treated with a cell permeable transnitrosation donor, *S*-nitrosocysteine (CysNO). After a 48-hour incubation period, soluble HEK293T lysates were obtained and an immunoblot was performed to observe the processing of CTSD in presence of increased NO levels

(Figure 2-9A). CTSD processing is decreased as the amount of CysNO increases in the cell media (Figure 2-9B). The decrease in processing to mature CTSD suggests that this phenomenon is caused by increased transnitrosation occurring in the HEK293T cells.

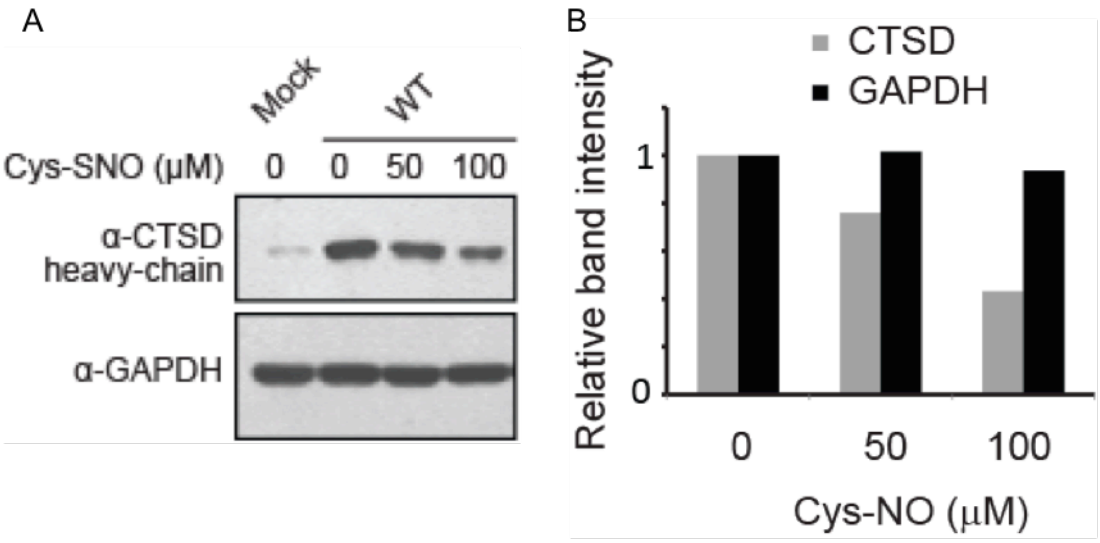

Figure 2-9 CTSD processing in the presence of CysNO. (A) Western blot of CTSD mature heavy chain after treatment of increasing concentrations of CysNO. (B) Quantification of Western blot bands from CysNO treated CTSD overexpressing cells.

Lastly, an additional activity assay was performed to confirm that CTSD activity is regulated by the inhibition of processing and not perturbation of mature enzyme activity. Lysates containing overexpressed CTSD WT were treated with GSNO prior to assessment of protease activity by the FRET-based assay described above. After treatment of these lysates with increasing levels GSNO, minimal changes were observed in the ability of CTSD WT to cleave the peptide substrate (Figure 2-7C). Since the active-site residue of CTSD is an aspartate, an amino acid residue is not known to undergo nitrosation, the insensitivity of the mature enzyme toward increasing NO-levels is plausible.

Conclusions and future directions

To our knowledge, *S*-nitrosation of Cys329 of CTSD is the first example of regulation of cellular protease activity by modification of processing of an enzyme. Upon mutagenesis of Cys329 to an alanine, abolishment of CTSD processing to its mature form is observed. Cells overexpressing CTSD WT grown in the presence of CysNO generate decreased levels of mature CTSD indicating that *S*-nitrosation also inhibits proper processing of the enzyme *in situ*.

Future studies will focus on the elucidation of the cellular compartmental localization of CTSD after *S*-nitrosothiol formation. Since CTSD travels from the ER to lysosome, there is a possibility that modification by NO leads to changes in the location of the enzyme that is atypical of unmodified CTSD. Pre-/pre-pro-CTSD is also secreted into the extracellular environment of breast cancer cells. Since levels of the pre-/pre-pro-CTSD are increased in breast cancer and oxidative PTMs are more likely to occur in in these tissues, *S*-nitrosation-induced inhibition in processing can serve as a mechanism for increased secretion of CTSD in cancer. The potential connection between Cys329 *S*-nitrosation and secretion of pre-/pre-pro-CTSD is an additional area that can be explored in future experiements.

Acknowledgments

I would like to acknowledge Yani Zhou for her preparation and analysis of the GSNO treated MS samples.

Experimental procedures

Materials and general procedure

All materials were purchased from Sigma Aldrich unless otherwise noted. DMEM/High glucose medium, Phosphate buffered saline (PBS) buffer, 2% Trypsin-EDTA and penicillin streptomycin (Pen/Strep) were purchased from Fisher Scientific (Pittsburgh, PA). The Myc-tag antibody, CTSD antibody, and anti-rabbit IgG HRP-linked antibody were purchased from Cell Signaling (Danvers, MA). Cathepsin D Activity Assay Kit was purchased from BioVision (Mountain View, CA). Potassium phosphate tribasic monohydrate was purchased from Fisher Scientific (Pittsburgh, PA). X-tremeGENE 9 DNA transfection reagent was purchased from Roche (Indianapolis, IN). All protein concentrations were determined using a Bio-Rad DC protein assay kit with reagents from Bio-Rad Life Science (Hercules, CA). Mini Trans-Blot Filter Paper was purchased from Bio-Rad Life Science (Hercules, CA). SuperSignal West Pico Chemiluminescent Substrate was purchased from Thermo Scientific (Armarillo, TX). QuickChange Site-Directed Mutagenesis Kit was purchased from Agilent Technologies (Santa Clara, CA). Illusta Nap-5 Columns were purchased from GE Healthcare Bio-Sciences (Piscataway, NJ). Micro Bio-Spin P-6 Columns were purchased from Bio-Rad Life Science (Hercules, CA). Streptavidin-agarose beads were purchase from Thermo Scientific (Armarillo, TX).

Preparation of cell lysate:

Cells were allowed to grow to 100% confluency and then harvested by scraping. The cells were washed three times with DPBS buffer, resuspended in an appropriate volume of DPBS and sonicated to obtain whole cell lysates. The lysates were then separated by ultracentrifugation at 45,000 rpm at 4°C under high vacuum for 45 minutes. The resulting supernatant was collected as the soluble proteome. Protein concentrations were then determined using a Bradford Protein Concentration Assay and further normalized as needed.

Construction of expression vectors:

The cDNA for CTSD was subcloned into a pcDNA3.1-(+)-Myc/His mammalian expression vector. The construct for subcloning into the vector was generated by polymerase chain reaction (PCR) from the corresponding cDNA using the primers: CTSD-WT pcDNA3.1(+) forward 5'-TTACTCGAGATGCAGCCCTCCAGCCTTCTG-3'; reverse 5'-TAAAGCTTGAGGCTGCCCGCCTC-3'. Site-directed mutagenesis was performed to obtain cysteine to alanine mutants using the QuickChange procedure (Stratagene) with the appropriate primers: CTSD-C91A pcDNA3.1(+) forward 5'-GACGCCCCCCCAGGCCTTCACAGTCGTC-3'; reverse 5'-GACGACTGTGAAGGCCTGGGGGGGCGTC-3'; CTSD-C329A pcDNA3.1(+) forward 5'-GAGTACATGATCCAGAAGGTGTCCAC-3'; reverse 5'-GTGGACACCTTCTGGATCATGTACTC-3'; CTSD-C366A pcDNA3.1(+) forward 5'-GCCGGGAAGACCCTCGCCCTGAGCGGCTTCATG-; reverse 5'-

CATGAAGCCGCTCAGGGCGAGGGTCTTCCCGGC-3'. All constructs were verified by DNA sequencing (Genewiz, Cambridge, MA).

Mass-spectrometry analysis of GSNO-treated MCF7 lysates.

S-nitrosoglutathione (GSNO) was dissolved in fresh HEN buffer (125 mM HEPES pH 7.7, 1 mM EDTA, 0.1 mM neocuproine). The GSNO concentration was determined by measuring the UV absorbance at 336 nm based on an extinction coefficient of 0.9 $mM^{-1}cm^{-1}$. MCF7 cell lysates (4 mg/mL) were aliquoted to 500 μL and incubated with 5 μL HEN buffer or 5 μL of GSNO (50 μM, 100 μM, 200 μM, or 500 μM final concentration) in HEN buffer at 37 °C for 1 hr. Excess GSNO was then removed by filtration through a Nap-5 column. Proteins were eluted with 1 mL PBS and aliquoted to produce two 500 μL samples. GSNO and buffer-treated samples were treated with the IA probe (100 μM) and subjected to CuAAC with light or heavy Azo-tags and subsequent mass-spectrometry analysis as described previously (Qian, Y. and Weerapana, E. et al. *Chem. Biol. Chem,* **2013**, *14*, 1410-14).

MS data analysis.

The generated tandem MS data was searched using the SEQUEST algorithm against the human IPI database. A static modification of +57.02146 on cysteine was specified to account for iodoacetamide alkylation and differential modifications of +456.2849 (Azo-L modification) and +462.2987 (Azo-H modification) were specified on cysteine to account for probe modifications. SEQUEST output files were filtered using DTASelect 2.0. Quantification of light/heavy ratios (R) was performed using the

CIMAGE quantification package as previously described (Weerapana, E., Speers, A. E. Cravatt, B. F. *Nat. Protoc.* **2007**, *2*, 1414-25).

Overexpression of CTSD in HEK293T cells.

HEK293T cells were transfected with CTSD (WT, C91A, C329A, or C366A). Specifically, serum free DMEM medium, 20μL of X-tremeGENE DNA transfection reagent and 6μg of either empty pcDNA-3.1(+)-Myc/His vector or recombinant vectors were combined in an eppendorf tube. After incubation at room temperature for 15 mins, the mixture was added to a plate of HEK293T cells with ~60% confluency. The cells were incubated at 37 ˚C for 48 hrs, harvested and then lysed in PBS. The concentrations of soluble proteins were normalized.

Protein overexpression was analyzed by western blot. Proteins were separated by 10% SDS-PAGE and transferred by electroblotting to nitrocellulose membrane at 150 volt hours. The membrane was first washed using Tris-buffered saline containing 1% Tween 20 (TBS-T), and exposed to Ponceau Stain to ensure that the protein was transferred from the gel to the membrane. The membrane was then washed three times with TBS-T until the membrane was free of stain, followed by blocking in TBS-T with 5% (w/v) non-fat dry milk at room temperature for 2 hrs. After washing three times with TBS-T, the membrane was incubated with CTSD primary anti-body (1:1000) at 4°C for 16 hrs. The membrane was then washed three times with TBS-T and incubated for another 2 hrs with horseradish peroxidase (HRP)-conjugated secondary antibody at room temperature. The membrane was washed three times with TBS-T and treated with both

SuperSignal® West Pico Chemiluminescent HRP and luminol substrate and exposed to film for 3 mins. Development took place using a Kodak X-OMAT 2000A processor.

CTSD activity assays

CTSD activity was monitored using the Cathepsin D Activity Assay Kit (BioVision Incorporated, Milpitas, CA). HEK293T cells transfected with pcDNA3.1(+)-CTSD (WT, C91A, C329A or C366A) constructs were lysed in DPBS buffer and normalized to a concentration of 11.4 μg/mL. To a 96-well plate was added 10μL of lysate (11.4ng lysate/well) and 40μL DPBS to bring the final volume to 50μL. Each well was mixed with 52µL of Master Mix (50µL of Reaction Buffer premixed with 2µL of Substrate), resulting in a final volume of 102μL/well. The 96-well plate was then incubated at 37°C for 1.5 hrs. Enzyme activity was measured by the resulting fluorescence released by the substrate once cleaved by CTSD using a Molecular Devices SpectraMax M5 plate reader. The fluorometer was set to read at 328nm excitation filter and 460nm emission filter, according to the instructions of the BioVision CTSD Assay Kit. The data collected for the mock lysate reactions were used to subtract out background fluorescence from the buffers not used by the kit (DPBS) for lysing cells as well as any endogenous CTSD that will be present in the cells prior to transfection. Each reaction was repeated two times and the data was analyzed using Microsoft Excel.

For the *S*-nitrosated CTSD activity assay, CTSD overexpressing lysates were exposed to GSNO to observe the effects of the nitrosating agent on fully processed CTSD activity. To each 10μL of lysate added to the wells was added GSNO in HEN buffer (1 mM stock), followed by DPBS to bring the final volume to 50μL and final concentrations

of GSNO to 0, 250 or 500 μM. The samples were then incubated at 37 ˚C for 30 mins. After incubation with GSNO, the master mix was added to each reaction, bringing the final volume to 102μL. The 96-well plate was incubated at 37˚C for 1.5 hours and then read using the plate reader. The data collected was analyzed as described above.

Monitoring processing of WT and mutant CTSD.

The Myc-tagged pcDNA3.1(+) vectors containing CTSD WT, C91A, C329A or C366A were transfected into HEK293T cells as described above. The cells were harvested and the soluble lysates were isolated by collection of the supernatant after ultracentrifugation (45 min, 45,000 rpm, 4 ˚C). The cell lysates were normalized to 4.0 mg/mL before immunoblotting with an anti-CTSD antibody (1:1000 dilution) followed by an anti-Rabbit HRP-linked antibody (1:3333 dilution) to evaluate the processing of CTSD.

Monitoring processing of WT CTSD in the presence of CysNO.

Three plates of HEK293T cells were transfected with pcDNA3.1(+)-CTSD WT. One plate remained untreated as a control. Six hours after transfection the other two plates were treated with 50 μM or 100 μM CysNO. Then 24 hours after transfection the plates were treated again with 50 μM and 100 μM CysNO, respectively. CysNO was generated following the preparation of *S*-Nitrosothiol procedure by Schoenfisch *et al* (Ricco, D. A., Nuts, S. T., Schoenfisch, M. H. *Anal Chem* **2012**, *84*, 851-6). After 48 hours, the cells were lysed and the soluble proteins were isolated and normalized to a

final concentration of 4.0 mg/mL. The proteins were analyzed using Western Blot and the bands were integrated using ImageJ.

References

(1) Jaffrey, S. R.; Erdjument-Bromage, H.; Ferris, C. D.; Tempst, P.; Snyder, S. H. Protein S-Nitrosylation: A Physiological Signal for Neuronal Nitric Oxide. *Nat. Cell Biol.* **2001**, *3*, 193–7.

(2) Jaffrey, S. R.; Snyder, S. H. The Biotin Switch Method for the Detection of S-Nitrosylated Proteins. *Sci. STKE* **2001**, *2001*, pl1.

(3) Benhar, M.; Thompson, J. W.; Moseley, M. A.; Stamler, J. S. Identification of S-Nitrosylated Targets of Thioredoxin Using a Quantitative Proteomic Approach. *Biochemistry* **2010**, *49*, 6963–9.

(4) Sinha, V.; Wijewickrama, G. T.; Chandrasena, R. E.; Xu, H.; Edirisinghe, P. D.; Schiefer, I. T.; Thatcher, G. R. Proteomic and Mass Spectroscopic Quantitation of Protein S-Nitrosation Differentiates NO-Donors. *ACS Chem. Biol.* **2010**, *5*, 667–80.

(5) Murray, C. I.; Uhrigshardt, H.; O'Meally, R. N.; Cole, R. N.; Van Eyk, J. E. Identification and Quantification of S-Nitrosylation by Cysteine Reactive Tandem Mass Tag Switch Assay. *Mol. Cell Proteomics* **2012**, *11*, M111.013441.

(6) Wang, H.; Xian, M. Fast Reductive Ligation of S-Nitrosothiols. *Angew. Chem. Int. Ed. Engl.* **2008**, *47*, 6598–601.

(7) Zhang, J.; Wang, H.; Xian, M. Exploration of the "Traceless" Reductive Ligation of S-Nitrosothiols. *Org. Lett.* **2009**, *11*, 477–80.

(8) Zhang, J.; Wang, H.; Xian, M. An Unexpected Bis-Ligation of S-Nitrosothiols. *J. Am. Chem. Soc.* **2009**, *131*, 3854–5.

(9) Zhang, J.; Li, S.; Zhang, D.; Wang, H.; Whorton, A. R.; Xian, M. Reductive Ligation Mediated One-Step Disulfide Formation of S-Nitrosothiols. *Org. Lett.* **2010**, *12*, 4208–11.

(10) Bechtold, E.; Reisz, J. A.; Klomsiri, C.; Tsang, A. W.; Wright, M. W.; Poole, L. B.; Furdui, C. M.; King, S. B. Water-Soluble Triarylphosphines as Biomarkers for Protein S-Nitrosation. *ACS Chem. Biol.* **2010**, *5*, 405–14.

(11) Seneviratne, U.; Godoy, L. C.; Wishnok, J. S.; Wogan, G. N.; Tannenbaum, S. R. Mechanism-Based Triarylphosphine-Ester Probes for Capture of Endogenous RSNOs. *J. Am. Chem. Soc.* **2013**, *135*, 7693–704.

(12) Forrester, M. T.; Foster, M. W.; Stamler, J. S. Assessment and Application of the Biotin Switch Technique for Examining Protein S-Nitrosylation under Conditions of Pharmacologically Induced Oxidative Stress. *J. Biol. Chem.* **2007**, *282*, 13977–83.

(13) Houk, K. N.; Hietbrink, B. N.; Bartberger, M. D.; McCarren, P. R.; Choi, B. Y.; Voyksner, R. D.; Stamler, J. S.; Toone, E. J. Nitroxyl Disulfides, Novel Intermediates in Transnitrosation Reactions. *J. Am. Chem. Soc.* **2003**, *125*, 6972–6.

(14) Perissinotti, L. L.; Turjanski, A. G. G.; Estrin, D. A. A.; Doctorovich, F. Transnitrosation of Nitrosothiols: Characterization of an Elusive Intermediate. *J. Am. Chem. Soc.* **2005**, *127*, 486–7.

(15) Weerapana, E.; Wang, C.; Simon, G. M.; Richter, F.; Khare, S.; Dillon, M. B.; Bachovchin, D. A.; Mowen, K.; Baker, D.; Cravatt, B. F. Quantitative Reactivity Profiling Predicts Functional Cysteines in Proteomes. *Nature* **2010**, *468*, 790–5.
(16) Qian, Y.; Martell, J.; Pace, N. J.; Ballard, T. E.; Johnson, D. S.; Weerapana, E. An Isotopically Tagged Azobenzene-Based Cleavable Linker for Quantitative Proteomics. *Chembiochem* **2013**, *14*, 1410–4.
(17) Hara, M. R.; Agrawal, N.; Kim, S. F.; Cascio, M. B.; Fujimuro, M.; Ozeki, Y.; Takahashi, M.; Cheah, J. H.; Tankou, S. K.; Hester, L. D.; et al. S-Nitrosylated GAPDH Initiates Apoptotic Cell Death by Nuclear Translocation Following Siah1 Binding. *Nat. Cell Biol.* **2005**, *7*, 665–74.
(18) Kornberg, M. D.; Sen, N.; Hara, M. R.; Juluri, K. R.; Nguyen, J. V.; Snowman, A. M.; Law, L.; Hester, L. D.; Snyder, S. H. GAPDH Mediates Nitrosylation of Nuclear Proteins. *Nat. Cell Biol.* **2010**, *12*, 1094–100.
(19) Minarowska, A.; Gacko, M.; Karwowska, A.; Minarowski, Ł. Human Cathepsin D. *Folia Histochem. Cytobiol.* **2008**, *46*, 23–38.
(20) Zaidi, N.; Maurer, A.; Nieke, S.; Kalbacher, H. Cathepsin D: A Cellular Roadmap. *Biochem. Biophys. Res. Commun.* **2008**, *376*, 5–9.
(21) Másа, M.; Maresová, L.; Vondrásek, J.; Horn, M.; Jezek, J.; Mares, M. Cathepsin D Propeptide: Mechanism and Regulation of Its Interaction with the Catalytic Core. *Biochemistry* **2006**, *45*, 15474–82.
(22) Kohr, M. J.; Aponte, A.; Sun, J.; Gucek, M.; Steenbergen, C.; Murphy, E. Measurement of S-Nitrosylation Occupancy in the Myocardium with Cysteine-Reactive Tandem Mass Tags: Short Communication. *Circ. Res.* **2012**, *111*, 1308–12.
(23) Lee, T.-Y. Y.; Chen, Y.-J. J.; Lu, C.-T. T.; Ching, W.-C. C.; Teng, Y.-C. C.; Huang, H.-D. D.; Chen, Y.-J. J. dbSNO: A Database of Cysteine S-Nitrosylation. *Bioinformatics* **2012**, *28*, 2293–5.
(24) Liaudet-Coopman, E.; Beaujouin, M.; Derocq, D.; Garcia, M.; Glondu-Lassis, M.; Laurent-Matha, V.; Prébois, C.; Rochefort, H.; Vignon, F. Cathepsin D: Newly Discovered Functions of a Long-Standing Aspartic Protease in Cancer and Apoptosis. *Cancer Lett.* **2006**, *237*, 167–79.
(25) Větvicka, V.; Fusek, M. Activation of Peripheral Blood Neutrophils and Lymphocytes by Human Procathepsin D and Insulin-like Growth Factor II. *Cell. Immunol.* **1994**, *156*, 332–41.
(26) Maynadier, M.; Farnoud, R.; Lamy, P.-J. J.; Laurent-Matha, V.; Garcia, M.; Rochefort, H. Cathepsin D Stimulates the Activities of Secreted Plasminogen Activators in the Breast Cancer Acidic Environment. *Int. J. Oncol.* **2013**, *43*, 1683–90.

Chapter 3

Monitoring cysteine *S*-nitrosation in living cells.

Introduction:

Methods available for the quantification and assessment of global cysteine nitrosation are only amenable in cell lysates (*in vitro*) due to lack of compatibility with live cells (*in situ*).[1] *S*-nitrosothiols are often disrupted upon cell lysis and exposure to light.[2] Therefore, maintenance of endogenous *S*-nitrosothiols in soluble protein lysates is difficult due to the highly labile nature of this modification. Additionally, decomposition and rearrangement of *S*-nitrosothiols renders *in vitro* methods insufficient for the accurate assessment of this PTM in living systems. Therefore, alternative methods must be developed to gain a physiologically relevant picture of this modification.

Moving our focus to whole cell analysis will allow for a physiologically relevant account of cysteine nitrosation. Study of cysteines in whole cells can be challenging since capping these residues, especially those that play critical functional roles in live cells can result in cell death. Consequently, the use of the iodoacetamide probe (IAA) employed in our *in vitro* MS platform is not ideal. IAA is highly toxic to cells at concentrations too low for adequate detection of a majority of cysteines within the proteome (Figure 1B). In an effort to overcome this limitation, we utilized a caged electrophile that can be used to probe cells at high concentrations without the cytotoxic effects exhibited by IAA.

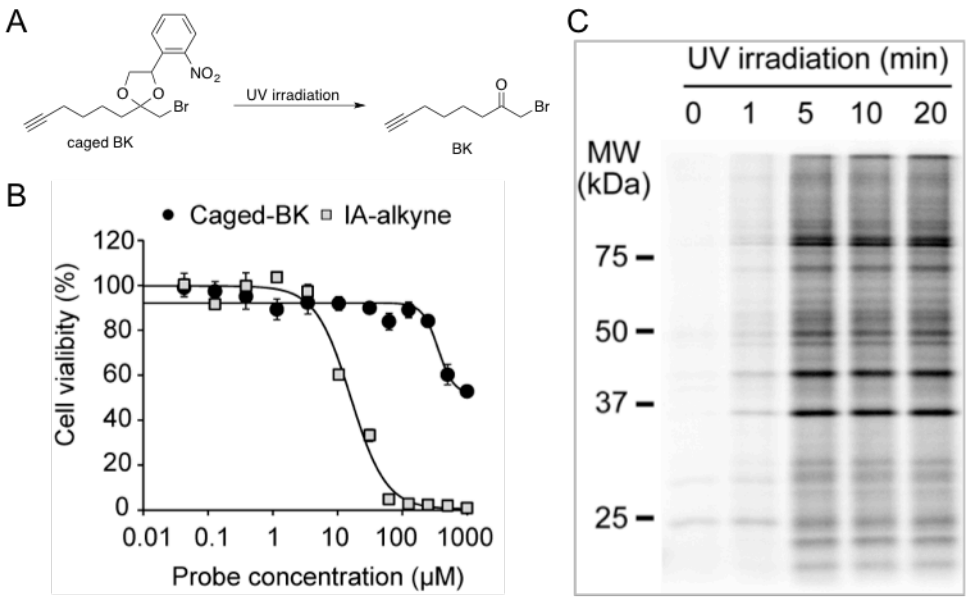

Figure 3-1 Caged BK as a probe to assess cysteine reactivity in living cells. (A) A cysteine reactive bromoketone electrophile is activated upon UV irradiation of Caged BK. (B) MTT assay displaying cytotoxic characteristics of CBK and IAA. (C) Fluorescent gel images of CBK labeling of HeLa cells after varying irradiation times. After 5 min of UV irradiation CBK fully uncaged and modifies proteins in living cells.

Caged bromomethylketone (CBK) is a photoprotected electrophilic probe that upon ultraviolet (UV) irradiation reveals a cysteine-reactive bromomethylketone (Figure 3-1A). [3] A 5-minute UV irradiation time allows for temporal and spatial control of bromomethylketone reactivity with cysteine residues (Figure 3-1C). Unlike IAA, CBK is amenable to the study of global cysteine reactivity in a whole cell context because this probe can be uncaged *in situ* and is not toxic to cells up to high micromolar concentrations (Figure 3-1B). After development of this caged electrophile, Abo et al. showcased the utility of CBK in a chemical probe-MS coupled platform to monitor cysteine oxidation events that result upon epidermal growth factor (EGF) activation of A431 cells. EGF stimulation of EGF receptor (EGFR) generates a burst of hydrogen peroxide, which oxidizes cellular cysteine residues. Using quantitative MS, cysteine

residues known to form redox-active disulfides and sulfenic acids were identified as oxidized upon cellular EGFR stimulation in living cells. This platform set the stage for identification and quantification of sites of cysteine nitrosation upon treatment with cell-permeable NO-donors and NOS inhibitors.

Unlike our *in vitro* study, we are unable to use GSNO to induce nitrosation in whole cells. Quantifying the amount of NO internalized by cells is difficult since GSNO is not completely cell permeable. [4–7] As an alternative to GSNO, *S*-nitrosocysteine (CysNO) was utilized since this smaller transnitrosation donor can traverse the cell membrane and increases overall NO levels (Figure 3-3B). [4–7] Exploration of cysteine sensitivity toward decreased NO levels upon NOS inhibition was also pursued. To achieve this, live cells were treated with N_{ω}-Nitro-L-arginine methyl ester (L-NAME), a pan NOS inhibitor (Figure 3-3C). [8] L-NAME treatment allows for a physiologically relevant and global account of cysteines sensitive toward *S*-nitrosation since this inhibitor regulates NOS directly in cells.

A Mass-spectrometry (MS) platform for the assessment of cysteine nitrosation *in situ*.

Our primary concern using a probe that is activated upon UV irradiation for the study of *S*-nitrosation is the tendency of *S*-nitrosothiols to photolyse when exposed to light. To quantify the extent of S-NO photocleavage of nitrosated peptides, GSNO was exposed to UV irradiation in PBS (Figure 3-2A). Relative concentrations of *S*-nitrosoglutathione in PBS were measured overtime and relative decrease in concentration was observed after 1 hour of UV irradiation (Figure 3-2B). However, for the short

photolysis time required to active CBK (5 min) minimal loss of *S*-nitrosothiols in the presence of UV light is observed. Additionally, reports have shown that protein SNOs are more difficult to photolyse, therefore, it is likely that under the CBK activation conditions the majority of protein SNOs are not disrupted. [9]

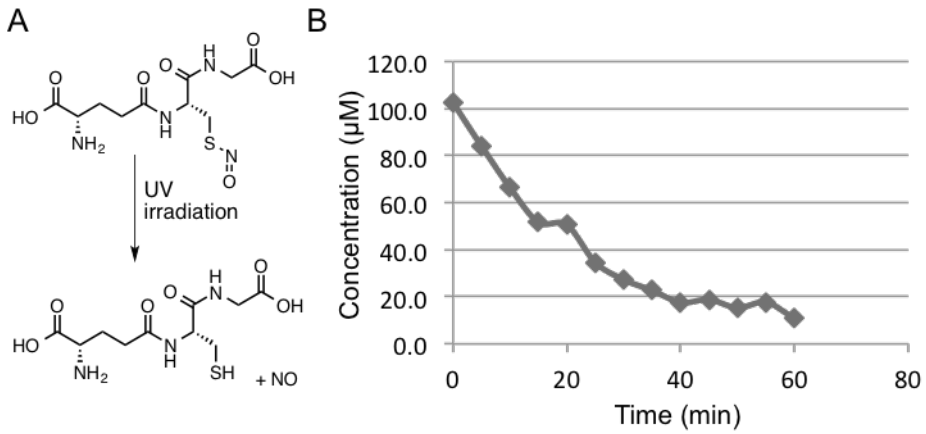

Figure 3-2 Quantification of GSNO S-NO photolysis up UV irradiation at room temperature. (A) *S*-nitrosothiol photocleavage after UV irradiation. GSNO concentrations are quantified at 335 nm (B) GSNO concentration decreases with longer exposure time to UV light. Decomposition of GSNO after 5 min of UV irradiation is minimal.

First, MCF-7 breast cancer cells were treated with either CysNO or L-NAME to increase or decrease cysteine nitrosation events, respectively (Figure 3-3A). Once treated, these cells are exposed to 200 μM CBK and allowed to incubate for one hour at 37 ˚C. These cells are then taken from the incubator for 5 minutes of UV irradiation on ice, to activate the bromomethylketone electrophile. Following irradiation, cells are incubated with the released electrophile at 37 ˚C for 20 minutes before being harvested and lysed. The cell lysates are subject to sodium borohydride reduction prior to MS preparation in order to reduce the ketone moiety, which is difficult to detect by MS. Once the sample is reduced and neutralized, soluble protein lysates are obtained and exposed to standard quantitative MS conditions. The CysNO and L-NAME treated samples undergo CuAAC

with the azo-light tag and the vehicle treated samples are tagged with azo-heavy tag. The light and heavy samples are combined to generate “CysNO versus vehicle” and “L-NAME versus vehicle” samples. These samples are analyzed using LC/LC-MS/MS and ratios are generated for the reactive cysteines based on their sensitivity toward nitrosation. A decrease in L:H ratio is expected upon a decrease in cysteine reactivity with CBK after CysNO treatment. When samples are treated with L-NAME cellular NO levels will decrease, leading to increased cysteine reactivity and L:H ratios greater than one. Upon data analysis, several cysteines were identified as susceptible toward *S*-nitrosation.

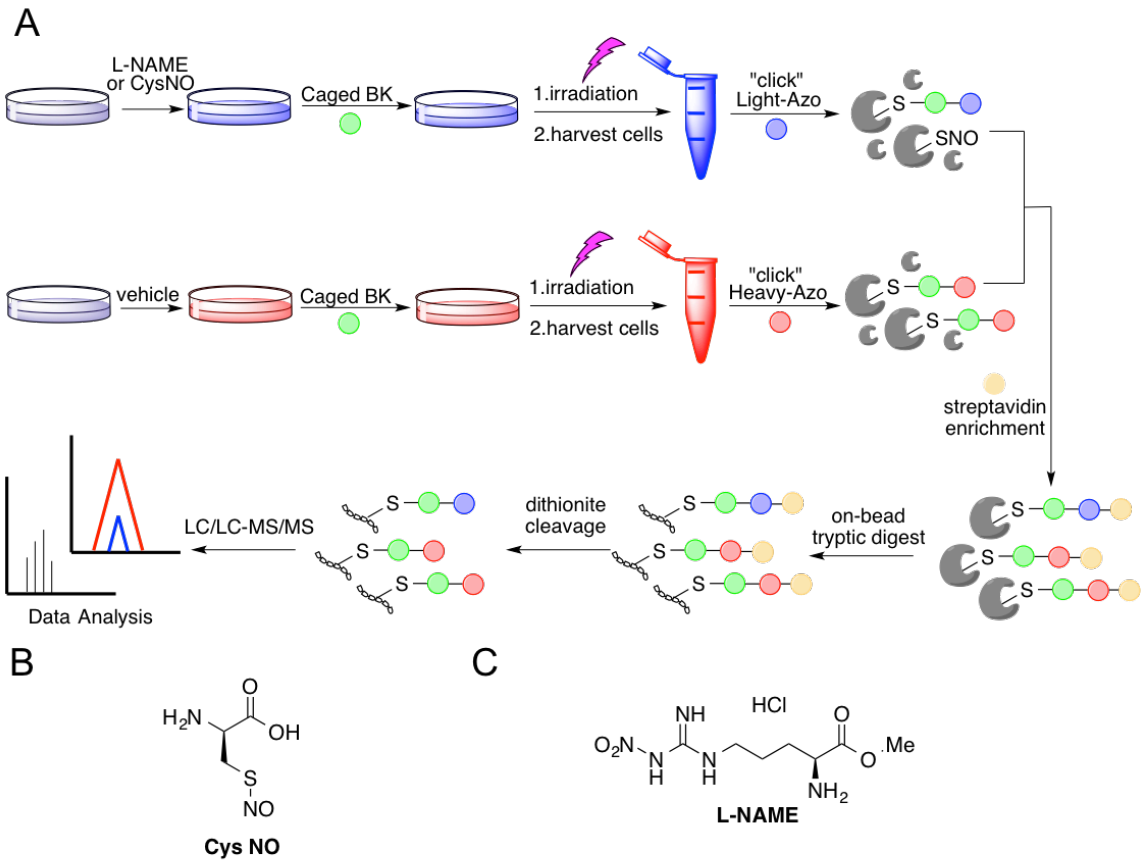

Figure 3-3 A MS platform for the assessment of cysteine nitrosation in living cells. (A) General MS workflow for analysis of cysteine reactivity changes resulting from Cys-NO or L-NAME treatment. (B) Structure of CysNO a low molecular weight transnitrosation donor. (C) Structure of L-NAME a pan NOS inhibitor.

The peptides identified after MS analysis were sorted by average ratios obtained from three biological replicates. Cysteines that possessed ratios <1 for the CysNO treated samples and >1 for the L-NAME treated data were then pooled. After sorting these data sets, we were able to rank and assemble a list of cysteines that show increased or decreased activity, in the L-NAME or CysNO samples respectively. Within the top 25 cysteines sensitive to *S*-nitrosation upon CysNO treatment, Cys413 of Aspartyl aminopeptidase (DNPEP), with an average L:H ratio of 0.68 ± 0.18, was identified. Subsequent comparison of the CysNO dataset with the L-NAME dataset, also found that Cys413 DNPEP increases in reactivity (L:H = 1.37±0.27) upon NOS inhibition. The appearance of Cys413 in both datasets strongly suggests that this cysteine is sensitive toward nitrosation. Cysteines present on Glutaredoxin 5 (Glrx5) and thymidine kinase 1 (TK1) also showed ratios greater than one indicating an increase in reactivity upon L-NAME treatment. These cysteines have been found to decrease in reactivity in previous *in vitro* GSNO MS experiments conducted by our laboratory.

Aspartyl amino peptidase (DNPEP)

Aspartyl amino peptidase, DNPEP, is a cytosolic aminopeptidase with specificity towards acidic residues at the N-terminus of protein substrates. [10] DNPEP is the only mammalian member of a poorly understood family of M18 peptidases that possess five metal coordinating residues forming a 'H.D.E.D.H' signature. This peptidase is termed aspartyl aminopeptidase due to its preference for aspartate over glutamate at the P1 position of the enzyme. Reports have found that DNPEP promotes the conversion of angiotensin I to angiotensin 2-10, as well as the conversion of angiotensin II to

angiotensin III *in vitro*, suggesting that this peptidase plays a role in the Renin-angiotensin system (RAS) and regulation of blood pressure. [11]

Members of the M18 family of peptidases tend to homo-oligomerize, similar to the self-compartmentalization strategy of proteasomes to confer specificity towards unfolded polypeptides over folded proteins. Specifically, DNPEP has been characterized as having a dodecameric architecture and is found to possess a dinuclear catalytic Zn^{2+} within its active site (Figure 3A). [12] During catalysis these Zn atoms activate water for nucleophilic attack at the amide-carbonyl of the substrate peptide, releasing the truncated peptide and aspartic acid. Recently, additional crystallographic evidence suggests a catalytic mechanism for DNPEP where H170, on a β8- β9 loop, is able to swap locations allowing for activation of peptide substrates for the hydrolysis by water within the metal-binding active site in the P1 pocket.

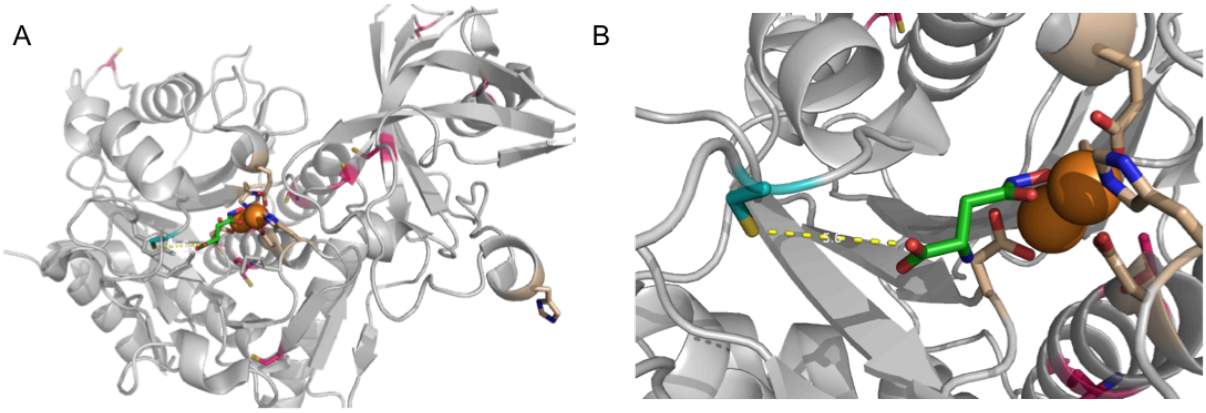

Figure 3-4 DNPEP possesses a cysteine with sensitivity toward *S*-nitrosation. (A) Crystal structure of DNPEP. Catalytic residues are highlighted in orange. (B) A close view of Cys314 in relation to P1 binding site of DNPEP.

Cys413 of DNPEP has not been previously annotated with a specific function.. After initial study of the DNPEP crystal structure, Cys314 is found on β17 loop, directly outside of the P1 binding pocket (Figure 3-4A). Using the co-crystalized inhibitor, L-aspartate-β-hydroxamate (ABH), as a mimic for substrate, the distance between the thiol

and substrate binding site is fairly small, 5.6Å (Figure 3-4B). Upon modification of Cys314 with NO, it is possible that this cysteine would occupy more space within the active site, interfering with substrate entering the P1 binding pocket. Alternatively, the *S*-nitrosothiol may inhibit the entry of the β8-β9 loop into the active site. Blocking the β8-β9 loop would decrease the activity of this enzyme since H107 will no longer be available for activation of the amide-carbonyl prior to hydrolysis.

Glutaredoxin 5 (Glrx5):

Glutaredoxins (Glrxs) are a family of GSH-disulfide oxidoreductases that possess a thioredoxin fold, a glutathione (GSH)-binding site, and a characteristic CSSC/S active site motif. [13] This enzyme family is involved in the maintenance of cellular redox homeostasis as well as cellular redox signaling. More specifically, Glrxs are implicated in the maintenance of cytosolic and mitochondrial iron homeostasis, and proteins within this family have been shown to coordinate [2Fe-2S] clusters. [13] To date four Glrxs have been identified in the human genome, two dithiol Glrxs (Glrx1 and Glrx2), a multidomain monothiol Glrx3, and a mitochondrial single-domain monothiol Glrx5.

Glutaredoxin 5 (Glrx5) is a 156 amino acid mitochondrial protein that plays an essential role in mitochondrial [Fe-S] transfer. [14] Glrx5 is highly conserved among eukaryotes and initial studies in yeast revealed that this enzyme plays an important role in mitochondrial iron-sulfur cluster biogenesis. Phylogenetic profiling suggests that Glrx5 is part of the Isc iron-sulfur assembly machinery. [14] Recent studies provide further evidence that Glrx5 is required for transfer and insertion of clusters into acceptor proteins after the clusters have been assembled on the IscU scaffold protein. Disruptions of [Fe-S]

biogenesis can lead to serious human diseases. [15] Deficiencies in Glrx5 cause severe microcytic anemia in zebrafish mutants and congenital sideroblastic anemia (CSA) or variant nonketotic hyperglycemia (vNKH) in their human counter parts.[16]

Upon treatment of MCF-7 cells with L-NAME and subsequent probing of reactive cysteines with CBK, we identified Cys67 of Glrx5 to increase in reactivity (L:H ratio = 1.34±0.16) upon reduction of cellular NO levels. Cys67 is known to coordinate to the [2Fe-2S] cluster within the dimeric form of Glrx5 (Figure 4). This cysteine is essential for proper maturation of iron-sulfur clusters. [16] Mutation of this cysteine to serine results in a significant decrease in activity of proteins, such as aconitase, that rely on iron-sulfur cluster maintained in cells. The increase in Cys67 reactivity toward CBK suggests that *S*-nitrosation of Glrx5 can potentially regulate iron-sulfur cluster synthesis and transfer. *S*-nitrosothiol formation on Cys67 may help facilitate the release of the iron-sulfur clusters from Glrx5 and promote transfer to other proteins that require the cluster for activity.

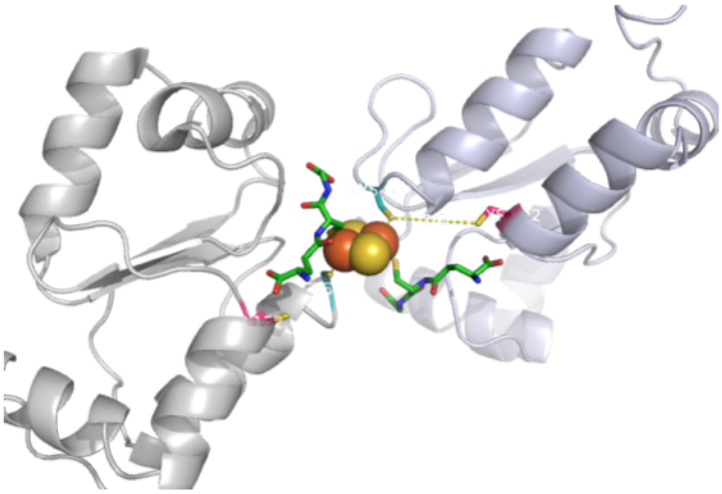

Figure 3-5 Metal binding cysteine of Glrx5 is sensitive to *S*-nitrosation. NO-modified cysteine is highlighted in cyan and only remaining cysteine in Glrx5 is highlighted in pink.

It is also of note that the only other cysteine residue present in Glrx5, Cys122, is in close proximity to Cys67. These two cysteines are separated by a 7.6-8.4 Å sulfur-to-sulfur distance, which could accommodate the formation of a disulfide within the protein upon removal of the iron-sulfur cluster (Figure 3-5). It is not uncommon for *S*-nitrosothiols to serve as precursors in disulfide bond formation on proteins. [17] Furthermore, there is evidence that formation of disulfide bonds within the active site of other Glrxs help maintain enzyme activity. [18,19] In the case of Glrx2, an intramolecular disulfide bond is made prior to regeneration of the active form of the enzyme to prevent overoxidation of the cysteine chelate. Therefore, a possible mechanism for iron-sulfur cluster release may involve *S*-nitrosation of Cys67 to release the iron-sulfur cluster from Glrx5. Subsequent formation of a disulfide bond with Cys122 may allow for resolution of the nitrosated cysteine to preserve the active site of Glrx5 for later iron-sulfur synthesis.

Summary and future directions

Using CBK as an alternative probe for the assessment of cysteine reactivity, we were able to develop a MS platform for the quantification of global cysteine nitrosation in living cells. Two complimentary NO-level perturbing small molecules were used: CysNO, a transnitrosation donor, and L-NAME, a NOS inhibitor, to modulate levels on NO within whole cells. We identified Cys413 of DNPEP as a cysteine sensitive to *S*-nitrosation upon CysNO and L-NAME treatment. Additionally, Cys67 of Glrx5 was identified to increase in activity upon L-NAME treatment. To elucidate the role of *S*-nitrosation on protein activity of these cysteines further experiments are necessary.

To characterize the role Cys413, WT DNPEP will be subcloned and a Cys413 mutant will be generated. After overexpression and purification of DNPEP WT and its C413S mutant, a BST experiment can be preformed to confirm that NO-modification of C415 occurs as a result of increasing the levels of NO in living cells. We expect to observe an enrichment of wild-type DNPEP upon cellular NO treatment, which will be monitored by western blot using a DNPEP antibody after pull-down of formerly-biotinylated proteins. When the C413S mutant is exposed to increased levels of NO, *S*-nitrosation should not occur thus decreasing the amount of biotinylated DNPEP observed by western blot. Overall, use of the BST would confirm that our MS platform is an efficient alternative for the identification and assessment of nitrosated cysteines in a complex system.

Next, recombinant WT DNPEP and the C413S mutant proteins will be utilized to study the effect of *S*-nitrosation on protease activity. A fluorometric Asp-*p*-nitroaniline or L-aspartic acid 7-amido-4-methylcoumarin (Asp-AMC) hydrolysis assay can be used to assess differences in wild-type and mutant activity.[20] A decrease in activity observed for the mutant protein would suggest that Cys413 plays a substantial role in DNPEP activity that was previously overlooked. It is of note that Cys413 is highly conserved in eukaryotes suggesting that this residue may play an essential role in protein function.[12]

If no change in activity between wild-type and mutant variants of the protein is observed, study of the WT DNPEP upon covalent modification with CBK or IAA may provide greater insight into potential regulatory roles that Cys413 has on protease activity. Known inhibitors of DNPEP function by occupying the activity site, blocking substrate from entering the enzyme for hydrolysis. Since the free thiol of Cys413 is

directed toward the active site of the enzyme, it is possible that modification by NO or a covalent small molecule could also occupy the active site preventing entry of substrate peptides. A decrease in enzyme activity upon IAA or CBK treatment would suggest that modification of Cys413 regulates enzyme function.

Further study of Cys67 of Glrx5 and the potential catalytic significance of *S*-nitrosothiol formation will require overexpression of WT and two cysteine mutants, C67S and C122S. Protein activities of each of the cysteine mutants will be assessed by monitoring the efficiency of iron-sulfur cluster synthesis and transfer through an aconitase coupled assay[15] as well as a fluorescence-based eosin 5-isothiocyanate assay.[21] A substantial decrease in Cys67 mutant activity has been previously reported.[15]

However, Cys122 has not been studied to the same extent. A decrease in activity upon Cys122 mutation would suggest that it plays significant a role in Glrx5 function. Further study of the changes in redox potentials of WT and Glrx5 mutants in the presence of NO-donor will be necessary to expose a link between *S*-nitrosothiol formation, cysteine oxidation and enzyme function. BST can be used to study Glrx5 WT and cysteine mutants to observe nitrosation of these proteins after transient transfection. This method will confirm whether Glrx5 undergoes nitrosation as well as identify which cysteine residue is modified by NO. Later studies can focus on the role that nitrosation may play on iron sulfur cluster biosynthesis and maturation, by monitoring iron sulfur formation in the presence of increasing concentrations of NO.

Acknowledgements.

I would like to acknowledge Masahiro Abo for providing the CBK probe used in these experiements.

Experimental procedures

Materials and general procedure

All materials were purchased from Sigma Aldrich unless otherwise noted. RPMI 1640 medium, DMEM/High glucose medium, Phosphate buffered saline (PBS) buffer, 2% Trypsin-EDTA and penicillin streptomycin (Pen/Strep) were purchased from Fisher Scientific (Pittsburgh, PA). Potassium phosphate tribasic monohydrate was purchased from Fisher Scientific (Pittsburgh, PA). All protein concentrations were determined using a Bio-Rad DC protein assay kit with reagents from Bio-Rad Life Science (Hercules, CA). Illusta Nap-5 Columns were purchased from GE Healthcare Bio-Sciences (Piscataway, NJ). Streptavidin-agarose beads were purchase from Thermo Scientific (Armarillo, TX).

Mass-spectrometry analysis of CysNO-treated MCF7 cells

S-*nitrosocysteine* (CysNO) was generated following the preparation of S-Nitrosothiol procedure by Schoenfisch *et al* (Ricco, D. A., Nuts, S. T., Schoenfisch, M. H. *Anal Chem* **2012**, *84*, 851-6). MCF-7 cells grown to ~100% confluency were treated with either 100 μM CysNO or the corresponding volume of buffer. Cells were incubated in the presence of CysNO for 1 hour before removal of media. New media containing 200 μM CBK was added followed by incubation at 37 ˚C for 1 hour. Media was then

removed and placed with PBS. The cells were then placed on ice and irradiated under UV-light for 5 min. The PBS is then removed and replaced with complete media. Cells then incubate at 37 ˚C for 20 min before harvest by scraping.

MCF-7 cell pellets were lysed in PBS and protein concentrations were determined and normalized. Subsequent lysates were subjected to standard CuAAC with light or heavy azo-tags and mass-spectrometry analysis as described previously (Qian, Y. and Weerapana, E. et al. *Chem. Biol. Chem,* **2013**, *14*, 1410-14).

Mass-spectrometry analysis of L-NAME-treated MCF7 cells

MCF-7 cells at ~100% confluency were treated with either 100 μM L-NAME or the corresponding volume of water. Cells were incubated in the presence of L-NAME overnight (~16 hours) before removal of media. New media containing 200 μM CBK was added followed by incubation at 37 ˚C for 1 hour. Media was then removed and replaced with PBS. The cells were then placed on ice and irradiated under UV-light for 5 min. The PBS is then removed and replaced with fresh media. Cells then incubate at 37 ˚C for 20 min before harvest by scraping.

MCF-7 cell pellets were lysed in PBS and protein concentrations were determined and normalized. Subsequent lysates were subjected to standard CuAAC with light or heavy azo-tags and mass-spectrometry analysis as described previously (Qian, Y. and Weerapana, E. et al. *Chem. Biol. Chem,* **2013**, *14*, 1410-14).

MS data analysis

The generated tandem MS data was searched using the SEQUEST algorithm against the human IPI database. A static modification of +57.02146 cysteine was specified to account for iodoacetamide alkylation and differential modifications of +443.2897 (Azo-L modification) and +449.3035 (Azo-H modification) were specified on cysteine to account for bromomethylketone probe modifications. SEQUEST output files were filtered using DTASelect 2.0. Quantification of light/heavy ratios (R) was performed using the CIMAGE quantification package as previously described (Weerapana, E., Speers, A. E. Cravatt, B. F. *Nat. Protoc.* **2007**, *2*, 1414-25).

References

(1) Couvertier, S. M.; Zhou, Y.; Weerapana, E. Chemical-Proteomic Strategies to Investigate Cysteine Posttranslational Modifications. *Biochim. Biophys. Acta* **2014**, *1844*, 2315–2330.

(2) Singh, R. J.; Hogg, N.; Joseph, J.; Kalyanaraman, B. Mechanism of Nitric Oxide Release from S-Nitrosothiols. *J. Biol. Chem.* **1996**, *271*, 18596–603.

(3) Abo, M.; Weerapana, E. A Caged Electrophilic Probe for Global Analysis of Cysteine Reactivity in Living Cells. *J. Am. Chem. Soc.* **2015**, *137*, 7087–90.

(4) Broniowska, K. A.; Zhang, Y.; Hogg, N. Requirement of Transmembrane Transport for S-Nitrosocysteine-Dependent Modification of Intracellular Thiols. *J. Biol. Chem.* **2006**, *281*, 33835–41.

(5) Zhang, Y.; Hogg, N. The Mechanism of Transmembrane S-Nitrosothiol Transport. *Proc. Natl. Acad. Sci. U.S.A.* **2004**, *101*, 7891–6.

(6) Broniowska, K. A.; Hogg, N. The Chemical Biology of S-Nitrosothiols. *Antioxid. Redox Signal.* **2012**, *17*, 969–80.

(7) Broniowska, K. A.; Diers, A. R.; Hogg, N. S-Nitrosoglutathione. *Biochim. Biophys. Acta* **2013**, *1830*, 3173–81.

(8) Pfeiffer, S.; Leopold, E.; Schmidt, K.; Brunner, F.; Mayer, B. Inhibition of Nitric Oxide Synthesis by NG-Nitro-L-Arginine Methyl Ester (L-NAME): Requirement for Bioactivation to the Free Acid, NG-Nitro-L-Arginine. *Br. J. Pharmacol.* **1996**, *118*, 1433–40.

(9) Gow, A.; Doctor, A.; Mannick, J.; Gaston, B. S-Nitrosothiol Measurements in Biological Systems. *J. Chromatogr. B Analyt. Technol. Biomed. Life Sci.* **2007**, *851*, 140–51.

(10) Wilk, S.; Wilk, E.; Magnusson, R. P. Purification, Characterization, and Cloning of a Cytosolic Aspartyl Aminopeptidase. *J. Biol. Chem.* **1998**, *273*, 15961–70.
(11) Banegas, I.; Prieto, I.; Vives, F.; Alba, F.; de Gasparo, M.; Segarra, A. B.; Hermoso, F.; Durán, R.; Ramírez, M. Brain Aminopeptidases and Hypertension. *J Renin Angiotensin Aldosterone Syst* **2006**, *7*, 129–34.
(12) Chaikuad, A.; Pilka, E. S.; De Riso, A.; von Delft, F.; Kavanagh, K. L.; Vénien-Bryan, C.; Oppermann, U.; Yue, W. W. Structure of Human Aspartyl Aminopeptidase Complexed with Substrate Analogue: Insight into Catalytic Mechanism, Substrate Specificity and M18 Peptidase Family. *BMC Struct. Biol.* **2012**, *12*, 14.
(13) Johansson, C.; Roos, A. K.; Montano, S. J.; Sengupta, R.; Filippakopoulos, P.; Guo, K.; von Delft, F.; Holmgren, A.; Oppermann, U.; Kavanagh, K. L. The Crystal Structure of Human GLRX5: Iron-Sulfur Cluster Co-Ordination, Tetrameric Assembly and Monomer Activity. *Biochem. J.* **2011**, *433*, 303–11.
(14) Alves, R.; Sorribas, A. In Silico Pathway Reconstruction: Iron-Sulfur Cluster Biogenesis in Saccharomyces Cerevisiae. *BMC Syst Biol* **2007**, *1*, 10.
(15) Liu, G.; Wang, Y.; Anderson, G. J.; Camaschella, C.; Chang, Y.; Nie, G. Functional Analysis of GLRX5 Mutants Reveals Distinct Functionalities of GLRX5 Protein. *J. Cell. Biochem.* **2016**, *117*, 207–17.
(16) Ye, H.; Jeong, S. Y.; Ghosh, M. C.; Kovtunovych, G.; Silvestri, L.; Ortillo, D.; Uchida, N.; Tisdale, J.; Camaschella, C.; Rouault, T. A. Glutaredoxin 5 Deficiency Causes Sideroblastic Anemia by Specifically Impairing Heme Biosynthesis and Depleting Cytosolic Iron in Human Erythroblasts. *J. Clin. Invest.* **2010**, *120*, 1749–61.
(17) Hogg, N. The Biochemistry and Physiology of S-Nitrosothiols. *Annu. Rev. Pharmacol. Toxicol.* **2002**, *42*, 585–600.
(18) Lundberg, M.; Johansson, C.; Chandra, J.; Enoksson, M.; Jacobsson, G.; Ljung, J.; Johansson, M.; Holmgren, A. Cloning and Expression of a Novel Human Glutaredoxin (Grx2) with Mitochondrial and Nuclear Isoforms. *J. Biol. Chem.* **2001**, *276*, 26269–75.
(19) Johansson, C.; Kavanagh, K. L.; Gileadi, O.; Oppermann, U. Reversible Sequestration of Active Site Cysteines in a 2Fe-2S-Bridged Dimer Provides a Mechanism for Glutaredoxin 2 Regulation in Human Mitochondria. *J. Biol. Chem.* **2007**, *282*, 3077–82.
(20) Chen, Y.; Tang, H.; Seibel, W.; Papoian, R.; Oh, K.; Li, X.; Zhang, J.; Golczak, M.; Palczewski, K.; Kiser, P. D. Identification and Characterization of Novel Inhibitors of Mammalian Aspartyl Aminopeptidase. *Mol. Pharmacol.* **2014**, *86*, 231–42.
(21) Coppo, L.; Montano, S. J.; Padilla, A. C.; Holmgren, A. Determination of Glutaredoxin Enzyme Activity and Protein S-Glutathionylation Using Fluorescent Eosin-Glutathione. *Anal. Biochem.* **2016**, *499*, 24–33.

Chapter 4

Development of a MS platform to study cysteine oxidation oscillation as a function of circadian rhythm.

Circadian rhythm and the peroxiredoxin cycle:

Circadian rhythms are characterized as any biological process that displays an endogenous oscillation of about 24 hours. The development of circadian rhythms is hypothesized to be evolutionarily advantageous, providing organisms the ability to regulate physiological processes to best align with temporal changes of a solar day. DNA damage induced by solar irradiation, for example, is preferentially repaired in the late afternoon and early evening, as opposed to early times in the day when sun exposure is at its peak. [1] The oscillation of biological functions is directly regulated by a circadian clock, which is genetically encoded in nearly every cell within an organism. Circadian rhythms are essential for normal cellular function. When circadian rhythms are altered diseases such as cancer have been shown to occur.[2]

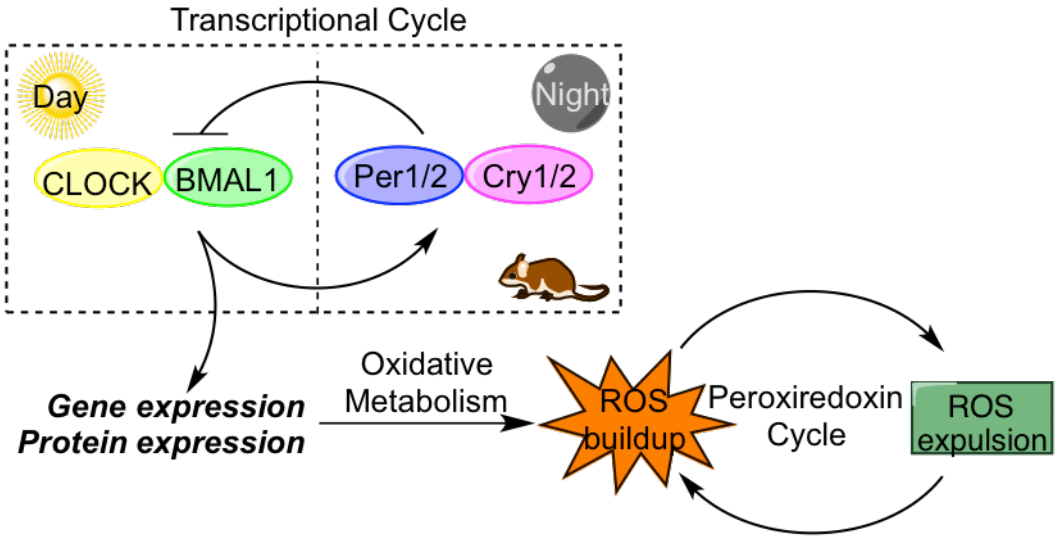

Figure 4-1 The circadian cycle. Fluctuations in gene and protein expression is representative of a circadian oscillation. Oxidative metabolism generates ROS, which is cleared from cells by the Peroxiredoxin cycle.

On a molecular level, a central circadian clock consisting of two proteins, CLOCK and BMAL in mammals or CLOCK and CYCLE in drosophila, controls daily

cycles (Figure 4-1). These proteins come together to form a heterodimeric complex, which activates the transcription of PERIOD and CRYPTOCHROME and PERIOD and TIM, in mammals and drosophila respectively.[3,4] These proteins are shuttled out of the nucleus where they become phosphorylated. Upon phosphorylation, these proteins reenter the nucleus and act as a negative feedback loop that downregulates the Clk-complexes. This activation and deactivation of cellular transcription creates a cycle, otherwise known as circadian rhythm.

The upregulation of transcription by Clk-complexes also increases the transcription of proteins responsible for oxidative metabolism. Oxidative metabolism not only results in energy production for the organism, but it also leads to the generation of reactive oxygen species (ROS) (Figure 4-1).[5] ROS, if not maintained, can lead to oxidative stress and damage the cell. To maintain cellular oxidation levels, proteins called peroxiredoxins (Prxs) have evolved to clear toxic ROS from cells and restore cellular homeostasis. This oscillation of ROS levels in cells is also known as the Peroxiredoxin cycle.[6]

Almost all living organisms possess peroxiredoxins. Recently, a link between circadian rhythms in metabolism and peroxiredoxin (Prx) oxidation oscillation has been purposed as a means of monitoring circadian processes.[7,8] Substrates of Prxs include cellular oxidants, such as hydrogen peroxide, and oxidized proteins. The peroxidase activity exhibited by Prxs is dependent on the oxidation of a 'peroxidatic' cysteine (C_p) residue in the active site of these proteins (Figure 4-3A). Across species this cysteine is highly conserved and is essential for efficient resolution of ROS.[9] The catalytic cysteine can also become hyperoxidized, rendering the Prx catalytically inactive. In the case of 2-

Cys peroxiredoxins, a 'resolving' cysteine (C_r) is essential for the regeneration of the active form of the enzyme by forming a disulfide with the 'peroxidatic' cysteine. The disulfide is reduced by thioredoxin to generate the active form of the enzyme. Under high oxidative stress Prxs can also be overoxidized to a sulfinic acid state, which until recently was thought to irreversibly inactivate peroxiredoxins. However, Biteau et al. has reported the overoxidized peroxiredoxins can be recycled by sulphiredoxin, by a process that requires ATP. [10,11]

When studying peroxiredoxin rhythms in the fruit fly *Drosophila melanogaster*, a direct correlation between the oscillation of TIM transcription and that of oxidation of Prx has been reported. [7] When key proteins responsible for the maintenance of circadian rhythm in the fly are mutated, non-cycling expression of the circadian components PER and TIM were observed. Further examination of the peroxiredoxin oxidation pattern found an altered circadian phase exhibited by the per^{01} and Clk^{Jrk} mutant flies with respect to wild-type. This indicates that the perturbed circadian timing in the mutants has a direct connection with relative peroxiredoxin oxidation over time. This finding has inspired our efforts to develop a method for the evaluation of changes in reactivity of cysteine residues sensitive to oxidation changes during a circadian cycle.

We used *Drosophila melanogaster* as our model organism, harvested at 4-hour time points during a 24-hour period. Using time = 0 as a control, we compared each of the subsequent time points with respect to cysteine reactivity with IA alkyne (IAA). These samples were analyzed using MS to quantify cysteine reactivity and assess the change in reactivity of a specific cysteine over time.

Mass Spectrometry Platform of the analysis of *Drosophila* cysteine oxidation oscillation

In collaboration with the Rosbash Lab, we were able to harvest *Drosophila* heads at time points 0, 4, 8, 12 16 and 20 hour of a circadian day. The fly heads were lysed and probed with IAA, to cap reactive cysteine free thiols. Cu(I)-catalyzed alkyne-azide cycloaddition (CuAAC) was performed using Azo-light and Azo-heavy tags as described for previous S-nitrosation MS platforms (Figure 2). For the fly samples, time = 0 samples were treated with azo-heavy tag and the later time points were treated with azo-light tag. Click chemistry reaction samples from time points 4, 8, 12, 16 and 20 hours were combined with a time point 0 hour control sample. The resulting combined samples were enriched on streptavidin beads overnight before exposure to denaturation, free-thiol capping and on-bead trypsin digestion steps. After removal of the free tryptic peptides, the bound modified cysteine-containing peptides were cleaved off the beads using sodium dithionite. These azo-samples were analyzed using LC/LC-MS/MS to identify cysteines with oscillations in reactivity toward IAA over a circadian day.

Initial analysis of the *Drosophila* data presented many cysteines that oscillate during the solar cycle. First, the data was analyzed for peroxiredoxins that oscillate, since previous studies suggest that Prxs are markers for circadian rhythm. Ratios obtained for a cysteine present on *Drosophila* Peroxiredoxin 5, Prx5, were found to oscillate during a circadian day. Additionally, we identified drosophila Thioredoxin reductase 1 (Trxr-1) and DJ-1 beta as two other novel proteins with cysteines that appear to oscillate during a circadian cycle.

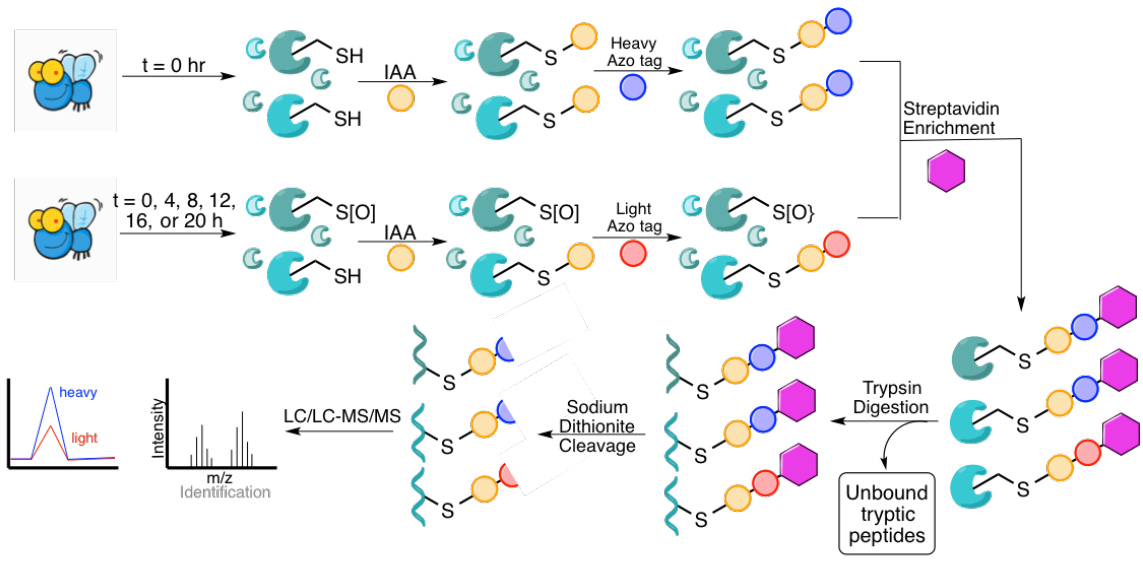

Figure 4-2 A MS platform for the assessment of cysteine oxidation during a circadian day. Cell lysates obtained from *Drosophila melanogaster* heads were probed with IAA. Probed lysates were subject to standard CuAAC conditions with azo-heavy (t = 0 h; control) or azo-light (t = 0, 4, 8, 12, 16, 20 h). Biotinylated proteins were enriched and later digested to afford tryptic peptides. MS analysis of tryptic peptides allowed for monitoring of cysteine reactivity changes over time.

Peroxiredoxin 5

Peroxiredoxin 5 (Prx5) is an atypical 2-Cys peroxiredoxin, which exhibits a wide subcellular distribution compared to other peroxiredoxin isoforms. [12,13] Interestingly, human Prdx5 was first described as a DNA-binding protein potentially implicated in RNA-polymerase-II-driven transcription regulation within the nucleus. [14] Later study of this enzyme found that it also functions within cellular peroxisomes, mitochondria, and cytosol. [15–18] Within these organelles, Prx5 exhibits thiol-peroxidase reactivity and cytoprotective antioxidant activity. More specifically, overexpression in the nucleus and mitochondria upon increased oxidative stress may help protect nuclear and mitochondrial DNA from oxidative damage. It is of note that orthologous Prx5 in *Drosophila melanogaster* is also expressed in mitochondria, nucleus and the cytosol, and

demonstrates not only protection from oxidative stress and apoptosis but also serves to promote longevity in the fly. [19]

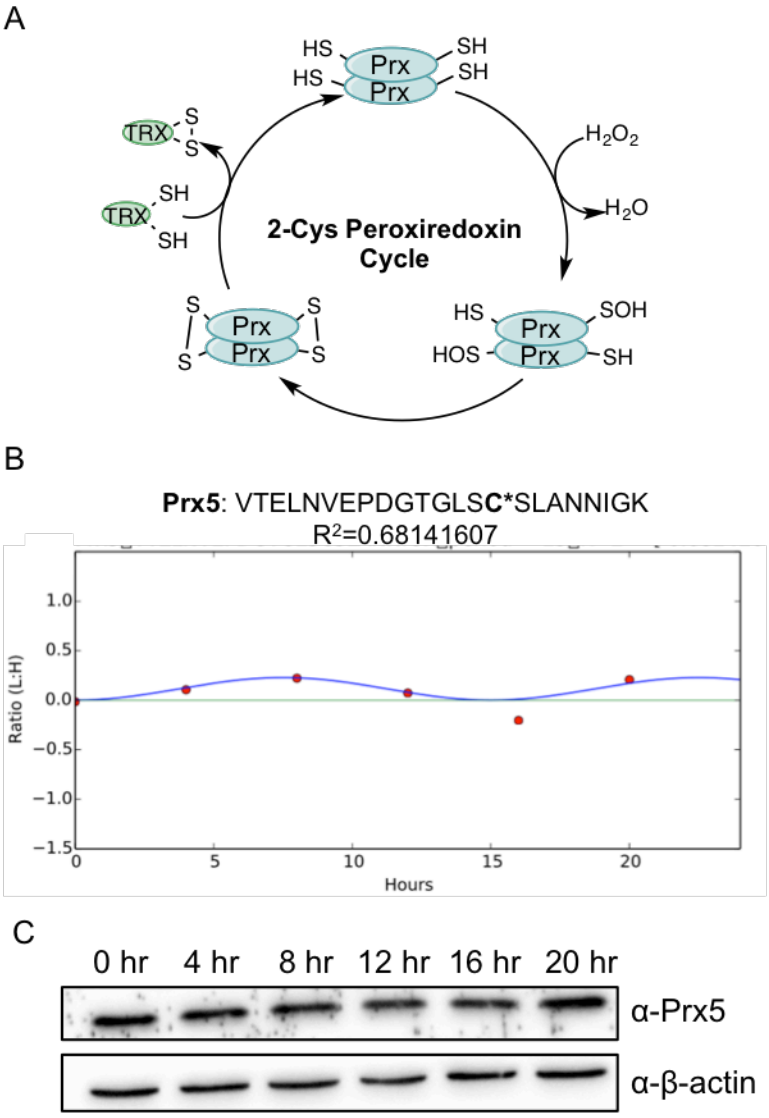

Figure 4-3 A cysteine on Peroxiredoxin 5 oscillates during a circadian cycle. (A) 2-Cys peroxiredoxin catalytic cycle. (B) The resolving Cys181 of *Drosophila* Prx5 oscillated in reactivity over a 20-hour period. (C) Immunoblot of relative Prx5 concentration in fly time point lysates. No fluctuation

Though Prx5 has conserved active-site cysteine residues similar to other 2-Cys peroxiredoxins, the mechanism by which this peroxiredoxin reduces cellular oxidants

varies. Typical resolution of the oxidized peroxidatic cysteine (C_p) occurs by intermolecular disulfide formation with dimer-pair resolving cysteine (C_r) (Figure 4-3A). Alternatively, crystallographic analysis of reduced Prx5 versus oxidized Prx5 suggests that resolution of oxidized C_p comes from the C_r within the same monomer forming an intramolecular disulfide in Prx5. [20,21] Therefore; the reduction of active Prx5 is directly catalyzed by cytosolic thioredoxin 1 and mitochondrial thioredoxin-2 in the cytosol and mitochondria, respectively.

MS analysis of the circadian *Drosophila* samples identified Cys181 to oscillate in reactivity during a 24-hour cycle (Figure 4-3B). Cys181 is homologous to resolving cysteine, Cys204, of human peroxiredoxin 5. Throughout the peroxiredoxin catalytic cycle the reactivity Cys204 fluctuates as this residue alternates between a reduced thiol and oxidized disulfide with the C_p. The oscillation in cysteine reactivity observed by MS supports the oscillatory mechanism of 2-Cys peroxiredoxins, where the resolving cysteine cycles between a free thiol and oxidized disulfide intermediate.

A western blot was utilized to confirm that the cysteine ratio oscillation observed is a product of cysteine reactivity changes over time and not of relative changes in Prx5 level at various time points (Figure 4-3C). Using a *Drosophila* Prx5 antibody, we analyzed the relative amount of Prx5 at each of the 4-hour intervals. Uniform Prx5 concentrations across each of the time points were observed, with respect to a β-actin control. Constant Prx5 levels indicate that the changes in cysteine reactivity measured are not the result of changing protein expression over time. These data further support that the change observed in Cys181 reactivity with IAA overtime is measure of changes in oxidation state of this cysteine.

Thioredoxin Reductase 1

Thioredoxin reductases (TrxRs) are homodimeric flavoproteins that belong to the pyridine nucleotide-disulfide oxidoreductase family. [22,23] TrxRs are the only enzymes known to catalyze the reduction of thioredoxin making these enzymes a central component of the thioredoxin system. *Drosophila* thioredoxin reductase 1 (Trxr1) is orthologous to mammalian thioredoxin reductase 2 (TrxR2). Bearing a mitochondrial targeting sequence, TrxR2 is the mitochondrial thioredoxin reductase in mammals. Like most pyridine nucleotide disulfide reductases TrxR2 possesses an N-terminal active site motif, **C***VNVG**C***. However, specific to TrxRs, TrxR2 also has a C-terminal extension sequence containing Gly-Cys-Sec-Gly. In *Drosophila*, the C-terminal extension sequence contains a Ser-Cys-Cys-Ser motif. [23]

Mammalian TrxR2 is found as a head to tail dimer when in its active form. Electrons are transferred from NADPH to the N-terminal redox-active dithiol motif, subsequently to the selenenylsulfide of the other subunit, and finally to disulfide substrates of mammalian TrxR2 (Figure 4-4A). [23] With two active sites, TrxR2 has a broad range of substrates including proteins such as thioredoxin 2 (Trx2) and glutaredoxin 2 (Glrx2). Therefore, as the first step of the thioredoxin antioxidant system within the mitochondria, TrxR2 is directly linked to maintaining mitochondrial ROS levels.

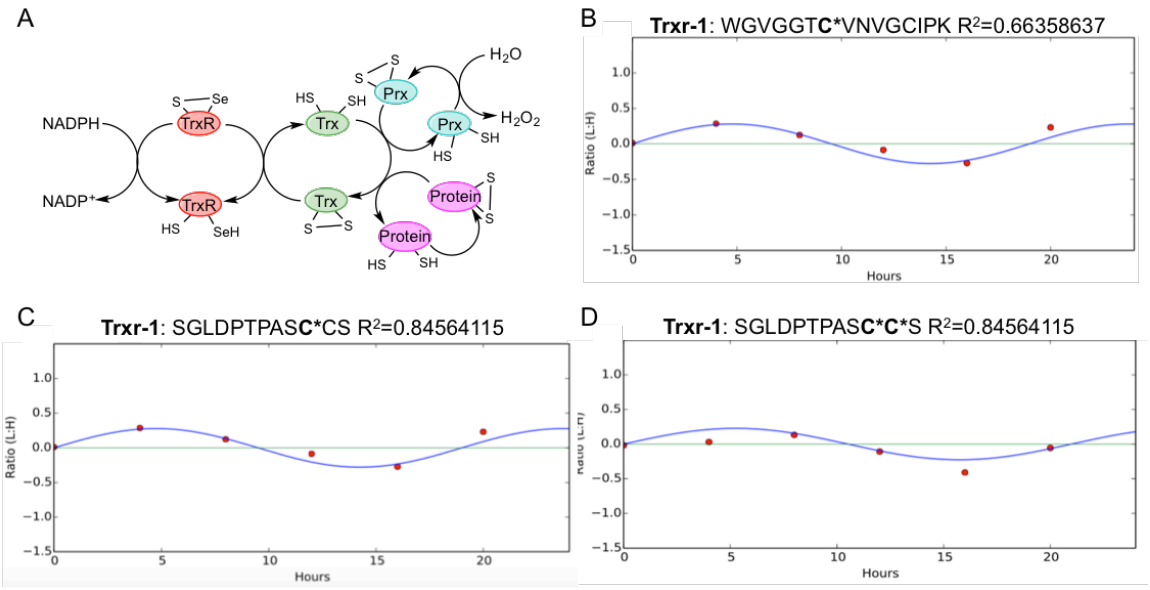

Figure 4-4 Trxr-1 oscillates during a circadian cycle. (A) The thioredoxin system is responsible the reduction of cellular oxidants and oxidized proteins in the cell. NADPH is the molecular reducing agent in this system. (B) Cys162 of *Drosophila* Trxr-1 oscillates over a 20-hour period. (C/D) Cys594/595 of *Drosophila* Trxr-1 oscillate over a 20-hour period.

The MS data obtained from the circadian *Drosophila* head samples identified multiple cysteines in fly Trxr-1 that cycle over a 24-hour period (Figure 4-4 A, B, C.) The three cysteines identified, Cys162, Cys594 and Cys595, are present in the thioredoxin disulfides required for thioredoxin function of Trxr-1. These cysteines oscillate with similar phase and intensity to Prx5. Being the central component of the thioredoxin system in the mitochondria; Trxr-1 is ultimately responsible for enzyme-regulated reduction of Prx5. Thus, the similar oscillating pattern observed for Trxr-1 and Prx5 may indicate a direct relationship between oxidation states of these two proteins over time. Further characterization of relative concentrations of Trxr-1 overtime is necessary. In the future, western blotting will be used to identify if the changes in cysteine reactivity observed by MS are a product of protein concentration fluctuations or change in oxidation state of Trxr-1.

DJ-1 beta

Protein deglycase DJ-1 in mammals is responsible for the repair of methylglyoxal- and glyoxal-glycated proteins by removal of the resulting lactate or glycolate-conjugates, respectively. [24] Removal of glycates from cysteine, arginine, and lysine residues reactivates protein substrates of DJ-1 and prevents the formation of advanced glycation endproducts (AGE). [25] AGE formation increases under oxidative stress, which is thought to be one factor in age-related chronic diseases. DJ-1 eliminates sources of redox-stress, such as hydrogen peroxide, and protects cells from hydrogen peroxide-induced cell death. Additionally, reports have shown that DJ-1 acts as an oxidative stress sensor as well as a redox-sensitive chaperone and protease. [26–28] Therefore, DJ-1 plays an important role in cell protection against oxidative stress.

A highly conserved cysteine residue is found within the active site of DJ-1 and mutagenesis of this residue abolishes enzymatic activity. [29,30] This cysteine residue acts a catalytic nucleophile and reacts with the carbonyl carbon of glyoxals, such as methylglyoxal, resulting in the formation of a hemithioacetal (Figure 4-5A). [30] Next, a *cis*-enediol is formed after proton abstraction by a basic residue within the active site. The enediol later reacts with a proton within the active affording D-lactoylcysteine. Subsequent hydrolysis of the thioester releases D-lactate from the active site and regenerates the catalytic nucleophile.

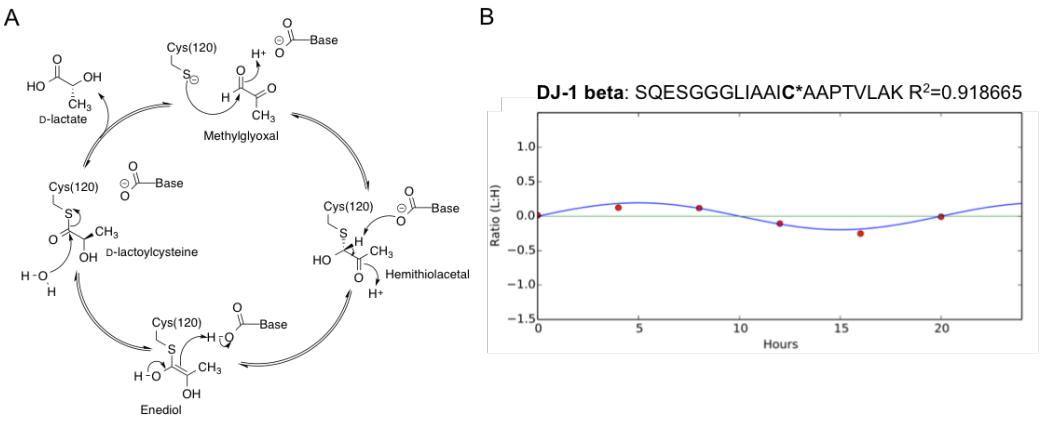

Figure 4-5 DJ-1 beta oscillates during a circadian cycle. (A) DJ-1 beta catalytic cycle. The catalytic nucleophilc cysteine is directly responsible for the transformation of toxic glyoxals (eg. Methylglyoxal) to carboxylic acids (eg. D-lactate). (B) The catalytic nucleophile Cys122 of *Drosophila* DJ-1 oscillates over a 20-hour period.

A cysteine present on DJ-1 beta, Cys122, was found to oscillate in the MS data mentioned above (Figure 4-5B). Cys122 is homologous with the active site cysteine, Cys106, of human DJ-1. It has been reported that Cys106 easily undergoes sulfinic acid formation. When levels of oxidative stress are high, the oxidation of Cys106 is responsible for the recruitment of this enzyme to the mitochondria. Translocation of DJ-1 into the mitochondria helps to protect this organelle from toxicity caused by ROS. Oxidation of the active site cysteine also allows DJ-1 to act as a sensor of oxidative stress. Interestingly, the oscillation pattern observed for DJ-1 beta is similar to that found for Prx5 and Trxr-1. Since sulfinic acid formation or decrease in activity of Cys106 acts as a sensor for changes in ROS levels in the cell, it is plausible that our data obtained for DJ-1 may be a direct record of the change in ROS over a circadian day. Further experiments are necessary to confirm that the changes in oxidation state of Cys106 are responsible for the oscillation of L:H ratios observed for this residue. First, we will conduct a western blot to quantify relative protein concentrations of DJ-1 beta across the different time points before measuring enzymatic activity of DJ-1 beta over time.

Cysteine circadian oscillation in a mammalian model, U2OS_P

In addition to monitoring cysteine circadian oscillation in *Drosophila*, the oscillations relatable to human circadian cycles were also explored. As a mammalian alternative to the *Drosophila* heads used initially, U2OS_P cells were used for MS analysis. The U2OS_P cell line is derived from osteosarcoma fibroblasts, which posses a Period 2 (Per2)-Luciferase (Luc) promoter. [32] The Per2-Luc promoter allows for visualization of oscillations of the mammalian cells upon treatment on a small molecule, forskolin. Forskolin binds to the adenylyl cyclize that cyclizes AMP to generate cyclic AMP (cAMP) (Figure 4-6A). [32,33] The increase in cAMP activates a cascade, which leads to increased gene expression.

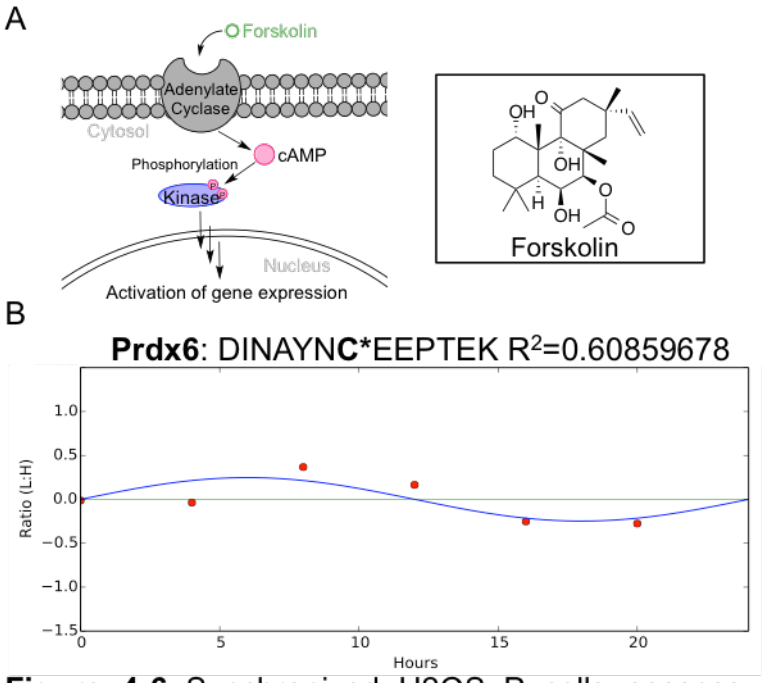

Figure 4-6 Synchronized U2OS_P cells possess proteins that oscillate during a circadian cycle. (A) Forskolin is a small molecule used to activate gene expression and synchronize cells. Forskolin binds to adenylate cyclase to activate gene expression in cells. (B) A cysteine on Human Prdx6 oscillates during a circadian day.

U2OS_P cells were treated for 2 hours with forskolin to induce synchronization. After removal of forskolin and replacement with standard media, cells were harvest for time = 0 hours. Remaining cell cultures grew under ambient conditions until 4, 8, 12, 16 and 20 hours past forskolin treatment, when they were harvested to afford each of the remaining time points necessary to assess protein oscillation during a circadian day. The cells were lysed and the lysates were treated with IAA to modify reactive cysteine residues. Each sample is exposed to CuAAC conditions to append azo-light (time = 0, 4, 8, 12, 16, 20) or azo-heavy (time = 0; control sample) tag to the appropriate samples. The azo-light samples are combined with the azo-heavy samples before enrichment on streptavidin beads. The enriched peptides are denatured and alkylated before trypsin digestion over night. The subsequent tryptic peptides are removed and the cysteine-containing peptides still bound to the streptavidin beads are cleaved using sodium dithionite to afford the azo-samples that are analyzed by LC/LC-MS/MS.

After analysis of the U2OS_P circadian samples, cysteines were identified that oscillate with phases and intensities similar to those found in the *Drosophila* data. Initially, this dataset was examined for peroxiredoxins that oscillate. To our delight, we identified Peroxiredoxin 6 (Prdx6) as a novel protein that oscillate in mammalian cells (Figure 4-6B).

Concluding remarks and future directions

In order to validate this MS platform, the relative protein abundance at each time point with be monitored by western blot to confirm whether the changes in cysteine activity are a function of cysteine oxidation changes overtime or a change in relative

protein abundance at each time point. If protein levels remain constant, these experiments would support that this platform can be used to detect changes in cysteine activities as a result of oxidative modification of the cysteine thiol. The change in cysteine reactivity will also be confirmed by preforming a pull-down assay. Lysates from the above MS experiments will be treated with IAA and then exposed to CuAAC conditions with biotin-azide. The biotinylated proteins will be enriched using streptavidin beads and then eluted from the beads upon boiling in the presence of SDS. The eluted proteins can be studied using Western blot to identify any changes in the amount of protein that is enriched across each of the time points. Presumably, as the oxidation states of these cysteines oscillate, the amount of protein enriched on the beads should also cycle based on the change reactivity with IAA.

Acknowledgements

The *Drosophila melanogaster* fly head samples were collected by the Rosbash Lab at Brandeis University. I would also like to thank Dan Bak for his assistance in data processing and development of the circadian-fitting program for CIMAGE data assessment of cysteine reactivity oscillation.

Experimental procedures

Materials and general procedure

All materials were purchased from Sigma Aldrich unless otherwise noted. DMEM/High glucose medium, Phosphate buffered saline (PBS) buffer, 2% Trypsin-EDTA and penicillin streptomycin (Pen/Strep) were purchased from Fisher Scientific (Pittsburgh, PA). The anti-*Drosophila* Prx-5 antibody was a gift from the Rosbash Lab and anti-rabbit IgG HRP-linked antibody was purchased from Cell Signaling (Danvers, MA). Potassium phosphate tribasic monohydrate was purchased from Fisher Scientific (Pittsburgh, PA). All protein concentrations were determined using a Bio-Rad DC protein assay kit with reagents from Bio-Rad Life Science (Hercules, CA). Mini Trans-Blot Filter Paper was purchased from Bio-Rad Life Science (Hercules, CA). SuperSignal West Pico Chemiluminescent Substrate was purchased from Thermo Scientific (Armarillo, TX). Illusta Nap-5 Columns were purchased from GE Healthcare Bio-Sciences (Piscataway, NJ). Streptavidin-agarose beads were purchase from Thermo Scientific (Armarillo, TX).

Mass-spectrometry analysis of circadian oxidation oscillation of cysteine reactivity in *Drosophila melanogaster*

Drosophila melanogaster heads collected at 0, 4, 8, 12, 16, and 20 hour time points were separated into eppendorf tubes (~200 heads/tube). The fly heads were homogenized in 0.5 mL of PBS and purified using filtration through a Nap-5 column. The resulting lysates were treated with the IA probe (100 μM) and subjected to CuAAC

with light (time = 0, 4, 8, 12, 16, 20) or heavy (time = 0) azo-tags and subsequent mass-spectrometry analysis as described previously (Qian, Y. and Weerapana, E. et al. *Chem. Biol. Chem,* **2013**, *14*, 1410-14).

Mass-spectrometry analysis of circadian oxidation oscillation of cysteine reactivity in U2OS_P cells

U2OS_P cells were grown to ~80-90% confluency before treatment with forskolin (10 μM) for 2 hours. The forskolin-containing media was removed and replaced with complete DMEM. Cells were collected at 0, 4, 8, 12, 16, 20-hour time points after forskolin-media removal. Cells were lysed and protein normalized to 1 mg/mL for all samples. The resulting lysates were treated with the IA probe (100 μM) and subjected to CuAAC with light (time = 0, 4, 8, 12, 16, 20) or heavy (time = 0) azo-tags and subsequent mass-spectrometry analysis as described previously (Qian, Y. and Weerapana, E. et al. *Chem. Biol. Chem,* **2013**, *14*, 1410-14).

MS data analysis

The generated tandem MS data was searched using the SEQUEST algorithm against the human IPI database. A static modification of +57.02146 on cysteine was specified to account for iodoacetamide alkylation and differential modifications of +443.2897 (Azo-L modification) and +449.3035 (Azo-H modification) were specified on cysteine to account for probe modifications. SEQUEST output files were filtered using DTASelect 2.0. Quantification of light/heavy ratios (R) was performed using the CIMAGE quantification package as previously described (Weerapana, E., Speers, A. E.

Cravatt, B. F. *Nat. Protoc.* **2007**, *2*, 1414-25). The ratios obtained from CIMAGE were plotted using the circadian-fitting program for CIMAGE developed by Daniel Bak in our laboratory. The traces generated were sorted by best fit (R^2) to sinusoidal curve then by greatest Max/Min ratio.

Monitoring protein expression levels of Prx5 in Drosophila melanogaster circadian samples

Protein expression was analyzed by western blot. Complete *Drosophila* head proteins were separated by 15% SDS-PAGE and transferred by electroblotting to nitrocellulose membrane at 150 volt hours. The membrane was first washed using Tris-buffered saline containing 1% Tween 20 (TBS-T), and exposed to Ponceau Stain to ensure that the protein was transferred from the gel to the membrane. The membrane was then washed three times with TBS-T until the membrane was free of stain, followed by blocking in TBS-T with 5% (w/v) non-fat dry milk at room temperature for 30 min. After washing with TBS-T three times, the membrane was incubated with *Drosophila* Prx5 primary anti-body (1:1000) at 4°C for 16hrs. The membrane was then washed three times with TBS-T, and incubated for another 2hrs with anti-Rabbit horseradish peroxidase (HRP)-conjugated secondary antibody (1:3333) at room temperature. The membrane was washed three times with TBS-T and treated with both SuperSignal® West Pico Chemiluminescent HRP and luminol substrate. A BioRad ChemiDoc MP Imaging System, using Chemi exposure setting, was used to quantify fluorescence bands.

References

(1) Kang, TH; Reardon, JT; Kemp, M Circadian Oscillation of Nucleotide Excision Repair in Mammalian Brain. *Proc. Natl. Acad. Sci. U. S. A.* **2009**, *106*, 2864-7.
(2) Shanmugam, V.; Wafi, A.; Al-Taweel, N.; Büsselberg, D. Disruption of Circadian Rhythm Increases the Risk of Cancer, Metabolic Syndrome and Cardiovascular Disease. *J Local Global Heal Sci* **2013**, 3.
(3) Partch, C. L.; Green, C. B.; Takahashi, J. S. Molecular Architecture of the Mammalian Circadian Clock. *Trends Cell Biol.* **2014**, *24*, 90–9.
(4) Abruzzi, K. C.; Rodriguez, J.; Menet, J. S.; Desrochers, J.; Zadina, A.; Luo, W.; Tkachev, S.; Rosbash, M. Drosophila CLOCK Target Gene Characterization: Implications for Circadian Tissue-Specific Gene Expression. *Genes Dev.* **2011**, *25*, 2374–86.
(5) Winterbourn, C. C. Reconciling the Chemistry and Biology of Reactive Oxygen Species. *Nat. Chem. Biol.* **2008**, *4*, 278–86.
(6) Andreyev, A. Y.; Kushnareva, Y. E.; Starkov, A. A. Mitochondrial Metabolism of Reactive Oxygen Species. *Biochemistry Mosc.* **2005**, *70*, 200–14.
(7) Edgar, R. S.; Green, E. W.; Zhao, Y.; van Ooijen, G.; Olmedo, M.; Qin, X.; Xu, Y.; Pan, M.; Valekunja, U. K.; Feeney, K. A.; et al. Peroxiredoxins Are Conserved Markers of Circadian Rhythms. *Nature* **2012**, *485*, 459–64.
(8) Hoyle, N. P.; O'Neill, J. S. Oxidation-Reduction Cycles of Peroxiredoxin Proteins and Nontranscriptional Aspects of Timekeeping. *Biochemistry* **2015**, *54*, 184–93.
(9) Rhee, S. G.; Chae, H. Z.; Kim, K. Peroxiredoxins: A Historical Overview and Speculative Preview of Novel Mechanisms and Emerging Concepts in Cell Signaling. *Free Radic. Biol. Med.* **2005**, *38*, 1543–52.
(10) Biteau, B.; Labarre, J.; Toledano, M. B. ATP-Dependent Reduction of Cysteine-Sulphinic Acid by S. Cerevisiae Sulphiredoxin. *Nature* **2003**, *425*, 980–4.
(11) Woo, H. A.; Jeong, W.; Chang, T.-S. S.; Park, K. J.; Park, S. J.; Yang, J. S.; Rhee, S. G. Reduction of Cysteine Sulfinic Acid by Sulfiredoxin Is Specific to 2-Cys Peroxiredoxins. *J. Biol. Chem.* **2005**, *280*, 3125–8.
(12) Knoops, B.; Goemaere, J.; Van der Eecken, V.; Declercq, J.-P. P. Peroxiredoxin 5: Structure, Mechanism, and Function of the Mammalian Atypical 2-Cys Peroxiredoxin. *Antioxid. Redox Signal.* **2011**, *15*, 817–29.
(13) Rhee, S. G. Overview on Peroxiredoxin. *Mol. Cells* **2016**, *39*, 1–5.
(14) Kropotov, A.; Sedova, V.; Ivanov, V.; Sazeeva, N.; Tomilin, A.; Krutilina, R.; Oei, S. L.; Griesenbeck, J.; Buchlow, G.; Tomilin, N. A Novel Human DNA-Binding Protein with Sequence Similarity to a Subfamily of Redox Proteins Which Is Able to Repress RNA-Polymerase-III-Driven Transcription of the Alu-Family Retroposons in Vitro. *Eur. J. Biochem.* **1999**, *260*, 336–46.
(15) Oberley, T. D.; Verwiebe, E.; Zhong, W.; Kang, S. W.; Rhee, S. G. Localization of the Thioredoxin System in Normal Rat Kidney. *Free Radic. Biol. Med.* **2001**, *30*, 412–24.
(16) Kropotov, A.; Usmanova, N.; Serikov, V.; Zhivotovsky, B.; Tomilin, N.

Mitochondrial Targeting of Human Peroxiredoxin V Protein and Regulation of PRDX5 Gene Expression by Nuclear Transcription Factors Controlling Biogenesis of Mitochondria. *FEBS J*. **2007**, *274*, 5804–14.
(17) Banmeyer, I.; Marchand, C.; Clippe, A.; Knoops, B. Human Mitochondrial Peroxiredoxin 5 Protects from Mitochondrial DNA Damages Induced by Hydrogen Peroxide. *FEBS Lett*. **2005**, *579*, 2327–33.
(18) Banmeyer, I.; Marchand, C.; Verhaeghe, C.; Vucic, B.; Rees, J.-F. F.; Knoops, B. Overexpression of Human Peroxiredoxin 5 in Subcellular Compartments of Chinese Hamster Ovary Cells: Effects on Cytotoxicity and DNA Damage Caused by Peroxides. *Free Radic. Biol. Med*. **2004**, *36*, 65–77.
(19) Radyuk, S. N.; Michalak, K.; Klichko, V. I.; Benes, J.; Rebrin, I.; Sohal, R. S.; Orr, W. C. Peroxiredoxin 5 Confers Protection against Oxidative Stress and Apoptosis and Also Promotes Longevity in Drosophila. *Biochem. J*. **2009**, *419*, 437–45.
(20) Seo, M. S.; Kang, S. W.; Kim, K.; Baines, I. C.; Lee, T. H.; Rhee, S. G. Identification of a New Type of Mammalian Peroxiredoxin That Forms an Intramolecular Disulfide as a Reaction Intermediate. *J. Biol. Chem*. **2000**, *275*, 20346–54.
(21) Smeets, A.; Marchand, C.; Linard, D.; Knoops, B.; Declercq, J.-P. P. The Crystal Structures of Oxidized Forms of Human Peroxiredoxin 5 with an Intramolecular Disulfide Bond Confirm the Proposed Enzymatic Mechanism for Atypical 2-Cys Peroxiredoxins. *Arch. Biochem. Biophys*. **2008**, *477*, 98–104.
(22) Lu, J.; Holmgren, A. The Thioredoxin Superfamily in Oxidative Protein Folding. *Antioxid. Redox Signal*. **2014**, *21*, 457–70.
(23) Lu, J.; Holmgren, A. The Thioredoxin Antioxidant System. *Free Radic. Biol. Med*. **2014**, *66*, 75–87.
(24) Lee, J.; Song, J.; Kwon, K.; Jang, S.; Kim, C.; Baek, K.; Kim, J.; Park, C. Human DJ-1 and Its Homologs Are Novel Glyoxalases. *Hum Mol Genet* **2012**, *21*, 3215–3225.
(25) Richarme, G.; Mihoub, M.; Dairou, J.; Bui, L.; Leger, T.; Lamouri, A. Parkinsonism-Associated Protein DJ-1/Park7 Is a Major Protein Deglycase That Repairs Methylglyoxal- and Glyoxal-Glycated Cysteine, Arginine, and Lysine Residues. *J Biol Chem* **2015**, *290*, 1885–1897.
(26) Chen, J.; Li, L.; Chin, L.-S. Parkinson Disease Protein DJ-1 Converts from a Zymogen to a Protease by Carboxyl-Terminal Cleavage. *Hum Mol Genet* **2010**, *19*, 2395–2408.
(27) Clements, C.; McNally, R.; Conti, B.; Mak, T.; Ting, J. DJ-1, a Cancer- and Parkinson's Disease-Associated Protein, Stabilizes the Antioxidant Transcriptional Master Regulator Nrf2. *P Natl Acad Sci Usa* **2006**, *103*, 15091–6.
(28) Xiong, H.; Wang, D.; Chen, L.; Choo, Y. S.; Ma, H.; Tang, C.; Xia, K.; Jiang, W.; Ronai, Z.; Zhuang, X.; et al. Parkin, PINK1, and DJ-1 Form a Ubiquitin E3 Ligase Complex Promoting Unfolded Protein Degradation. *J. Clin. Invest*. **2009**, *119*, 650–60.
(29) Shendelman, S.; Jonason, A.; Martinat, C.; Leete, T.; Abeliovich, A. DJ-1 Is a Redox-Dependent Molecular Chaperone That Inhibits Alpha-Synuclein Aggregate Formation. *PLoS Biol*. **2004**, *2*, e362.
(30) McNally, R. S.; Davis, B. K.; Clements, C. M.; Accavitti-Loper, M. A.; Mak, T. W.; Ting, J. P. DJ-1 Enhances Cell Survival through the Binding of Cezanne, a Negative Regulator of NF-kappaB. *J. Biol. Chem*. **2011**, *286*, 4098–106.
(31) Choi, D.; Kim, J.; Ha, S.; Kwon, K.; Kim, E.-H. H.; Lee, H.-Y. Y.; Ryu, K.-S. S.;

Park, C. Stereospecific Mechanism of DJ-1 Glyoxalases Inferred from Their Hemithioacetal-Containing Crystal Structures. *FEBS J.* **2014**, *281*, 5447–62.
(32) Lande-Diner, L.; Boyault, C.; Kim, J. Y.; Weitz, C. J. A Positive Feedback Loop Links Circadian Clock Factor CLOCK-BMAL1 to the Basic Transcriptional Machinery. *Proc. Natl. Acad. Sci. U.S.A.* **2013**, *110*, 16021–6.
(33) Misra, U. K.; Pizzo, S. V. Coordinate Regulation of Forskolin-Induced Cellular Proliferation in Macrophages by Protein Kinase A/cAMP-Response Element-Binding Protein (CREB) and Epac1-Rap1 Signaling: Effects of Silencing CREB Gene Expression on Akt Activation. *J. Biol. Chem.* **2005**, *280*, 38276–89.

Chapter 5

The design and evaluation of a cysteine-reactive small-molecule probe library based on a modular 4-aminopipridine scaffold.

A significant portion of the work described in this chapter has been published in:

Couvertier, S. M.; Weerapana, E. Cysteine-reactive chemical probes based on a modular 4-aminopiperidine scaffold. *MedChemComm* **2014**, *5*, 358–362.

Paige Carleen, Alexander Warshauer, and Inchul You assisted in probe library synthesis. Inchul You performed site-of-labeling experiements with recombinant PDIA1.

Introduction

Many functional cysteines display enhanced nucleophilicity relative to other non-functional cysteines in the proteome. [1,2] Small molecules bearing thiol-reactive electrophiles can be used to selectively target these nucleophilic residues. [3] Cysteine-mediated protein activities are known to be dysregulated in diseases such as cancer, including cysteine proteases, [4,5] phosphatases, [6,7] kinases, [8,9] oxidoreductases [10] and metabolic enzymes. [11] Despite the well-characterized roles of cysteine in disease, very few pharmacological tools exist to perturb and investigate these activities *in vivo*. In an effort to expand the tools available to modulate protein function, we have developed a library of chemical probes to target diverse protein activities by exploiting the inherent reactivity of functional cysteines.

An ideal cysteine-reactive probe requires a central scaffold that has optimal cell permeability and cellular stability. Additionally, the central scaffold must have the ability to possess three essential functionalities: (1) a cysteine-reactive electrophile for covalent modification of reactive cysteine residues; (2) a bio-orthogonal alkyne handle for downstream target identification; and (3) various diversity elements to direct the library toward distinct subsets of the proteome. Previously, our lab has developed a cell-permeable tri-functionalized triazine probe library, which afforded several selective covalent modifiers of β-tubulin and protein disulfide isomerase A 1 (PDIA1). [12] Despite the early successes demonstrated for triazine-based covalent small molecules, one limitation of the triazine scaffold is the rigidity, which positions each of the three functionalities with a spatial separation of 120°. [13] We postulate that the orientation of these functional moieties is non-ideal in situations where the binding interaction provided

by the diversity element needs to be positioned adjacent to the covalent interaction provided by the electrophile. To overcome these limitations, we sought an alternative scaffold with increase conformational flexibility and modularity relative to the tri-functionalized 1,3,5-triazine.

Scaffold Design

We focused our attention to substituted piperidines, which are central to a variety of bioactive alkaloid natural products, and have gained popularity in drug discovery platforms due to their ease of functionalization and conformational flexibility. [14–17] Incorporation of the three desired probe functionalities (the electrophile, the alkyne and diversity element) required a piperidine scaffold that would allow for modular tri-functionalization with synthetic ease. We arrived at a 4-aminopiperidine scaffold for our application. This scaffold is flexible and allows for diverse spatial orientations of the alkyne, diversity element and electrophile. [18] The 4-aminopiperidine scaffold has been utilized in a variety of pharmaceutical applications, [19] alluding to its favorable pharmacokinetic properties. A recent computational study on fentanyl, a widely utilized synthetic opioid analgesic, identified a lowest energy chair conformation for the piperidine ring with an equatorial exocyclic 4-N-substituent (Figure 5-1A). [20] Given the predicted conformation of this scaffold, we designed our probe library to incorporate the electrophile and diversity elements in close proximity as substituents on the exocyclic 4-amino group (Figure 5-1B). We hypothesize that these two elements synergistically contribute to binding and modification of target proteins thereby warranting their proximity to each other. The alkyne group was installed in the form of a pentynyl-group

on the ring-nitrogen of the piperidine heterocycle. For this initial library, we incorporated a chloroacetamide (CA) electrophile into all compounds since this group is known to be of moderate activity and specific to thiol groups over other nucleophilic amino-acid side chains (Figure 5-1C). The diversity elements varied across the library members, ranging from aliphatic and aromatic groups with diverse size, hydrophobicity and aromaticity, including both D- and L-isomers of amino acid methyl esters (Figure 5-1D).

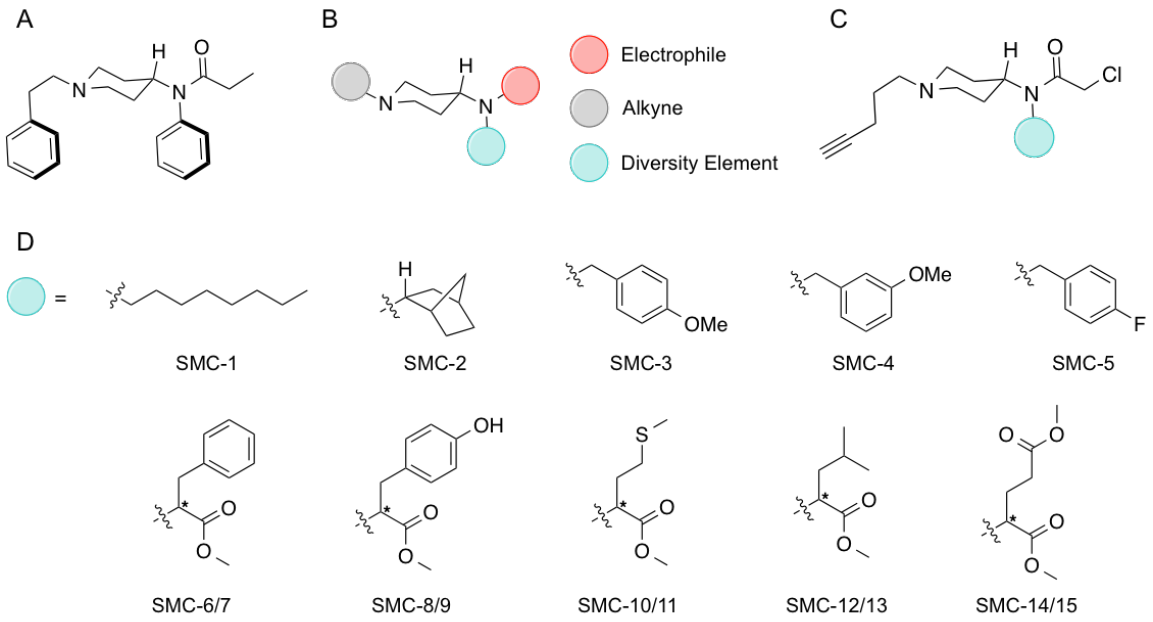

Figure 5-1 Design of cysteine-reactive probe library. (A) Lowest-energy chair conformation of fentanyl, a 4-aminopiperidine-based opioid analgesic. (B) Proposed incorporation of the required electrophile, alkyne and diversity element functionalities into the 4-aminopiperidine scaffold. (C) The central core comprised of a pentynyl-group and a chloroacetamide attached to the 4-aminopiperidine scaffold. (D)Structures of the diversity elements incorporated at the beginning of this study.

4-aminopiperidine probe synthesis

Upon designing the general probe architecture, we sought to develop a divergent synthetic route that would allow efficient access to these tri-functionalized 4-aminopiperidine probes. The synthetic route begins with commercially available 4-pentynyl-1-ol, which undergoes a tosylation reaction to form intermediate **2** in high yield

(93% yield) (Scheme 5-1). This resulting tosylate is subjected to a substitution reaction with 1,4-dioxa-8-azaspiro[4.5]decane to obtain the alkyne functionalized ketal intermediate **3** (80% yield). This ketal intermediate is deprotected to afford a ketone (**4**), which constitutes a common intermediate that is diversified through incorporation of the diversity elements. Addition of the diversity elements to ketone **4** is achieved via a mild reductive amination reaction with the corresponding primary amines in the presence of sodium triacetoxyborohydride (71-98% yield). The secondary amine **5**, resulting from the reductive amination, is then coupled to chloroacetylchloride to afford the final electrophile-bearing compounds that constitute the probe library. It is of note the synthetic route is carried out under mild conditions that support incorporation of diversity elements containing esters and other labile function groups. Furthermore, the divergent nature of the synthesis allows for functionalization of the common ketone intermediate (**4**) with a variety of diversity elements as well as different electrophiles, supporting the eventual modular expansion of the library through variation of both these groups.

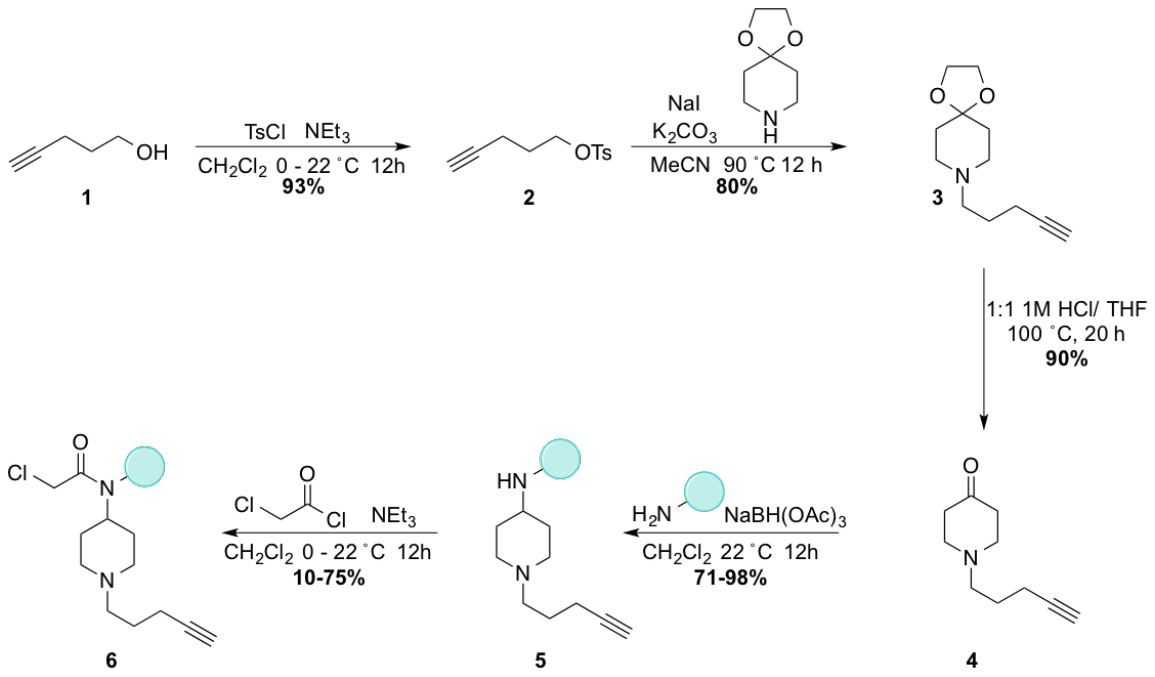

Scheme 5-1 Synthesis of cysteine-reactive 4-aminopiperidine probes.

Evaluation of the cell-permeability and target diversity of the probes

Using the synthesis described above, we generated an initial library of 15 probes with varying diversity elements. A subset of these probes was evaluated in MCF-7 breast cancer cells to determine cell permeability and target diversity. MCF-7 cells in culture were treated with either 1 or 5 μM concentrations of each of the probes for 1 hour. The cells were then lysed, and the lysates were treated with rhodamine azide (Rh-N_3) and standard reagents for copper-catalyzed click chemistry (CuAAC). [21,22] The resulting fluorescently tagged lysates were separated by SDS-PAGE and protein labeling was visualized by in-gel fluorescence (Figure 5-2). The 4-aminopiperidine probes were cell permeable and demonstrated diverse protein labeling profiles. Comparing aliphatic diversity elements (SMC-1) to aromatic groups (SMC-3) showed distinct and diverse protein targets. Similarly, probes with amino acid methyl ester directing groups labeled

protein targets with noticeable difference observed between the L- and D-stereoisomers (SMC-8 and SMC-9). These data highlight the utility of the modular 4-aminopiperidine scaffold to generate cell permeable covalent probes with diverse cellular protein targets.

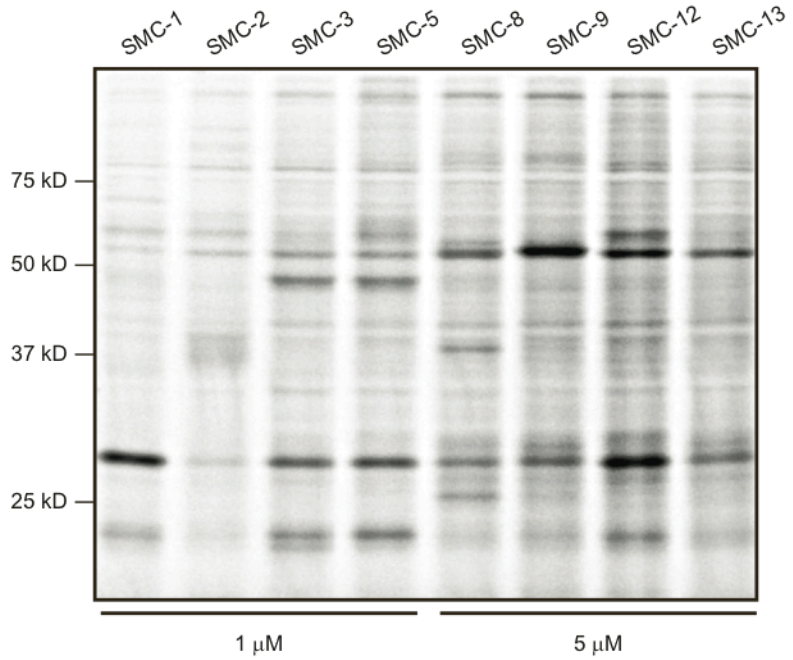

Figure 5-2 In-gel fluorescence evaluation of probe labeling in cells. MCF-7 cells were treated with either 1μM (SMC-1 to SMC-5) of 5 μM (SMC-8 to SMC-13) probe for 1 hour. Cells were then lysed, and probe-labeled proteins were conjugated to rhodamine azide using click chemistry, separated by SDS-PAGE and visualized using in-gel fluorescence.

Protein target identification by tryptic MS analysis

Our ultimate goal is to expand the size of the probe library to further increase the structural diversity and potential protein targets. We envision screening this expanded library against cell lysates overexpressing a protein of interest to identify covalent modifiers. However, upon initial gel analysis, identification of protein targets of probes

(SMC-1, SMC-8 and SMC-9) that appear to be selective and potent for single proteins was pursued. In order to identify the protein targets, HeLa cell lysates were exposed to each of the probes for 1 hour (Figure 5-3A). The probed lysates undergo standard click chemistry conditions with biotin-azide (biotin-N_3). The biotinylated proteins are enriched on streptavidin beads and digested by trypsin to afford tryptic peptides of the modified proteins. These tryptic samples are analyzed by LC/LC-MS/MS and the most abundant protein that corresponds to the molecular weight observed by fluorescence gel analysis were identified. After MS analysis, we discovered SMC-1 as a covalent modifier for GSTO1, SMC-8 as a probe for AKT1 and PDIA1 as the protein target for SMC-9 (Figure 5-3B).

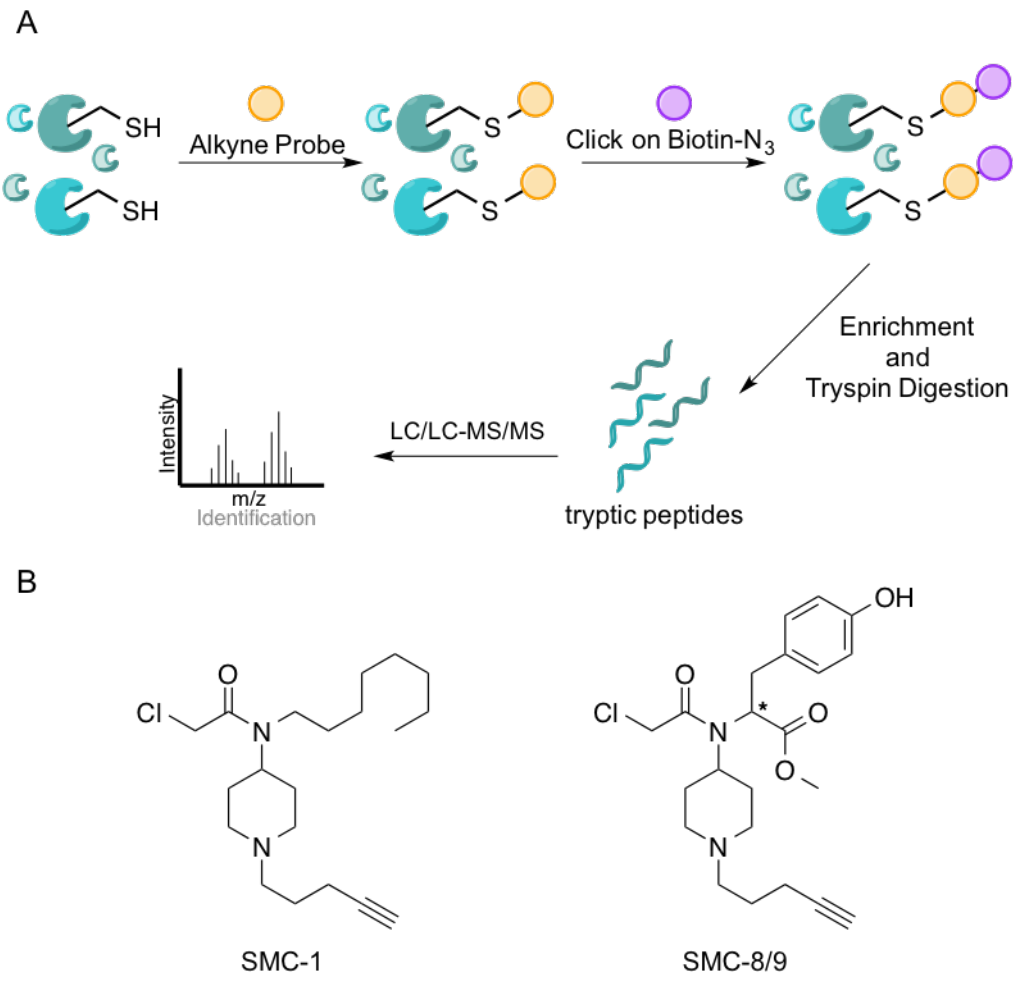

Figure 5-3 Identification of protein targets by MS. (A) MS workflow for identification of probe-modified proteins using Biotin-azide (B) Alkyne probes used for MS protein identification. SMC-1 contains an n-octyl directing group. SMC-8 and SMC-9 contain an L-Tyr methyl ester and D-Tyr methyl ester, respectively.

Identification of a cysteine-reactive chemical probe for GSTO1

Glutathione *S*-transferase 1 (GSTO1) is a member of the GST superfamily of enzymes involved in cellular detoxification and redox homeostasis in cells. Unlike the other members of this family, GSTO1 contains an active site cysteine and catalyzes a variety of thioltransferase reactions (Figure 5-4B).[23] GSTO1 is overexpressed at high levels in numerous cancers and is implicated in cancer-cell resistance to

chemotherapeutic drugs, such a cisplatin.[24] Several cysteine-reactive GSTO1 inhibitors have been previously described.[25,26]

MS analysis identified GSTO1 as the protein target of SMC-1. SMC-1 contains an *n*-octyl group as a diversity element, which potentially has a high affinity for the active site of this enzyme. To confirm that SMC-1 was covalently modifying the known active site cysteine (Cys32) of GSTO1, we treated cells expressing GSTO1 WT and C32A mutant with 0.5 μM SMC-1. Observation of in-gel fluorescence of probe-modified WT GSTO1 and complete loss of labeling for the C32A mutant demonstrates the specificity of this probe for the active site (Figure 5-4A). Furthermore, this live-cell analysis confirms that SMC-1 is both cell-permeable and selective for GSTO1 in cells. Given that Cys32 is present in the active site of GSTO1 and is essential for activity, SMC-1 reports on the nucleophilicity of this catalytic residue and can be used to screen for inhibitors of GSTO1 in cells.

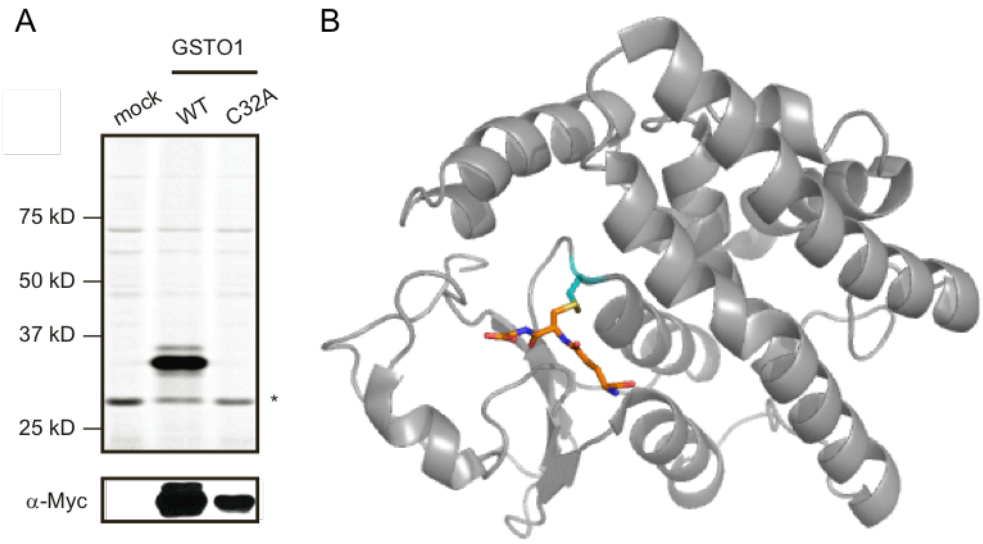

Figure 5-4 A chemical probe for GSTO1. (A) Cells transfected with empty plasmid (mock), GSTO1 (wild-type; WT) or C32A mutant were treated with 0.5 μM SMC-1 and analyzed by in-gel fluorescence. The lower band (*) is endogenous GSTO1 and the upper band is the Myc-tagged overexpressed variant. Expression of wild-type and mutant is confirmed by western blotting with a α-Myc antibody. (B) Crystal structure of GSTO1 (PDB: 1eem). Active-site Cys32 is highlighted in cyan.

Identification of a chemical probe for AKT1

AKT1, also known as Protein Kinase B (PKB), is implicated in many cellular processes, such as metabolism, proliferation, cell survival and growth.[27] Dysregulated AKT1 activity is characteristic of a variety of diseases such as cancer and diabetes.[28,29] In particular, increased AKT1 activity in cancer has been shown to support tumor growth, rendering AKT1 an attractive therapeutic target.[27] It has also been reported that oxidative stress and nitrosating agents modulate AKT1 activity. Human AKT1 contains 7 cysteine residues and of these cysteines, Cys296 and Cys310 have been shown to form a disulfide bond under oxidative stress, and Cys296 and Cys224 have been identified as targets of *S*-nitrosation (Figure 5-5A).[29–31] The disulfide-linked form of AKT1 is thought to be

catalytically inactive, and furthermore, covalent modification of Cys310 by hydroquinones inhibits enzyme function, [28] suggesting the importance of cysteine residues in regulating AKT1 activity.

After MS analysis, we identified SMC-8 as a selective covalent modifier of AKT1. This compound contains an L-tyrosine methyl ester as the diversity element. Interesting, the D-isomer of the tyrosine methyl ester (SMC-9) did not afford significant covalent modification of AKT1, alluding to the importance of the structure and stereochemistry of the diversity element in target determination.

In an effort to elucidate the specific site of labeling of AKT1, each of the 7 cysteine residues present on the protein were mutated to serine. Cell lysates from cells that had been transiently transfected with empty plasmid (mock), AKT1 (WT), and the Cys to Ser mutants (C60S, C77S, C224S, C268S, C296S, C310S, C366S, C480S) were subject to fluorescent gel analysis to identify the specific cysteine modified by the probes. Similar to GSTO1, we expect to observe a decrease in labeling when the cysteine residue is no longer present in the AKT1 mutant. After initial gel analysis, we were unable to deduce which cysteine is specifically modified. As seen in the fluorescent image, some AKT1 mutants (C60S and C224S) appear to yield a slight reduction in fluorescent signal. However, the difference in fluorescence with respect to the wild-type is likely due to the lower expression of these mutants as seen in the western blot (Figure 5-5B). Further mutagenesis to generate the double and even triple cysteine to serine mutants appears necessary to identify the site of labeling for SMC-8.

Despite the inconclusive experiment to identify the site of labeling of SMC-8, we sought to determine if covalent modification of AKT1 by the probe occurred in an

activity-based manner. To achieve this, AKT1 lysates were incubated with increasing concentration of staurosporine (STS), a pan kinase inhibitor,[32] prior to addition of SMC-8. These STS and SMC-8 treated lysates were then subject to click chemistry with Rh-N_3 followed by in-gel fluorescence analysis. A dose-dependent decrease in SMC-8 labeling of AKT1 is observed in the presence of STS, alluding to the activity-based nature of this labeling event (Figure 5-5C). Interestingly, several previously reported non-covalent inhibitors of AKT1 contain a piperidine or 4-aminopiperidine scaffolds,[27,33,34] suggesting this heterocycle to be a preferred chemotype for AKT1. Although the exact cysteine modified by SMC-8 is as yet unidentified, this probe could still be a useful tool for monitoring AKT1 activity in lysates, and for screening AKT1 inhibitors in cells. In the future, we will identify the cysteine(s) in AKT1 that is modified by SMC-8 and perform structure-activity relationship studies to arrive at a more potent covalent modifier of this enzyme.

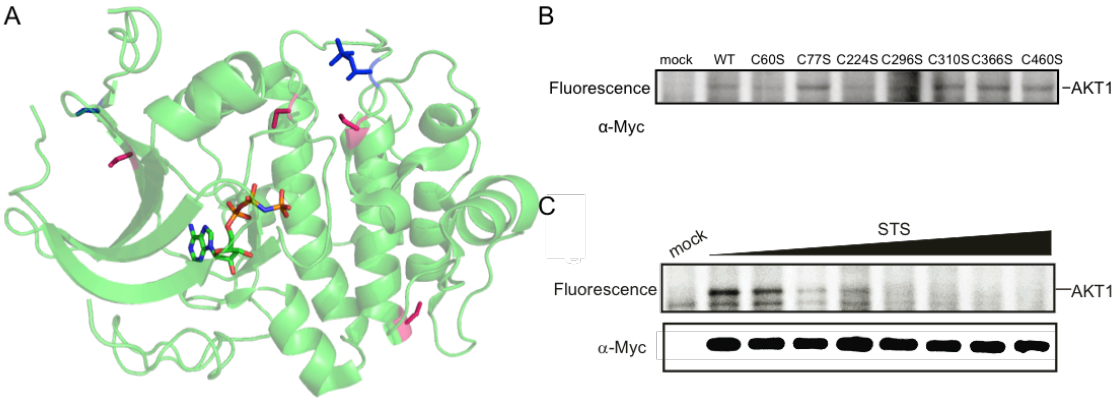

Figure 5-5 A chemical probe for AKT1. (A) Crystal structure of kinase domain of AKT1 (PDB: 4ekk1). Cysteines sensitive to oxidative PTMs highlighted in pink. (B) HEK293T cells transfected with empty plasmid (mock), AKT1 (wild-type; WT) or Cys to Ser mutants (C60S, C77S, C224S, C296S, C310S, C366S, C460S) were treated with 5 μM SMC-8 and analyzed by in-gel fluorescence. (C) AKt1 over-expressing lysates were pre-treated with increasing concentrations of staurosporine (STS) (0.5-100 mM) followed by SMC-8 (5 μM). AKT1 inhibition by STS resulting in decreased labeling by SMC-8 alluding to the activity-based nature of SMC-8 labeling of AKT1.

4-aminopiperidine probes specific for each active site of PDIA1

The Protein Disulfide Isomerase (PDI) family of enzymes consists of 21 different members predominately found within the endoplasmic reticulum (ER).[35] These enzyme have 3 different domains: (1) the thioredoxin-like domains (a domains), which possess the proteins active sites and bear CGHC motifs; (2) the b domains which are non-catalytic, hypothesized to help with protein substrate recognition; and (3) the c-terminal extension which contains an ER retrieval signal (e.g. KDEL and KEEL) (Figure 5-6A).[36] Protein Disulfide Isomerase 1 (PDIA1) is the most abundant PDI and is responsible for the rearrangement of misfolded disulfides and disulfide formation of nascent proteins in the ER. PDIA1 contains two thioredoxin-like domains, a and a' domains, which share 34% sequence homology.[37] This dissimilarity between the a-domains suggests that these active sites have distinct catalytic functions. As a protein also overexpressed in cancer tissues, PDIA1 has been found to facilitate tumor growth, making this an interesting protein of study.

Despite the fact that PDIA1 has been studied intensively over past decades, no selective PDIA1 inhibitors have been developed for clinical use. Among the small number of PDIA1 inhibitors, many are neither potent nor selective and show significant off-target toxicity. However, recent discoveries of synthetic small-molecular PDIA1 inhibitors, such as propynoic acid carbamoyl methyl amide (PACMA) 31[38] and 16F16,[39] have proved to be necessary tools to further understand the role of PDIA1 in disease. Additionally, our laboratory has developed a 1,3,5-trisubstitued triazine probe, RB-11-ca,[12] for the specific modification of the a-domain of PDIA1, which has shown to induced cell death upon treatment of HeLa cells. In an effort to add to the number of small

molecules available to study PDIA1, we screened the 4-aminopiperidine-probe library for any potential modifiers of this enzyme. Upon screening, three members of the 4-aminopiperidine library, SMC-9, SMC18 and SMC-11, were identified to target either both sites, the a site or the a' active site of PDIA1, respectively.

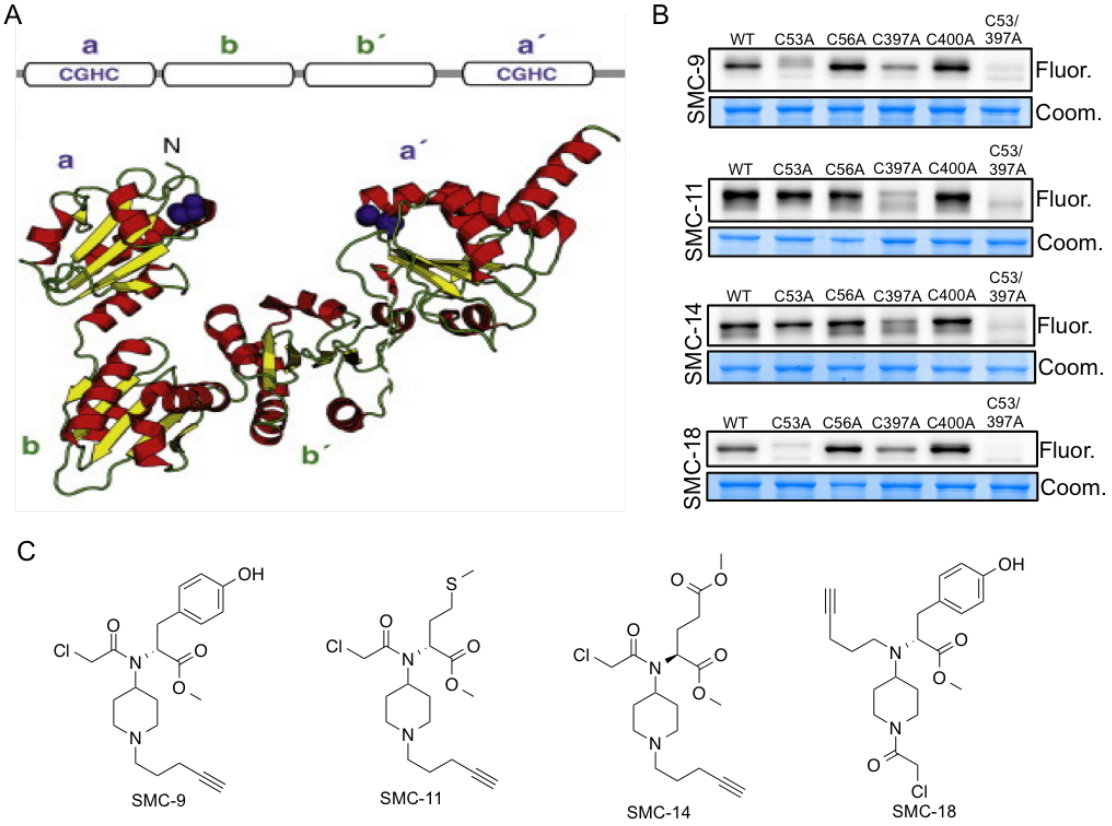

Figure 5-6 Chemical probes for PDIA1 active sites. (A) Illustration of PDIA1. Catalytic domains a and a' possess CGHC motifs highlighted in deep purple. (B) PDIA1 wild-type (WT) and Cys to Ala mutants (C53A, C56A, C397A, C400A, and C53/397A) were recombinantly expressed and spiked into MCF7 lysates. These lysates were probed with 5uM of SMC-9, SMC-11, SMC-14 and SMC-18. SMC-9 is selective for both a and a' domains. SMC-11 and SMC-14 target C397 in the a' domain. SMC-18 shows selectivity for C53 in the a-domain. (C) Structures of probes used site of labeling experiments.

The small molecule modifier, SMC-9, possesses a D-tyrosine methyl ester directing group and appears to be highly selective for PDIA1 upon whole cell labeling (Figure 5-2B). To discern which of the active site cysteines were modified by SMC-9, PDIA1 was mutated to afford each of the resulting alanine mutants: C53A, C56A,

C397A, C400A as well as a C53/397A double mutant. Upon incubation with SMC-9 and subsequent click chemistry with Rh-N_3, protein lysates possessing overexpressed mutants were separated by SDS-PAGE gel. The fluorescent gel analysis revealed a decrease in labeling for C53A and C397A mutants as well as complete loss of labeling for the C53/397A mutant (Figure 5-6B). This suggests that SMC-9, though selective for PDIA1, has the ability to modify cysteines in each of the active sites. The ability to label cysteines within the a and a' domains indicates that SMC-9 can be a useful tool for the elucidation of the roles of each active site of PDIA1. Integration of the PDIA1 bands in the fluorescent gel report that SMC-9 has a 2-fold preference for the modification of the a-domain over the a'-domain of PDIA1, which is similar to commercially available inhibitor, 16F16, proving that probes capable of targeting both sites is beneficial to the field.

A later screen of the remaining library members revealed several probes selective for either the a or a' sites of PDIA1, exclusively (Figure 5-6B/C). We identified SMC-11 and SMC-14 as probes selective for the a' domain (C397), though SMC-11 appears to be more potent and selective upon fluorescent gel analysis. Additionally, we found several probe library members that are selective for the a domain of PDIA1, the most potent library member appears to be SMC-18. After site of labeling experiments, we confirmed that SMC-18 is a selective modifier for C53 of PDIA1.

Our lab is currently using these probes to assess how each active sites relates to specific enzymatic functions of PDIA1. To assess the oxidase activity of PDIA1 upon probe treatment, a coupled reduced RNase assay has been pursued. This RNase assay reports the absorbance of cleaved cCMP as measure of the ability of PDIA1 to properly

oxidize RNase to its active form.[40,41] Furthermore, we plan to use experiments that focus on reductase, isomerase and chaperone activity. Reductase activity can be measured by the use of fluorescent probes, such as di-(o-aminobenzoyl)-GSSG (diabz-GSSG) or dieosin-GSSG (Di-E-GSSG), which upon exposure to active PDIA1 will cause the reduction of the GSSG disulfide leading to a substantial increase in fluorescence intensity.[42,43] Chaperone activity can be measured using green fluorescent protein (GFP) assay. This assay monitors the refolding of acid-denatured GFP by PDIA1 by the resulting increase in the fluorescence intensity. GFP serves as a model substrate to study the chaperone activity of PDIA1 because not only does this protein lack disulfide bonds but also upon acid-denaturation exhibits low fluorescence compare to the active form.[44] Finally, a scrambled RNase (sRNase) assay can be used to monitor the isomerase activity of PDIA1. sRNase is used as a substrate of PDIA1 and RNase enzyme activity, upon proper intramolecular disulfide formation, is used to measure PDIA1 isomerase activity.[45]

Identification of additional 4-aminopiperidine probes for other PDI family members

PDIs also of interest to our laboratory include PDIA3 and PDIA4. PDIA3 shows high homology with PDIA1, sharing similar amino acid sequences (CGHC) in their active sites.[46] PDIA3 is highly expressed in aggressive ovarian cancer cell line, YDOV-139, and may be a potential biomarker for this cancer type. PDIA4 mediates resistance to cisplatin-induced death and upon activation of the Unfolded Protein Response (UPR), PDIA4 levels increase 2-5 fold.[47,48] Several studies have suggested links between both PDIA3 and PDIA4 with cellular stress tolerance and chemoresistance in disease. Unlike

PDIA1, both of these PDIs have no known selective inhibitors. To add to potential tools and inhibitors for PDIA3 and PDIA4, recombinant protein for each PDI has been screened against the 4-aminopiperidine probe library. After fluorescent gel analysis SMC-20 was found as a covalent modifier for PDIA3 as well as SMC-19 and SMC-20 as covalent modifiers for PDIA4. The cysteine residues modified by these probes are currently being characterized. In future experiments, these probes will be used to modulate protein activities of these two enzymes to elucidate the roles each of these enzymes play in cellular homeostasis.

Acknowledgements

I would like to thank the three undergraduate students that have helped me with synthesis and evaluation of this probe library. Alexander Warshauer contributed to early optimization of synthetic procedures used for intermediate synthesis. Paige Carleen worked on synthesis of SMC-8 derivatives. Inchul You performed the PDIA1 site of labeling experiments.

Experimental Procedures

General procedures and materials

All reagents were purchased from Sigma Aldrich unless otherwise noted. Dimethyl D-Glutamate hydrochloride, L-methionine methyl ester hydrochloride, and D-leucine methyl ester hydrochloride were all purchased from TCI America (Tokyo, Japan). D-Methionine methyl ester hydrochloride was purchased from MP Biomedicals, LLG (Solon, OH). D-Tyrosine methyl ester hydrochloride was purchased from AK Scientific Inc. (Union City, CA). All compounds were characterized by proton and/or carbon NMR on either a Varian (Palo Alto, CA) 400 MHz or 500 MHz spectrometer. Chemical shifts (δ) are reported in parts per million (ppm) with chemical shifts referenced to internal standards: CDCl3 (7.26 ppm for 1H, 77.8 ppm for 13C). Coupling constants (J) are reported in Hertz (Hz) and multiplicities are abbreviated as singlet (s), broad singlet (bs), doublet (d), triplet (t), pentet (p), multiplet (m), doublet of doublets (dd), and doublet of triplets (dt). High resolution Mass Spectra (HRMS) were obtained at the Mass Spectrometry Facility at Boston College (Chestnut Hill, MA). Analytical thin layer chromatography (TLC) was performed on Sorbent Technologies Silica G TLC Plates w/UV354 (0.25 mm). All compounds were visualized on TLC by UV and/or KMnO4 staining. Column chromatography was carried out using forced flow of indicated solvent on Sorbent Technology Standard grade silica gel, 40-63 μm particle size, 60 Å pore size (Sorbent Technologies). PBS buffer, DMEM/High glucose media, RPMI 1640 media, and penicillin streptomycin (Pen/Strep) were purchased from Thermo Scientific (Waltham, MA). The anti-Myc-tag antibody and the anti-rabbit IgG HRP-linked antibody

were purchased from Cell Signaling (Danvers, MA). X-tremeGENE 9 DNA transfection reagent was purchased from Roche (Indianapolis, IN). Staurosporine (STS) was purchased from Cell Signaling (Danvers, MA). All chemical probes were added to samples at the indicated concentration from a 10mM stock in dimethyl sulfoxide (DMSO) unless otherwise noted.

General Synthetic Method of piperidine-based probes

Synthesis of pent-4-yn-1-yl 4-methylbenzenesulfonate (Compound 1)

To an oven dried flask equipped with stir bar was added, 4-pentyn-1-ol (59.4 mmol) and dichloromethane (DCM) (120 mL) under nitrogen (N_2) atmosphere. The resulting mixture was allowed to cool to 0 ˚C in an ice bath. Next, triethylamine (63.0 mmol) and tosyl chloride (63.0 mmol) was added in one portion. The reaction vessel was purged with N_2 and allowed to slowly warm to room temperature. The reaction is quenched, after 12 hours, with water and extracted with DCM (3x 50 mL). The combined organic layers were dried with sodium sulfate (Na_2SO_4) and then concentrated in vacuo. The crude oil was purified by silica column chromatography (9:1 Hexanes (Hex):Ethyl acetate (EtOAc)). The product was isolated as a clear oil (93% yield). 1H NMR (500 MHz, CDCl3): δ 7.79 (d, *J* = 8.30, 2H), 7.34 (d, *J* = 7.80, 2H), 4.14 (t, *J* = 6.35, 2H), 2.44 (s, 3H), 2.25 (td, *J* = 2.44, 6.83, 2H), 1.88-1.82 (m, 3H)ppm. 13C NMR (125 MHz, CDCl3): δ 145.05, 133.26, 130.11, 128.18, 82.36, 69.67, 68.98, 27.99, 21.88, 14.96. HRMS m/z calculated for C12H15O3S (M+H+): 239.0742. Found: 239.0739.

Synthesis of 8-(pent-4-yn-1-yl)-1,4-dioxa-8-azaspiro[4.5]decane (Compound 2)

To an oven dried flask, under N_2, equipped with stir bar and reflux condenser was added, sodium iodide (15.1 mmol), potassium carbonate (90.6 mmol) and acetonitrile (64 mL). To the suspension was added 1,4-dioxa-8-azaspiro[4.5]decane (30.2 mmol). The resulting mixture was allowed to heat to 90 ˚C and stirred for 20 min before the drop-wise addition of tosylated alcohol (1) (45.3 mmol). The reaction was allowed to mix for 18 hours before being cooled and diluted with DCM. The suspension was filtered to remove solid precipitate. The remaining supernatant was concentrated *in vacuo* and then the resulting residue was dissolved in DCM (25 mL) and washed with 5% aq. NaOH (3x 25 mL) and brine (3x 25mL). The aqueous layer was extracted with DCM (3x 25 mL) and the combined layers were first dried with Na_2SO_4, filtered then concentrated *in vacuo*. The crude oil was purified by silica column chromatography (9:1-1:1 Hex: EtOAc). The resulting product was isolated as a clear light yellow oil (80% yield). 1H NMR (500 MHz, CDCl3): δ 3.93 (s, 4H), 2.51 (bs, 4H), 2.44 (t, *J* = 7.56, 2H), 2.21 (td, *J* = 2.44, 7.32, 2H), 1.92 (t, *J* = 2.64, 1H), 1.74-1.68 (m, 6H). 13C NMR (125 MHz, CDCl3): δ 107.98, 84.91, 69.05, 64.88, 57.06, 52.05, 35.52, 26.86, 17.15. HRMS m/z calculated for C12H20NO3 (M+H+): 210.1494. Found: 210.1493.

Synthesis of 1-(pent-4-yn-1-yl)piperidin-4-one (Compound 3)

To a round bottom flask was added ketal (2) (9.6 mmol), 1N HCl aq. (95 mL) and tetrahydrofuran (THF) (95 mL). The resulting mixture was heated to 100 ˚C for 20 hours. The reaction was allowed to cool and then slowly quenched with sodium bicarbonate. The aqueous layer was extracted with DCM (3x 100 mL). The solution of the crude

product was concentrated in vacuo and purified on silica column chromatography (9:1-1:1 Hex: EtOAc) to yield a light yellow oil (90% yield). 1H NMR (500 MHz, CDCl3): δ 2.74 (t, *J* = 6.34, 4H), 2.56 (t, *J* = 7.06, 2H), 2.45 (t, *J* = 6.10, 4H), 2.28 (td, *J* = 2.44, 7.08, 2H), 1.96 (t, *J* = 2.69, 1H), 1.74 (p, *J* =7.32, 2H). 13C NMR (125 MHz, CDCl3): δ 210.02, 84.80, 69.45, 61.22, 56.83, 42.07, 27.14, 17.16. HRMS m/z calculated for C10H15NO (M+H+): 166.1232. Found: 166.1228.

S***ynthesis of N-octyl-1-(pent-4-yn-1-yl)piperidin-4-amine (Compound 4)***

To a flame dried vial equipped with stir bar was added ketone (3) (0.3 mmol), 1˚ *n*-octylamine (0.3 mmol) and DCM (1 mL). The resulting mixture was allowed to stir at room temperature for 5 minutes before the addition of sodium triacetoxyborohydride in one portion (0.4 mmol). The vial was purged with N_2 and the resulting mixture was allowed to stir at room temperature for 12 hours before it was diluted with DCM (1 mL) and quenched with sodium bicarbonate (2 mL). The aqueous layer was extracted with DCM (3x 3 mL). The resulting DCM solution was concentrated in vacuo to obtain a crude oil. The oil was purified by silica column chromatography (9:1 DCM: Hex, 1:1 DCM: Hex, DCM, DCM/2% Methanol (MeOH)) to obtain a clear yellow oil (>98% yield).

Synthesis of 2-chloro-N-octyl-N-(1-(pent-4-yn-1-yl)piperidin-4-yl)acetamide (SMC-1)

To a flame dried vial equipped with stir bar was added the 2˚ amine intermediate (4) (0.9 mmol), as described above, and DCM (2 mL). The reaction vessel was purged with N_2 and cooled to 0 ˚C. Next, chloroacetyl chloride (1.2 mmol) was added drop-wise

followed by triethylamine (1.2 mmol) added dropwise as well. The resulting mixture was allowed to warm to room temperature and stir for 8 hours. The reaction was quenched by the addition of sodium bicarbonate (2 mL), extracted with DCM (3x 2mL) and concentrated *in vacuo* to yield a crude oil. The resulting mixture was purified by column chromatography (Base wash column with 2% NEt3, 9:1 DCM: Hex, 1:1 DCM: Hex, DCM, DCM/2%MeOH) to obtain a viscous, light yellow oil (66% yield).

Characterization of probe library members

Compound SMC-1:

The synthesis for SMC-1 is described above. Due to the sterically encumbered directing group, SMC-1 was found to have atropic isomers. 1H NMR (400 MHz, CDCl3): δ 4.32-4.29 (m, 0.5H), 4.05 (d, *J* = 4.69, 2H), 3.55-3.49 (m, 0.5H), 3.21-3.16 (m, 2H), 3.01-2.95 (m, 2H), 2.45-2.41 (m, 2H), 2.25-2.19 (m, 2H), 2.05-1.99 (m, 2H), 1.95-1.93 (m, 1H), 1.89-1.80 (m, 1H), 1.73-1.66 (m, 5H), 1.61-1.54 (m, 3H), 1.26 (bs, 10H), 0.89-0.85 (m, 3H). 13C NMR (100 MHz, CDCl3): δ 166.82 (d), 84.66, 69.20, 57.81 (d), 53.43, 44.66, 43.42, 42.35 (d), 32.57, 32.40 (d), 30.35, 29.906 (m), 29.69, 27.87 (d), 26.67, 23.27 (d), 17.10, 14.74. HRMS m/z calculated for C20H36ClN2O (M+H+): 355.2516. Found: 355.2522.

Compound SMC-2:

Synthesized using the general procedure described above, using (exo)-norbonylamine as the source of diversity element. 1H NMR (400 MHz, CDCl3): δ 4.07-3.99 (m, 2H), 3.22

(bs, 1H), 2.99-2.94 (m, 2H), 2.43-2.39 (m, 2H), 2.32 (bs, 1H), 2.21 (td, *J* = 2.73, 7.05, 2H), 2.16 (bs, 1H), 1.99-1.94 (m, 2H), 1.92 (t, *J* = 2.73, 1H), 1.72-1.65 (m, 3H), 1.57-1.45 (m, 6H), 1.23-1.20 (m, 4H), 1.13-1.09 (m, 2H). 13C NMR (100 MHz, CDCl3): δ 166.63, 84.79, 69.11, 61.09, 57.55, 54.17, 44.21, 42.79, 39.02, 38.21, 36.97, 31.16, 30.35, 28.18, 26.26, 22.36, 17.08. HRMS m/z calculated for C19H30ClN2O (M+H+): 337.2047. Found: 337.2044.

Compound SMC-3:

Synthesized using the general procedure described above, using 4- methoxybenzylamine as the source of diversity element. 1H NMR (400 MHz, CDCl3): δ 7.14-7.06 (m, 2H), 6.88-6.80 (m, 2H), 4.52 (s, 2H), 4.04 (d, *J* = 95.86, 2H), 3.79 (s, 3H), 2.94-2.87 (m, 2H), 2.41-2.38 (m, 2H), 2.19 (bs, 2H), 2.04-1.96 (m, 2H), 1.92 (bs, 1H), 1.83-1.80 (m, 1H), 1.69-1.62 (m, 5H). 13C NMR (100 MHz, CDCl3): δ 168.14, 154.65, 129.98, 127.31, 115.04, 84.65, 69.17, 57.75, 55.98, 53.44, 46.73, 42,68, 31.77, 30.02, 26.60, 17.06. HRMS m/z calculated for C20H28ClN2O2 (M+H+): 363.1839. Found:363.1837.

Compound SMC-4:

Synthesized using the general procedure described above, using 3-methoxybenzylamine as the source of diversity element. 1H NMR (500 MHz, CDCl3): δ 7.28-7.19 (m, 1H), 6.81-6.69 (m, 3H), 2.56 (bs, 2H), 4.05 (d, *J* = 129.81, 2H), 3.79 (bs, 3H), 2.96-2.90 (m, 2H), 2.42-2.39 (m, 2H), 2.22-2.19 (m, 2H), 2.08-1.97 (3H), 1.92 (bs, 1H), 1.84-1.78 (m, 1H), 1.69-1.62 (m, 5H). HRMS m/z calculated for C20H28ClN2O2 (M+H+): 363.1839. Found: 363.1835.

Compound SMC-5:

Synthesized using the general procedure described above, using 4-fluorobenzylamine as the source of diversity element. 1H NMR (500 MHz, CDCl3): δ 7.17-7.14 (m, 2H), 7.05-7.02 (m, 1H), 6.96-6.92 (m, 1H), 4.54 (d, *J* = 6.34, 2H), 4.17 (bs, 1H), 3.90 (bs, 1H), 3.70-3.66 (m, 1H), 2.94-2.91 (m, 2H), 2.41-2.38 (m, 2H), 2.19-2.18 (m, 2H), 2.07-1.97 (m, 2H), 1.92 (bs, 2H), 1.82-1.75 (m, 1H), 1.68-1.64 (m, 5H). 13C NMR (125 MHz, CDCl3): δ 167.9, 134.42 (d), 128.48 (d), 116.63 (d), 115.92 (d), 84.61, 69.25, 57.72, 46.68, 42.37 (d), 31.75, 29.96, 26.54, 17.05. HRMS m/z calculated for C19H25ClFN2O (M+H+): 351.1639. Found: 351.1643.

Compound SMC-6:

Synthesized using the general procedure described above, using L-phenylalanine methyl ester (HCl salt) as the source of diversity element. 1H NMR (500 MHz, CDCl3): δ 7.27-7.24 (m, 2H), 7.21-7.16 (m, 3H), 4.07 (dd, *J* = 12.2, 79.43, 2H), 3.86-3.83 (m, 1H), 3.73 (s, 3H), 3.50-3.37 (m, 3H), 2.97-2.95 (m, 1H), 2.72-2.70 (m, 1H), 2.37-2.34 (m, 2), 2.19-2.16 (m, 2H), 2.04-1.78 (m, 4), 1.71-1.59 (m, 3H), 1.07-1.01 (m, 1H), 0.58-0.55 (m, 1H). HRMS m/z calculated for C22H30ClN2O3 (M+H+): 405.1945. Found: 405.1952.

Compound SMC-7:

Synthesized using the general procedure described above, using D-phenylalanine methyl ester (HCl salt) as the source of diversity element.1H NMR (500 MHz, CDCl3): δ 7.29-7.25 (m, 2H), 7.21-7.16 (m, 3H), 4.07 (dd, *J* = 12.2, 36.36, 2H), 3.85-3.82 (m, 1H), 3.73

(s, 3H), 3.51-3.37 (m, 3H), 2.94-2.92 (m, 1H), 2.71-2.68 (m, 1H), 2.35-2.31 (m, 2H), 2.19-2.16 (m, 2H), 1.93-1.80 (m, 4H), 1.65-1.60 (m, 3H), 1.20-0.96 (m, 1H), 0.58-0.54 (m, 1H). HRMS m/z calculated for C22H30ClN2O3 (M+H+): 405.1945. Found: 405.1934.

Compound SMC-8:

Synthesized using the general procedure described above, using L-tyrosine methyl ester (HCl salt) as the source of diversity element. 1H NMR (500 MHz, CDCl3): δ 6.96 (d, *J* = 7.56, 2H), 6.67 (d, *J* = 7.57, 2H), 4.06 (dd, *J* = 12.45, 37.71, 2H), 3.78-3.75 (m, 1H), 3.70 (s, 3H), 3.49-3.38 (m, 2H), 3.27-3.22 (m, 1H), 2.97-2.95 (m, 1H), 2.79-2.77 (m, 1H), 2.39-2.36 (m, 2H), 2.19-2.16 (m, 2H), 1.98-1.82 (m, 3H), 1.72-1.63 (m, 3H), 1.20-1.17 (m, 2H), 0.80-0.77 (m, 1H). 13C NMR (100 MHz, CDCl3): δ 170.78, 166.54, 154.92, 131.12, 130.01, 115.36, 83.82, 68.63, 58.59, 57.06, 53.11, 53.41, 41.76, 34.08, 30.47, 29.67, 25.72, 16.40. HRMS m/z calculated for C22H30ClN2O4 (M+H+): 421.1894. Found: 421.1877.

Compound SMC-9:

Synthesized using the general procedure described above, using D-tyrosine methyl ester (HCl salt) as the source of diversity element. 1H NMR (500 MHz, CDCl3): δ 6.96 (d, *J* = 8.54, 2H), 6.67 (d, *J* = 8.3, 2H), 4.06 (dd, *J* = 12.2, 73.3, 2H), 3.78-3.75 (m, 1H), 3.71 (s, 3H), 3.48-3.37 (m, 2H), 3.28-3.24 (m, 1H), 2.96-2.94 (m, 1H), 2.76-2.74 (m, 1H), 2.38-2.34 (m, 2H), 2.19-2.16 (m, 2H), 1.96-1.80 (m, 3H), 1.71-1.62 (m, 3H), 1.14-1.10 (m, 2H), 0.77-0.74 (m, 1H). 13C NMR (100 MHz, CDCl3): δ 171.47, 167.24, 155.69,

131.79, 130.62, 116.08, 84.50, 69.32, 59.28, 57.75, 53.80, 53.11, 42.44, 34.77, 31.15, 30.35, 26.40, 17.09. HRMS m/z calculated for C22H30ClN2O4 (M+H+): 421.1894. Found: 421.1899.

Compound SMC-10:

Synthesized using the general procedure described above, using L-methionine methyl ester (HCl salt) as the source of diversity element. 1H NMR (500 MHz, CDCl3): 4.07 (dd, *J* = 15.37, 38.68, 2H), 3.90-3.88 (m, 1H), 3.68 (s, 3H), 3.66-3.58 (m, 1H), 3.02-3.00 (m, 2H), 2.78-2.71 (m, 1H), 2.67-2.62 (m, 2H), 2.45-2.42 (m, 2H), 2.24-2.01 (m, 2H), 2.09 (s, 3H), 2.05-2.03 (m, 2H), 1.95-1.79 (m, 6H), 1.72-1.66 (m, 2H). HRMS m/z calculated for C18H30ClN2O3S (M+H+): 389.1666. Found: 389.1658.

Compound SMC-11:

Synthesized using the general procedure described above, using D-methionine methyl ester (HCl salt) as the source of diversity element. 1H NMR (500 MHz, CDCl3): 4.06 (dd, *J* = 12.21, 37.10, 2H), 3.90-3.88 (m, 1H), 3.68 (s, 3H), 3.65-3.59 (m, 1H), 3.02-3.00 (m, 2H), 2.78-2.71 (m, 1H), 2.66-2.63 (m, 2H), 2.44-2.41 (m, 2H), 2.24-2.01 (m, 2H), 2.09 (s, 3H), 2.06-2.02 (m, 2H), 1.95-1.79 (m, 6H), 1.72-1.66 (m, 2H). HRMS m/z calculated for C18H30ClN2O3S (M+H+): 389.1666. Found: 389.1667.

Compound SMC-12:

Synthesized using the general procedure described above, using L-leucine methyl ester (HCl salt) as the source of diversity element. 1H NMR (400 MHz, CDCl3): δ 4.05 (dd, *J*

= 12.12, 13.70, 2H), 3.70-3.56 (m, 5H), 3.02-3.29 (m, 2H), 2.48-2.41 (m, 3H), 2.24-2.20 (m, 2H), 2.07-2.02 (m, 2H), 1.94-1.93 (m, 2H), 1.87-1.77 (m, 4H), 1.73-1.65 (m, 2H), 1.31-1.24 (m, 1H), 0.94-0.92 (m, 6H). 13C NMR (100 MHz, CDCl3): δ 172.21, 166.85, 84.78, 69.33, 58.39, 57.77, 55.58, 53.91, 52.98, 42.50, 40.55, 31.76 (d), 26.68, 24.02, 23.21, 17.17. HRMS m/z calculated for C19H32ClN2O3 (M+H+): 371.2101. Found: 371.2085.

Compound SMC-13:

Synthesized using the general procedure described above, using D-leucine methyl ester (HCl salt) as the source of diversity element.1H NMR (400 MHz, CDCl3): δ 4.05 (dd, *J* = 12.20, 30.74, 2H), 3.70-3.57 (m, 5H), 3.01-2.99 (m, 2H), 2.43-2.41 (m, 3H), 2.22-2.19 (m, 2H), 2.05-2.01 (m, 2H), 1.93 (bs, 2H), 1.85-1.76 (m, 4H), 1.71-1.65 (m, 4H), 1.29-1.23 (m, 1H), 0.93-0.92 (m, 6H). 13C NMR (100 MHz, CDCl3): δ 171.32, 166.01, 83.67, 68.82, 57.20, 56.80, 54.75, 52.91, 52.15, 41.71, 39.73, 29.62 (d), 25.83, 23.20, 22.39, 16.28. HRMS m/z calculated for C19H32ClN2O3 (M+H+): 371.2101. Found: 371.2101.

Compound SMC-14:

Synthesized using the general procedure described above, using L-glutamate dimethyl ester (HCl salt) as the source of diversity element. 1H NMR (500 MHz, CDCl3): δ 4.07 (dd, *J* = 12.2, 33.31, 2H), 3.79-3.77 (m, 1H), 3.69 (s, 3H), 3.68 (s, 3H), 3.66-3.58 (m, 1H), 3.20-2.98 (m, 2H), 2.70-2.65 (m, 1H), 2.55-2.52 (m, 2H), 2.45-2.42 (m, 2H), 2.41-

2.22 (m, 2H), 2.08-1.91 (m, 5H), 1.84-1.78 (m, 3H), 1.70-1.68 (m, 2H). HRMS m/z calculated for C19H30ClN2O5 (M+H+): 401.1843. Found: 401.1849.

Compound SMC-15:

Synthesized using the general procedure described above, using D-glutamate dimethyl ester (HCl salt) as the source of diversity element. 1H NMR (500 MHz, CDCl3): δ 4.06 (dd, *J* = 12.2, 32.94, 2H), 3.79-3.77 (m, 1H), 3.69 (s, 3H), 3.67 (s, 3H), 3.66-3.61 (m, 1H), 3.05-3.01 (m, 2H), 2.69-2.63 (m, 1H), 2.55-2.52 (m, 2H), 2.46-2.43 (m, 2H), 2.25-2.21 (m, 2H), 2.09-1.92 (m, 5H), 1.86-1.78 (m, 3H), 1.74-1.67 (m, 2H). HRMS m/z calculated for C19H30ClN2O5 (M+H+): 401.1843. Found: 401.1858.

Preparation of cell lysates:

Cells (MCF-7 or HEK 293T) were grown to 100% confluency under 5% CO2 at 37 ˚C before they were scraped, washed (3x 5 mL Phosphate buffered saline (PBS)) and pelleted (by centrifugation; 3,500 rpm, 5 min, 4 ˚C). After the supernatant was removed, the cells were lysed in PBS. The lysates were separated to obtain the soluble lysates by ultracentrifugation (45,000 rpm, 45 min, 4˚C). The soluble lysates were normalized to 2 mg mL-1 and used in subsequent experiments.

Click chemistry and fluorescent analysis:

Cell lysates, described above, were aliquoted into 50 μL samples and exposed to probe for 1 hour at room temperature. Samples underwent click chemistry combining

rhodamine-azide (0.025 mM), TCEP (0.28 mg mL-1), tris[(1-benzyl-1H-1,2,3-triazol-4-yl)methyl]amine (TBTA ligand) (100 μM, 17X stock in DMSO: *t*-Butanol 1:4), and CuSO4 (1 mM). The reaction was mixed after 30 minutes of incubation at room temperature and then allowed to proceed for another 30 minutes before being quenched with 2x SDS loading dye. The samples were then separated by SDS-PAGE and visualized with a Hitachi FMBIO II multiview flatbed laser-induced fluorescent scanner at 585 nm or with a BioRad ChemiDoc MT Imaging System set to the Rhodamine filter.

***In situ* gel profiling**

MCF-7 cells were grown to 100% confluency, in RPMI media supplemented with 10% fetal calf serum (FCS), 2 mM glutamine, and 1% Penn/strep (under 5% CO2 at 37 ˚C), before being introduced to probes. The probes were diluted into 5 mL of serum free RPMI media supplemented with Penn/strep from 5 mM DMSO stocks to the desired probing concentrations (1μM or 5μM) under a sterile environment. Next, the probe containing media was gently added to the cells and the cells were allowed to incubate under 5% CO2 at 37 ˚C for 1 hour. The cells were then scraped from the plate and transferred to a 15 mL conical tube. The cells were washed 3x (5 mL) with PBS, by resuspending the pellet in the PBS followed by centrifugation (3,500 rpm for 5 minutes at 4 ˚C) and removal of supernatant. When washing was complete, the cells were resuspended in PBS and lysed by sonication. The soluble lysates were separated by ultracentrifugation (45,000 rpm for 45 min at 4 ˚C). After, the lysates were normalized to a protein concentration of 2 mg mL-1 and aliquoted into 50 μL reaction volumes. Each reaction sample was exposed to click chemistry conditions with rhodamine-azide for

visualization, as described above. After analysis, gels underwent a typical procedure for coomassie staining and destaining. Stained gels were visualized on a Stratagene Eagle Eye apparatus by a COHU High performance CCD camera or with a BioRad ChemiDoc MT Imaging System using the Coomassie Blue setting.

Transfection procedure

The cDNA for WT-GSTO1 and WT-AKT1 were subcloned into a pcDNA3.1-myc/His mammalian expression vector. Site-directed mutagenesis was used to obtain the C32A GSTO1 mutant, and all constructs were verified by sequencing (Genewiz, Cambridge, MA). HEK 293T cells were grown at 37 °C under 5% CO2 in DMEM media supplemented with 10% fetal bovine serum (FBS), 2 mM glutamine, and 1% Penn/strep. Transfections were performed on 10 cm cell plates of ~50% confluency. Serum free DMEM media (600 μL) and X-tremeGENE DNA transfection reagent (20 μL) were combined in an eppendorf tube and vortexed. Plasmids of WT-GSTO1, WT-AKT1 or C32A GSTO1 (6 μg) were added and the sample was shaken and remained at room temperature for 15 minutes. This plasmid solution was added dropwise to the HEK 293T cells. was incubated at 37 °C under 5% CO2 for 48 hours. HEK 293T cells transfected with the pcDNA3.1-myc/His plasmid was used as a mock negative control. The lysates were prepared as described above.

***In vitro* gel profiling**

The procedure for preparation of lysates, described above, was used to obtain the lysates used in the following experiment. After, the lysates are normalized to a protein

concentration of 2 mg mL-1 and aliquoted into 50 μL reaction volumes. To each sample was added equal volume of probe to achieve the desired final concentration of probe in 50 μL (GSTO1 at 1μM and AKT1 at 5μM) and the sample was allowed to incubate at room temperature for 1 hour. Each reaction sample was exposed to click chemistry conditions with Rhodamine-azide for visualization. The click chemistry reaction was allowed to proceed at room temperature for 1 hour, and then the proteins were separated by SDS-PAGE. The gel was then scanned to obtain a fluorescent image, as described above, and then proteins were transferred to nitrocellulose membrane for a
Western Blot. The concentrations of GSTO1 or AKT1 were evaluated by Western Blot analysis, described below.

GSTO1 site of labeling experiment

HEK 293T cells were transfected with either WT-GSTO1 or C32A-GSTO1 mammalian constructs, as described above. The cells were grown to 100% confluency and then exposed to SMC-1 (0.5 μM) by diluting 5 mM probe stock into 5 mL of serum free DMEM media, supplemented with 1% Penn/strep. The cells were allowed to incubate with probe for 1 hour before being scraped, washed, pelleted, and sonicated as described above. After the soluble protein lysates was normalized to 2 mg mL-1 and aliquoted into 50 μL reaction volumes, they were exposed to click chemistry conditions and visualized by fluorescence, as described above. The protein was then transferred to nitrocellulose paper and the GSTO1 protein concentrations were evaluated by Western Blot analysis, described below.

Staurosporine AKT1 inhibition experiment with SMC-8

Cell lysates were prepared as described above and normalized to 2 mg mL-1. The lysates were aliquoted into 50 μL samples and then treated with Staurosporine (STS) in DMSO to obtain samples with final STS concentrations of 0, 0.5, 1, 5, 10, 25, 50, 100 μM. The STS treated samples were mixed and then allowed to incubate for 1 hour at room temperature. Then each sample was exposed to SMC-8 (5 μM). The samples were incubated at room temperature for another hour before being exposed to click chemistry conditions, as described above. Then the proteins were separated by SDS-PAGE. The gel was then scanned to obtain a fluorescent image and then proteins were transferred to nitrocellulose membrane for Western Blot analysis. The concentrations of AKT1 were evaluated by Western Blot analysis, described below.

Western Blot Analysis

After the protein was transferred to nitrocellulose paper (75mV, 120 min), the membrane was washed with tris-buffered saline with 1% Tween 20 (TBST) and then stained by Ponceau S stain to detect transferred proteins. The membrane was washed 3x (~10 mL for 5 min) with TBST until completely destained. The membrane was then allowed to milk block (2.5g in 50 mL of TBST) for 2 hours at room temperature before being washed again with TBST (3x ~10 mL for 5 min). The membrane was then exposed to 1˚ anti-Myc antibody (Ab) (1:1000) in TBST and allowed to incubate over night at 4 ˚C. Then the membrane is washed with TBST (3x ~10 mL for 5 min) and exposed to antirabbit-HRP conjugated 2˚ Ab (1:3333) in TBST for 2 hours at room temperature. After 2˚ Ab incubation the membrane is washed 3x (~10 mL for 5 min) with TBST

before being treated with HRP super signal chemiluminescence reagents and exposed to film for one minute before development, using Kodak X-OMAT 2000A processor.

Expression and purification of PDIA1 and mutants in BL21 (DE3) cells

PDIA1 (WT or C53A, C56A, C397A, C400A, and C53/397A mutants) were subcloned into pET23a for expressions as a C-terminal 6-His fusion protein in *Escherichia coli* BL21 (DE3) cells. Cells were then inoculated in a 5mL LB medium containing 100μM Ampicillin (LB-Amp medium) at 37°C overnight. The overnight culture was added to a 500mL LB-Amp medium and allowed to grow at 37°C until OD_{600} ~ 0.8. Expression was then induced by the addition of 0.3 mM IPTG for 5hrs at 37°C. Cells were harvested and lysed in DPBS. The expressed fusion protein was purified using a Ni-NTA packed chromatography column. After loading whole cell lysate on the column, the unspecific proteins were washed away with 50mM imidazole in PBS. PDIA1 protein was eluted with 500mM imidazole in PBS.

Protein expression and purification were then analyzed by 10% SDS-PAGE. After analysis, gels underwent a silver staining. Excess imidazole was then removed by use of a Nap-5 column. The purified protein was eluted by a 20mM potassium phosphate buffer, pH 7.4, containing 5% glycerol and 5mM β-mercaptoethanol, and stored at -80°C.

Evaluation of 4-aminopiperidine probes for PDIA1

The 4-aminopiperidine library was screened against the WT and mutant recombinant PDIA1 proteins. The purified protein (0.1 mg/ mL) was added to 2 mg/mL MCF7 lysates before incubation SMC-9, SMC-11, SMC-14, SMC-18. The samples were exposed to

standard CuAAC conditions in the presence of Rhodamine-azide. The fluorescent samples were separated by 10% SDS-PAGE gel and the gels were imaged on a BioRad ChemiDoc MP Imaging System, using the Rhodamine fluorescence exposure setting. Decreases of fluorescence in the mutant samples were observed.

References

(1) Pace, N.; Weerapana, E. Diverse Functional Roles of Reactive Cysteines. *ACS chemical biology* **2012**.
(2) Weerapana, E.; Wang, C.; Simon, G. M.; Richter, F.; Khare, S.; Dillon, M. B.; Bachovchin, D. A.; Mowen, K.; Baker, D.; Cravatt, B. F. Quantitative Reactivity Profiling Predicts Functional Cysteines in Proteomes. *Nature* **2010**, *468*, 790–5.
(3) Weerapana, E.; Simon, G. M.; Cravatt, B. F. Disparate Proteome Reactivity Profiles of Carbon Electrophiles. *Nat. Chem. Biol.* **2008**, *4*, 405–7.
(4) Hensley, P.; Mishra, M.; Kyprianou, N. Targeting Caspases in Cancer Therapeutics. *Biol. Chem.* **2013**, *394*, 831–43.
(5) Palermo, C.; Joyce, J. A. Cysteine Cathepsin Proteases as Pharmacological Targets in Cancer. *Trends Pharmacol. Sci.* **2008**, *29*, 22–8.
(6) Song, M. S.; Salmena, L.; Pandolfi, P. P. The Functions and Regulation of the PTEN Tumour Suppressor. *Nat. Rev. Mol. Cell Biol.* **2012**, *13*, 283–96.
(7) Lessard, L.; Stuible, M.; Tremblay, M. L. The Two Faces of PTP1B in Cancer. *Biochim. Biophys. Acta* **2010**, *1804*, 613–9.
(8) Liu, Q.; Sabnis, Y.; Zhao, Z.; Zhang, T.; Buhrlage, S. J.; Jones, L. H.; Gray, N. S. Developing Irreversible Inhibitors of the Protein Kinase Cysteinome. *Chem. Biol.* **2013**, *20*, 146–59.
(9) Leproult, E.; Barluenga, S.; Moras, D.; Wurtz, J.-M. M.; Winssinger, N. Cysteine Mapping in Conformationally Distinct Kinase Nucleotide Binding Sites: Application to the Design of Selective Covalent Inhibitors. *J. Med. Chem.* **2011**, *54*, 1347–55.
(10) Montero, A. J.; Jassem, J. Cellular Redox Pathways as a Therapeutic Target in the Treatment of Cancer. *Drugs* **2011**, *71*, 1385–96.
(11) Anastasiou, D.; Poulogiannis, G.; Asara, J. M.; Boxer, M. B.; Jiang, J. K.; Shen, M.; Bellinger, G.; Sasaki, A. T.; Locasale, J. W.; Auld, D. S.; et al. Inhibition of Pyruvate Kinase M2 by Reactive Oxygen Species Contributes to Cellular Antioxidant Responses. *Science* **2011**, *334*, 1278–83.
(12) Banerjee, R.; Pace, N. J.; Brown, D. R.; Weerapana, E. 1,3,5-Triazine as a Modular Scaffold for Covalent Inhibitors with Streamlined Target Identification. *J. Am. Chem. Soc.* **2013**, *135*, 2497–500.

(13) Directors, I. PREFACE. *Acta Hortic* **2005**, 5–5.
(14) O'Hagan, D. Pyrrole, Pyrrolidine, Pyridine, Piperidine and Tropane Alkaloids. *Nat Prod Rep* **2000**, *17*, 435–46.
(15) Arbiser, J. L.; Kau, T.; Konar, M.; Narra, K.; Ramchandran, R.; Summers, S. A.; Vlahos, C. J.; Ye, K.; Perry, B. N.; Matter, W.; et al. Solenopsin, the Alkaloidal Component of the Fire Ant (Solenopsis Invicta), Is a Naturally Occurring Inhibitor of Phosphatidylinositol-3-Kinase Signaling and Angiogenesis. *Blood* **2007**, *109*, 560–5.
(16) Tang, Y.; Fu, Y.; Xiong, J.; Li, M.; Ma, G.-L. L.; Yang, G.-X. X.; Wei, B.-G. G.; Zhao, Y.; Zhang, H.-Y. Y.; Hu, J.-F. F. Casuarinines A-J, Lycodine-Type Alkaloids from Lycopodiastrum Casuarinoides. *J. Nat. Prod.* **2013**, *76*, 1475–84.
(17) Lee, S. T.; Green, B. T.; Welch, K. D.; Jordan, G. T.; Zhang, Q.; Panter, K. E.; Hughes, D.; Chang, C.-W. T. W.; Pfister, J. A.; Gardner, D. R. Stereoselective Potencies and Relative Toxicities of Γ-Coniceine and N-Methylconiine Enantiomers. *Chem. Res. Toxicol.* **2013**, *26*, 616–21.
(18) Blackburne, I. D.; Katritzky, A. R.; Takeuchi, Y. Conformation of Piperidine and of Derivatives with Additional Ring Hetero Atoms. *Acc. Chem. Res. 8*, 300–306.
(19) Källström, S.; Leino, R. Synthesis of Pharmaceutically Active Compounds Containing a Disubstituted Piperidine Framework. *Bioorg. Med. Chem.* **2008**, *16*, 601–35.
(20) Došen-Mićović, L.; Roglić; Mićović; Ivanović Conformational Study of Fentanyl and Its analogs.1. Conformational Space of the N-phenethyl Substituent. *Electronic Journal of Theoretical Chemistry* **1996**, *1*, 199–210.
(21) Speers, A. E.; Adam, G. C.; Cravatt, B. F. Activity-Based Protein Profiling in Vivo Using a Copper(i)-Catalyzed Azide-Alkyne [3 + 2] Cycloaddition. *J. Am. Chem. Soc.* **2003**, *125*, 4686–7.
(22) Speers, A. E.; Cravatt, B. F. Profiling Enzyme Activities in Vivo Using Click Chemistry Methods. *Chem. Biol.* **2004**, *11*, 535–46.
(23) Bachovchin, D. A.; Brown, S. J.; Rosen, H.; Cravatt, B. F. Identification of Selective Inhibitors of Uncharacterized Enzymes by High-Throughput Screening with Fluorescent Activity-Based Probes. *Nat. Biotechnol.* **2009**, *27*, 387–94.
(24) Piaggi, S.; Raggi, C.; Corti, A.; Pitzalis, E.; Mascherpa, M. C.; Saviozzi, M.; Pompella, A.; Casini, A. F. Glutathione Transferase Omega 1-1 (GSTO1-1) Plays an Anti-Apoptotic Role in Cell Resistance to Cisplatin Toxicity. *Carcinogenesis* **2010**, *31*, 804–11.
(25) Tsuboi, K.; Bachovchin, D. A.; Speers, A. E.; Spicer, T. P.; Fernandez-Vega, V.; Hodder, P.; Rosen, H.; Cravatt, B. F. Potent and Selective Inhibitors of Glutathione S-Transferase Omega 1 That Impair Cancer Drug Resistance. *J. Am. Chem. Soc.* **2011**, *133*, 16605–16.
(26) Pace, N. J.; Pimental, D. R.; Weerapana, E. An Inhibitor of Glutathione S-Transferase Omega 1 That Selectively Targets Apoptotic Cells. *Angew. Chem. Int. Ed. Engl.* **2012**, *51*, 8365–8.
(27) Wu, W.-I. I.; Voegtli, W. C.; Sturgis, H. L.; Dizon, F. P.; Vigers, G. P.; Brandhuber, B. J. Crystal Structure of Human AKT1 with an Allosteric Inhibitor Reveals a New Mode of Kinase Inhibition. *PLoS ONE* **2010**, *5*, e12913.
(28) Lee, J. Y.; Lee, Y. G.; Lee, J.; Yang, K.-J. J.; Kim, A. R.; Kim, J. Y.; Won, M.-H. H.; Park, J.; Yoo, B. C.; Kim, S.; et al. Akt Cys-310-Targeted Inhibition by Hydroxylated

Benzene Derivatives Is Tightly Linked to Their Immunosuppressive Effects. *J. Biol. Chem.* **2010**, *285*, 9932–48.
(29) Yasukawa, T.; Tokunaga, E.; Ota, H.; Sugita, H.; Martyn, J. A.; Kaneki, M. S-Nitrosylation-Dependent Inactivation of Akt/protein Kinase B in Insulin Resistance. *J. Biol. Chem.* **2005**, *280*, 7511–8.
(30) Murata, H.; Ihara, Y.; Nakamura, H.; Yodoi, J.; Sumikawa, K.; Kondo, T. Glutaredoxin Exerts an Antiapoptotic Effect by Regulating the Redox State of Akt. *J. Biol. Chem.* **2003**, *278*, 50226–33.
(31) Lu, X.-M. M.; Lu, M.; Tompkins, R. G.; Fischman, A. J. Site-Specific Detection of S-Nitrosylated PKB alpha/Akt1 from Rat Soleus Muscle Using CapLC-Q-TOF(micro) Mass Spectrometry. *J Mass Spectrom* **2005**, *40*, 1140–8.
(32) Bertrand, R.; Solary, E.; O'Connor, P.; Kohn, K. W.; Pommier, Y. Induction of a Common Pathway of Apoptosis by Staurosporine. *Exp. Cell Res.* **1994**, *211*, 314–21.
(33) Calleja, V.; Laguerre, M.; Parker, P. J.; Larijani, B. Role of a Novel PH-Kinase Domain Interface in PKB/Akt Regulation: Structural Mechanism for Allosteric Inhibition. *PLoS Biol.* **2009**, *7*, e17.
(34) Addie, M.; Ballard, P.; Buttar, D.; Crafter, C.; Currie, G.; Davies, B. R.; Debreczeni, J.; Dry, H.; Dudley, P.; Greenwood, R.; et al. Discovery of 4-Amino-N-[(1S)-1-(4-Chlorophenyl)-3-Hydroxypropyl]-1-(7H-pyrrolo[2,3-D]pyrimidin-4-Yl)piperidine-4-Carboxamide (AZD5363), an Orally Bioavailable, Potent Inhibitor of Akt Kinases. *J. Med. Chem.* **2013**, *56*, 2059–73.
(35) Xu, S.; Sankar, S.; Neamati, N. Protein Disulfide Isomerase: A Promising Target for Cancer Therapy. *Drug Discov. Today* **2014**, *19*, 222–40.
(36) Appenzeller-Herzog, C.; Ellgaard, L. The Human PDI Family: Versatility Packed into a Single Fold. *Biochim. Biophys. Acta* **2008**, *1783*, 535–48.
(37) Wang, C.; Li, W.; Ren, J.; Fang, J.; Ke, H.; Gong, W.; Feng, W.; Wang, C.-C. C. Structural Insights into the Redox-Regulated Dynamic Conformations of Human Protein Disulfide Isomerase. *Antioxid. Redox Signal.* **2013**, *19*, 36–45.
(38) Xu, S.; Butkevich, A. N.; Yamada, R.; Zhou, Y.; Debnath, B.; Duncan, R.; Zandi, E.; Petasis, N. A.; Neamati, N. Discovery of an Orally Active Small-Molecule Irreversible Inhibitor of Protein Disulfide Isomerase for Ovarian Cancer Treatment. *Proc. Natl. Acad. Sci. U.S.A.* **2012**, *109*, 16348–53.
(39) Hoffstrom, B. G.; Kaplan, A.; Letso, R.; Schmid, R. S.; Turmel, G. J.; Lo, D. C.; Stockwell, B. R. Inhibitors of Protein Disulfide Isomerase Suppress Apoptosis Induced by Misfolded Proteins. *Nat. Chem. Biol.* **2010**, *6*, 900–6.
(40) Lyles, M. M.; Gilbert, H. F. Catalysis of the Oxidative Folding of Ribonuclease A by Protein Disulfide Isomerase: Dependence of the Rate on the Composition of the Redox Buffer. *Biochemistry* **1991**, *30*, 613–9.
(41) Hong, B. X.; Soong, L. Identification and Enzymatic Activities of Four Protein Disulfide Isomerase (PDI) Isoforms of Leishmania Amazonensis. *Parasitol. Res.* **2008**, *102*, 437–46.
(42) Raturi, A.; Vacratsis, P. O.; Seslija, D.; Lee, L.; Mutus, B. A Direct, Continuous, Sensitive Assay for Protein Disulphide-Isomerase Based on Fluorescence Self-Quenching. *Biochem. J.* **2005**, *391*, 351–7.
(43) Tomazzolli, R.; Serra, M. D.; Bellisola, G.; Colombatti, M.; Guella, G. A Fluorescence-Based Assay for the Reductase Activity of Protein Disulfide Isomerase.

Anal. Biochem. **2006**, *350*, 105–12.
(44) Mares, R. E.; Meléndez-López, S. G.; Ramos, M. A. Acid-Denatured Green Fluorescent Protein (GFP) as Model Substrate to Study the Chaperone Activity of Protein Disulfide Isomerase. *Int J Mol Sci* **2011**, *12*, 4625–36.
(45) Ibbetson, A. L.; Freedman, R. B. Thiol-Protein Disulphide Oxidoreductases. Assay of Microsomal Membrane-Bound Glutathione-Insulin Transhydrogenase and Comparison with Protein Disulphide-Isomerase. *Biochem. J.* **1976**, *159*, 377–84.
(46) Kullmann, M.; Kalayda, G. V.; Hellwig, M.; Kotz, S.; Hilger, R. A.; Metzger, S.; Jaehde, U. Assessing the Contribution of the Two Protein Disulfide Isomerases PDIA1 and PDIA3 to Cisplatin Resistance. *J. Inorg. Biochem.* **2015**, *153*, 247–52.
(47) Tufo, G.; Jones, A. W.; Wang, Z.; Hamelin, J.; Tajeddine, N.; Esposti, D. D.; Martel, C.; Boursier, C.; Gallerne, C.; Migdal, C.; et al. The Protein Disulfide Isomerases PDIA4 and PDIA6 Mediate Resistance to Cisplatin-Induced Cell Death in Lung Adenocarcinoma. *Cell Death Differ.* **2014**, *21*, 685–95.
(48) Shoulders, M. D.; Ryno, L. M.; Genereux, J. C.; Moresco, J. J.; Tu, P. G.; Wu, C.; Yates, J. R.; Su, A. I.; Kelly, J. W.; Wiseman, R. L. Stress-Independent Activation of XBP1s And/or ATF6 Reveals Three Functionally Diverse ER Proteostasis Environments. *Cell Rep* **2013**, *3*, 1279–92.

Appendix I

Mass spectrometry tables

Figure 3A-1 The peptides identified after MS analysis were sorted by average ratios obtained from three biological replicates (L-NAME1 (L1), L-NAME2 (L2), and L-NAME3 (L3)). Cysteines that possessed ratios >1 for the L-NAME treated samples were pooled, ranked and assembled into a list of increasing reactivity. Within the top 25 cysteines sensitive to L-NAME treatment (highlighted in blue), Cys413 of Aspartyl aminopeptidase (DNPEP) was identified. Glutaredoxin 5 (Glrx5) and thymidine kinase 1 (TK1) also showed ratios greater than one indicating an increase in reactivity upon L-NAME treatment.

ipi	description	symbol	sequence	LN1	LN2	LN3	Avg	Rank
Q13561	DCTN2 Dynactin subunit 2	DCTN2	R.C*DQDAQNPLSAGLQGACLMETVELLQAK.V	10.6	1.1	1.07	4.26	1
Q96GX2	ATXN7L3B Putative ataxin-7-like protein 3B	ATXN7L3B	R.LPLC*SLPGEPGNGPDQQLQR.S	2.34	5.57	1.48	3.13	2
O00299	CLIC1 Chloride intracellular channel protein 1	CLIC1	K.LC*PGGQLPFLLYGTEVHTDTNK.I	2.11	5.87	1.18	3.05	3
Q9UJY4	GGA2 ADP-ribosylation factor-binding protein GGA2	GGA2	R.NLLDLLSAQPAPC*PLNYVSQK.S	1.6	5.83	1	2.81	4
P04183	TK1 Thymidine kinase, cytosolic	TK1	R.NTMEALPAC*LLR.D	1.85	2.15	1.76	1.92	5
Q99439	CNN2 Calponin-2	CNN2	K.C*ASQVGMTAPGTR.R	1.74	2.83	1.09	1.89	6
P20073	ANXA7 Annexin A7	ANXA7	R.LGTDESC*FNMILATR.S	1.83	2.46	1.19	1.83	7
Q13155	AIMP2 Aminoacyl tRNA synthase complex-interacting multif	AIMP2	R.VELPTC*MYR.L	2.46	2.05	0.89	1.80	8

Q7RTV0	PHF5A PHD finger-like domain-containing protein 5A	PHF5A	R.ICDEC*NYGSYQGR.C	1.4	2.63	1.26	1.76	9
Q99873	PRMT1 Protein arginine N-methyltransferase 1	PRMT1	K.VEDLTFTSPFC*LQVK.R	1.36	2.42	1.43	1.74	10
P55786	NPEPPS Puromycin-sensitive aminopeptidase	NPEPPS	R.LPADVSPINYSLC*LKPDLLDFTFEGK.L	2.14	1.78	1.27	1.73	11
P62826	RAN GTP-binding nuclear protein Ran	RAN	R.VC*ENIPIVLCGNK.V	1.67	2.17	1.31	1.72	12
Q92598	HSPH1 Heat shock protein 105 kDa	HSPH1	R.C*TPSVISFGSK.N	1.58	1.93	1.52	1.68	13
P04183	TK1 Thymidine kinase, cytosolic	TK1	K.LFAPQQILQC*SPAN.-	1.36	2.15	1.42	1.64	14
Q99873	PRMT1 Protein arginine N-methyltransferase 1	PRMT1	K.GQLCELSC*STDYR.M	1.38	2.01	1.49	1.63	15
Q9ULA0	DNPEP Aspartyl aminopeptidase	DNPEP	R.NDTPC*GTTIGPILASR.L	1.38	1.64	1.81	1.61	16
Q86SX6	GLRX5 Glutaredoxin-related protein 5, mitochondrial	GLRX5	K.GTPEQPQC*GFSNAVVQILR.L	1.57	1.78	1.44	1.60	17
P52292	KPNA2 Importin subunit alpha-2	KPNA2	R.TDC*SPIQFESAWALTNIASGTSEQTK.A	1.8	1.2	1.76	1.59	18

O00515	LAD1 Ladinin-1	LAD1	R.GLPC*TELFVAPVGVASK.R	1.42	2.17	1.15	1.58	19
O14561	NDUFAB1 Acyl carrier protein, mitochondrial	NDUFAB1	K.LMC*PQEIVDYIADK.K	1.73	1.77	1.22	1.57	20
Q13526	PIN1 Peptidyl-prolyl cis-trans isomerase NIMA-interacti	PIN1	K.IKSGEEDFESLASQFSDC*SSAK.A	1.44	2.08	1.12	1.55	21
Q14247	CTTN Src substrate cortactin	CTTN	K.HC*SQVDSVR.G	1.39	1.89	1.35	1.54	22
Q9UNF1	MAGED2 Melanoma-associated antigen D2	MAGED2	R.MGIGLGSENAAGPC*NWDEADIGPWAK.A	2.26	1.34	1.01	1.54	23
P57721	PCBP3 Poly(rC)-binding protein 3	PCBP3	R.LVVPASQC*GSLIGK.G	1.49	1.74	1.35	1.53	24
P68366	TUBA4A Tubulin alpha-4A chain	TUBA4A	K.YMAC*CLLYR.G	1.7	1.55	1.32	1.52	25
P22102	GART Trifunctional purine biosynthetic protein adenosin	GART	K.AFTKPEEAC*SFILSADFPALVVK.A	1.12	1.85	1.57	1.51	26
P30040	ERP29 Endoplasmic reticulum resident protein 29	ERP29	K.GQGVYLGMPGC*LPVYDALAGEFIR.A	2.16	1.49	0.84	1.50	27
P60709	ACTB Actin, cytoplasmic 1	ACTB	R.CPEALFQPSFLGMESC*GIHETTFNSIMK.C	1.42	1.75	1.31	1.49	28

P09429	HMGB1 High mobility group protein B1	HMGB1	K.MSSYAFFVQTC*R.E	1.3	2.07	1.1	1.49	29
Q9Y570	PPME1 Protein phosphatase methylesterase 1	PPME1	R.FAEPIGGFQC*VFPGC*.-	1.56	1.71	1.17	1.48	30
P08238	HSP90AB1 Heat shock protein HSP 90-beta	HSP90AB1	R.LVSSPC*CIVTSTYGWTANMER.I	1.47	1.71	1.23	1.47	31
Q9UI30	TRMT112 tRNA methyltransferase 112 homolog	TRMT112	R.IC*PVEFNPNFVAR.M	1.67	1.48	1.2	1.45	32
P52895	AKR1C2 Aldo-keto reductase family 1 member C2	AKR1C2	R.EEPWVDPNSPVLLEDPVLC*ALAK.K	1.54	1.5	1.3	1.45	33
P61077	UBE2D3 Ubiquitin-conjugating enzyme E2 D3	UBE2D3	K.VLLSIC*SLLCDPNPDDPLVPEIAR.I	1.1	1.94	1.29	1.44	34
P62888	RPL30 60S ribosomal protein L30	RPL30	R.VC*TLAIIDPGDSDIIR.S	1.4	1.6	1.3	1.43	35
O95433	AHSA1 Activator of 90 kDa heat shock protein ATPase homo	AHSA1	K.NGETELC*MEGR.G	1.53	1.4	1.37	1.43	36
P13489	RNH1 Ribonuclease inhibitor	RNH1	R.SNELGDVGVHC*VLQGLQTPSCK.I	1.5	1.5	1.28	1.43	37
O75179	ANKRD17 Ankyrin repeat domain-	ANKRD17	R.LTSSVSC*ALDEAAAALTR.M	1.25	1.88	1.14	1.42	38

	containing protein 17							
P55786	NPEPPS Puromycin-sensitive aminopeptidase	NPEPPS	R.SKDGVC*VR.V	1.64	1.4	1.21	1.42	39
O00244	ATOX1 Copper transport protein ATOX1	ATOX1	K.VC*IESEHSMDTLLATLK.K	1.49	1.55	1.2	1.41	40
P30041	PRDX6 Peroxiredoxin-6	PRDX6	K.DINAYNC*EEPTEK.L	1.94	1.46	0.83	1.41	41
P42575	CASP2 Caspase-2	CASP2	R.SDMICGYAC*LK.G	1.23	1.79	1.2	1.41	42
P30084	ECHS1 Enoyl-CoA hydratase, mitochondrial	ECHS1	K.ALNALC*DGLIDELNQALK.T	1.37	1.56	1.28	1.40	43
Q96RN5	MED15 Mediator of RNA polymerase II transcription subuni	MED15	K.QQYLC*QPLLDAVLANIR.S	1.29	1.31	1.6	1.40	44
P23610	F8A3 Factor VIII intron 22 protein	F8A3	R.LVC*PAAYGEPLQAAASALGAAVR.L	1.27	1.8	1.08	1.38	45
P07900	HSP90AA1 Heat shock protein HSP 90-alpha	HSP90AA1	R.VFIMDNC*EELIPEYLNFIR.G	1.5	1.53	1.1	1.38	46
P23396	RPS3 40S ribosomal protein S3	RPS3	R.GLC*AIAQAESLR.Y	1.31	1.69	1.13	1.38	47
P55072	VCP Transitional endoplasmic reticulum ATPase	VCP	K.AIANEC*QANFISIK.G	1.29	1.73	1.1	1.37	48

P12814	ACTN1 Alpha-actinin-1	ACTN1	K.IC*DQWDNLGALTQK.R	1.26	1.65	1.19	1.37	49
Q9UNH7	SNX6 Sorting nexin-6	SNX6	R.IGSSLYALGTQDSTDIC*K.F	1.28	1.48	1.34	1.37	50
P30153	PPP2R1A Serine/threonine-protein phosphatase 2A 65 kDa reg	PPP2R1A	R.LNIISNLDC*VNEVIGIR.Q	1.42	1.55	1.11	1.36	51
P62993	GRB2 Growth factor receptor-bound protein 2	GRB2	K.VLNEEC*DQNWYK.A	1.3	1.26	1.51	1.36	52
Q52LJ0	FAM98B Protein FAM98B	FAM98B	K.SLC*NLEESITSAGR.D	1.44	0.88	1.75	1.36	53
Q96I99	SUCLG2 Succinyl-CoA ligase	SUCLG2	R.SC*NGPVLVGSPQGGVDIEEVAASNPELIFK.E	1.52	1.34	1.19	1.35	54
P49458	SRP9 Signal recognition particle 9 kDa protein	SRP9	K.VTDDLVC*LVYK.T	1.71	1.07	1.27	1.35	55
P19784	CSNK2A2 Casein kinase II subunit alpha	CSNK2A2	K.EQSQPC*ADNAVLSSGLTAAR.-	1.27	1.46	1.32	1.35	56
P24752	ACAT1 Acetyl-CoA acetyltransferase, mitochondrial	ACAT1	K.IHMGSC*AENTAK.K	1.12	1.63	1.28	1.34	57
P60981	DSTN Destrin	DSTN	K.HEC*QANGPEDLNR.A	1.44	1.44	1.15	1.34	58
P54136	RARS Arginine--tRNA ligase, cytoplasmic	RARS	K.NC*GC*LGASPNLEQLQEENLK.L	1.43	1.37	1.19	1.33	59

O15382	BCAT2 Branched-chain-amino-acid aminotransferase, mitoch	BCAT2	R.EVFGSGTAC*QVCPVHR.I	1.14	1.59	1.25	1.33	60
P62258	YWHAE 14-3-3 protein epsilon	YWHAE	K.LICC*DILDVLDK.H	1.58	1.26	1.14	1.33	61
Q9Y5P6	GMPPB Mannose-1-phosphate guanyltransferase beta	GMPPB	R.LC*SGPGIVGNVLVDPSAR.I	1.36	1.29	1.32	1.32	62
P49915	GMPS GMP synthase	GMPS	K.TVGVQGDC*R.S	1.34	1.26	1.36	1.32	63
P60981	DSTN Destrin	DSTN	K.LGGSLIVAFEGC*PV.-	1.4	1.3	1.23	1.31	64
P62879	GNB2 Guanine nucleotide-binding protein G(I)/G(S)/G(T)	GNB2	K.AC*GDSTLTQITAGLDPVGR.I	1.71	1.08	1.14	1.31	65
P37802	TAGLN2 Transgelin-2	TAGLN2	K.NMAC*VQR.T	1.42	1.33	1.16	1.30	66
P36405	ARL3 ADP-ribosylation factor-like protein 3	ARL3	K.LSC*VPVLIFANK.Q	1.43	1.47	1	1.30	67
Q7Z4W1	DCXR L-xylulose reductase	DCXR	R.GVPGAIVNVSSQC*SQR.A	1.27	1.53	1.1	1.30	68
P41250	GARS Glycine--tRNA ligase	GARS	R.SC*YDLSCHAR.A	1.35	1.29	1.25	1.30	69
O43175	PHGDH D-3-phosphoglycerate dehydrogenase	PHGDH	K.NAGNC*LSPAVIVGLLK.E	1.23	1.6	1.04	1.29	70

P61289	PSME3 Proteasome activator complex subunit 3	PSME3	R.LDEC*EEAFQGTK.V	1.41	1.29	1.17	1.29	71
Q7L0Y3	TRMT10C Mitochondrial ribonuclease P protein 1	TRMT10C	K.SSVQEEC*VSTISSSKDEDPLAATR.E	1.47	1.38	1.02	1.29	72
O75153	KIAA0664 Clustered mitochondria protein homolog	KIAA0664	K.C*LTQQAVALQR.T	1.22	1.36	1.28	1.29	73
Q14258	TRIM25 E3 ubiquitin/ISG15 ligase TRIM25	TRIM25	K.NTVLC*NVVEQFLQADLAR.E	1.25	1.41	1.19	1.28	74
P21333	FLNA Filamin-A	FLNA	R.VTYC*PTEPGNYIINIK.F	1.31	1.41	1.13	1.28	75
P38606	ATP6V1A V-type proton ATPase catalytic subunit A	ATP6V1A	R.VLDALFPCVQGGTTAIPGAFGC*GK.T	1.43	1.36	1.05	1.28	76
P62306	SNRPF Small nuclear ribonucleoprotein F	SNRPF	R.C*NNVLYIR.G	1.31	1.25	1.26	1.27	77
P62879	GNB2 Guanine nucleotide-binding protein G(I)/G(S)/G(T)	GNB2	R.TFVSGAC*DASIK.L	1.46	1.07	1.28	1.27	78
P35568	IRS1 Insulin receptor substrate 1	IRS1	K.LC*GAAGGLENGLNYIDLDLVK.D	1.34	1.38	1.07	1.26	79
Q96FW1	OTUB1 Ubiquitin thioesterase OTUB1	OTUB1	K.QEPLGSDSEGVNC*LAYDEAIMAQQDR.I	1.19	1.43	1.16	1.26	80

Q6P1X6	C8orf82 UPF0598 protein C8orf82	C8orf82	R.YEAAFPFLSPC*GR.E	1.3	1.12	1.36	1.26	81
P49458	SRP9 Signal recognition particle 9 kDa protein	SRP9	R.HSDGNLC*VK.V	1.48	1.01	1.28	1.26	82
P14618	PKM Pyruvate kinase isozymes M1/M2	PKM	K.C*CSGAIIVLTK.S	1.38	1.59	0.8	1.26	83
Q9UNE7	STUB1 E3 ubiquitin-protein ligase CHIP	STUB1	R.AQQAC*IEAK.H	1.33	1.2	1.23	1.25	84
P68366	TUBA4A Tubulin alpha-4A chain	TUBA4A	R.SIQFVDWC*PTGFK.V	1.44	1.07	1.25	1.25	85
Q7Z4W1	DCXR L-xylulose reductase	DCXR	R.SGMTTGSTLPVEGGFWAC*.-	1.61	1.05	1.09	1.25	86
P23528	CFL1 Cofilin-1	CFL1	K.HELQANC*YEEVK.D	1.3	1.18	1.25	1.24	87
Q13642	FHL1 Four and a half LIM domains protein 1	FHL1	K.CFDKFC*ANTCVECR.K	1.38	1.38	0.97	1.24	88
P04406	GAPDH Glyceraldehyde-3-phosphate dehydrogenase	GAPDH	K.IISNASC*TTNCLAPLAK.V	1.34	1.23	1.15	1.24	89
O95373	IPO7 Importin-7	IPO7	R.GIDQC*IPLFVEAALER.L	1.25	1.28	1.19	1.24	90
Q8TEX9	IPO4 Importin-4	IPO4	K.LC*PQLMPMLEEALR.S	1.4	1.12	1.19	1.24	91
Q9BSD7	NTPCR Cancer-related nucleoside-triphosphata	NTPCR	R.NADC*SSGPGQR.V	1.13	1.24	1.34	1.24	92

	se							
Q16186	ADRM1 Proteasomal ubiquitin receptor ADRM1	ADRM1	R.VPQC*PSGR.V	1.28	0.96	1.47	1.24	93
Q9Y2S7	POLDIP2 Polymerase delta-interacting protein 2	POLDIP2	R.DC*PHISQR.S	1.44	1.12	1.14	1.23	94
Q9UJU6	DBNL Drebrin-like protein	DBNL	R.AEEDVEPEC*IMEK.V	1.46	1.03	1.2	1.23	95
O95671	ASMTL N-acetylserotonin O-methyltransferase-like protein	ASMTL	K.LTAC*QVATAFNLSR.F	1.21	1.42	1.06	1.23	96
Q15257	PPP2R4 Serine/threonine-protein phosphatase 2A activator	PPP2R4	R.IDYGTGHEAAFAAFLCCLC*K.I	1.36	1.57	0.75	1.23	97
P14868	DARS Aspartate--tRNA ligase, cytoplasmic	DARS	R.LEYC*EALAMLR.E	1.33	1.29	1.06	1.23	98
Q969T9	WBP2 WW domain-binding protein 2	WBP2	K.DC*EIKQPVFGANYIK.G	1.57	1.03	1.08	1.23	99
P46527	CDKN1B Cyclin-dependent kinase inhibitor 1B	CDKN1B	K.TDPSDSQTGLAEQC*AGIR.K	1.31	1.06	1.31	1.23	100
Q9BQ52	ELAC2 Zinc phosphodiesterase ELAC protein 2	ELAC2	R.GPSGC*SGGPNTVYLQVVAAGSR.D	1.17	1.11	1.4	1.23	101
Q00610	CLTC Clathrin	CLTC	R.IHEGC*EEPATHNALAK.I	1.18	1.19	1.3	1.22	102

	heavy chain 1							
Q99873	PRMT1 Protein arginine N-methyltransferase 1	PRMT1	K.VIGIEC*SSISDYAVK.I	1.28	1.28	1.1	1.22	103
P04406	GAPDH Glyceraldehyde-3-phosphate dehydrogenase	GAPDH	K.IISNASC*TTN.C	1.33	1.16	1.16	1.22	104
Q9Y508	RNF114 RING finger protein 114	RNF114	R.DC*GGAAQLAGPAAEADPLGR.F	1.17	1.4	1.07	1.21	105
O00273	DFFA DNA fragmentation factor subunit alpha	DFFA	R.EQHGVAASC*LEDLR.S	1.6	1.08	0.95	1.21	106
Q15370	TCEB2 Transcription elongation factor B polypeptide 2	TCEB2	R.ADDTFEALC*IEPFSSPPELPDVMKPQDSGSSANEQAVQ.-	1.28	1.23	1.12	1.21	107
Q7L1Q6	BZW1 Basic leucine zipper and W2 domain-containing prot	BZW1	R.FDPTQFQDC*IIQGLTETGTDLEAVAK.F	1.16	1.35	1.12	1.21	108
Q8IU81	IRF2BP1 Interferon regulatory factor 2-binding protein 1	IRF2BP1	K.LFTEYPC*GSGNVYAGVLAVAR.Q	1.11	1.13	1.39	1.21	109
Q96CP2	FLYWCH2 FLYWCH family member 2	FLYWCH2	R.TEDSGLAAGPPEAAGENFAPC*SVAPGK.S	1.4	1.28	0.94	1.21	110
P49327	FASN Fatty acid synthase	FASN	K.AINC*ATSGVVGLVNCLR.R	1.22	1.21	1.19	1.21	111

Q15185	PTGES3 Prostaglandin E synthase 3	PTGES3	K.HLNEIDLFHC*IDPNDSK.H	1.36	1.14	1.1	1.20	112
Q9UPY8	MAPRE3 Microtubule-associated protein RP/EB family member	MAPRE3	R.LSNVAPPC*ILR.K	1.16	1.27	1.17	1.20	113
P62879	GNB2 Guanine nucleotide-binding protein G(I)/G(S)/G(T)	GNB2	R.VSC*LGVTDDGMAVATGSWDSFLK.I	1.12	1.17	1.31	1.20	114
Q13748	TUBA3D Tubulin alpha-3C/D chain	TUBA3D	R.TIQFVDWC*PTGFK.V	1.45	1.04	1.1	1.20	115
Q15813	TBCE Tubulin-specific chaperone E	TBCE	R.NCAVSC*AGEK.G	1.34	1.19	1.05	1.19	116
P26641	EEF1G Elongation factor 1-gamma	EEF1G	K.AAAPAPEEEMDEC*EQALAAEPK.A	1.27	1.17	1.13	1.19	117
P27348	YWHAQ 14-3-3 protein theta	YWHAQ	R.YLAEVAC*GDDR.K	1.14	1.26	1.17	1.19	118
O75663	TIPRL TIP41-like protein	TIPRL	K.VAC*AEEWQESR.T	1.78	1.01	0.77	1.19	119
O15075	DCLK1 Serine/threonine-protein kinase DCLK1	DCLK1	R.YQDDFLLDESEC*R.V	1.32	0.98	1.26	1.19	120
Q15365	PCBP1 Poly(rC)-binding protein 1	PCBP1	R.LVVPATQC*GSLIGK.G	1.26	1.17	1.12	1.18	121

P04183	TK1 Thymidine kinase, cytosolic	TK1	R.YSSSFC*THDR.N	1.36	1.14	1.03	1.18	122
O14745	SLC9A3R1 Na(+)/H(+) exchange regulatory cofactor NHE-RF1	SLC9A3R1	R.IVEVNGVC*MEGK.Q	1.31	1.17	1.05	1.18	123
P08238	HSP90AB1 Heat shock protein HSP 90-beta	HSP90AB1	R.VFIMDSC*DELIPEYLNFIR.G	1.34	1.06	1.12	1.17	124
Q53T59	HS1BP3 HCLS1-binding protein 3	HS1BP3	K.LFDDPDLGGAIPLGDSLLLPAAC*ESGGPTPSLSHR.D	1.34	1.25	0.92	1.17	125
P57721	PCBP3 Poly(rC)-binding protein 3	PCBP3	R.INISEGNC*PER.I	1.21	1.16	1.14	1.17	126
O14929	HAT1 Histone acetyltransferase type B catalytic subunit	HAT1	K.VDENFDC*VEADDVEGK.I	1.22	1.04	1.25	1.17	127
P13489	RNH1 Ribonuclease inhibitor	RNH1	R.ELDLSNNC*LGDAGILQLVESVR.Q	1.2	1.22	1.08	1.17	128
Q15796	SMAD2 Mothers against decapentaplegic homolog 2	SMAD2	K.AITTQNC*NTK.C	1.49	1.12	0.88	1.16	129
Q9Y5Y2	NUBP2 Cytosolic Fe-S cluster assembly factor NUBP2	NUBP2	R.AVHQC*DR.G	1.24	1.13	1.12	1.16	130

Q9ULA0	DNPEP Aspartyl aminopeptidase	DNPEP	R.ISASC*QHPTAFEEAIPK.S	1.1	1.27	1.11	1.16	131
Q9BWD1	ACAT2 Acetyl-CoA acetyltransferase, cytosolic	ACAT2	R.QASVGAGIPYSVPAWSC*QMICGSGLK.A	1.3	1.26	0.92	1.16	132
Q5MNZ6	WDR45L WD repeat domain phosphoinositide-interacting prot	WDR45L	R.C*NYLALVGGGK.K	1.04	1.26	1.18	1.16	133
P07437	TUBB Tubulin beta chain	TUBB	K.LTTPTYGDLNHLVSATMSGVTTC*LR.F	1.32	0.96	1.19	1.16	134
Q9Y4P1	ATG4B Cysteine protease ATG4B	ATG4B	K.NFPAIGGTGPTSDTGWGC*MLR.C	1.12	1.19	1.16	1.16	135
Q96RS6	NUDCD1 NudC domain-containing protein 1	NUDCD1	K.FFACAPNYSYAALC*ECLR.R	1.27	1.08	1.11	1.15	136
Q6UWE0	LRSAM1 E3 ubiquitin-protein ligase LRSAM1	LRSAM1	K.SC*SLLSLATIK.V	1.1	1.18	1.18	1.15	137
Q9UHD8	SEPT9 Septin-9	9-Sep	R.SQEATEAAPSC*VGDMADTPR.D	1.14	1.15	1.16	1.15	138
P31749	AKT1 RAC-alpha serine/threonine-protein kinase	AKT1	K.TFC*GTPEYLAPEVLEDNDYGR.A	1.18	1.1	1.16	1.15	139

Q99714	HSD17B10 3-hydroxyacyl-CoA dehydrogenase type-2	HSD17B10	K.VC*NFLASQVPFPSR.L	1.2	1.08	1.15	1.14	140
P30044	PRDX5 Peroxiredoxin-5, mitochondrial	PRDX5	K.ALNVEPDGTGLTC*SLAPNIISQL.-	1.36	1	1.06	1.14	141
P67936	TPM4 Tropomyosin alpha-4 chain	TPM4	K.EENVGLHQTLDQTLNELNC*I.-	1.29	1.27	0.86	1.14	142
Q9P2T1	GMPR2 GMP reductase 2	GMPR2	R.VTQQVNPIFSEAC*.-	1.44	1.07	0.91	1.14	143
O00299	CLIC1 Chloride intracellular channel protein 1	CLIC1	K.IGNC*PFSQR.L	1.17	1.24	1.01	1.14	144
P09110	ACAA1 3-ketoacyl-CoA thiolase, peroxisomal	ACAA1	R.QC*SSGLQAVASIAGGIR.N	1.27	1.18	0.96	1.14	145
P45984	MAPK9 Mitogen-activated protein kinase 9	MAPK9	R.TAC*TNFMMTPYVVTR.Y	1.24	1.08	1.09	1.14	146
P47756	CAPZB F-actin-capping protein subunit beta	CAPZB	K.DETVSDC*SPHIANIGR.L	1.23	1.19	0.98	1.13	147
P10599	TXN Thioredoxin	TXN	K.C*MPTFQFFK.K	1.16	1.21	1.02	1.13	148
Q96RS6	NUDCD1 NudC domain-containing protein 1	NUDCD1	R.DSAQC*AAIAER.L	1.14	1.1	1.15	1.13	149

Q5T160	RARS2 Probable arginine--tRNA ligase, mitochondrial	RARS2	K.LLGITPVC*R.M	1.22	0.98	1.19	1.13	150
P61962	DCAF7 DDB1- and CUL4-associated factor 7	DCAF7	R.VPC*TPVAR.L	0.84	1.28	1.27	1.13	151
O14980	XPO1 Exportin-1	XPO1	K.DLLGLC*EQK.R	1.18	1.04	1.16	1.13	152
O60232	SSSCA1 Sjoegren syndrome/scleroderma autoantigen 1	SSSCA1	K.AAQGPPAPAVPPNTDVMAC*TQTALLQK.L	1.16	1.23	0.98	1.12	153
Q9UPM8	AP4E1 AP-4 complex subunit epsilon-1	AP4E1	K.VTEQPGC*CLPVMEAESTK.S	1.3	1.03	1.04	1.12	154
Q9Y3A3	MOB4 MOB-like protein phocein	MOB4	R.HTLDGAAC*LLNSNK.Y	1.17	1.03	1.17	1.12	155
Q15366	PCBP2 Poly(rC)-binding protein 2	PCBP2	R.YSTGSDSASFPHTTPSMC*LNPDLEGPPLEAYTIQGQY.A	1.07	1.21	1.08	1.12	156
Q16576	RBBP7 Histone-binding protein RBBP7	RBBP7	R.VHIPNDDAQFDASHC*DSDKGEFGGFGSVTGK.I	1.29	1.14	0.91	1.11	157
P23921	RRM1 Ribonucleoside-diphosphate reductase large subunit	RRM1	R.NTAAMVCSLENRDEC*LMCGS.-	0.88	1.42	1.02	1.11	158

Q9BRA2	TXNDC17 Thioredoxin domain-containing protein 17	TXNDC17	W.C*PDCVQAEPVVR.E	1.16	1.1	1.06	1.11	159
O15355	PPM1G Protein phosphatase 1G	PPM1G	K.C*SGDGVGAPR.L	1.2	0.96	1.16	1.11	160
Q96EY8	MMAB Cob(I)yrinic acid a,c-diamide adenosyltransferase,	MMAB	K.IQC*TLQDVGSALATPCSSAR.E	1.29	1.03	0.99	1.10	161
P13639	EEF2 Elongation factor 2	EEF2	K.STLTDSLVC*K.A	1.08	1.06	1.16	1.10	162
P32119	PRDX2 Peroxiredoxin-2	PRDX2	R.LVQAFQYTDEHGEVC*PAGWKPGSDTIKPNVDDSK.E	1.11	1.02	1.17	1.10	163
P15924	DSP Desmoplakin	DSP	K.YC*YLQNEVFGLFQK.L	1.21	0.83	1.26	1.10	164
Q9NQR4	NIT2 Omega-amidase NIT2	NIT2	R.VGLGIC*YDMR.F	1.15	1.1	1.02	1.09	165
Q9NP81	SARS2 Serine--tRNA ligase, mitochondrial	SARS2	R.FC*ACPEEAAHALELR.K	1.18	0.89	1.2	1.09	166
P13716	ALAD Delta-aminolevulinic acid dehydratase	ALAD	R.C*YQLPPGAR.G	1.1	1.12	1.03	1.08	167
Q9BRA2	TXNDC17 Thioredoxin domain-containing protein 17	TXNDC17	K.DAGGKSWC*PDCVQAEPVVR.E	1.06	1.06	1.11	1.08	168

Q96CM8	ACSF2 Acyl-CoA synthetase family member 2, mitochondrial	ACSF2	R.MVSTPIGGLSYVQGC*TK.K	1	1.11	1.12	1.08	169
P00492	HPRT1 Hypoxanthine-guanine phosphoribosyltransferase	HPRT1	K.SYC*NDQSTGDIK.V	1.1	1.15	0.98	1.08	170
P12277	CKB Creatine kinase B-type	CKB	H.LGYILTC*PSNLGTGLR.A	1	1.19	1.04	1.08	171
P24468	NR2F2 COUP transcription factor 2	NR2F2	R.FGSQC*MQPNNIMGIENICELAAR.M	1	0.96	1.27	1.08	172
P37198	NUP62 Nuclear pore glycoprotein p62	NUP62	K.DIIEHLNTSGAPADTSDPLQQIC*K.I	1.25	0.97	1.01	1.08	173
Q8NBF2	NHLRC2 NHL repeat-containing protein 2	NHLRC2	K.AILFSQPLQITDTQQGC*IAPVELR.Y	1.09	1.01	1.12	1.07	174
O14556	GAPDHS Glyceraldehyde-3-phosphate dehydrogenase, testis-s	GAPDHS	S.C*TTNCLAPLAK.V	1.24	1.01	0.97	1.07	175
O14980	XPO1 Exportin-1	XPO1	K.LDINLLDNVVNC*LYHGEGAQQR.M	1.1	1.03	1.09	1.07	176
O75934	BCAS2 Pre-mRNA-splicing factor SPF27	BCAS2	K.NDITAWQEC*VNNSMAQLEHQAVR.I	1.1	1.06	1.05	1.07	177
P50570	DNM2 Dynamin-2	DNM2	K.LQDAFSSIGQSC*HLDLPQIAVVGGQSAGK.S	1.1	1.05	1.06	1.07	178

P15924	DSP Desmoplakin	DSP	K.LENINGVTDGYLNSLC*TVR.A	1.36	0.65	1.2	1.07	179
P53602	MVD Diphosphomevalonate decarboxylase	MVD	R.DGDPLPSSLSC*K.V	1.1	0.98	1.12	1.07	180
Q13185	CBX3 Chromobox protein homolog 3	CBX3	R.LTWHSC*PEDEAQ.-	1.07	1.17	0.95	1.06	181
Q9Y365	STARD10 PCTP-like protein	STARD10	R.MEC*CDVPAETLYDVLHDIEYR.K	1.06	1.14	0.99	1.06	182
O00233	PSMD9 26S proteasome non-ATPase regulatory subunit 9	PSMD9	K.GIGMNEPLVDC*EGYPR.S	1.12	0.95	1.11	1.06	183
Q99757	TXN2 Thioredoxin, mitochondrial	TXN2	R.VVNSETPVVVDFHAQWC*GPCK.I	1.02	1.08	1.08	1.06	184
P30048	PRDX3 Thioredoxin-dependent peroxide reductase, mitochon	PRDX3	K.AFQYVETHGEVC*PANWTPDSPTIKPSPAASK.E	1.09	1.06	1.02	1.06	185
Q8N806	UBR7 Putative E3 ubiquitin-protein ligase UBR7	UBR7	K.VEQNSEPC*AGSSSESDLQTVFK.N	1.26	1.07	0.84	1.06	186
Q9BXJ9	NAA15 N-alpha-acetyltransferase 15, NatA auxiliary subun	NAA15	R.LFNTAVC*ESK.D	0.75	1.53	0.88	1.05	187
Q9NXJ5	PGPEP1 Pyroglutamyl-peptidase 1	PGPEP1	R.YLC*DFTYYTSLYQSHGR.S	1.3	0.88	0.98	1.05	188

Q9Y3F4	STRAP Serine-threonine kinase receptor-associated protei	STRAP	K.IGFPETTEEELEEIASENSDC*IFPSAPDVK.A	1.07	1.05	1.04	1.05	189
Q15019	SEPT2 Septin-2	2-Sep	R.LTVVDTPGYGDAINC*R.D	1.12	0.95	1.09	1.05	190
Q13630	TSTA3 GDP-L-fucose synthase	TSTA3	K.VVSCLSTC*IFPDK.T	1	1.06	1.1	1.05	191
Q96FV2	SCRN2 Secernin-2	SCRN2	S.C*DCFVSVPPASAIPAVIFAK.N	1.05	1.17	0.94	1.05	192
P16455	MGMT Methylated-DNA--protein-cysteine methyltransferase	MGMT	R.VVC*SSGAVGNYSGGLAVK.E	1.08	1.06	0.98	1.04	193
P49189	ALDH9A1 4-trimethylaminobutyraldehyde dehydrogenase	ALDH9A1	K.GALMANFLTQGQVC*CNGTR.V	1.22	0.93	0.96	1.04	194
P33240	CSTF2 Cleavage stimulation factor subunit 2	CSTF2	K.LC*VQNSPQEAR.N	1.12	0.86	1.13	1.04	195
P37235	HPCAL1 Hippocalcin-like protein 1	HPCAL1	R.LLQC*DPSSASQF.-	1.06	1.09	0.95	1.03	196
Q2TAA2	IAH1 Isoamyl acetate-hydrolyzing esterase 1 homolog	IAH1	R.VILITPTPLC*ETAWEEQCIIQGCK.L	1.12	1.02	0.94	1.03	197

Q9UPM8	AP4E1 AP-4 complex subunit epsilon-1	AP4E1	R.SSC*STLPDYLLYQCQK.V	1	0.96	1.12	1.03	198
P10599	TXN Thioredoxin	TXN	K.LVVVDFSATWC*GPCK.M	1.03	1.24	0.8	1.02	199
Q5JPI3	C3orf38 Uncharacterized protein C3orf38	C3orf38	K.FEQSDLEAFYNVITVC*GTNEVR.H	0.76	1.48	0.83	1.02	200
O43865	AHCYL1 Putative adenosylhomocysteinase 2	AHCYL1	K.LC*VPAMNVNDSVTK.Q	1.11	0.93	1.03	1.02	201
Q9Y3D2	MSRB2 Methionine-R-sulfoxide reductase B2, mitochondrial	MSRB2	R.GQAGGGGPGTGPGLGEAGSLATC*ELPLAK.S	1.13	0.89	1.05	1.02	202
P78347	GTF2I General transcription factor II-I	GTF2I	R.SILSPGGSC*GPIK.V	1.03	0.71	1.33	1.02	203
Q9BUL9	RPP25 Ribonuclease P protein subunit p25	RPP25	R.SEEAPAGC*GAEGGGPGSGPFADLAPGAVHMR.V	1.19	1.04	0.84	1.02	204
Q15365	PCBP1 Poly(rC)-binding protein 1	PCBP1	R.VMTIPYQPMPASSPVIC*AGGQDR.C	1.12	1.05	0.9	1.02	205
Q9UKV8	EIF2C2 Protein argonaute-2	EIF2C2	R.SFFTASEGC*SNPLGGGR.E	0.94	1	1.12	1.02	206
O15355	PPM1G Protein phosphatase 1G	PPM1G	R.GTEAGQVGEPGIPTGEAGPSC*SSASDK.L	1.04	1.04	0.97	1.02	207
P21333	FLNA Filamin-A	FLNA	K.AEISC*TDNQDGTCSVSYLPVLPGDYSILVK.Y	1.04	0.95	1.06	1.02	208

E9PPU0	EPPK1 Epiplakin	EPPK1	R.LLDAQLATGGLVC*PAR.R	0.98	0.93	1.14	1.02	209
Q86X76	NIT1 Nitrilase homolog 1	NIT1	K.IGLAVC*YDMR.F	1.14	0.9	0.99	1.01	210
Q9Y3E2	BOLA1 BolA-like protein 1	BOLA1	R.VC*LCQGSAGSGAIGPVEAAIR.T	1.17	0.93	0.91	1.00	211
Q9P258	RCC2 Protein RCC2	RCC2	K.AVQDLC*GWR.I	0.94	1.13	0.93	1.00	212
P53396	ACLY ATP-citrate synthase	ACLY	K.FIC*TTSAIQNR.F	0.99	0.9	1.09	0.99	213
P31947	SFN 14-3-3 protein sigma	SFN	K.GAVEKGEELSC*EER.N	1.2	0.9	0.88	0.99	214
Q96CD2	PPCDC Phosphopantothenoylcysteine decarboxylase	PPCDC	K.KLVC*GDEGLGAMAEVGTIVDK.V	1	0.94	1.04	0.99	215
Q9HAV7	GRPEL1 GrpE protein homolog 1, mitochondrial	GRPEL1	E.KATQC*VPKEEIKDDNPHLK.N	1.09	0.94	0.9	0.98	216
Q14980	NUMA1 Nuclear mitotic apparatus protein 1	NUMA1	R.QFC*STQAALQAMER.E	0.84	1.19	0.9	0.98	217
Q6XZF7	DNMBP Dynamin-binding protein	DNMBP	R.SLDQTSPC*PLVLVR.I	0.85	0.74	1.3	0.96	218
Q96QR8	PURB Transcriptional activator protein Pur-beta	PURB	R.GGGGGPC*GFQPASR.G	0.96	1.03	0.89	0.96	219
Q9UHQ1	NARF Nuclear prelamin A	NARF	K.VLVVSVC*PQSLPYFAAK.F	0.88	1.08	0.92	0.96	220

	recognition factor							
Q6KB66	KRT80 Keratin, type II cytoskeletal 80	KRT80	R.C*HIDLSGIVEEVK.A	0.92	1.02	0.88	0.94	221
P68366	TUBA4A Tubulin alpha-4A chain	TUBA4A	R.AVC*MLSNTTAIAEAWAR.L	1.2	0.76	0.84	0.93	222
O75362	ZNF217 Zinc finger protein 217	ZNF217	R.C*IPQLDPFTTFQAWQLATK.G	0.84	0.73	1.16	0.91	223
P42765	ACAA2 3-ketoacyl-CoA thiolase, mitochondrial	ACAA2	R.LC*GSGFQSIVNGCQEICVK.E	0.8	0.96	0.86	0.87	224
Q09666	AHNAK Neuroblast differentiation-associated protein AHNA	AHNAK	K.LEGDLTGPSVDVEVPDVELEC*PDAK.L	0.99	0.91	0.71	0.87	225
Q14694	USP10 Ubiquitin carboxyl-terminal hydrolase 10	USP10	R.TPSYSISSTLNPQAPEFILGC*TASK.I	0.73	0.77	1.05	0.85	226
Q15366	PCBP2 Poly(rC)-binding protein 2	PCBP2	D.ASAQTTSHELTIPNDLIGC*IIGR.Q	0.8	0.61	1.04	0.82	227
Q12959	DLG1 Disks large homolog 1	DLG1	K.LLAVNNVC*LEEVTHEEAVTALK.N	1.2	0.4	0.83	0.81	228
Q9UHI6	DDX20 Probable ATP-dependent RNA helicase DDX20	DDX20	K.EALPVSLPQIPC*LSSFK.I	0.6	0.55	1.28	0.81	229

Q09666	AHNAK Neuroblast differentiation-associated protein AHNA	AHNAK	K.GPFVEAEVPDVDLEC*PDAK.L	0.82	0.75	0.78	0.78	230
E7EQZ4	SMN1 Survival motor neuron protein	SMN1	K.NGDIC*ETSGKPK.T	0.88	0.63	0.81	0.77	231

Table 3A-2 The peptides identified after MS analysis were sorted by average ratios obtained from three biological replicates (CysNO1 (C1), CysNO2 (C2), and CysNO3 (C3)). Cysteines that possessed ratios <1 for the CysNO treated samples were pooled, ranked and assembled into a table by decreasing reactivity. Within the top 25 cysteines sensitive to *S*-nitrosation upon CysNO treatment (highlighted in purple), Cys413 of Aspartyl aminopeptidase (DNPEP), with an average L:H ratio of 0.68 ± 0.18, was identified.

ipi	description	symbol	sequence	C1	C2	C3	Avg	Rank
O75131	CPNE3 Copine-3	CPNE3	K.NC*LNPQFSK.T	0.14	1.42	0.28	0.61	1
P23921	RRM1 Ribonucleoside-diphosphate reductase large subunit	RRM1	K.IIDINYYPVPEAC*LSNK.R	0.69	0.94	0.77	0.80	2
Q14790	CASP8 Caspase-8	CASP8	K.VFFIQAC*QGDNYQK.G	0.93	0.92	0.82	0.89	3
O76075	DFFB DNA fragmentation factor subunit beta	DFFB	R.VLGSMC*QR.L	1.07	0.62	1.04	0.91	4
Q9ULA0	DNPEP Aspartyl aminopeptidase	DNPEP	R.NDTPC*GTTIGPILASR.L	1.47	1.01	0.41	0.96	5
Q8NEC7	GSTCD Glutathione S-transferase C-terminal domain-contai	GSTCD	K.AC*AEVSQWTR.L	0.76	1.33	0.88	0.99	6
P49189	ALDH9A1 4-trimethylaminobutyraldehyde dehydrogenase	ALDH9A1	K.GALMANFLTQGQVC*CNGTR.V	0.94	1.11	0.95	1.00	7
Q13630	TSTA3 GDP-L-fucose synthase	TSTA3	K.VVSCLSTC*IFPDK.T	0.98	1.04	1.04	1.02	8

Q9UKX7	NUP50 Nuclear pore complex protein Nup50	NUP50	K.AC*VGNAYHK.Q	1.02	1.22	0.84	1.03	9
Q9H3U1	UNC45A Protein unc-45 homolog A	UNC45A	K.TESPVLTSSC*R.E	1.74	0.81	0.53	1.03	10
Q96ED9	HOOK2 Protein Hook homolog 2	HOOK2	R.AGQLEATLTSC*R.R	1.56	0.96	0.58	1.03	11
Q04637	EIF4G1 Eukaryotic translation initiation factor 4 gamma 1	EIF4G1	R.LQGINC*GPDF.T	1.43	0.93	0.78	1.05	12
O14745	SLC9A3R1 Na(+)/H(+) exchange regulatory cofactor NHE-RF1	SLC9A3R1	R.IVEVNGVC*MEGK.Q	1.42	1.11	0.61	1.05	13
O15382	BCAT2 Branched-chain-amino-acid aminotransferase, mitoch	BCAT2	R.EVFGSGTAC*QVCPVHR.I	1.75	0.62	0.79	1.05	14
P35520	CBS Cystathionine beta-synthase	CBS	M.PSETPQAEVGPTGC*PHR.S	1.34	0.99	0.86	1.06	15
P61158	ACTR3 Actin-related protein 3	ACTR3	R.YSYVC*PDLVK.E	1.44	1.22	0.53	1.06	16
Q9BRA2	TXNDC17 Thioredoxin domain-containing protein 17	TXNDC17	K.DAGGKSWC*PDCVQAEPVVR.E	1.05	1.10	1.06	1.07	17

Q5TH69	ARFGEF3 Brefeldin A-inhibited guanine nucleotide-exchange	ARFGEF3	R.GSGC*SCTAPALSGPVAR.T	1.49	0.89	0.84	1.07	18
Q99497	PARK7 Protein DJ-1	PARK7	K.GLIAAIC*AGPTAL.L	0.93	1.10	1.20	1.08	19
Q9H0W8	SMG9 Protein SMG9	SMG9	R.REDFC*PR.K	1.25	1.03	0.98	1.09	20
P42575	CASP2 Caspase-2	CASP2	R.SDMICGYAC*LK.G	1.14	1.19	0.93	1.09	21
Q7L2J0	MEPCE 7SK snRNA methylphosphate capping enzyme	MEPCE	R.NSC*NVGGGGGGFK.H	1.22	1.14	0.90	1.09	22
Q16204	CCDC6 Coiled-coil domain-containing protein 6	CCDC6	S.SC*SSTSGGGGGGGGGGGK.S	1.41	1.03	0.82	1.09	23
Q16186	ADRM1 Proteasomal ubiquitin receptor ADRM1	ADRM1	R.VPQC*PSGR.V	1.62	0.89	0.75	1.09	24
O14980	XPO1 Exportin-1	XPO1	K.DLLGLC*EQK.R	1.27	1.08	0.94	1.10	25
O14976	GAK Cyclin-G-associated kinase	GAK	R.AIIQEVC*FMK.K	1.48	0.93	0.88	1.10	26
Q9BRA2	TXNDC17 Thioredoxin domain-containing protein 17	TXNDC17	W.C*PDCVQAEPVVR.E	1.07	1.10	1.13	1.10	27
Q9UPM8	AP4E1 AP-4 complex subunit epsilon-1	AP4E1	R.SSC*STLPDYLLYQCQK.V	1.19	1.04	1.07	1.10	28

Q14258	TRIM25 E3 ubiquitin/ISG15 ligase TRIM25	TRIM25	K.NTVLC*NVVEQF.L	1.58	1.10	0.64	1.11	29
P54136	RARS Arginine--tRNA ligase, cytoplasmic	RARS	K.NC*GCLGASPNLEQLQEENLK.L	1.40	1.04	0.90	1.11	30
Q96QR8	PURB Transcriptional activator protein Pur-beta	PURB	R.GGGGGPC*GFQPASR.G	1.34	1.21	0.80	1.12	31
Q8N1F7	NUP93 Nuclear pore complex protein Nup93	NUP93	K.SSGQSAQLLSHEPGDPPC*LR.R	1.23	1.06	1.07	1.12	32
Q9Y5Y2	NUBP2 Cytosolic Fe-S cluster assembly factor NUBP2	NUBP2	R.AVHQC*DR.G	1.29	1.40	0.69	1.13	33
A0AVT1	UBA6 Ubiquitin-like modifier-activating enzyme 6	UBA6	R.KPNVGC*QQDSEELLK.L	1.27	1.09	1.05	1.14	34
Q13671	RIN1 Ras and Rab interactor 1	RIN1	R.VAYQDPSSGC*TSK.T	1.34	1.02	1.05	1.14	35
Q00765	REEP5 Receptor expression-enhancing protein 5	REEP5	K.NC*MTDLLAK.L	1.23	1.12	1.08	1.14	36
Q9HAV7	GRPEL1 GrpE protein homolog 1, mitochondrial	GRPEL1	K.ATQC*VPKEEIKDDNPHLK.N	1.22	1.13	1.10	1.15	37

Q6XZF7	DNMBP Dynamin-binding protein	DNMBP	R.SLDQTSPC*PLVLVR.I	1.32	1.13	1.00	1.15	38
Q14980	NUMA1 Nuclear mitotic apparatus protein 1	NUMA1	R.QFC*STQAALQAMER.E	1.59	1.19	0.67	1.15	39
O43663	PRC1 Protein regulator of cytokinesis 1	PRC1	R.RSEVLAEESIVC*LQK.A	1.42	1.09	0.95	1.15	40
Q8N806	UBR7 Putative E3 ubiquitin-protein ligase UBR7	UBR7	R.VQQVELIC*EYNDLK.T	1.52	1.36	0.58	1.15	41
Q9NV70	EXOC1 Exocyst complex component 1	EXOC1	R.NFDKC*ISNQIR.Q	1.29	1.21	0.97	1.16	42
P13639	EEF2 Elongation factor 2	EEF2	K.STLTDSLVC*K.A	1.42	1.22	0.84	1.16	43
Q9Y3E2	BOLA1 BolA-like protein 1	BOLA1	R.VC*LCQGSAGSGAIGPVEAAIR.T	1.48	1.16	0.84	1.16	44
P46379	BAG6 Large proline-rich protein BAG6	BAG6	R.CNLAC*TPPR.H	1.50	1.23	0.75	1.16	45
Q9Y4P1	ATG4B Cysteine protease ATG4B	ATG4B	K.NFPAIGGTGPTSDTGWGC*MLR.C	1.29	1.18	1.02	1.16	46
Q96Q11	TRNT1 CCA tRNA nucleotidyltransferase 1, mitochondrial	TRNT1	K.YQGEHC*LLK.E	1.52	1.18	0.79	1.16	47
Q15149	PLEC Plectin	PLEC	K.AFC*GFEDPR.T	1.52	1.19	0.79	1.17	48

Q06203	PPAT Amidophosphoribosyltransferase	PPAT	K.C*ELENCQPFVVETLHGK.I	1.43	1.07	1.01	1.17	49
O95671	ASMTL N-acetylserotonin O-methyltransferase-like protein	ASMTL	M.VLC*PVIGK.L	1.37	1.21	0.94	1.17	50
P26641	EEF1G Elongation factor 1-gamma	EEF1G	K.AAAPAPEEEMDEC*EQALA.A	1.48	1.19	0.85	1.17	51
P35658	NUP214 Nuclear pore complex protein Nup214	NUP214	K.AC*FQVGTSEEMK.M	1.40	1.05	1.08	1.18	52
O43390	HNRNPR Heterogeneous nuclear ribonucleoprotein R	HNRNPR	K.SAFLC*GVMK.T	1.61	1.25	0.67	1.18	53
Q8N2W9	PIAS4 E3 SUMO-protein ligase PIAS4	PIAS4	R.VSLIC*PLVK.M	1.37	1.14	1.04	1.18	54
Q9NZL4	HSPBP1 Hsp70-binding protein 1	HSPBP1	R.LLDRDAC*DTVR.V	1.56	1.15	0.84	1.18	55
P53602	MVD Diphosphomevalonate decarboxylase	MVD	R.DGDPLPSSLSC*K.V	1.50	1.26	0.79	1.18	56
Q9NQ88	TIGAR Fructose-2,6-bisphosphatase TIGAR	TIGAR	K.AAREEC*PVFTPPGGETLDQVK.M	1.63	1.38	0.54	1.18	57
Q13618	CUL3 Cullin-3	CUL3	K.LKTECGC*QFTSK.L	1.52	1.28	0.76	1.19	58

O15355	PPM1G Protein phosphatase 1G	PPM1G	R.GTEAGQVGEPGIPTGEAGPSC*SSASDK.L	1.53	1.31	0.72	1.19	59
Q96CD2	PPCDC Phosphopantothenoylcysteine decarboxylase	PPCDC	K.KLVC*GDEGLGAMAEVGTIVDK.V	1.27	1.05	1.24	1.19	60
Q15021	NCAPD2 Condensin complex subunit 1	NCAPD2	K.VACC*PLER.C	1.23	1.10	1.23	1.19	61
Q15366	PCBP2 Poly(rC)-binding protein 2	PCBP2	R.YSTGSDSASFPHTTPSMC*LNPDLE.G	1.55	1.19	0.82	1.19	62
Q8WXE1	ATRIP ATR-interacting protein	ATRIP	K.LGVQSPLPPVTGSNCQC*NVEVVR.A	1.28	1.06	1.23	1.19	63
Q8WV74	NUDT8 Nucleoside diphosphate-linked moiety X motif 8, mi	NUDT8	R.LAGLTC*SGAEGLAR.P	1.23	1.14	1.20	1.19	64
Q9HCC0	MCCC2 Methylcrotonoyl-CoA carboxylase beta chain, mitoch	MCCC2	K.AATGEEVSAEDLGGADLHC*R.K	1.36	1.20	1.01	1.19	65
P53396	ACLY ATP-citrate synthase	ACLY	K.FIC*TTSAIQNR.F	1.58	1.16	0.83	1.19	66
Q96FW1	OTUB1 Ubiquitin thioesterase OTUB1	OTUB1	G.SDSEGVNC*LAYDEAIMAQQDR.I	1.66	1.22	0.70	1.19	67
Q99996	AKAP9 A-kinase anchor protein 9	AKAP9	K.LTGQQGEEPSLVSPSTSC*GSLTER.L	1.46	1.23	0.90	1.20	68

Q16576	RBBP7 Histone-binding protein RBBP7	RBBP7	R.VHIPNDDAQFDASHC*DSDKGEFGGFGSVTGK.I	1.58	1.23	0.78	1.20	69
Q9Y3A3	MOB4 MOB-like protein phocein	MOB4	R.HTLDGAAC*LLNSNK.Y	1.29	1.49	0.81	1.20	70
Q9BW61	DDA1 DET1- and DDB1-associated protein 1	DDA1	R.FHADSVC*K.A	1.57	1.19	0.84	1.20	71
Q9H3U1	UNC45A Protein unc-45 homolog A	UNC45A	K.C*DAERENFHR.L	1.60	1.19	0.81	1.20	72
P29590	PML Protein PML	PML	R.LQDLSSC*ITQGK.D	1.49	1.29	0.83	1.20	73
E9PPU0	EPPK1 Epiplakin	EPPK1	R.LLDAQLATGGLVC*PAR.R	1.64	1.15	0.82	1.20	74
Q9C0B1	FTO Alpha-ketoglutarate-dependent dioxygenase FTO	FTO	K.ANEDAVPLC*MSADFPR.V	1.31	1.38	0.93	1.21	75
Q4G176	ACSF3 Acyl-CoA synthetase family member 3, mitochondrial	ACSF3	R.EAC*SYTIHAEGDER.G	1.54	1.24	0.85	1.21	76
Q53H82	LACTB2 Beta-lactamase-like protein 2	LACTB2	R.DHSGGIGDIC*K.S	1.30	1.34	1.00	1.21	77
E7EVH7	KLC1 Kinesin light chain 1	KLC1	K.AC*KVDSPTVTTTLK.N	1.53	1.14	0.98	1.22	78

Q93009	USP7 Ubiquitin carboxyl-terminal hydrolase 7	USP7	K.MKGTC*VEGTIPK.L	1.59	1.10	0.97	1.22	79
Q15257	PPP2R4 Serine/threonine-protein phosphatase 2A activator	PPP2R4	R.AGHC*APSEAIEK.L	1.51	1.33	0.82	1.22	80
P48506	GCLC Glutamate--cysteine ligase catalytic subunit	GCLC	K.GGNAVVDGC*GK.A	1.56	1.23	0.88	1.22	81
O15075	DCLK1 Serine/threonine-protein kinase DCLK1	DCLK1	R.YQDDFLLDESEC*R.V	1.53	1.40	0.75	1.23	82
P16455	MGMT Methylated-DNA--protein-cysteine methyltransferase	MGMT	R.VVC*SSGAVGNYSGGLAVK.E	1.50	1.25	0.93	1.23	83
Q5T4S7	UBR4 E3 ubiquitin-protein ligase UBR4	UBR4	K.AVQC*LNTSSK.E	1.56	1.25	0.87	1.23	84
P31749	AKT1 RAC-alpha serine/threonine-protein kinase	AKT1	K.TFC*GTPEYLAPEVLEDNDYGR.A	1.64	1.38	0.67	1.23	85
Q15365	PCBP1 Poly(rC)-binding protein 1	PCBP1	R.VMTIPYQPMPASSPVIC*AGGQDR.C	1.59	1.29	0.81	1.23	86
Q86VY4	TSPYL5 Testis-specific Y-encoded-like protein 5	TSPYL5	K.KAPETC*STAGR.G	1.62	1.38	0.69	1.23	87

O00233	PSMD9 26S proteasome non-ATPase regulatory subunit 9	PSMD9	K.GIGMNEPLVDC*EGYPR.S	1.53	1.27	0.90	1.23	88
P49588	AARS Alanine--tRNA ligase, cytoplasmic	AARS	K.C*LSVMEAK.V	1.51	1.27	0.92	1.23	89
Q15019	SEPT2 Septin-2	2-Sep	R.LTVVDTPGYGDAINC*R.D	1.48	1.20	1.04	1.24	90
Q8N6M0	OTUD6B OTU domain-containing protein 6B	OTUD6B	K.DC*ALTVVALR.S	1.52	1.26	0.94	1.24	91
Q7Z4W1	DCXR L-xylulose reductase	DCXR	R.GVPGAIVNVSSQC*SQR.A	1.80	1.17	0.76	1.24	92
P35568	IRS1 Insulin receptor substrate 1	IRS1	R.SKSQSSSNC*.S	1.57	1.20	0.96	1.24	93
Q9P258	RCC2 Protein RCC2	RCC2	K.AVQDLC*GWR.I	1.62	1.19	0.92	1.24	94
I3L2F9	Uncharacterized protein	Uncharacterized	S.ATMSGVTTC*LR.F	1.78	1.16	0.79	1.24	95
Q9ULV4	CORO1C Coronin-1C	CORO1C	K.C*DLISIPK.K	1.62	1.31	0.81	1.25	96
Q9UHB9	SRP68 Signal recognition particle 68 kDa protein	SRP68	R.FETFC*LDPSLVTK.Q	1.51	1.53	0.71	1.25	97
Q9UL40	ZNF346 Zinc finger protein 346	ZNF346	K.NQC*LFTNTQCK.V	1.33	1.19	1.24	1.25	98
P62879	GNB2 Guanine nucleotide-binding protein G(I)/G(S)/G(T)	GNB2	K.AC*GDSTLTQITAGLDPVGR.I	1.70	1.26	0.80	1.25	99

O95833	CLIC3 Chloride intracellular channel protein 3	CLIC3	K.ASEDGESVGHC*PSCQR.L	1.48	1.18	1.10	1.25	100
Q9Y3D2	MSRB2 Methionine-R-sulfoxide reductase B2, mitochondrial	MSRB2	R.GQAGGGGPGTGPGLGEAGSLATC*ELPLAK.S	1.50	1.36	0.90	1.25	101
Q6NXG1	ESRP1 Epithelial splicing regulatory protein 1	ESRP1	K.FESGTC*SK.M	1.75	1.33	0.69	1.26	102
E7EQZ4	SMN1 Survival motor neuron protein	SMN1	K.NGDIC*ETSGKPK.T	1.67	1.30	0.81	1.26	103
Q9UL25	RAB21 Ras-related protein Rab-21	RAB21	K.VVLLGEGC*VGK.T	1.74	1.36	0.68	1.26	104
O15327	INPP4B Type II inositol 3,4-bisphosphate 4-phosphatase	INPP4B	K.SLNC*IIAMVDK.L	1.75	1.38	0.65	1.26	105
P78406	RAE1 mRNA export factor	RAE1	K.VFTASC*DKTAK.M	1.91	1.36	0.51	1.26	106
O60271	SPAG9 C-Jun-amino-terminal kinase-interacting protein 4	SPAG9	R.ITALMVSC*NR.L	1.84	1.25	0.70	1.26	107
Q96RS6	NUDCD1 NudC domain-containing protein 1	NUDCD1	K.QGELIRDSAQC*AAIAER.L	1.66	1.27	0.87	1.27	108

O15091	KIAA0391 Mitochondrial ribonuclease P protein 3	KIAA0391	K.TIESIQLSPEEYEC*LK.G	1.70	1.21	0.89	1.27	109
Q96P48	ARAP1 Arf-GAP with Rho-GAP domain, ANK repeat and PH dom	ARAP1	R.AVFPEGPC*EEPLQLR.K	1.48	1.19	1.14	1.27	110
P49753	ACOT2 Acyl-coenzyme A thioesterase 2, mitochondrial	ACOT2	K.SEFYANEAC*KR.L	1.46	1.44	0.91	1.27	111
O60502	MGEA5 Bifunctional protein NCOAT	MGEA5	R.ANSSVVSVNC*K.G	1.63	1.27	0.91	1.27	112
O14929	HAT1 Histone acetyltransferase type B catalytic subunit	HAT1	K.VDENFDC*VEADDVEGK.I	1.66	1.26	0.89	1.27	113
P21333	FLNA Filamin-A	FLNA	K.AEISC*TDNQDGTCSVSYLPVLPGDYSILVK.Y	1.76	1.28	0.77	1.27	114
Q9UNE7	STUB1 E3 ubiquitin-protein ligase CHIP	STUB1	R.AQQAC*IEAK.H	1.72	1.31	0.78	1.27	115
Q9Y3D2	MSRB2 Methionine-R-sulfoxide reductase B2, mitochondrial	MSRB2	Q.AGGGGPGTGPGLGEAGSLATC*ELPLAK.S	1.72	1.24	0.86	1.27	116

P07814	EPRS Bifunctional glutamate/proline--tRNA ligase	EPRS	K.ERPTPSLNNNC*TTSEDSLVLYNR.V	1.64	1.34	0.84	1.27	117
O14980	XPO1 Exportin-1	XPO1	R.QMSVPGIFNPHEIPEEMC*D.-	1.70	1.39	0.74	1.28	118
P57721	PCBP3 Poly(rC)-binding protein 3	PCBP3	R.INISEGNC*PER.I	1.74	1.36	0.73	1.28	119
Q8WUM4	PDCD6IP Programmed cell death 6-interacting protein	PDCD6IP	K.AVQADGQVKEC*YQSHR.D	1.66	1.33	0.86	1.28	120
P51649	ALDH5A1 Succinate-semialdehyde dehydrogenase, mitochondria	ALDH5A1	R.NTGQTC*VCSNQFLVQR.G	1.82	1.28	0.75	1.28	121
Q9NYL2	MLTK Mitogen-activated protein kinase kinase kinase MLT	MLTK	K.FDDLQFFENC*GGGSFGSVYR.A	1.66	1.44	0.76	1.29	122
Q15633	TARBP2 RISC-loading complex subunit TARBP2	TARBP2	R.SC*SLGSLGALGPACCR.V	1.79	1.14	0.93	1.29	123
P33240	CSTF2 Cleavage stimulation factor subunit 2	CSTF2	K.LC*VQNSPQEAR.N	1.73	1.33	0.80	1.29	124

Q99996	AKAP9 A-kinase anchor protein 9	AKAP9	R.TELTALGTTDAVGLLNC*LEQR.I	1.55	1.63	0.69	1.29	125
P49327	FASN Fatty acid synthase	FASN	K.ADEASELAC*PTPK.E	1.77	1.40	0.70	1.29	126
P40763	STAT3 Signal transducer and activator of transcription 3	STAT3	R.QQIACIGGPPNIC*LDR.L	1.56	1.44	0.88	1.29	127
Q8IU81	IRF2BP1 Interferon regulatory factor 2-binding protein 1	IRF2BP1	R.SFREPAPAEALPQQYPEPAPAALC*.G	1.88	1.12	0.88	1.29	128
P31689	DNAJA1 DnaJ homolog subfamily A member 1	DNAJA1	K.GAVEC*CPNCR.G	1.79	1.33	0.76	1.29	129
P49458	SRP9 Signal recognition particle 9 kDa protein	SRP9	R.HSDGNLC*VK.V	1.58	1.56	0.74	1.29	130
Q9NVG8	TBC1D13 TBC1 domain family member 13	TBC1D13	R.LLQDYPITDVC*QILQK.A	1.80	1.17	0.92	1.30	131
O75663	TIPRL TIP41-like protein	TIPRL	K.VAC*AEEWQESR.T	1.70	1.31	0.88	1.30	132
Q5T440	IBA57 Putative transferase CAF17, mitochondrial	IBA57	R.VWAVLPSSPEAC*GAASLQER.A	1.57	1.49	0.83	1.30	133

Q96FW1	OTUB1 Ubiquitin thioesterase OTUB1	OTUB1	K.EFCQQEVEPMC*K.E	1.76	1.59	0.54	1.30	134
E7EQ34	GOSR2 Golgi SNAP receptor complex member 2	GOSR2	K.QVHEIQSC*MGR.L	2.16	1.21	0.52	1.30	135
P15924	DSP Desmoplakin	DSP	R.ETQTEC*EWTVDTSK.L	1.81	1.10	0.99	1.30	136
Q7Z6Z7	HUWE1 E3 ubiquitin-protein ligase HUWE1	HUWE1	R.SSESELC*IETPK.L	1.56	1.44	0.90	1.30	137
P11940	PABPC1 Polyadenylate-binding protein 1	PABPC1	K.VVC*DENGSK.G	1.74	1.40	0.77	1.30	138
Q86VP6	CAND1 Cullin-associated NEDD8-dissociated protein 1	CAND1	K.HC*ECAEEGTR.N	1.79	1.37	0.76	1.31	139
O00299	CLIC1 Chloride intracellular channel protein 1	CLIC1	K.IGNC*PFSQR.L	1.78	1.29	0.85	1.31	140
P27707	DCK Deoxycytidine kinase	DCK	R.SC*PSFSASSEGTR.I	1.80	1.29	0.84	1.31	141
Q9NR33	POLE4 DNA polymerase epsilon subunit 4	POLE4	K.DAYC*CAQQGK.R	1.69	1.41	0.83	1.31	142
Q92817	EVPL Envoplakin	EVPL	R.VTQEC*AEYR.A	1.72	1.40	0.81	1.31	143
P15924	DSP Desmoplakin	DSP	K.YQAEC*SQFK.A	1.77	1.50	0.66	1.31	144

Q6PCE3	PGM2L1 Glucose 1,6-bisphosphate synthase	PGM2L1	R.GQVTSSC*SSQR.L	1.40	1.56	0.98	1.31	145
Q7Z406	MYH14 Myosin-14	MYH14	K.ADLLLEPC*SHYR.F	1.68	1.33	0.93	1.31	146
P62879	GNB2 Guanine nucleotide-binding protein G(I)/G(S)/G(T)	GNB2	R.TFVSGAC*DASIK.L	1.71	1.35	0.88	1.31	147
Q04726	TLE3 Transducin-like enhancer protein 3	TLE3	K.SPISQLDC*LNR.D	1.78	1.35	0.81	1.31	148
Q9HAV4	XPO5 Exportin-5	XPO5	R.AVMEQIPEIQKDSLDQFDC*K.L	1.76	1.38	0.80	1.31	149
Q15631	TSN Translin	TSN	K.ETAAAC*VEK.-	1.70	1.47	0.77	1.31	150
Q9NP81	SARS2 Serine--tRNA ligase, mitochondrial	SARS2	R.FC*ACPEEAAHALELR.K	1.49	1.39	1.07	1.32	151
P55735	SEC13 Protein SEC13 homolog	SEC13	R.FASGGC*DNLIK.L	1.70	1.40	0.85	1.32	152
P23528	CFL1 Cofilin-1	CFL1	K.HELQANC*YEEVK.D	1.71	1.42	0.82	1.32	153
P62306	SNRPF Small nuclear ribonucleoprotein F	SNRPF	R.C*NNVLYIR.G	1.83	1.32	0.80	1.32	154
P34932	HSPA4 Heat shock 70 kDa protein 4	HSPA4	R.C*TPACISFGPK.N	1.71	1.57	0.67	1.32	155

P63208	SKP1 S-phase kinase-associated protein 1	SKP1	R.KENQWC*EEK.-	1.65	1.49	0.82	1.32	156
Q9NUU7	DDX19A ATP-dependent RNA helicase DDX19A	DDX19A	K.VLVTTNVC*AR.G	1.58	1.59	0.79	1.32	157
Q9Y3P9	RABGAP1 Rab GTPase-activating protein 1	RABGAP1	K.NNTDTLYEVVC*LESESER.E	1.90	1.31	0.75	1.32	158
P49327	FASN Fatty acid synthase	FASN	K.AINC*ATSGVVGLVNCLR.R	1.88	1.36	0.72	1.32	159
P78347	GTF2I General transcription factor II-I	GTF2I	R.SILSPGGSC*GPIK.V	1.81	1.38	0.78	1.32	160
P46782	RPS5 40S ribosomal protein S5	RPS5	K.AQC*PIVER.L	1.57	1.27	1.14	1.33	161
P41250	GARS Glycine--tRNA ligase	GARS	R.SC*YDLSCHAR.A	1.65	1.61	0.72	1.33	162
O15067	PFAS Phosphoribosylformylglycinamidine synthase	PFAS	K.FC*DNSSAIQGK.E	1.54	1.42	1.02	1.33	163
P18858	LIG1 DNA ligase 1	LIG1	K.QPEQATTSAQVAC*LYR.K	1.92	1.17	0.89	1.33	164
P47756	CAPZB F-actin-capping protein subunit beta	CAPZB	K.DETVSDC*SPHIANIGR.L	1.73	1.34	0.91	1.33	165
P26641	EEF1G Elongation factor 1-gamma	EEF1G	K.AAAPAPEEEMDEC*EQALAAEPK.A	1.87	1.41	0.70	1.33	166

O43865	AHCYL1 Putative adenosylhomocysteinase 2	AHCYL1	K.LC*VPAMNVNDSVTK.Q	1.61	1.40	0.98	1.33	167
Q9NZT2	OGFR Opioid growth factor receptor	OGFR	R.DC*NGDTPNLSFYR.N	1.70	1.43	0.86	1.33	168
Q4ZG55	GREB1 Protein GREB1	GREB1	R.LINSSC*LVR.T	1.89	1.25	0.85	1.33	169
Q96FW1	OTUB1 Ubiquitin thioesterase OTUB1	OTUB1	K.QEPLGSDSEGVNC*LAYDEAIMAQQDR.I	1.73	1.61	0.65	1.33	170
P60981	DSTN Destrin	DSTN	K.C*STPEEIKKR.K	1.72	1.48	0.79	1.33	171
P49915	GMPS GMP synthase	GMPS	K.TVGVQGDC*R.S	1.74	1.53	0.72	1.33	172
P04183	TK1 Thymidine kinase, cytosolic	TK1	R.YSSSFC*THDR.N	1.92	1.37	0.70	1.33	173
P54886	ALDH18A1 Delta-1-pyrroline-5-carboxylate synthase	ALDH18A1	R.GDEC*GLALGR.L	1.77	1.37	0.86	1.33	174
O95071	UBR5 E3 ubiquitin-protein ligase UBR5	UBR5	K.LPNLEC*IQNANK.G	1.90	1.27	0.83	1.33	175
P67936	TPM4 Tropomyosin alpha-4 chain	TPM4	K.EENVGLHQTLDQTLNELNC*I.-	1.60	1.63	0.77	1.33	176
Q9UBW7	ZMYM2 Zinc finger MYM-type protein 2	ZMYM2	R.MDVFYLQPEC*SSSTDSPVWYTSTSLDR.N	1.91	1.33	0.76	1.33	177
O75348	ATP6V1G1 V-type proton ATPase	ATP6V1G1	R.GSC*STEVEKETQEK.M	1.66	1.34	1.01	1.34	178

	subunit G 1							
P38606	ATP6V1A V-type proton ATPase catalytic subunit A	ATP6V1A	R.DIKWDFTPC*K.N	1.45	1.30	1.27	1.34	179
P15924	DSP Desmoplakin	DSP	K.NQC*TQVVQER.E	1.91	1.40	0.71	1.34	180
P52292	KPNA2 Importin subunit alpha-2	KPNA2	R.TDC*SPIQFESAWALTNIASGTSEQTK.A	1.96	1.41	0.65	1.34	181
P27348	YWHAQ 14-3-3 protein theta	YWHAQ	R.DNLTLWTSDSAGEEC*DAAEGAEN.-	1.80	1.42	0.81	1.34	182
Q9NX70	MED29 Mediator of RNA polymerase II transcription subuni	MED29	R.LAHEC*LSQSCDSAK.H	1.98	1.10	0.95	1.34	183
O00232	PSMD12 26S proteasome non-ATPase regulatory subunit 12	PSMD12	R.AIYDTPC*IQAESEK.W	1.86	1.61	0.56	1.34	184
P22102	GART Trifunctional purine biosynthetic protein adenosin	GART	K.QVLVAPGNAGTAC*SEK.I	1.77	1.54	0.74	1.35	185
P34932	HSPA4 Heat shock 70 kDa protein 4	HSPA4	R.WNSPAEEGSSDC*EVFSK.N	1.70	1.71	0.64	1.35	186

Q9H8W4	PLEKHF2 Pleckstrin homology domain-containing family F mem	PLEKHF2	R.ICDFCYDLLSAGDMATC*QPAR.S	1.67	1.39	1.00	1.35	187
P45984	MAPK9 Mitogen-activated protein kinase 9	MAPK9	R.TAC*TNFMMTPYVVTR.Y	1.90	1.32	0.84	1.35	188
Q4ZG55	GREB1 Protein GREB1	GREB1	R.VPC*SPLAVVAYER.L	1.77	1.23	1.06	1.35	189
P36873	PPP1CC Serine/threonine-protein phosphatase PP1-gamma cat	PPP1CC	R.GNHEC*ASINR.I	1.97	1.40	0.69	1.35	190
Q15459	SF3A1 Splicing factor 3A subunit 1	SF3A1	R.EVLDQVC*YR.V	1.75	1.48	0.85	1.36	191
P00492	HPRT1 Hypoxanthine-guanine phosphoribosyltransferase	HPRT1	K.SYC*NDQSTGDIK.V	1.80	1.48	0.80	1.36	192
P49137	MAPKAPK2 MAP kinase-activated protein kinase 2	MAPKAPK2	K.ETTSHNSLTTPC*YTPYYVAPEVLGPEK.Y	1.77	1.36	0.96	1.36	193
O95671	ASMTL N-acetylserotonin O-methyltransferase-like protein	ASMTL	K.VDASAC*GMER.L	1.78	1.35	0.96	1.36	194
Q9UNH7	SNX6 Sorting nexin-6	SNX6	R.IGSSLYALGTQDSTDIC*K.F	1.70	1.52	0.88	1.37	195

P60981	DSTN Destrin	DSTN	K.HEC*QANGPEDLNR.A	1.69	1.68	0.73	1.37	196
Q7L576	CYFIP1 Cytoplasmic FMR1-interacting protein 1	CYFIP1	K.C*NEQPNRVEIYEK.T	1.90	1.47	0.73	1.37	197
Q16555	DPYSL2 Dihydropyrimidinase-related protein 2	DPYSL2	R.GLYDGPVC*EVSVTPK.T	1.88	1.65	0.57	1.37	198
E7EVH7	KLC1 Kinesin light chain 1	KLC1	R.LC*QENQWLR.D	1.68	1.26	1.17	1.37	199
Q8WW01	TSEN15 tRNA-splicing endonuclease subunit Sen15	TSEN15	R.GDSEPTPGC*SGLGPGGVR.G	1.67	1.34	1.10	1.37	200
Q5T4S7	UBR4 E3 ubiquitin-protein ligase UBR4	UBR4	R.HTAC*NEQQR.T	1.72	1.42	0.97	1.37	201
P30153	PPP2R1A Serine/threonine-protein phosphatase 2A 65 kDa reg	PPP2R1A	K.EFCENLSADC*R.E	1.97	1.44	0.70	1.37	202
P37802	TAGLN2 Transgelin-2	TAGLN2	K.NMAC*VQR.T	1.92	1.40	0.80	1.37	203
P27348	YWHAQ 14-3-3 protein theta	YWHAQ	R.YLAEVAC*GDDR.K	1.78	1.57	0.77	1.37	204
Q13185	CBX3 Chromobox protein homolog 3	CBX3	R.LTWHSC*PEDEAQ.-	1.83	1.56	0.73	1.37	205
O95433	AHSA1 Activator of 90 kDa heat shock protein ATPase	AHSA1	K.NGETELC*MEGR.G	1.73	1.68	0.71	1.37	206

	homo							
P15924	DSP Desmoplakin	DSP	K.LENINGVTDGYLNSLC*TVR.A	2.07	1.35	0.70	1.37	207
Q8NFF5	FLAD1 FAD synthase	FLAD1	R.LHYGTDPC*TGQPFR.F	1.47	1.74	0.92	1.38	208
P30044	PRDX5 Peroxiredoxin-5, mitochondrial	PRDX5	K.ALNVEPDGTGLTC*SLAPNIISQL.-	1.82	1.45	0.86	1.38	209
Q7L2H7	EIF3M Eukaryotic translation initiation factor 3 subunit	EIF3M	K.VAASC*GAIQYIPTELDQVR.K	1.87	1.54	0.72	1.38	210
P62888	RPL30 60S ribosomal protein L30	RPL30	R.VC*TLAIIDPGDSDIIR.S	1.85	1.30	0.98	1.38	211
Q9Y696	CLIC4 Chloride intracellular channel protein 4	CLIC4	K.AGSDGESIGNC*PFSQR.L	1.75	1.43	0.96	1.38	212
Q15365	PCBP1 Poly(rC)-binding protein 1	PCBP1	R.LVVPATQC*GSLIGK.G	1.91	1.52	0.71	1.38	213
Q15796	SMAD2 Mothers against decapentaplegic homolog 2	SMAD2	K.AITTQNC*NTK.C	1.81	1.41	0.93	1.38	214
P31947	SFN 14-3-3 protein sigma	SFN	K.GAVEKGEELSC*EER.N	1.73	1.48	0.94	1.38	215

P46527	CDKN1B Cyclin-dependent kinase inhibitor 1B	CDKN1B	K.TDPSDSQTGLAEQC*AGIR.K	1.86	1.43	0.86	1.38	216
P12814	ACTN1 Alpha-actinin-1	ACTN1	K.IC*DQWDNLGALTQK.R	1.78	1.66	0.71	1.38	217
Q52LJ0	FAM98B Protein FAM98B	FAM98B	K.SLC*NLEESITSAGR.D	1.66	1.50	1.00	1.39	218
Q13057	COASY Bifunctional coenzyme A synthase	COASY	R.YATSCYSCC*PR.L	1.83	1.51	0.82	1.39	219
Q9ULV4	CORO1C Coronin-1C	CORO1C	K.SIKDTIC*NQDER.I	1.87	1.55	0.74	1.39	220
Q96CM8	ACSF2 Acyl-CoA synthetase family member 2, mitochondrial	ACSF2	R.MVSTPIGGLSYVQGC*TK.K	1.67	1.39	1.11	1.39	221
Q9BTW9	TBCD Tubulin-specific chaperone D	TBCD	K.AGAPDEAVCGENVSQIYC*ALLGCMDDYTTDSR.G	1.67	1.65	0.85	1.39	222
Q13526	PIN1 Peptidyl-prolyl cis-trans isomerase NIMA-interacti	PIN1	K.IKSGEEDFESLASQFSDC*SSAK.A	1.82	1.66	0.69	1.39	223
Q6P1X6	C8orf82 UPF0598 protein C8orf82	C8orf82	R.YEAAFPFLSPC*GR.E	1.60	1.54	1.04	1.39	224
Q04724	TLE1 Transducin-like enhancer protein 1	TLE1	K.SPVSQLDC*LNR.D	1.93	1.46	0.79	1.39	225

Q9H3U1	UNC45A Protein unc-45 homolog A	UNC45A	R.AIQTVSCLLQGPC*DAGNR.A	1.76	1.75	0.67	1.39	226
Q9Y4P8	WIPI2 WD repeat domain phosphoinositide-interacting prot	WIPI2	R.LDGSLETTNEILDSASHDC*PLV.T	2.27	0.99	0.94	1.40	227
Q9UNF1	MAGED2 Melanoma-associated antigen D2	MAGED2	R.MGIGLGSENAAGPC*NWDEADIGPWAK.A	1.73	1.74	0.73	1.40	228
P37235	HPCAL1 Hippocalcin-like protein 1	HPCAL1	R.LLQC*DPSSASQF.-	2.06	1.40	0.76	1.41	229
Q9NNW7	TXNRD2 Thioredoxin reductase 2, mitochondrial	TXNRD2	R.SGLDPTVTGC*.U	1.79	1.62	0.81	1.41	230
P52630	STAT2 Signal transducer and activator of transcription 2	STAT2	K.GLSC*LVSYQDDPLTK.G	1.77	1.37	1.09	1.41	231
E9PPU0	EPPK1 Epiplakin	EPPK1	R.YLC*GLGAVGGVR.L	1.90	1.52	0.81	1.41	232
O75153	KIAA0664 Clustered mitochondria protein homolog	KIAA0664	K.C*LTQQAVALQR.T	1.83	1.44	0.97	1.41	233
Q13148	TARDBP TAR DNA-binding protein 43	TARDBP	R.NPVSQC*MR.G	1.83	1.57	0.84	1.41	234
P21333	FLNA Filamin-A	FLNA	K.AHVVPC*FDASK.V	1.86	1.62	0.76	1.41	235

A6NDG6	PGP Phosphoglycolate phosphatase	PGP	K.NNQESDC*VSK.K	1.39	1.10	1.76	1.42	236
Q92598	HSPH1 Heat shock protein 105 kDa	HSPH1	R.AGGIETIANEFSDRC*TPSVISFGSK.N	1.86	1.53	0.86	1.42	237
Q9Y224	C14orf166 UPF0568 protein C14orf166	C14orf166	K.LTALDYHNPAGFNC*K.D	1.71	1.81	0.73	1.42	238
P57721	PCBP3 Poly(rC)-binding protein 3	PCBP3	R.LVVPASQC*GSLIGK.G	1.88	1.69	0.69	1.42	239
Q9BSD7	NTPCR Cancer-related nucleoside-triphosphatase	NTPCR	R.NADC*SSGPGQR.V	1.91	1.56	0.80	1.42	240
Q9H2U2	PPA2 Inorganic pyrophosphatase 2, mitochondrial	PPA2	K.C*NGGAINCTNVQISDSPFR.C	1.75	1.75	0.77	1.42	241
P30281	CCND3 G1/S-specific cyclin-D3	CCND3	R.ASYFQC*VQR.E	1.96	1.38	0.94	1.43	242
P21333	FLNA Filamin-A	FLNA	K.THEAEIVEGENHTYC*IR.F	1.83	1.64	0.81	1.43	243
Q9Y508	RNF114 RING finger protein 114	RNF114	R.DC*GGAAQLAGPAAEADPLGR.F	1.92	1.55	0.81	1.43	244
Q6IA69	NADSYN1 Glutamine-dependent NAD(+) synthetase	NADSYN1	K.NSSQETC*TR.A	1.99	1.60	0.69	1.43	245

P40222	TXLNA Alpha-taxilin	TXLNA	R.VTEAPC*YPGAPSTEASGQTGPQEPTSAR.A	1.82	1.75	0.71	1.43	246
Q9UP83	COG5 Conserved oligomeric Golgi complex subunit 5	COG5	R.ELLQDGC*YSDFLNEDFDVK.T	2.15	1.41	0.73	1.43	247
O15355	PPM1G Protein phosphatase 1G	PPM1G	K.C*SGDGVGAPR.L	1.88	1.52	0.89	1.43	248
Q15366	PCBP2 Poly(rC)-binding protein 2	PCBP2	R.YSTGSDSASFPHTTPSMC*LNPDLEGPPLEAYTIQGQY.A	1.87	1.80	0.62	1.43	249
Q12765	SCRN1 Secernin-1	SCRN1	K.TQSPC*FGDDDPAK.K	1.71	1.81	0.78	1.43	250
O95685	PPP1R3D Protein phosphatase 1 regulatory subunit 3D	PPP1R3D	R.APPPTPAPSGC*DPR.L	1.92	1.47	0.92	1.44	251
Q14C86	GAPVD1 GTPase-activating protein and VPS9 domain-containi	GAPVD1	R.LIITSAEASPAEC*CQHAK.I	1.87	1.70	0.75	1.44	252
Q27J81	INF2 Inverted formin-2	INF2	K.LGPQDSDPTEANLESADPELC*IR.L	1.58	1.45	1.31	1.45	253
Q93052	LPP Lipoma-preferred partner	LPP	K.TYITDPVSAPC*APPLQPK.G	2.11	1.45	0.79	1.45	254
P78417	GSTO1 Glutathione S-transferase omega-1	GSTO1	K.LNEC*VDHTPK.L	1.87	1.71	0.77	1.45	255

P04406	GAPDH Glyceraldehyde-3-phosphate dehydrogenase	GAPDH	K.IISNASC*TTNCLAPLAK.V	2.17	1.41	0.77	1.45	256
Q9H6T0	ESRP2 Epithelial splicing regulatory protein 2	ESRP2	R.AEAAALSTQC*R.E	2.25	1.42	0.68	1.45	257
P49790	NUP153 Nuclear pore complex protein Nup153	NUP153	K.CVACETPKPGTC*VK.R	1.77	1.44	1.15	1.45	258
Q8TEX9	IPO4 Importin-4	IPO4	K.AC*QSCPSEPNTAALQAALAR.V	2.17	1.58	0.62	1.46	259
P12814	ACTN1 Alpha-actinin-1	ACTN1	R.MVSDINNAWGC*LEQVEK.G	1.96	1.54	0.88	1.46	260
Q7Z6Z7	HUWE1 E3 ubiquitin-protein ligase HUWE1	HUWE1	R.HIIEDPC*TLR.H	2.14	1.54	0.70	1.46	261
Q9Y5P6	GMPPB Mannose-1-phosphate guanyltransferase beta	GMPPB	R.LC*SGPGIVGNVLVDPSAR.I	1.84	1.60	0.94	1.46	262
Q96BF6	NACC2 Nucleus accumbens-associated protein 2	NACC2	R.NTLANSC*GTGIR.S	1.92	1.73	0.74	1.46	263
P68366	TUBA4A Tubulin alpha-4A chain	TUBA4A	K.RSIQFVDWC*PTGFK.V	1.83	1.79	0.77	1.46	264
Q7L2J0	MEPCE 7SK snRNA methylphosphate capping enzyme	MEPCE	R.SC*FPASLTASR.G	1.98	1.57	0.85	1.47	265

P23396	RPS3 40S ribosomal protein S3	RPS3	R.GLC*AIAQ AESLR.Y	2.12	1.60	0.68	1.47	266
Q99497	PARK7 Protein DJ-1	PARK7	K.GLIAAIC* AGPTALLA.H	1.46	1.01	1.95	1.47	267
P61962	DCAF7 DDB1- and CUL4-associated factor 7	DCAF7	R.VPC*TPVA R.L	2.19	1.43	0.80	1.47	268
P17987	TCP1 T-complex protein 1 subunit alpha	TCP1	R.SLHDALC* VVK.R	1.78	1.93	0.72	1.48	269
P51808	DYNLT3 Dynein light chain Tctex-type 3	DYNL T3	R.HC*DEVGF NAEEAHNIV K.E	2.11	1.66	0.66	1.48	270
O95817	BAG3 BAG family molecular chaperone regulator 3	BAG3	R.SQSPAASD C*SSSSSSAS LPSSGR.S	2.00	1.68	0.76	1.48	271
P30041	PRDX6 Peroxiredoxi n-6	PRDX6	K.DINAYNC* EEPTEK.L	1.98	1.61	0.86	1.48	272
P55786	NPEPPS Puromycin-sensitive aminopeptid ase	NPEPP S	R.SKDGVC*V R.V	1.99	1.68	0.79	1.49	273
Q12931	TRAP1 Heat shock protein 75 kDa, mitochondri al	TRAP1	K.FEDRSPAA EC*LSEK.E	1.64	1.92	0.92	1.49	274
P68366	TUBA4A Tubulin alpha-4A chain	TUBA4 A	K.YMACC*L LYR.G	1.76	1.98	0.74	1.49	275
I3L2F9	Uncharacteri zed protein	Unchar acterize d	K.NMMAAC* DPR.H	1.92	1.84	0.73	1.50	276

P46940	IQGAP1 Ras GTPase-activating-like protein IQGAP1	IQGAP1	K.QLSSSVTGLTNIEEENC*QR.Y	2.01	1.68	0.81	1.50	277
P14868	DARS Aspartate--tRNA ligase, cytoplasmic	DARS	R.LEYC*EALAMLR.E	2.11	1.58	0.82	1.50	278
P12277	CKB Creatine kinase B-type	CKB	H.LGYILTC*PSNLGTGLR.A	2.12	1.42	0.98	1.51	279
P04406	GAPDH Glyceraldehyde-3-phosphate dehydrogenase	GAPDH	K.IISNASC*TTN.C	2.25	1.42	0.85	1.51	280
O75150	RNF40 E3 ubiquitin-protein ligase BRE1B	RNF40	R.LREIQPC*LAESR.A	2.20	1.31	1.01	1.51	281
Q13642	FHL1 Four and a half LIM domains protein 1	FHL1	K.CFDKFC*ANTCVECR.K	1.78	1.86	0.88	1.51	282
Q6UWE0	LRSAM1 E3 ubiquitin-protein ligase LRSAM1	LRSAM1	R.QNLVQQAC*SSMAEMDER.F	1.86	1.20	1.47	1.51	283
O95299	NDUFA10 NADH dehydrogenase	NDUFA10	R.KQC*VDHYNEVK.S	2.06	1.56	0.92	1.51	284
Q14980	NUMA1 Nuclear mitotic apparatus protein 1	NUMA1	R.KVEELQAC*VETAR.Q	1.95	1.67	0.93	1.52	285

Q6AI08	HEATR6 HEAT repeat-containing protein 6	HEATR6	R.LC*ALRPDDSSSAR.T	2.11	1.64	0.83	1.53	286
Q9UGI8	TES Testin	TES	R.TQYSCYC*CK.L	2.02	1.93	0.67	1.54	287
Q14247	CTTN Src substrate cortactin	CTTN	K.HC*SQVDSVR.G	1.64	2.21	0.78	1.54	288
Q9Y2S2	CRYL1 Lambda-crystallin homolog	CRYL1	R.VILSSSTSC*LMPSK.L	1.90	1.92	0.82	1.55	289
Q00610	CLTC Clathrin heavy chain 1	CLTC	R.IHEGC*EEPATHNALAK.I	2.09	1.59	0.97	1.55	290
Q71U36	TUBA1A Tubulin alpha-1A chain	TUBA1A	R.TIQFVDWC*PTGFK.V	1.90	2.03	0.75	1.56	291
Q9UPN9	TRIM33 E3 ubiquitin-protein ligase TRIM33	TRIM33	R.C*DPVPAANGAIR.F	2.27	1.69	0.72	1.56	292
P62993	GRB2 Growth factor receptor-bound protein 2	GRB2	K.VLNEEC*DQNWYK.A	1.81	2.07	0.82	1.57	293
Q04637	EIF4G1 Eukaryotic translation initiation factor 4 gamma 1	EIF4G1	R.LQGINC*GPDFTPSFANLGR.T	2.24	1.70	0.76	1.57	294
Q5VZL5	ZMYM4 Zinc finger MYM-type protein 4	ZMYM4	K.C*GGVEQASSSPR.S	2.03	1.98	0.70	1.57	295

Q07864	POLE DNA polymerase epsilon catalytic subunit A	POLE	R.IHC*GLQD SQK.A	2.21	1.73	0.78	1.57	296
Q969T 9	WBP2 WW domain-binding protein 2	WBP2	K.DC*EIKQP VFGANYIK.G	2.08	1.70	0.94	1.57	297
Q9H91 0	HN1L Hematologic al and neurological expressed 1-like pr	HN1L	K.DHVFLC*E GEEPK.S	1.86	1.75	1.15	1.59	298
Q7RTV 0	PHF5A PHD finger-like domain-containing protein 5A	PHF5A	R.ICDEC*NY GSYQGR.C	1.88	2.17	0.71	1.59	299
Q9NX G2	THUMPD1 THUMP domain-containing protein 1	THUM PD1	R.RC*DAGGP R.Q	1.76	2.12	0.90	1.59	300
P62258	YWHAE 14-3-3 protein epsilon	YWHA E	K.LICC*DILD VLDK.H	2.21	1.79	0.79	1.60	301
P17516	AKR1C4 Aldo-keto reductase family 1 member C4	AKR1 C4	L.WVDPNSP VLLEDPVLC *ALAK.K	2.20	1.65	1.03	1.63	302
P28340	POLD1 DNA polymerase delta catalytic subunit	POLD1	R.VAGLC*SN IR.D	2.62	1.45	0.82	1.63	303
O95372	LYPLA2 Acyl-protein thioesterase 2	LYPLA 2	K.TYPGVMH SSC*PQEMA AVK.E	2.29	1.83	0.80	1.64	304
Q04917	YWHAH 14-3-3	YWHA H	K.NC*NDFQ YESK.V	2.29	1.70	0.99	1.66	305

	protein eta							
P00338	LDHA L-lactate dehydrogenase A chain	LDHA	R.VIGSGC*NLDSAR.F	2.67	1.61	0.80	1.69	306
Q96EY8	MMAB Cob(I)yrinic acid a,c-diamide adenosyltransferase,	MMAB	K.IQC*TLQDVGSALATPCSSAR.E	1.84	2.51	0.82	1.72	307
P24752	ACAT1 Acetyl-CoA acetyltransferase, mitochondrial	ACAT1	K.IHMGSC*AENTAK.K	2.99	1.33	0.94	1.75	308
O43719	HTATSF1 HIV Tat-specific factor 1	HTATSF1	K.RGFEGSC*SQK.E	1.89	2.75	0.63	1.76	309
P21333	FLNA Filamin-A	FLNA	K.IEC*DDKGDGSCDVR.Y	2.39	2.24	0.72	1.78	310
P00390	GSR Glutathione reductase, mitochondrial	GSR	K.LGGTC*VNVGCVPK.K	2.80	1.57	1.00	1.79	311
Q9NVM4	PRMT7 Protein arginine N-methyltransferase 7	PRMT7	K.QVSSSAAC*HSR.R	2.48	1.76	1.16	1.80	312
P13646	KRT13 Keratin, type I cytoskeletal 13	KRT13	K.AGLENTVAETEC*R.Y	2.94	1.82	0.68	1.81	313
P13639	EEF2 Elongation factor 2	EEF2	K.DLEEDHAC*IPIK.K	1.96	3.04	0.86	1.95	314
P11216	PYGB Glycogen phosphorylase, brain	PYGB	R.TC*FETFPDK.V	2.35	1.52	2.08	1.98	315

	form							
O14733	MAP2K7 Dual specificity mitogen-activated protein kinase	MAP2K7	K.LC*DFGISGR.L	2.66	2.22	1.19	2.02	316
P55072	VCP Transitional endoplasmic reticulum ATPase	VCP	K.AIANEC*QANFISIK.G	1.95	1.75	2.46	2.05	317
Q99873	PRMT1 Protein arginine N-methyltransferase 1	PRMT1	K.VIGIEC*SSISDYAVK.I	2.53	2.36	1.35	2.08	318
Q06124	PTPN11 Tyrosine-protein phosphatase non-receptor type 11	PTPN11	K.QGFWEEFETLQQQEC*K.L	1.84	3.54	0.88	2.09	319
Q04760	GLO1 Lactoylglutathione lyase	GLO1	K.C*DFPIMK.F	3.02	2.50	1.60	2.37	320
Q96ER3	SAAL1 Protein SAAL1	SAAL1	R.VLQNMEQC*QK.K	3.04	2.32	4.86	3.41	321
Q9BTE3	MCMBP Mini-chromosome maintenance complex-binding protei	MCMBP	R.DASALLDPMEC*TDTAEEQR.V	10.75	1.47	0.85	4.36	322
Q9HA64	FN3KRP Ketosamine-3-kinase	FN3KRP	R.ATGHSGGGC*ISQGR.S	1.89	10.66	0.80	4.45	323

Table 4A-1 Azo-sample data collected from *Drosophila melanogaster* heads collected at 4-hour intervals (0, 4, 8, 12, 16, 20) over a 20 hour period. Cysteines with oscillating reactivity were sorted by R^2 and intensity (max/min) and ranked from strongest to weakest oscillators. Known mRNA cyclers are highlighted in purple. Novel cyclers and Prx cyclers are highlighted in yellow. Potential mRNA cyclers are highlighted in orange. Oscillators that do not show substantial decrease in activity are highlighted in grey.

Rank	protein	peptide	intensity	period	R^2	0	4	8	12	16	20	Max/Min
1	Arr1	ASDESQPCGVQYFVK	2.1	21	0.913	1.05	1.82	1.32	0.58	0.41	0.80	4.43
2	Arr1	VMYLVPTLVANCDR	1.9	20	0.908	1.08	2.04	1.16	0.75	0.46	1.10	4.42
3	Mlp60A	GYGFGGGAGCLSTDTGAHLNR	1.9	19	0.951	0.93	2.09	1.30	0.72	0.53	1.16	3.98
4	tsr	YGLFDFEYMHQCQGTSESSK	1.8	20	0.761	0.98	2.07	1.61	1.11	0.53	1.22	3.91
5	sesB-RD, sesB	YFAGNLASGGAAGATSLCFVYPLDFAR	0.6	24	0.801	1.32	0.90	1.72	3.46	1.45	1.45	3.84
6	Eb1, Eb1-RA, Eb1-	INACANSTGTVK	1.8	21	0.866	0.98	1.52	2.02	0.88	0.53	0.97	3.81

	RF											
7	Arr1	QGIQPCTVVR	1.8	20	0.755	1.03	1.46	2.34	0.65	0.64	1.03	3.66
8	ninaC	NPSMTSCALTYNAYK	2.0	19	0.865	0.93	1.51	1.27	0.56	0.42	1.15	3.64
9	Trxr-1	SGLDPTPASCCS	1.9	19	0.846	1.03	1.93	1.33	0.82	0.54	1.70	3.61
10	Arr2	STGDACGIVISYSVR	1.7	21	0.783	1.03	1.55	1.97	0.99	0.57	1.09	3.45
11	rtp	SQCEHPY	1.9	20	0.775	1.12	1.34	1.18	0.60	0.39	0.96	3.44
12	CG9368, CG9368-RA	IFDAICNCANNNAAAATTR	1.8	20	0.855	1.12	1.57	1.29	0.83	0.47	1.22	3.34
13	ninaC	GTCIGSPCWMAPEVVSAMESR	1.8	19	0.882	0.88	1.59	1.13	0.67	0.49	1.16	3.27
14	Gale	AVGESCR	1.8	18	0.774	0.96	1.31	0.99	0.48	0.51	1.52	3.17
15	CG6330-RB, CG6330	LDGAFCDFSENEK	1.6	18	0.775	1.05	1.37	1.32	0.79	0.58	1.76	3.03
16	rtp	NEGFFQDCR	1.7	20	0.763	1.03	1.20	1.36	0.69	0.45	1.17	3.01

17	Mlp60A	ALDSTNCTEHEK	1.8	20	0.938	0.98	1.50	1.36	0.63	0.53	1.10	2.85
18	cl	CSNQDLVEMMFEDED	1.6	20	0.842	1.10	1.32	1.39	0.87	0.52	1.04	2.67
19	Arr2	LNCGTLGGEMQTDVPFK	1.5	21	0.843	1.01	1.18	1.55	0.80	0.62	0.89	2.51
20	Mlp60A	ELFCK	1.6	19	0.910	0.94	1.49	1.07	0.64	0.60	1.16	2.50
21	CtBP	DCSIEMPILK	1.5	22	0.788	0.95	1.18	1.72	0.82	0.71	0.82	2.42
22	ninaC	SCQDQDLIMDR	1.6	19	0.866	0.99	1.36	1.28	0.81	0.56	1.24	2.42
23	Cat	DGAMNVTDNQDGAPNYFPNSFNGPQECPR	1.5	19	0.781	1.05	1.29	1.33	0.81	0.62	1.50	2.42
24	dj-1beta	SQESGGGLIAAICAAPTVLAK	1.6	20	0.919	1.03	1.33	1.31	0.78	0.56	0.98	2.38
25	RpS5a, RpS5b	AQCPIVER	1.5	21	0.824	0.95	1.20	1.28	0.80	0.54	0.94	2.37

26	beta Tub56D,	NMMAACDPR	1.5	20	0.850	1.00	1.25	1.47	0.82	0.63	1.13	2.33
27	CtBP	EAAHGCAR	1.3	30	0.807	0.95	1.12	0.98	0.49	0.60	0.70	2.31
28	mub	INISDGSCPER	1.4	25	0.866	0.99	0.67	0.64	0.58	0.43	0.93	2.30
29	GstO3	FCPYAQR	1.4	23	0.758	0.97	1.44	1.02	1.06	0.63	0.71	2.29
30	alpha Tub84D,	TIQFVDWCPTGFK	1.5	19	0.855	0.91	1.42	1.26	0.86	0.63	1.33	2.27
31	beta Tub56D,	TAVCDIPPR	1.5	19	0.830	0.97	1.31	1.27	0.84	0.59	1.29	2.21
32	Gs2-RC, Gs2	NGFPGPQGPYYCGVGANK	1.4	23	0.789	0.96	1.31	1.39	1.18	0.64	0.91	2.18
33	Tina-1	MLNSLDNLEDCEEIYTR	1.5	22	0.817	1.01	1.34	1.20	0.70	0.62	0.68	2.16
34	Arr1	ELTLVSQQVCPPQK	1.4	21	0.898	1.11	1.51	1.11	0.86	0.71	0.91	2.14
35	CG32444-RA, BcDNA:GH08902	VDDVCLGFDDIASYLANK	0.8	28	0.776	0.80	1.33	1.32	1.65	1.26	1.51	2.06

	, CG32444											
36	Uba1	ICSGNTCPLDAAVGGIVAQEVLK	1.4	22	0.865	1.11	1.24	1.39	1.01	0.70	0.91	1.99
37	alphaTub84D,	YMACCMLYR	1.4	20	0.841	0.95	1.22	1.24	0.82	0.63	1.14	1.98
38	Arr2,	DFIDHIDYCDPVDGVIVVEPDYLK	1.4	20	0.888	1.04	1.29	1.14	0.75	0.66	0.91	1.96
39	CanA-14F	LTCADVFDAR	1.5	18	0.864	0.96	1.34	1.30	0.79	0.77	1.49	1.95
40	TBCB	LEILTGGCAGTMK	1.4	21	0.758	0.83	1.13	1.30	0.84	0.67	0.92	1.94
41	GstT1	LCQYNVNEK	1.4	20	0.787	1.00	1.53	1.29	0.98	0.79	1.14	1.93
42	Arr1	NTIAFMETSEGCPLNPGSSLQK	1.4	21	0.955	1.05	1.30	1.33	0.80	0.69	0.88	1.93

43	Gapdh2, Gapdh1	VVSNASCTTNCLAPLAK	1.4	20	0.909	1.07	1.25	1.29	0.76	0.67	1.06	1.93
44	rtp	CPEVVQR	1.4	19	0.790	1.06	1.14	1.36	0.73	0.72	1.10	1.88
45	CG16985	MAYLDCILR	0.8	29	0.757	0.89	1.21	1.02	1.65	1.28	1.32	1.85
46	Act5C	CPEALFQPSFLGMEACGIHETTYNSIMK	1.4	23	0.931	1.08	1.33	1.25	0.90	0.78	0.72	1.84
47	Ran, ran	VCENIPIVLCGNK	1.3	21	0.773	0.97	1.13	1.36	0.92	0.75	1.03	1.83
48	oho23B-RE, RpS21	TYAICGEIR	1.3	20	0.850	0.96	1.30	1.06	0.92	0.71	1.08	1.82
49	Arr2	EGCPITPGANLTK	1.3	20	0.952	1.03	1.33	1.14	0.91	0.73	0.98	1.82
50	tsr	LFLMSWCPDTAK	1.3	23	0.775	1.06	1.15	1.45	0.97	0.82	0.92	1.77
51	CstF-64	LCIVSNPSEAR	1.3	19	0.760	1.18	1.25	1.04	0.76	0.74	0.99	1.69
52	Act42A, Act5C	LCYVALDFEQEMATA	1.3	20	0.909	0.90	1.36	1.28	0.85	0.81	1.03	1.68

		ASSSSLEK										
53	regucalcin-RD, regucalcin	PQEFAVGCGR	0.8	29	0.864	1.21	1.15	1.14	1.88	1.50	1.40	1.66
54	CG9156, flw, Pp1-87B, Pp1alpha-96A, Pp1-13C	GNHECASINR	1.2	19	0.914	0.96	1.19	1.11	0.91	0.79	1.11	1.51
55	Scp2	DNDGQVSVDEWCNMWDAYAK	1.2	20	0.888	0.95	1.18	1.09	0.94	0.81	1.06	1.46
56	mgr	FMACNLEAR	1.2	20	0.769	0.86	1.22	1.19	0.93	0.85	1.03	1.44
57	Henna, Hn	AYGAGLLSSYGELEYCLTDK	1.3	30	0.877	0.89	0.72	0.77	0.70	0.62	0.70	1.43
58	CG11089	YTQSNSVCYAR	0.8	27	0.924	1.06	1.04	1.24	1.48	1.22	1.26	1.42

59	Prx2540-1, CG12896-RA, Prx2540-2, CG12896	SYCLDIPGDFPYPIIADPTR	0.8	26	0.956	1.07	1.06	1.36	1.36	1.46	1.14	1.38
60	CG30116, BcDNA:GH04922, BcDNA.GH04922	TMTVSGTGCIR	0.9	29	0.853	0.97	1.06	1.21	1.34	1.12	1.28	1.38
61	Scp2, cimageipi-tr|Q6NL47|Q6NL47_DROME	TECEEAFAK	1.1	19	0.754	1.03	1.19	1.03	0.99	0.91	1.09	1.31
62	CG10512-RA, CG10512-RD, CG10512	TCANLAEILK	0.9	28	0.953	1.00	1.12	1.20	1.25	1.22	1.21	1.25
63	chic	LGDYLITCGY	1.1	20	0.836	0.95	1.08	1.04	0.91	0.91	1.00	1.19

64	14-3-3zeta, Egfr	EICYEVLGLLDK	0.9	29	0.767	1.13	1.05	1.10	1.12	1.15	1.11	1.10

Table 4A-2 Azo-sample data collected from U2OS_P cells collected at 4-hour intervals (0, 4, 8, 12, 16, 20) over a 20 hour period. Cysteines with oscillating reactivity were sorted by R^2 and intensity (max/min) and ranked from strongest to weakest oscillators. Data was analyzed for Prxs present in the data that oscillate with similar phase found in the *Drosophila* data. Prx6 is highlighted in yellow.

#	protein	peptide	intensity	period	R^2	0	4	8	12	16	20	Max/Min
1	TTC1	VTDTQEAECAGPPVPDPK	2.98	23	0.633	1.02	2.05	0.87	0.90	0.15	0.32	13.67
2	BAG3	SQSPAASDCSSSSSSASLPSSGR	2.66	19	0.630	1.33	2.37	0.89	0.83	0.20	1.82	11.85
3	PDLIM5	QPTVTSVCSETSQELAEGQR	2.14	20	0.528	1.32	1.05	1.84	0.84	0.23	1.39	8.00
4	TNKS1BP1	NLEVSSCVGSGGSSEAR	2.60	25	0.922	0.86	3.08	1.80	1.31	0.45	0.44	7.00
5	PPP4R2	LCELLTDPR	0.65	23	0.264	5.77	1.09	0.99	5.81	1.18	1.03	5.89
6	FLNA	YWPQEAGEYAVHVLCNSEDIR	0.65	22	0.636	0.50	1.28	2.75	1.51	2.17	0.95	5.50
7	EIF3D	TQGNVFATDAILATLMSCTR	0.65	21	0.627	0.93	1.00	1.32	4.30	1.10	0.84	5.15
8	MAP4	CSLPAEEDSVLE	1.98	25	0.802	1.26	1.36	1.63	1.47	0.42	0.50	3.87

		K										
9	ALDH2	LLCGGGIAADR	1.36	20	0.232	1.13	0.83	1.82	0.48	0.85	0.82	3.79
10	CTTN	HCSQVDSVR	1.35	25	0.186	2.87	1.44	1.42	1.19	0.77	0.94	3.70
11	RPL10, RPL10L	MLSCAGADR	1.66	23	0.528	1.92	1.91	1.24	1.34	0.55	0.77	3.49
12	CHMP5	APPPSLTDCIGTVDSR	1.68	21	0.687	1.41	1.16	1.50	0.82	0.45	0.85	3.37
13	VDAC2	SCSGVEFSTSGSSNTDTGK	1.62	19	0.673	0.98	1.90	1.28	1.11	0.59	1.37	3.25
14	IBA57	VWAVLPSSPEACGAASLQER	1.56	23	0.683	0.96	1.25	2.24	0.91	0.71	0.87	3.15
15	CNN2	CASQSGMTAYGTR	1.58	24	0.511	1.51	1.18	0.99	1.13	0.48	0.50	3.14
16	TCF20	SVICDISPLR	1.59	24	0.603	1.05	1.31	2.57	0.84	0.82	0.82	3.13
17	WAPAL	CSSYSESSEAAQLEEVTSVLEANSK	1.60	23	0.669	1.02	1.52	0.96	0.87	0.59	0.50	3.03
18	CRKL	DSSTCPGDYVLSVSENSR	1.51	26	0.568	1.06	1.13	1.16	0.97	0.85	0.40	2.89

19	SSSCA1	MLGETCADCGTILLQDK	1.43	25	0.530	1.23	0.87	1.75	0.89	0.72	0.62	2.82
20	TIGAR	CSLPATLSR	1.42	24	0.461	0.97	1.27	1.76	0.64	1.06	0.63	2.79
21	UBE3A	AACSAAAMEEDSEASSSR	1.54	20	0.625	0.90	2.13	1.01	0.77	0.81	0.80	2.77
22	NHP2L1	LLDLVQQSCNYK	1.25	19	0.181	2.08	1.26	1.02	0.76	0.87	1.01	2.74
23	MYH9, MYH10, MYH11, MYH14	EDQSILCTGESGAGK	1.76	18	0.769	0.85	2.00	1.75	0.73	0.86	1.52	2.74
24	KIN	GACSSSGATSSK	1.60	22	0.907	1.02	1.27	1.67	0.84	0.61	0.76	2.74
25	FAM129B	EELCK	1.60	24	0.673	1.04	1.08	1.22	1.06	0.46	0.56	2.65
26	RPL5	DIICQIAYAR	1.46	24	0.849	0.98	1.06	0.40	0.56	0.60	0.74	2.65
27	TXNDC17	SWCPDCVQAEPVVR	1.56	25	0.894	1.00	1.19	1.55	1.12	0.60	0.65	2.58
28	PLEC	LCFEGLR	1.47	19	0.528	0.57	1.47	1.18	0.84	0.67	1.21	2.58
29	PTPN11	QGFWEEFETLQQQECK	1.49	21	0.633	1.06	1.18	1.14	0.96	0.46	0.99	2.56

30	CLTC	IHEGCEEPATHNALAK	1.40	18	0.564	0.87	1.09	1.52	0.60	0.91	1.31	2.53
31	PRDX6	DINAYNCEEPTEK	0.76	18	0.773	0.97	1.12	1.96	1.46	0.80	0.89	2.44
32	RPS5	VNQAIWLLCTGAR	0.81	25	0.634	0.68	0.90	1.66	1.40	1.36	1.24	2.44
33	SUCLA2	ICNQVLVCER	1.40	19	0.569	0.87	1.32	1.03	1.00	0.58	1.37	2.36
34	PLIN3	DIAQQLQATCTSLGSSIQGLPTNVK	1.33	26	0.524	1.06	0.97	1.28	0.89	0.88	0.54	2.36
35	EIF3D	FMTPVIQDNPSGWGPCAVPEQFR	1.26	19	0.229	0.53	1.25	1.04	0.70	0.89	0.96	2.36
36	ACAT1	IHMGSCAENTAK	1.40	19	0.628	1.04	1.34	1.53	0.65	0.96	1.04	2.35
37	RPS5	TIAECLADELINAAK	1.49	20	0.791	1.00	1.46	1.30	0.64	0.79	0.82	2.28
38	PLEC	CDNFTSSWR	0.61	26	0.907	1.12	1.86	2.12	2.12	2.55	1.50	2.28
39	LANCL2	SVVCQESDLPDELLYGR	0.74	19	0.815	1.01	1.35	1.43	2.18	0.97	1.02	2.25
40	ACSF2	MVSTPIGGLSYVQGCT	1.34	18	0.548	0.91	1.17	1.28	0.57	0.96	1.04	2.25

		K										
41	SOD1	LACGVIGIAQ	0.69	20	0.929	0.90	1.28	1.98	1.99	1.29	1.30	2.20
42	VAPA	CVFEMPNENDK	0.69	22	0.648	0.78	0.95	0.78	1.23	1.70	1.42	2.18
43	Uncharacterized, RPL36AL	LECVEPNCR	1.36	23	0.609	1.13	1.05	1.51	0.74	0.79	0.70	2.16
44	PLOD1	VGVDYEGGGCR	0.73	24	0.841	0.84	1.54	1.80	1.62	1.52	1.37	2.16
45	9-Sep	SQEATEAAPSCVGDMADTPR	1.34	20	0.645	1.12	1.31	0.95	0.93	0.61	0.98	2.15
46	TXLNA	VTEAPCYPGAPSTEASGQTGPQEPTSAR	1.45	20	0.768	0.94	1.46	1.38	0.99	0.68	1.23	2.15
47	TIPRL	CVNNYQGMLK	1.34	25	0.596	0.91	1.31	0.94	1.09	0.73	0.61	2.15
48	NHLRC2	AILFSQPLQITDTQQGCIAPVELR	1.38	24	0.695	0.87	1.10	1.26	1.14	0.59	0.77	2.14
49	G6PD	TQVCGILR	1.46	20	0.748	1.39	1.33	1.28	0.82	0.65	0.99	2.13
50	RPL24	VELCSFSGYK	1.30	19	0.456	0.79	1.67	1.24	0.96	1.00	1.08	2.13

51	RNF2	FCADCIITALR	0.77	26	0.824	0.89	1.12	1.88	1.34	1.62	1.36	2.12
52	UPP1	AESHNDCPVR	1.30	23	0.492	1.30	1.18	1.16	1.21	0.61	0.93	2.12
53	NIT2	TLSPGDSFSTFDTPYCR	0.78	18	0.490	1.15	0.85	0.97	1.00	1.50	0.71	2.11
54	PLEC	VLSSSGSEAAVPSVCFLVPPPNQEAQEAVTR	1.22	20	0.260	0.62	1.28	1.30	0.83	0.99	0.98	2.10
55	NAA10	GNSPPSSGEACR	1.37	20	0.714	0.91	1.23	1.06	0.89	0.60	1.13	2.05
56	OXCT1	STGCDFAVSPK	0.81	18	0.373	0.95	0.99	1.14	1.16	1.52	0.74	2.05
57	PITPNB	VVLPCSVQEYQVGQLYSVAEASK	1.32	18	0.843	1.09	1.05	0.54	0.64	0.95	0.91	2.04
58	SH3PXD2B	GPQCEGHESR	1.44	23	0.893	1.23	1.42	1.27	0.98	0.70	0.75	2.04
59	SARS	YAGLSTCFR	1.38	21	0.815	1.03	1.15	1.24	0.86	0.61	0.99	2.03
60	ACTR3	LPACVVDCGTGYTK	1.29	18	0.483	0.95	1.75	0.86	0.89	0.91	1.04	2.03
61	TRMT10C	SSVQEECVSTISSSK	1.22	23	0.517	0.69	1.01	0.90	0.50	0.90	0.96	2.02
62	XPO	DSLD	1.39	18	0.74	0.9	1.2	1.2	0.8	0.7	1.4	2.01

	5	QFDCK			6	3	4	9	7	3	7	
63	ACAA2	LCGSGFQSIVNGCQEICVK	1.27	19	0.517	0.99	1.18	1.30	0.65	0.97	0.95	2.00
64	PLOD2	LDPDMALCR	1.27	18	0.495	0.90	1.08	1.22	0.62	0.91	1.02	1.98
65	GNB2L1	VWNLANCK	1.41	23	0.875	0.83	0.91	0.46	0.62	0.60	0.88	1.98
66	GLOD4	ALLGYADNQCK	0.78	23	0.680	0.95	0.97	0.76	0.93	1.49	1.15	1.96
67	ALDH7A1	GEVITTYCPANNEPIAR	0.86	22	0.613	1.02	0.99	1.09	1.71	1.11	0.87	1.95
68	DCTN1	VTFSCAAGFGQR	1.15	25	0.566	1.13	1.19	0.93	0.61	0.85	0.96	1.95
69	MT2A, MT1E, MT1G, MT1X, MT1M	SCCSCCPVGCAK	1.18	24	0.274	1.54	1.02	1.13	1.00	0.82	0.80	1.93
70	MT2A, MT1G, MT1X	CAQGCICK	1.32	25	0.618	1.13	1.10	1.07	0.96	0.76	0.59	1.92
71	ERP29	GQGVYLGMPGCLPV	0.81	25	0.468	1.14	1.07	0.77	1.16	1.14	1.47	1.91

		YDALAGEFIR										
72	MACROD1	LEVDAIVNAANSSLLGGGGVDGCIHR	1.25	20	0.466	0.90	1.21	1.52	0.80	0.99	1.02	1.90
73	SPR	TVVNISSLCALQPFK	1.27	18	0.654	0.97	1.25	1.07	0.66	0.96	1.01	1.89
74	WASF2	SELECVTNITLANVIR	1.35	23	0.945	1.05	1.38	1.21	1.04	0.74	0.81	1.86
75	DOCK6	AGCALSAESSR	1.45	21	0.855	0.89	1.46	1.44	0.80	0.81	0.85	1.84
76	METAP1	VCETDGCSSEAK	1.27	19	0.629	0.96	1.19	1.43	0.79	0.92	1.04	1.82
77	MAPKAPK3	ETTQNALQTPCYTPYYVAPEVLGPEK	1.32	21	0.720	1.14	1.32	1.32	1.07	0.73	1.05	1.82
78	TPRKB	LSSQEESIGTLLDAIICR	1.37	23	0.926	1.00	1.19	1.25	0.93	0.69	0.74	1.81
79	PSMD4	SNPENNVGLITLANDCEVLTTLTPDTGR	1.23	21	0.517	0.98	1.01	1.36	0.76	0.85	0.91	1.80
80	EEF2	STLTDSLV	1.30	20	0.487	0.70	1.12	1.25	0.89	0.70	1.13	1.79

		CK										
81	LAP3	QVVDCQLADVNNIGK	1.24	21	0.386	0.90	1.03	0.99	1.04	0.58	0.94	1.79
82	SUCLG1	IICQGFTGK	1.25	19	0.524	0.82	1.45	0.94	0.81	0.89	0.95	1.79
83	CLIC1, CLIC4, CLIC6, CLIC5	IGNCPFSQR	1.35	19	0.901	1.10	1.27	1.10	0.78	0.71	1.04	1.79
84	CNP	PELQFPFLQDEDTVATLLECK	1.22	22	0.575	0.91	0.98	1.28	0.98	0.72	0.93	1.78
85	CLIC4	IEEFLEEVLCPPK	1.17	26	0.372	1.10	0.95	1.34	0.86	1.00	0.76	1.77
86	GLRX5	GTPEQPQCGFSNAVVQILR	1.21	18	0.429	0.95	1.14	1.14	0.65	0.99	0.93	1.76
87	HUWE1	DQSAQCTASK	1.25	23	0.638	0.88	1.50	1.06	1.01	0.88	0.85	1.76
88	ACAT1	QAVLGAGLPISTPCTTINK	1.28	19	0.717	1.06	1.26	1.25	0.72	0.94	1.02	1.75
89	NPEPPS	DGVCVR	1.30	19	0.846	1.00	1.26	1.12	0.72	0.83	0.98	1.75
90	ACAA1	DCLIPMGITSENVAER	1.29	19	0.659	0.97	1.48	1.28	0.85	1.00	1.06	1.75
91	MAP2K	LCDFGISG	1.30	19	0.759	0.98	1.12	1.22	0.70	0.83	1.10	1.74

	4	QLVDSIAK										
92	UPP1	CVGAELGLDCPGR	1.35	22	0.817	1.08	1.26	1.11	0.82	0.73	0.74	1.73
93	PTBP1	LSLDGQNIYNACCTLR	0.89	25	0.483	0.79	1.36	1.07	1.23	1.28	1.06	1.73
94	RASSF2	ILQGPCEQISK	0.85	18	0.716	0.85	1.01	1.47	1.33	0.89	0.98	1.72
95	FDXR	AVPTGDMEDLPCGLVLSSIGYK	0.81	18	0.527	0.88	1.03	0.93	1.39	1.26	0.81	1.72
96	EEF1A1	PMCVESFSDYPPLGR	1.24	24	0.651	1.24	1.09	1.28	1.04	0.75	0.88	1.71
97	SMAD2	AITTQNCNTK	1.25	21	0.742	0.88	1.36	1.04	0.96	0.80	0.90	1.70
98	TPX2	TVEICPFSFDSR	0.81	26	0.776	1.04	1.35	1.07	1.77	1.35	1.23	1.70
99	ERC1	TGEPCVAELTEENFQR	1.31	18	0.645	0.79	1.14	1.11	0.67	0.83	1.13	1.70
100	HSDL2	TAIHTAAMDMLGGPGIESQCR	1.18	21	0.396	0.87	1.02	1.36	0.80	0.93	0.92	1.70
101	SARS	TICAILENYQTEK	1.34	20	0.608	1.17	1.52	1.44	0.90	0.95	1.06	1.70
102	RPS12	QAHLCVLASNCD	1.32	19	0.945	1.02	1.31	1.06	0.78	0.77	1.04	1.69

		EPMYVK										
103	MAP2K3, MAP2K6	MCDFGISGYLVDSVAK	1.26	21	0.886	1.08	1.27	1.08	0.93	0.75	0.97	1.69
104	UPP1	DYPNICAGTDR	1.20	26	0.674	0.94	1.25	1.01	1.03	0.91	0.74	1.69
105	RCC2	AVQDLCGWR	1.27	21	0.698	0.85	1.43	1.19	0.98	0.86	0.99	1.68
106	UBE2O	CYNEMALIR	1.22	19	0.483	0.79	1.32	1.04	1.02	0.81	1.16	1.68
107	MLTK	ICDFGASR	1.29	21	0.933	1.05	1.36	1.18	0.95	0.81	0.93	1.68
108	NSUN2	YEPDSANPDALQCPIVLCGWR	0.88	22	0.540	0.91	1.20	1.00	1.44	1.24	0.86	1.67
109	RB1	INQMVCNSDR	1.24	21	0.827	1.07	1.35	1.06	0.95	0.81	0.97	1.67
110	PSAP	LGPGMADICK	0.81	21	0.702	0.95	0.93	0.86	1.05	1.42	0.98	1.65
111	TBC1D13	SLDDSQCGITYK	1.23	19	0.683	0.91	1.43	1.02	0.96	0.86	1.07	1.65
112	TK1	YSSSFCTHDR	0.76	22	0.869	1.04	1.44	1.71	1.48	1.38	1.21	1.64
113	PKM	CDENILWLDYK	0.84	21	0.519	1.01	0.87	1.03	0.95	1.43	1.01	1.64
114	NARS	LMTDTINEPILLCR	1.30	19	0.720	1.13	1.41	1.24	0.95	0.87	1.20	1.63

115	TIGAR	EQFSQGSPSNCLETSLAEIFPLGK	1.28	23	0.539	1.39	1.25	1.43	0.92	0.88	0.90	1.63
116	FLII	TGLCYLPEELAALQK	1.32	22	0.964	1.05	1.31	1.27	0.90	0.81	0.84	1.62
117	ACTB	CPEALFQPSFLGMESCGIHETTFNSIMK	1.24	19	0.743	1.05	1.28	1.21	0.79	0.95	0.99	1.62
118	BZW1	IQEYCYDNIHFMK	1.14	20	0.350	0.94	1.02	1.31	0.81	0.97	1.00	1.62
119	YWHAE	LICCDILDVLDK	1.11	18	0.193	1.41	1.04	1.12	0.88	0.92	1.08	1.61
120	PGM2L1	CPNPEEGESVLELSLR	1.32	19	0.792	1.20	1.19	1.22	0.78	0.76	1.07	1.61
121	GSTO1	FCPFAER	1.21	22	0.480	1.04	1.14	1.17	0.73	0.94	0.77	1.60
122	ARF5	NICFTVWDVGGQDK	1.30	19	0.897	1.07	1.33	1.21	0.89	0.83	1.15	1.60
123	HSPD1	AAVEEGIVLGGGCALLR	1.25	24	0.819	1.17	1.15	1.24	1.04	0.78	0.85	1.59
124	DUT	IAQLICER	1.21	26	0.567	0.99	1.02	1.04	1.08	0.83	0.68	1.59
125	MDH2	SQETECTYFSTPLLLG	0.85	21	0.543	0.90	0.99	0.87	1.02	1.37	1.02	1.58

		K										
126	DDX39B	HFILDECDK	1.20	18	0.601	0.88	1.13	1.12	0.95	0.83	1.31	1.58
127	ARF4	NICFTVWDVGGQDR	1.25	21	0.551	1.26	1.28	1.27	0.82	0.94	0.91	1.57
128	PABPC1, PABPC4	VVCDENGSK	1.19	23	0.574	1.02	1.24	0.93	1.03	0.79	0.80	1.57
129	CAPZB	GCWDSIHVVEVQEK	1.21	21	0.724	1.03	1.07	1.31	0.86	0.83	0.97	1.57
130	PSME2	CGFLPGNEK	1.25	18	0.874	1.09	1.22	1.14	0.78	0.89	1.08	1.56
131	MLTK	FDDLQFFENCGGGSFGSVYR	1.24	20	0.867	0.99	1.16	1.27	0.90	0.82	1.02	1.56
132	KIAA0664	CLTQQAVALQR	1.23	25	0.682	1.11	1.21	1.04	1.17	0.78	0.81	1.56
133	LGALS1	FNAHGDANTIVCNSK	1.13	18	0.659	1.18	0.92	0.86	0.76	1.01	0.91	1.56
134	ACTB	CDVDIR	0.83	18	0.586	0.86	0.94	0.96	1.18	1.31	0.85	1.55
135	FAM49B	VLTCTDLEQGPNFFLDFENAQPTESEK	1.19	21	0.565	1.06	1.14	1.22	0.79	0.96	0.89	1.55
136	MYPN, PAL	NEAGIVSCTAR	0.74	18	0.923	1.18	1.44	1.66	1.61	1.08	1.14	1.54

	LD											
137	CORIN	NVMGLVSECGEK	1.20	21	0.502	0.82	1.25	1.15	0.81	0.96	0.88	1.54
138	HNRNPH1, HNRNPH2	GLPFGCSK	1.12	18	0.632	0.96	0.98	0.70	0.92	1.08	1.07	1.54
139	AHCYL1, AHCYL2	LCVPAMNVNDSVTK	1.25	23	0.912	0.92	1.21	1.13	0.99	0.79	0.82	1.54
140	SUCLG2	IDATQVEVNPFGETPEGQVVCFDAK	1.19	20	0.681	0.98	1.06	1.17	0.94	0.77	1.10	1.53
141	SGTA	AICIDPAYSK	1.11	25	0.219	0.72	1.10	1.04	0.96	0.96	0.82	1.53
142	TRAPPC4	CELFDQNLK	1.25	20	0.751	1.01	1.16	1.04	0.76	0.78	0.93	1.53
143	HAT1	VDENFDCVEADDVEGK	1.25	24	0.741	1.25	1.22	1.20	1.00	0.84	0.82	1.52
144	CTSB	EQWPQCPTIK	1.23	24	0.657	0.90	1.03	1.11	1.04	0.73	0.77	1.52
145	PSMD9	GIGMNEPLVDCEGYPR	1.23	24	0.848	0.91	1.19	1.24	0.92	0.89	0.82	1.51
146	MDH2	TIIPLISQCTPK	1.21	23	0.683	0.89	1.19	1.34	0.91	0.93	0.91	1.51
147	TIGAR	EECPVFTPPGGE	1.27	23	0.934	1.03	1.17	1.19	0.91	0.79	0.80	1.50

		TLDQVK										
148	UPP1	IGTSGGIGLEPGTVVITEQAVDTCFK	1.28	21	0.914	1.01	1.20	1.20	0.81	0.80	0.91	1.50
149	TBC1D13	LLQDYPITDVCQILQK	1.25	21	0.850	1.11	1.23	1.12	0.84	0.82	0.88	1.50
150	DPYSL2	FQLTDCQIYEVLSVIR	1.21	26	0.849	0.98	1.27	1.12	1.12	0.86	0.87	1.49
151	CCT7	QLCDNAGFDATNILNK	1.16	19	0.363	1.20	1.34	1.13	0.90	1.05	0.97	1.49
152	PPFIBP1	INNFEPNCLR	1.25	18	0.887	1.03	1.16	1.19	0.80	0.87	1.17	1.49
153	CLIC4	AGSDGESIGNCPFSQR	1.21	20	0.722	1.08	1.18	1.27	0.96	0.86	1.07	1.49
154	FHL2	DNQNFCVPCYEK	1.26	18	0.886	0.89	1.19	1.11	0.81	0.85	1.18	1.48
155	RPL27A	NQSFCPTVNLDK	1.15	18	0.543	0.98	1.25	0.94	1.01	0.85	1.12	1.47
156	TLE3	SPISQLDCLNR	1.07	19	0.131	0.79	1.02	1.16	0.89	1.00	1.01	1.47
157	MECR	LALNCVGGK	1.18	19	0.481	0.88	1.24	1.28	0.87	1.02	1.03	1.47
158	SKP1	ENQWCEEK	1.17	24	0.759	1.00	1.18	1.02	0.96	0.87	0.80	1.47

159	SART1	SLPSAVYCIEDK	1.18	22	0.693	1.10	1.29	1.05	0.90	0.91	0.88	1.47
160	CSTF2, CSTF2T	GYGFCEYQDQETALSAMR	0.93	24	0.460	0.92	1.02	1.03	1.15	1.32	0.90	1.47
161	HSP90AB1	LVSSPCCIVTSTYGWTANMER	1.08	24	0.473	1.04	1.07	0.98	0.73	0.98	0.96	1.47
162	SFN	GEELSCEER	1.23	23	0.804	1.07	1.09	1.15	0.89	0.80	0.79	1.46
163	ACTN1, ACTN4	EGLLLWCQR	0.81	23	0.842	1.13	0.88	0.84	1.10	1.23	1.20	1.46
164	TKT	QAFTDVATGSLGQGLGAACGMAYTGK	1.14	21	0.453	1.03	0.96	1.22	0.83	0.87	0.92	1.46
165	P4HB	EECPAVR	0.86	18	0.540	0.88	0.95	1.03	1.14	1.20	0.82	1.46
166	DSTN	CSTPEEIK	1.15	25	0.682	0.97	1.19	0.99	1.03	0.89	0.82	1.46
167	PRKAA2, PRKAA1	TSCGSPNYAAPEVISGR	1.15	22	0.905	0.98	0.99	0.84	0.71	0.85	1.04	1.46
168	GRPEL1	LYGIQAFCK	1.12	20	0.675	0.94	1.00	0.88	0.70	1.01	1.02	1.46
169	PPM1G	GTEAGQVGEPGIPTGEAGP	1.15	18	0.587	1.01	1.13	1.04	1.00	0.86	1.25	1.46

		SCSSASDK										
170	PPP1CC, PPP1CA, PPP1CB	TFTDCFNCLPIAAIVDEK	0.86	19	0.493	0.88	0.99	0.90	1.27	1.19	1.01	1.45
171	ATP6V1G1	GSCSTEVEK	1.14	26	0.706	0.99	1.22	1.03	1.03	0.96	0.85	1.45
172	GSTO1	LNECVDHTPK	1.19	24	0.730	0.95	1.14	1.03	1.07	0.79	0.81	1.44
173	CCT4	TLSGMESYCVR	1.18	20	0.651	0.96	1.13	1.10	0.78	0.91	0.93	1.44
174	VAT1	ACGLNFADLMAR	0.81	26	0.937	1.09	1.14	1.32	1.56	1.29	1.30	1.44
175	GAPDH	IISNASCTTNCLAPLAK	1.20	21	0.800	0.89	1.11	1.16	0.89	0.81	0.94	1.43
176	DPYSL2	GLYDGPVCEVSVTPK	1.19	21	0.791	1.12	1.13	1.15	0.95	0.81	1.01	1.42
177	OTUB1	QEPLGSDSEGVNCLAYDEAIMAQQDR	1.19	23	0.927	1.05	1.24	1.13	0.97	0.87	0.89	1.42
178	PGP	NNQESDCVSK	1.19	23	0.698	1.12	1.09	1.06	0.95	0.79	0.81	1.42
179	TRNT1	YQGEHCLLK	1.16	19	0.587	1.03	1.16	1.28	0.91	0.97	1.06	1.41
180	NTMT1	IICSAGLSLLAEE	1.21	18	0.784	1.14	1.14	1.15	0.83	0.88	1.14	1.39

		R										
181	HMGB1, HMGB2	MSSYAFFVQTCR	1.09	23	0.673	1.17	1.00	0.86	0.86	0.84	1.03	1.39
182	FLNB	SSTETCYSAIPK	1.17	18	0.671	0.98	1.25	1.05	1.01	0.91	1.20	1.38
183	ABL1	ELQICPATAGSGPAATQDFSK	1.17	18	0.560	1.13	1.31	1.10	1.01	0.95	1.16	1.38
184	TCP1	SLHDALCVVK	1.18	18	0.773	1.03	1.18	1.20	0.87	0.96	1.11	1.38
185	LAP3	SAGACTAAAFLK	1.15	23	0.768	0.96	1.08	1.12	1.06	0.81	0.93	1.38
186	EEF1G	AAAPAPEEEMDECEQALAAEPK	1.18	19	0.950	0.97	1.22	1.08	0.89	0.90	1.05	1.37
187	YWHAQ	DNLTLWTSDSAGEECDAAEGAEN	1.17	18	0.662	1.09	1.11	1.14	0.93	0.90	1.24	1.37
188	UROD	AAQDFFSTCR	1.12	22	0.380	1.20	1.15	1.05	0.89	0.97	0.88	1.37
189	CSRP1	SCFLCMVCK	1.11	19	0.380	1.05	1.09	1.10	0.81	1.01	0.94	1.36
190	ACTB, POTEE	LCYVALDFEQEMATAASSSSLEK	0.89	25	0.538	0.86	0.96	0.86	0.94	1.16	1.08	1.35

191	SF3B5	MLQPCGPPADK	1.11	20	0.438	1.17	1.06	1.09	0.99	0.87	1.07	1.35
192	MGEA5	ANSSVVSVNCK	1.18	19	0.744	1.04	1.06	1.06	0.85	0.79	1.03	1.35
193	DDX19A, DDX19B	VLVTTNVCAR	1.06	24	0.410	0.91	1.05	1.00	0.79	0.98	0.96	1.34
194	SSBP3	DTCEHSSEAK	1.08	23	0.338	0.87	1.16	1.03	1.05	0.94	0.98	1.34
195	OLA1	STFFNVLTNSQASAENFPFCTIDPNESR	1.11	25	0.530	1.08	1.08	1.05	0.92	0.96	0.81	1.34
196	HSPA4	SVMDATQIAGLNCLR	1.07	22	0.149	1.18	1.06	1.16	0.88	1.06	0.94	1.34
197	PIN1	SGEEDFESLASQFSDCSSAK	1.17	19	0.567	1.16	1.17	1.16	0.98	0.88	1.16	1.33
198	BLVRB	CLTTDEYDGHSTYPSHQYQ	1.08	18	0.226	0.99	1.12	0.89	1.05	0.84	1.11	1.33
199	GDI1, GDI2	NTNDANSCQIIIPQNQVNR	1.16	18	0.690	1.08	1.09	0.97	0.83	0.84	1.09	1.32
200	CAPZB	DETVSDCSPHIANIGR	1.14	19	0.790	1.06	1.17	0.98	0.89	0.89	1.03	1.31
201	TRMT112	ICPVEFNPNFVA	1.13	18	0.822	0.98	1.16	1.10	0.88	0.98	1.05	1.31

		R										
202	TLN1	MVAAATNNLCEAANAAVQGHASQEK	0.91	19	0.733	1.10	1.02	1.29	1.10	1.08	0.98	1.31
203	PYCR1	CMTNTPVVVR	1.13	23	0.692	1.13	1.13	1.08	0.95	0.92	0.88	1.28
204	PSME1	EDLCTK	1.16	23	0.814	1.11	1.15	1.16	0.96	0.91	0.91	1.28
205	OAT	VLPMNTGVEAGETACK	1.14	21	0.470	0.86	1.08	1.05	0.85	0.90	0.88	1.28
206	YWHAQ	YLAEVACGDDR	1.13	20	0.635	1.08	1.13	1.17	0.99	0.92	1.07	1.28
207	EIF3M	VAASCGAIQYIPTELDQVR	1.14	23	0.897	1.05	1.16	1.14	0.96	0.92	0.91	1.27
208	DSTN	LGGSLIVAFEGCPV	1.14	19	0.872	1.01	1.18	1.09	0.94	0.94	1.06	1.27
209	CCT8	IAVYSCPFDGMITETK	1.14	19	0.754	1.12	1.16	1.08	0.92	0.92	1.03	1.26
210	PSMA4	ATCIGNNSAAAVSMLK	0.91	25	0.904	1.00	1.02	1.07	1.26	1.20	1.03	1.26
211	YWHAZ	YDDMAACMK	0.91	21	0.614	0.98	1.00	0.89	1.11	1.12	1.03	1.25
212	PPIA	IIPGFMCQ	0.92	21	0.599	1.08	0.98	0.93	1.03	1.16	1.00	1.24

		GGDFTR										
213	ALDH7A1	STCTINYSK	1.07	19	0.324	1.08	1.09	1.00	0.88	1.00	0.95	1.24
214	TCEB1	VCMYFTYK	1.09	24	0.442	0.79	0.93	0.91	0.79	0.97	0.89	1.24
215	RBM22	NVCQTCLLDLEYGLPIQVR	1.13	20	0.780	1.07	1.09	1.07	0.88	0.89	0.96	1.23
216	HSP90AB1	VFIMDSCDELIPEYLNFIR	1.10	22	0.778	1.00	1.06	1.13	0.93	0.94	0.93	1.22
217	TAGLN2	DGTVLCELINALYPEGQAPVK	1.03	22	0.336	1.09	0.97	0.99	0.90	1.01	0.97	1.22
218	YWHAQ	YDDMATCMK	0.89	20	0.820	0.93	0.91	0.94	1.11	1.11	0.99	1.22
219	PPIA	ITIADCGQLE	0.92	25	0.915	1.02	0.98	1.13	1.18	1.19	1.03	1.22
220	TPI1	IIYGGSVTGATCK	0.93	22	0.813	1.03	0.96	1.17	1.13	1.08	1.00	1.22
221	FKBP4	TQLAVCQQR	0.97	18	0.087	1.14	0.94	1.02	1.00	1.01	0.99	1.21
222	GSTM3	YTCGEAPDYDR	1.06	18	0.432	0.98	1.04	1.03	1.01	0.92	1.11	1.21
223	HSD17B10	LGNNCVFAPADVTSEK	1.09	19	0.385	0.87	1.04	1.00	0.88	0.91	1.00	1.20
224	CLIC1	FLDGNELT	1.06	26	0.523	0.88	0.95	0.93	0.95	0.84	0.99	1.18

		LADCNLLPK									
225	TPI1	VPADTEVVCAPPTAYIDFAR	0.95	23	0.379	1.19	1.01	1.16	1.05	1.08	1.04	1.17
226	MIF	LLCGLLAER	1.05	18	0.950	1.02	0.97	0.92	0.92	1.00	0.98	1.11
227	ARPC2	NCFASVFEK	0.96	24	0.509	1.07	1.11	1.03	1.07	1.09	1.01	1.10
228	PFN1	CYEMASHLR	1.04	18	0.811	1.01	0.92	0.94	0.94	0.97	0.98	1.09
229	ACTN4, ACTN1	ELPPDQAEYCIAR	0.94	25	0.879	1.04	1.04	1.14	1.10	1.10	1.06	1.09

Table 5A-1 Tryptic digests of MCF-7 lysates treated with DMSO or SMC1 (5μM).After sorting tryptic data by MW, analysis was focused on proteins less than 40 kDa, corresponding to the molecular weight of the protein band fluorescently labeled in SMC1 treated MCF7 lysates. GSTO1 (highlighted in blue) showed the most specific enrichment in the SMC1 treated samples with respect to the DMSO treated sample (control).

		DMSO		SMC1 (5 μM)	
Protein	MW (Da)	1	2	1	2
IPI00788737 - Gene_Symbol=GAPDH 39 kDa	38791	31	146	23	56
IPI00329801 - Gene_Symbol=ANXA5 Annexin	35937	3	22	12	14
IPI00291006 - Gene_Symbol=MDH2 Malate dehydrogenase, mitochondrial precursor	35531	38	27	25	14
IPI00604590 - Gene_Symbol=NME1;NME2 Nucleoside diphosphate kinase	32642	37	24	34	37
IPI00465028 - Gene_Symbol=TPI1 Isoform 1 of Triosephosphate isomerase	30791	14	19	15	36
IPI00021263 - Gene_Symbol=YWHAZ 14-3-3 protein zeta/delta	27745	14	46	19	15
IPI00019755 - Gene_Symbol=GSTO1 Glutathione transferase omega-1	27566	0	0	131	46
IPI00419258 - Gene_Symbol=HMGB1 High mobility group protein B1	24894	3	31	11	68
IPI00784459 - Gene_Symbol=CFL1 Uncharacterized protein CFL1	24041	2	30	16	111
IPI00025512 - Gene_Symbol=HSPB1 Heat shock protein beta-1	22783	15	41	28	27
IPI00007427 - Gene_Symbol=AGR2 AGR2	22238	10	20	19	17

IPI00335132 - Gene_Symbol=- 22 kDa protein	22066	3	31	11	68
IPI00028618 - Gene_Symbol=MGMT Methylated-DNA--protein-cysteine methyltransferase	21646	0	0	79	38
IPI00419585 - Gene_Symbol=PPIA;LOC654188;PPIAL3 Peptidyl-prolyl cis-trans isomerase A	18012	52	75	66	62
IPI00291764 - Gene_Symbol=HIST1H2AI;HIST1H2AJ;HIST1H2AM;HIST1H2AL;HIST1H2AK;HIST1H2AG Histone H2A type 1	14091	24	44	12	16

Table 5A-2 Tryptic digests of HeLa and MCF-7 lysates treated with DMSO or SMC8/SMC9 (5μM). After sorting tryptic data by MW, analysis was focused on proteins between 66 and 48kDa, corresponding to the molecular weight of the protein bands fluorescently labeled in SMC8 and SMC9 treated MCF7 lysates.

		HeLa						MCF7					
		DMSO		SMC9		SMC8		DMSO		SMC9		SMC8	
Protein	MW (Da)	1	2	1	2	1	2	1	2	1	2	1	2
IPI00639957 - Gene_Symbol= CARM1 coactivator-associated arginine methyltransferase 1	65854	0	0	3	6	5	7	0	0	3	4	5	4
IPI00554737 - Gene_Symbol= PPP2R1A Serine/threonine-protein phosphatase 2A 65 kDa regulatory subunit A alpha isoform	65309	10	0	15	11	34	19	22	3	23	22	31	19
IPI00220299 - Gene_Symbol= FLAD1 Isoform 1 of FAD synthetase	65266	0	0	9	0	4	0	0	0	11	9	5	4
IPI00289499 - Gene_Symbol= ATIC Bifunctional purine biosynthesis protein PURH	64616	6	0	8	0	13	4	47	7	62	11	70	19

IPI00554777 - Gene_Symbol= ASNS Asparagine synthetase	64370	16	4	155	173	87	52	16	3	195	223	70	74
IPI00641635 - Gene_Symbol= FTO 64 kDa protein	64336	0	0	0	6	5	0	0	0	4	5	2	4
IPI00294943 - Gene_Symbol= ARIH1 Protein ariadne-1 homolog	64118	0	0	0	0	2	0	5	0	4	0	2	0
IPI00006181 - Gene_Symbol= EIF3D Eukaryotic translation initiation factor 3 subunit 7	63973	0	0	2	0	0	0	7	0	6	0	5	0
IPI00216008 - Gene_Symbol= G6PD Isoform Long of Glucose-6-phosphate 1-dehydrogenase	63827	0	0	0	3	0	0	48	5	44	8	53	8
IPI00027497 - Gene_Symbol= GPI Glucose-6-phosphate isomerase	63147	3	0	0	3	2	0	49	0	26	9	50	5
IPI00306960 - Gene_Symbol= NARS Asparaginyl-tRNA synthetase, cytoplasmic	62943	0	0	0	0	0	0	5	0	10	0	14	5
IPI00257508 - Gene_Symbol= DPYSL2 Dihydropyrimidinase-related protein 2	62294	0	0	0	3	0	2	4	0	2	0	2	0

IPI00103026 - Gene_Symbol= PRMT3 PRMT3 protein (Fragment)	619 67	0	0	4	0	3	0	0	0	2	0	0	0
IPI00219649 - Gene_Symbol= CBS Isoform 2 of Cystathionine beta-synthase	618 63	0	0	4	0	0	0	27	0	16	0	31	5
IPI00549569 - Gene_Symbol=I SYNA1 Myo-inositol 1-phosphate synthase A1	610 68	0	0	4	0	7	0	0	0	2	0	3	0
IPI00011603 - Gene_Symbol= PSMD3 26S proteasome non-ATPase regulatory subunit 3	609 78	0	0	4	0	0	0	5	0	6	0	5	0
IPI00009662 - Gene_Symbol= NT5DC2 Isoform 1 of 5'-nucleotidase domain-containing protein 2	607 19	2	0	15	12	12	7	0	0	5	6	6	7
IPI00553185 - Gene_Symbol= CCT3 T-complex protein 1 subunit gamma	605 34	6	0	9	4	7	5	3	0	5	0	3	2

IPI00386448 - Gene_Symbol= RELA Isoform 1 of Transcription factor p65	602 19	0	0	3	0	2	0	0	0	3	2	0	3
IPI00030116 - Gene_Symbol= PGM3 Isoform 1 of Phosphoacetylglucosamine mutase	598 52	2	0	3	0	3	0	0	0	4	6	4	2
IPI00302925 - Gene_Symbol= CCT8 Uncharacterized protein CCT8	597 79	7	8	8	10	12	16	3	0	7	0	5	3
IPI00010720 - Gene_Symbol= CCT5 T-complex protein 1 subunit epsilon	596 71	4	0	4	5	6	0	7	2	9	0	8	3
IPI00018465 - Gene_Symbol= CCT7 T-complex protein 1 subunit eta	593 67	8	4	5	3	6	20	4	2	5	0	7	2
IPI00018402 - Gene_Symbol= TBCE Tubulin-specific chaperone	593 46	0	0	10	2	10	7	3	0	8	4	9	5

IPI00006167 - Gene_Symbol= PPM1G Protein phosphatase 1G	59272	2	2	7	5	4	0	3	0	8	3	6	0
IPI00007074 - Gene_Symbol= YARS Tyrosyl-tRNA synthetase, cytoplasmic	59144	0	0	4	0	2	0	6	0	9	0	9	0
IPI00026105 - Gene_Symbol= SCP2 Isoform SCPx of Nonspecific lipid-transfer protein	58994	5	0	19	11	16	21	0	0	8	18	10	8
IPI00182938 - Gene_Symbol= AHCYL1 Isoform 1 of Putative adenosylhomocysteinase 2	58951	0	0	2	0	0	0	0	0	3	0	4	0
IPI00029764 - Gene_Symbol= SF3A3 Splicing factor 3A subunit 3	58849	2	0	2	0	0	0	0	0	2	0	3	2

IPI00828081 - Gene_Symbol= CAMK2D Isoform Delta 4 of Calcium/calmodulin-dependent protein kinase type II delta chain	58344	0	0	2	0	0	0	0	0	5	0	0	2
IPI00007247 - Gene_Symbol= PCCB Propionyl-CoA carboxylase beta chain, mitochondrial precursor	58216	27	38	10	25	13	49	6	34	11	22	7	31
IPI00783061 - Gene_Symbol= PKM2 Uncharacterized protein PKM2	58066	37	17	46	53	86	102	92	33	96	113	202	92
IPI00302927 - Gene_Symbol= CCT4 T-complex protein 1 subunit delta	57924	2	3	6	7	6	2	5	0	5	0	2	0
IPI00002214 - Gene_Symbol= KPNA2 Importin subunit alpha-2	57862	4	0	8	10	9	17	3	0	5	0	0	0
IPI00299033 - Gene_Symbol= KPNA3 Importin subunit alpha-3	57811	0	0	0	0	2	0	2	0	6	0	5	0

IPI00790937 - Gene_Symbol= NMD3 Protein NMD3 homolog	57603	0	0	0	0	0	0	18	0	11	6	16	7
IPI00297779 - Gene_Symbol= CCT2 T-complex protein 1 subunit beta	57488	7	0	13	7	9	0	8	0	7	2	11	0
IPI00021808 - Gene_Symbol= HARS Histidyl-tRNA synthetase, cytoplasmic	57411	0	0	2	5	5	0	6	0	7	10	7	4
IPI00029534 - Gene_Symbol= PPAT Amidophosphoribosyltransferase precursor	57399	0	0	0	3	0	0	0	0	3	0	0	0
IPI00103467 - Gene_Symbol= ALDH1B1 Aldehyde dehydrogenase X, mitochondrial precursor	57238	6	4	14	4	5	4	0	0	8	4	4	0
IPI00010796 - Gene_Symbol= P4HB Protein disulfide-isomerase precursor	57116	15	2	97	198	18	8	111	3	573	802	161	99

IPI00306127 - Gene_Symbol= THUMPD3 THUMP domain-containing protein 3	57003	0	0	0	0	2	0	0	0	5	0	4	0
IPI00019812 - Gene_Symbol= PPP5C Serine/threonine -protein phosphatase 5	56879	0	0	4	0	0	0	3	0	10	0	6	0
IPI00025252 - Gene_Symbol= PDIA3 Protein disulfide-isomerase A3 precursor	56782	3	0	7	3	2	4	26	2	24	7	36	8
IPI00011200 - Gene_Symbol= PHGDH D-3-phosphoglycerate dehydrogenase	56651	18	5	31	31	33	59	9	4	14	16	17	23
IPI00220566 - Gene_Symbol= TXNRD2 Isoform 1 of Thioredoxin reductase 2, mitochondrial precursor	56460	0	0	10	10	86	69	0	0	14	9	11	14

IPI00329629 - Gene_Symbol= DNAJC7 DnaJ homolog subfamily C member 7	56441	2	0	9	5	7	13	0	0	8	0	3	6
IPI00479877 - Gene_Symbol= ALDH9A1 aldehyde dehydrogenase 9A1	56292	2	0	6	4	10	36	3	0	2	0	7	7
IPI00016862 - Gene_Symbol= GSR Isoform Mitochondrial of Glutathione reductase, mitochondrial precursor	56257	0	0	4	0	0	11	16	0	16	8	19	8
IPI00011237 - Gene_Symbol= NARF Isoform 2 of Nuclear prelamin A recognition factor	56141	0	0	3	2	0	0	0	0	5	3	0	2
IPI00465044 - Gene_Symbol= RCC2 Protein RCC2	56085	3	0	6	5	3	8	21	3	28	12	29	5
IPI00556027 - Gene_Symbol= BAG5 BCL2-associated athanogene 5 isoform a	56027	0	0	3	0	0	0	0	0	9	6	8	9

IPI00002520 - Gene_Symbol= SHMT2 Serine hydroxymethyltransferase, mitochondrial precursor	55993	7	0	10	3	5	8	11	3	15	4	15	6
IPI00291510 - Gene_Symbol=IMPDH2 Inosine-5'-monophosphate dehydrogenase 2	55805	3	0	10	10	4	0	0	0	0	5	2	0
IPI00746278 - Gene_Symbol= STX16 56 kDa protein	55774	0	0	0	0	0	0	4	0	19	39	11	14
IPI00012870 - Gene_Symbol= AKT2 RAC-beta serine/threonine -protein kinase	55769	0	0	2	0	7	0	0	0	13	28	32	42
IPI00012866 - Gene_Symbol= AKT1 RAC-alpha serine/threonine -protein kinase	55686	0	0	2	0	11	20	4	0	29	76	60	110
IPI00787501 - Gene_Symbol= LOC727737 similar to APG4 autophagy 4 homolog B isoform b	55446	0	0	11	2	9	0	0	0	8	4	7	8

IPI00004968 - Gene_Symbol= PRPF19 Pre-mRNA-processing factor 19	55181	0	0	2	0	0	0	8	0	2	0	7	0
IPI00013774 - Gene_Symbol= HDAC1 Histone deacetylase 1	55103	0	0	5	2	5	0	4	0	7	11	9	5
IPI00031420 - Gene_Symbol= UGDH UDP-glucose 6-dehydrogenase	55024	0	0	0	0	0	0	105	19	92	61	108	30
IPI00007102 - Gene_Symbol= GLOD4 Uncharacterized protein C17orf25	55012	3	3	6	4	5	0	0	0	3	4	3	8
IPI00747810 - Gene_Symbol= FSCN1 Uncharacterized protein FSCN1 E	54640	0	0	2	2	0	2	2	0	3	0	4	0
IPI00749487 - Gene_Symbol= PMPCB 55 kDa protein	54524	0	0	5	0	0	0	0	0	8	12	8	4
IPI00304596 - Gene_Symbol= NONO Non-POU domain-containing octamer-binding protein	54232	2	0	0	0	4	9	3	0	6	11	17	12

IPI00015911 - Gene_Symbol= DLD Dihydrolipoyl dehydrogenase, mitochondrial precursor	54150	3	0	6	0	0	2	7	0	15	2	11	3
IPI00019918 - Gene_Symbol= DDX19A ATP-dependent RNA helicase DDX19A	53975	2	0	2	0	4	0	5	0	3	0	2	0
IPI00793953 - Gene_Symbol= TUBA8 Putative uncharacterized protein DKFZp686L04275 (Fragment)	53969	0	30	124	251	175	0	19	0	20	0	35	25
IPI00299571 - Gene_Symbol= PDIA6 Isoform 2 of Protein disulfide-isomerase A6 precursor	53901	6	2	14	24	11	10	22	5	53	17	27	22
IPI00003606 - Gene_Symbol= RNF14 E3 ubiquitin-protein ligase RNF14	53837	0	0	3	0	44	51	0	0	2	0	17	24
IPI00001636 - Gene_Symbol= ATXN10 Ataxin-10	53489	7	0	8	7	16	15	0	0	5	0	2	0

IPI00747533 - Gene_Symbol= PGD Uncharacterized protein PGD	53339	2	0	4	4	0	0	33	4	22	2	48	6
IPI00220906 - Gene_Symbol= ACOT2 Isoform 1 of Acyl-coenzyme A thioesterase 2, mitochondrial precursor	53257	0	0	3	0	2	0	0	0	3	5	0	0
IPI00008453 - Gene_Symbol= CORO1C Coronin-1C	53249	0	0	0	4	0	0	13	0	9	0	11	2
IPI00165092 - Gene_Symbol= YARS2 Tyrosyl-tRNA synthetase, mitochondrial precursor	53199	0	0	5	2	0	0	0	0	5	3	0	0
IPI00295400 - Gene_Symbol= WARS Tryptophanyl-tRNA synthetase, cytoplasmic	53165	0	0	0	0	2	0	13	0	14	4	21	6
IPI00745729 - Gene_Symbol= SELENBP1 Uncharacterized protein SELENBP1	53062	0	0	0	0	0	0	2	0	6	8	12	12
IPI00550852 - Gene_Symbol= DCTN4 Dynactin subunit 4	52337	0	0	3	0	12	11	0	0	2	0	0	5

IPI00646512 - Gene_Symbol= RBBP7 Retinoblastoma binding protein 7	523 14	3	2	5	10	3	15	7	0	6	0	11	0
IPI00177965 - Gene_Symbol= NT5DC1 5'-nucleotidase domain-containing protein 1	518 45	0	0	3	6	6	2	2	0	10	2	8	3
IPI00219005 - Gene_Symbol= FKBP4 FK506-binding protein 4	518 05	4	0	5	2	0	0	41	4	23	6	45	10
IPI00479191 - Gene_Symbol= HNRPH1 HNRPH1 protein	512 30	6	0	28	31	28	25	9	0	24	3	15	7
IPI00002270 - Gene_Symbol= C6orf211 UPF0364 protein C6orf211	511 72	0	0	0	0	0	0	27	0	18	4	32	7
IPI00009104 - Gene_Symbol= RUVBL2 RuvB-like 2	511 57	2	0	3	0	3	3	0	0	3	0	2	0
IPI00297982 - Gene_Symbol= EIF2S3 Eukaryotic translation initiation factor 2 subunit 3	511 10	0	0	4	0	2	0	2	0	5	9	3	4

IPI00216746 - Gene_Symbol= HNRPK Isoform 2 of Heterogeneous nuclear ribonucleoprotein K	51028	10	7	26	23	30	15	13	3	23	42	14	15
IPI00011107 - Gene_Symbol=IDH2 Isocitrate dehydrogenase [NADP], mitochondrial precursor	50909	2	0	0	0	0	3	39	3	37	4	46	6
IPI00291570 - Gene_Symbol= CASP2 Isoform ICH-1L of Caspase-2 precursor	50685	0	0	7	0	3	0	0	0	2	7	2	0
IPI00031461 - Gene_Symbol= GDI2 Rab GDP dissociation inhibitor beta	50663	4	6	5	0	8	0	49	7	36	6	53	12
IPI00010154 - Gene_Symbol= GDI1 Rab GDP dissociation inhibitor alpha	50583	5	7	7	5	9	8	25	8	26	7	35	12
IPI00014424 - Gene_Symbol= EEF1A2 Elongation factor 1-alpha 2	50470	0	11	0	0	0	0	128	12	96	71	71	19
IPI00021187 - Gene_Symbol= RUVBL1 Isoform 1 of RuvB-like 1	50228	2	0	7	4	7	0	0	3	6	0	4	2

IPI00472724 - Gene_Symbol=- Elongation factor 1-alpha	50185	51	11	366	142	158	85	125	10	163	38	126	0
IPI00093057 - Gene_Symbol=CPOX Coproporphyrinogen III oxidase, mitochondrial precursor	50152	2	0	6	0	4	0	0	0	2	0	0	0
IPI00396485 - Gene_Symbol=EEF1A1 Elongation factor 1-alpha	50141	51	11	366	142	158	85	125	10	163	38	126	0
IPI00000875 - Gene_Symbol=EEF1G Elongation factor 1-gamma	50119	8	5	26	75	24	61	219	2	179	10	128	16
IPI00026833 - Gene_Symbol=ADSS Adenylosuccinate synthetase isozyme 2	50097	3	0	4	5	11	0	0	0	4	3	8	4
IPI00550069 - Gene_Symbol=RNH1 Ribonuclease inhibitor	49974	5	0	4	6	4	9	23	2	20	15	20	15
IPI00297261 - Gene_Symbol=PTPN1 Tyrosine-protein phosphatase non-receptor type 1	49967	0	0	0	0	0	0	13	0	15	5	23	7

IPI00027107 - Gene_Symbol= TUFM Tu translation elongation factor, mitochondrial	49875	5	8	5	21	7	29	0	0	3	2	0	5
IPI00549993 - Gene_Symbol= C10orf97 chromosome 10 open reading frame 97	49725	4	0	15	15	0	0	0	0	5	9	0	0
IPI00217223 - Gene_Symbol= PAICS Multifunctional protein ADE2	49679	7	8	10	43	44	25	12	0	12	18	19	14
IPI00174849 - Gene_Symbol=- Uncharacterized protein	49573	22	0	101	56	55	140	0	0	0	0	0	0
IPI00024719 - Gene_Symbol= HAT1 Histone acetyltransferase type B catalytic subunit	49513	7	0	10	6	12	11	0	0	5	5	5	4
IPI00026230 - Gene_Symbol= HNRPH2 Heterogeneous nuclear ribonucleoprotein H'	49264	2	0	20	0	0	0	0	0	13	3	6	4
IPI00018398 - Gene_Symbol= PSMC3 26S protease regulatory subunit 6A	49204	4	0	2	0	0	0	8	0	3	0	9	2

IPI00644431 - Gene_Symbol= DDX39 ATP-dependent RNA helicase DDX39	49130	5	5	4	5	4	0	16	0	24	6	19	4
IPI00101968 - Gene_Symbol= DBNL Isoform 3 of Drebrin-like protein	49042	0	0	0	0	2	0	0	0	3	0	5	0
IPI00848161 - Gene_Symbol= ATP6V1G2;BAT1 Isoform 1 of Spliceosome RNA helicase BAT1	48991	5	0	4	5	4	0	23	4	23	7	24	3

Appendix II

Representative NMR Spectra

pent-4-yn-1-yl 4-methylbenzenesulfonate (Compound 1)

^{1}H-NMR

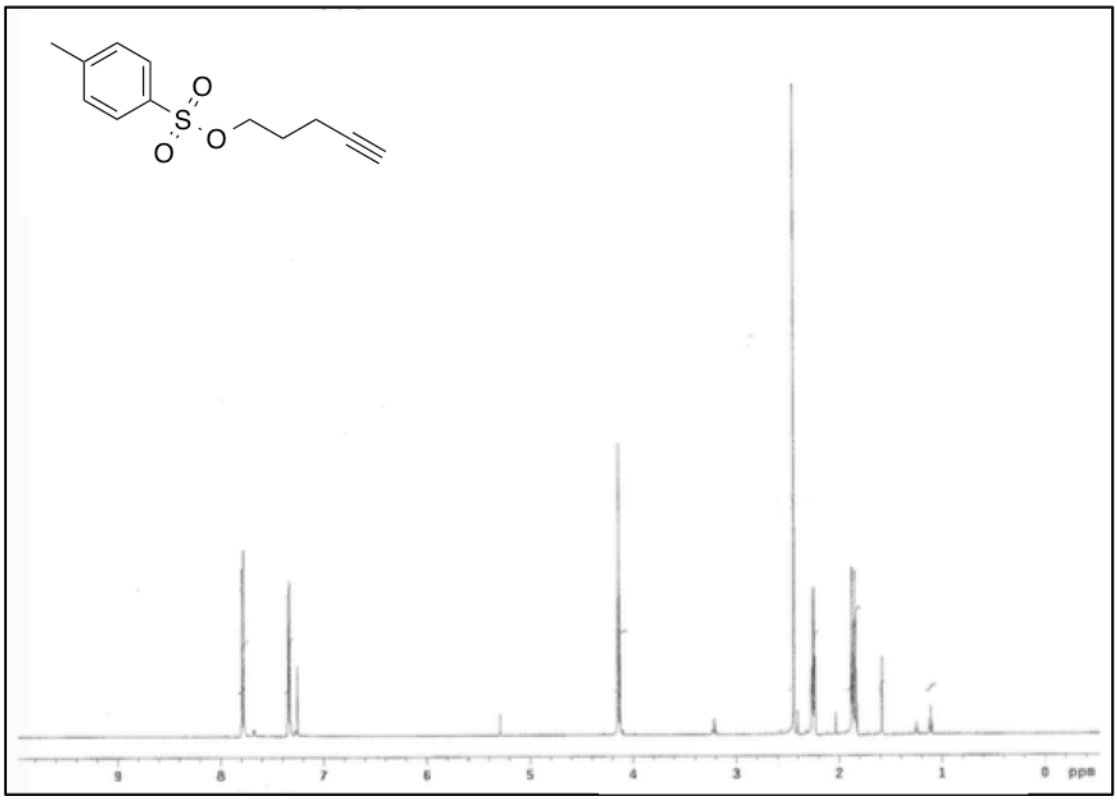

^{13}C-NMR

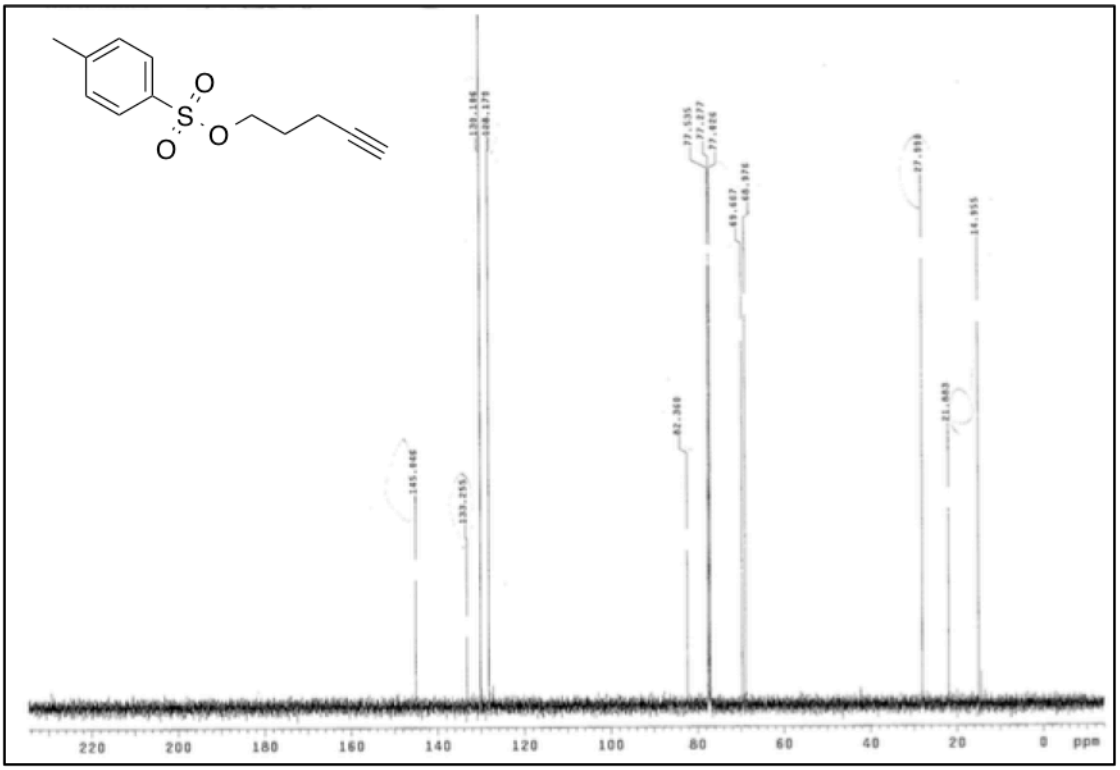

8-(pent-4-yn-1-yl)-1,4-dioxa-8-azaspiro[4.5]decane (Compound 2)

^{1}H-NMR

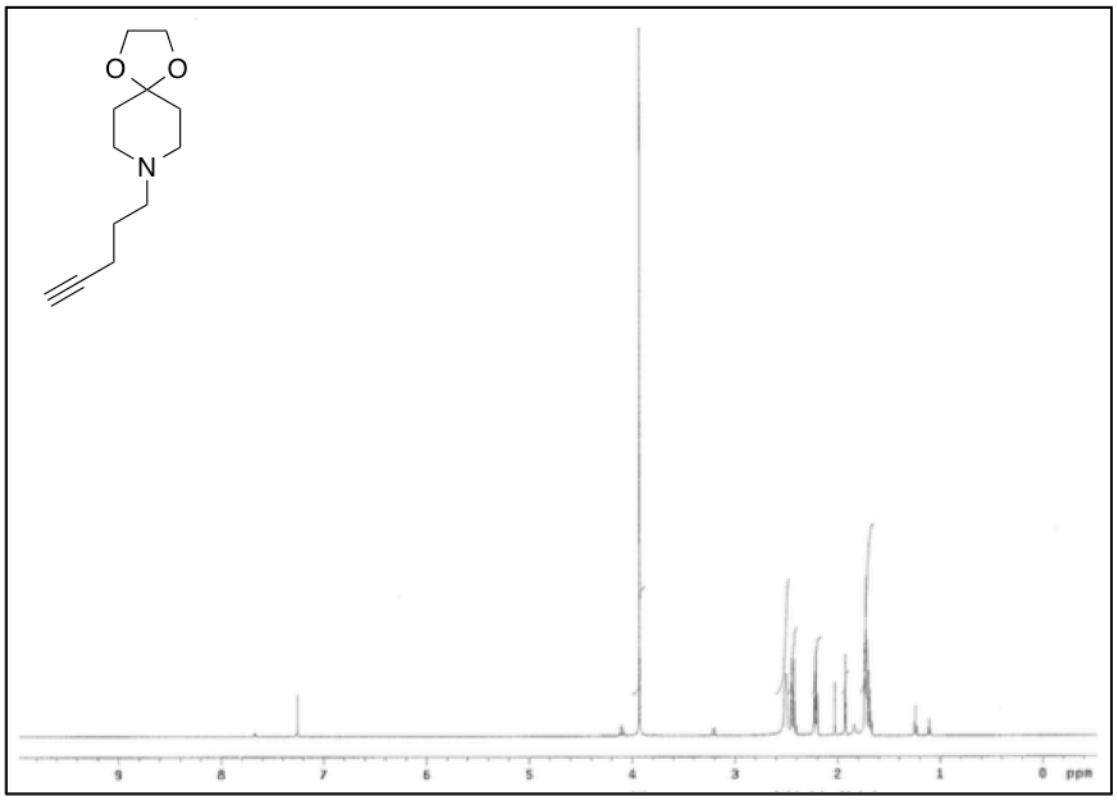

^{13}C-NMR

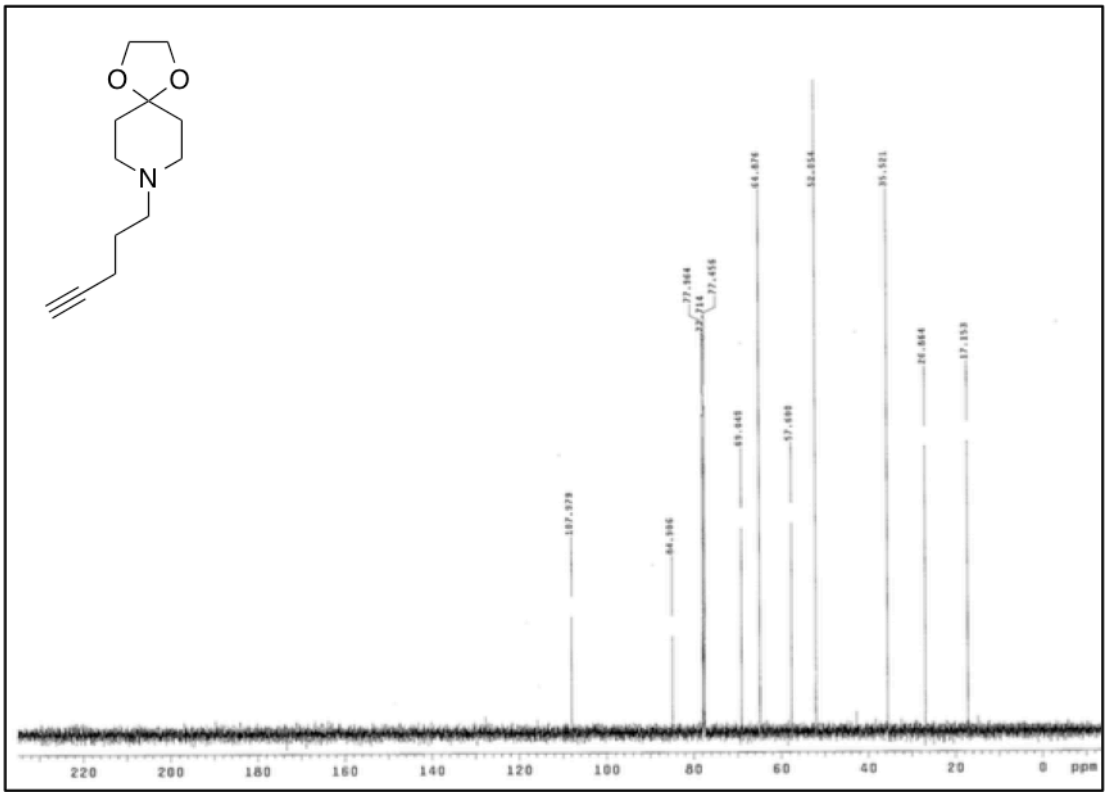

1-(pent-4-yn-1-yl)piperidin-4-one (Compound 3)

^{1}H-NMR

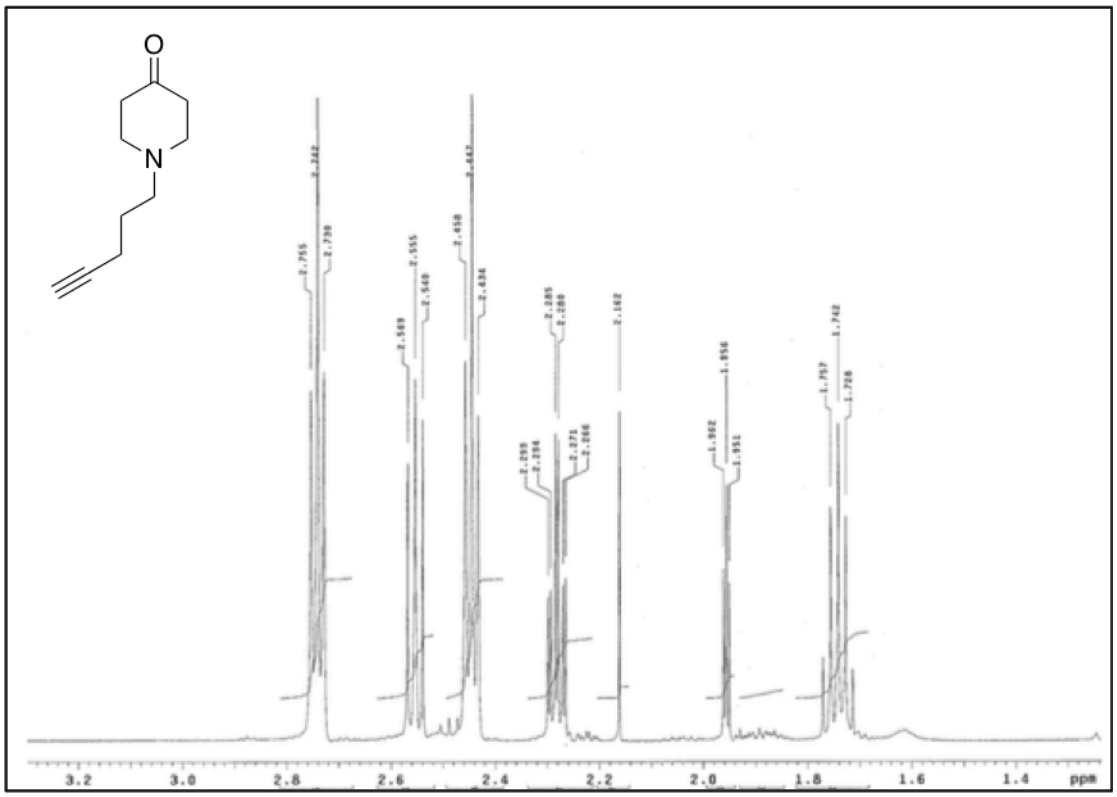

^{13}C-NMR

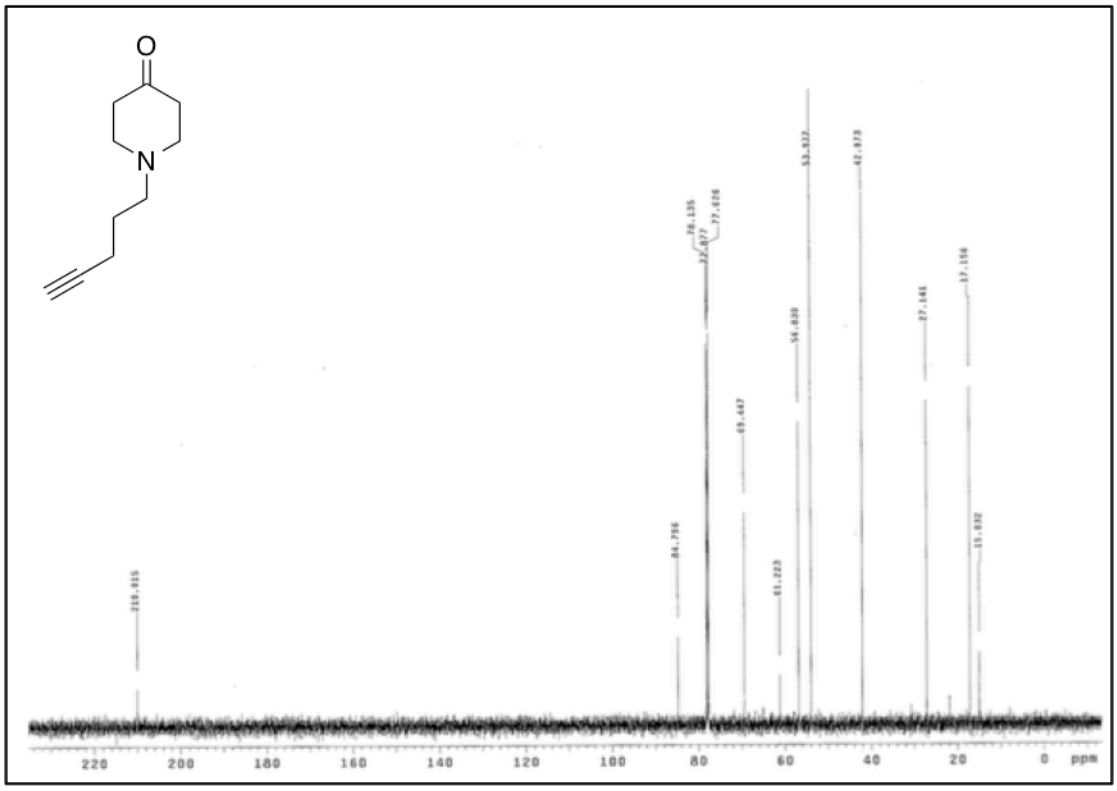

2-chloro-N-octyl-N-(1-(pent-4-yn-1-yl)piperidin-4-yl)acetamide (SMC-1)

^{1}H-NMR

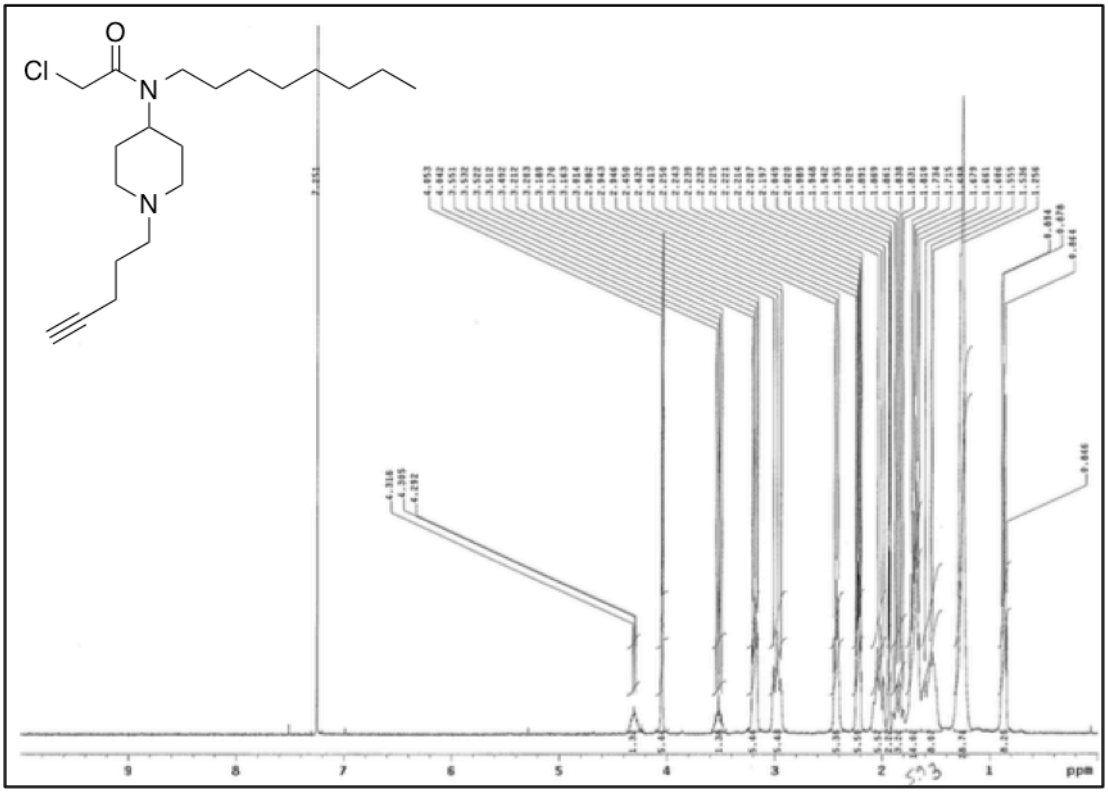

^{13}C-NMR

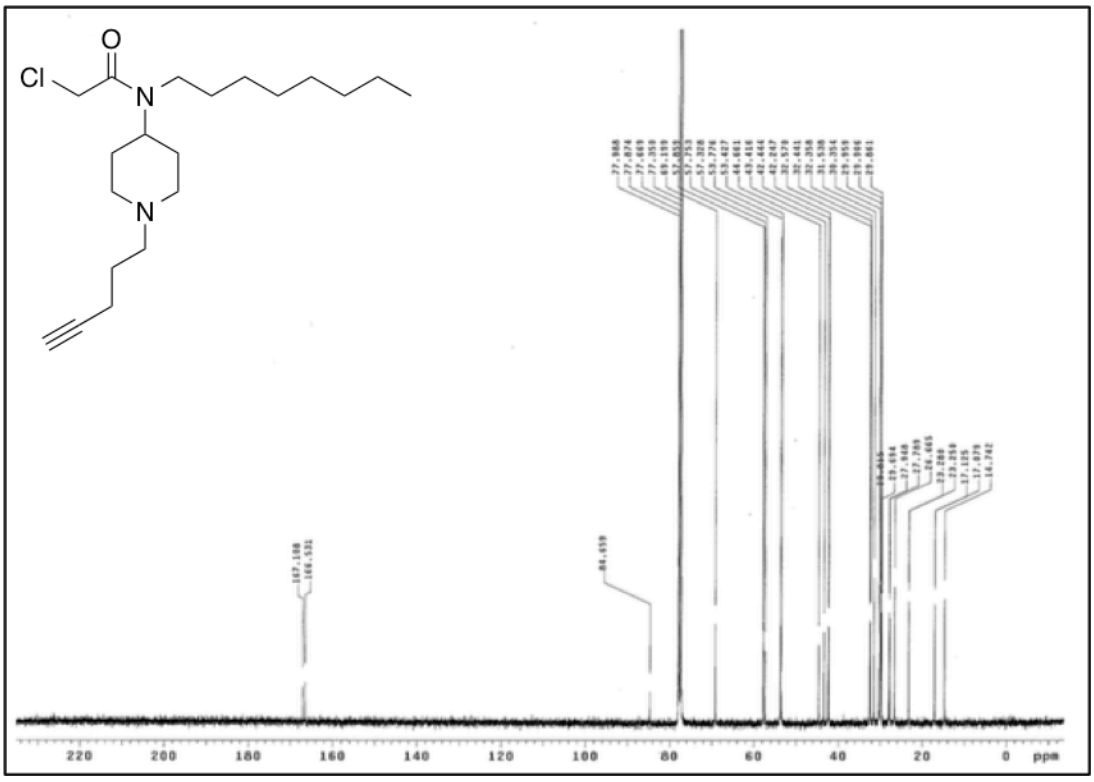

methyl *N*-(2-chloroacetyl)-*N*-(1-(pent-4-yn-1-yl)piperidin-4-yl)-*D*-tyrosinate (SMC-9)

^{1}H-NMR

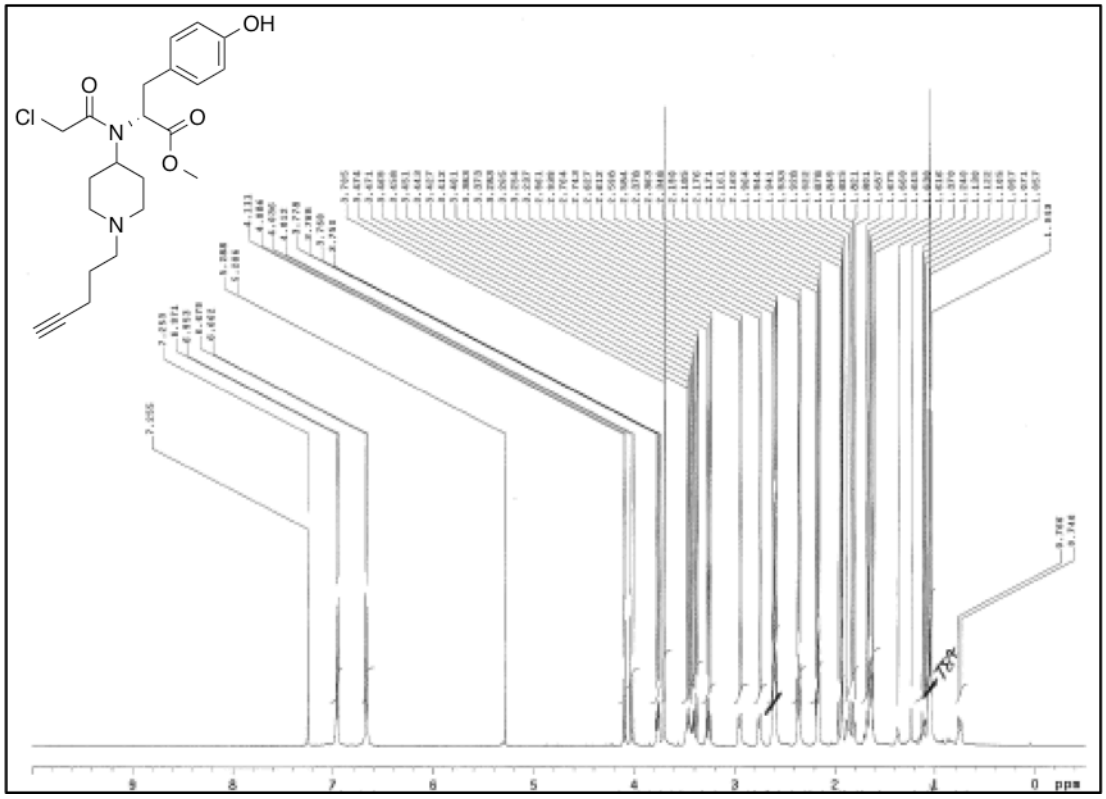

^{13}C-NMR